Appendixes

Appendix A

A.1. Pyrite distribution description

TorA1 (Toraro Mt.): lithiotid accumulation dominated by *Lithiotis problematica*

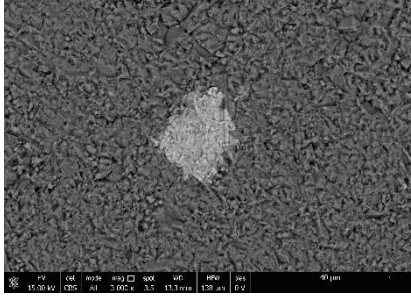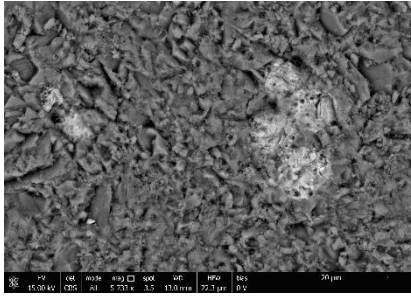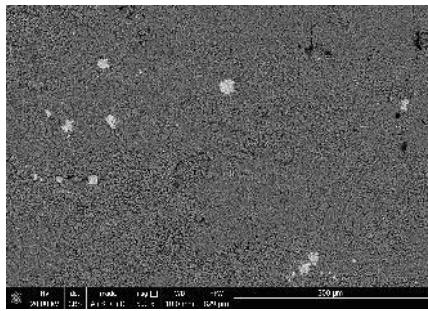| Sample	Photo	Notes SEM Analysis	Image		Measuring
A1-1	8_029	Pyrite		One well-defined framboid (diameter: ~22.33 µm) and another framboid, less defined (diameter: ~18.67 µm). The size of each crystallite varies from 1.5 to 3.5 µm.	The two framboids were considered in the next photo
	8_030	Pyrite		Overview of the previous photo. Framboids pyrite with altered surface, small euhedral crystal (?) and not well-defined pyrite forms.	(Considering also the previous two framboids) **Total amount of framboids (S):** 13 **Mean framboid diameter (md):** 8.66 µm **Maximum framboid diameter (MFD):** 22.33 µm **Minimum framboid diameter:** 2.58 µm **Standard deviation (SD):** 5.61 µm
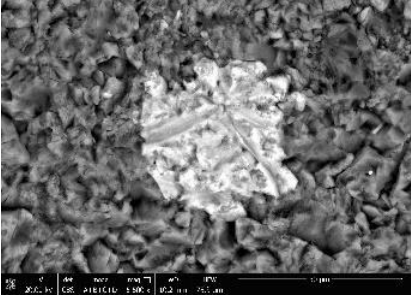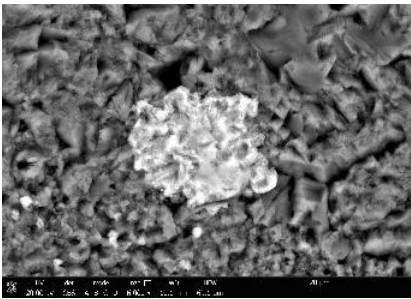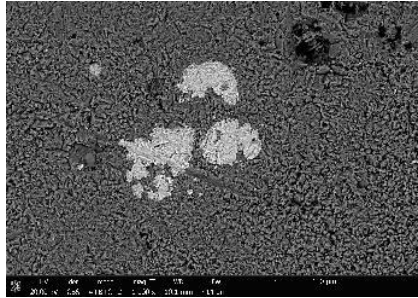
	8_031	Pyrite		Only one framboid with altered surface. The analysed framboid exhibits granular pyrite overgrowth (according to Morse and Cornwell, 1987) where each crystallite varies from 1 to 28 µm.	Diameter: ~12.77 µm
			Considering all the pyrite framboids **Total amount of framboids (S):** 14 **Mean framboid diameter (md):** 8.95 µm **Maximum framboid diameter (MFD):** 22.33 µm **Minimum framboid diameter:** 2.58 µm **Standard deviation (SD):** 5.50 µm		
A1-2	No pyrite				
A1-4	15_003	?		Altered pyrite (?) with undefined morphology (maximum size: 35 µm; minimum: 28 µm).	/
A1-7	No pyrite				
A1-8	No pyrite				
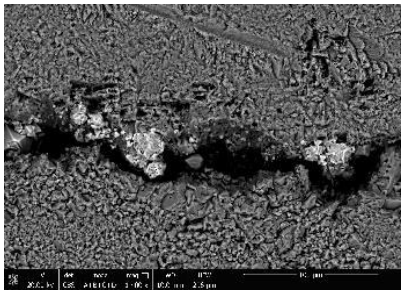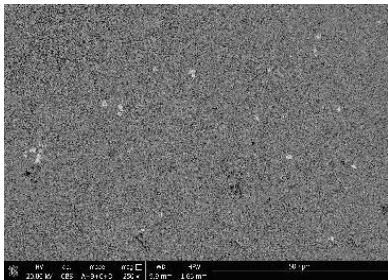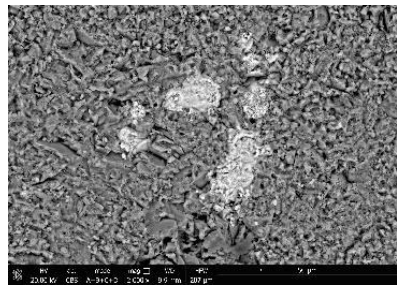
A1-11	17_004	Pyrite		Pyrite with undefined morphology (maximum size: 30 µm; minimum: 27.79 µm).	/
	17_005	Pyrite		Six pyrite framboids with altered surface.	**Total amount of framboids (S):** 6 **Mean framboid diameter (md):** 6.99 µm **Maximum framboid diameter (MFD):** 10.07 µm **Minimum framboid diameter:** 4.39 µm **Standard deviation (SD):** 2.13 µm
	17_006	Pyrite		Only one framboid with altered surface.	Diameter: ~12.01 µm
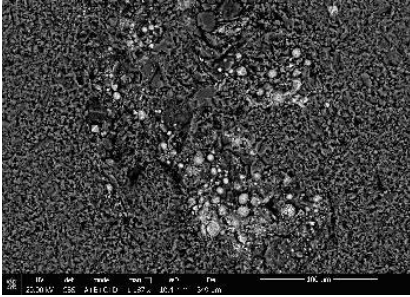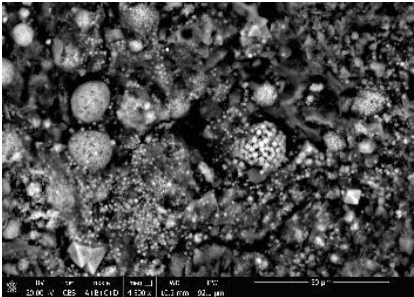
Sample	Photo	Notes SEM Analysis	Image		Measuring
17_007	Pyrite			Only one framboid with altered morphology and surface. The analysed framboid exhibits amorphous pyrite overgrowth where each crystallite diameter is ~2.5 µm.	Diameter: ~9.14 µm
Considering all the pyrite framboids **Total amount of framboids (S):** 8 **Mean framboid diameter (md):** 7.89 µm **Maximum framboid diameter (MFD):** 12.01 µm **Minimum framboid diameter:** 4.39 µm **Standard deviation (SD):** 2.57 µm					

TorA2 (Toraro Mt.): small lithiotid accumulation dominated by *Lithiotis problematica*
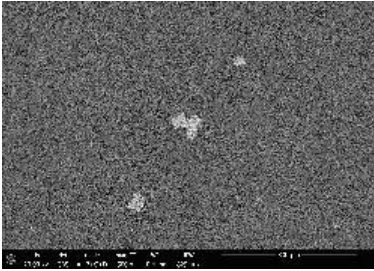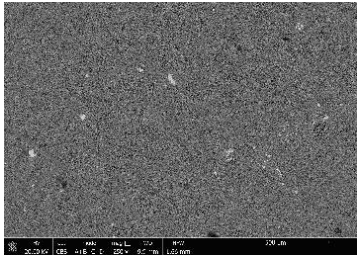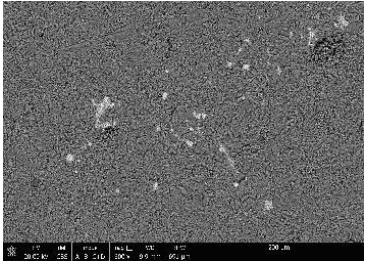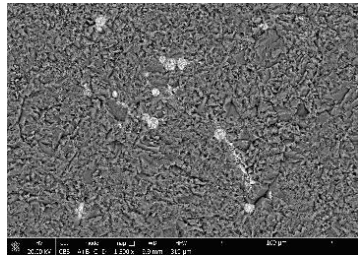
Sample	Photo	Notes SEM Analysis	Image		Measuring
18a (lower part block C)	1			Few framboidal structures with altered surface. Few undefined forms (from ~3 to ~31 µm). Rare not well-defined euhedral crystals (from ~13 µm to ~24 µm).	**Total amount of framboids (S):** 8 **Mean framboid diameter (md):** 17.53 µm **Maximum framboid diameter (MFD):** 29.73 µm **Minimum framboid diameter:** 5.70 µm **Standard deviation (SD):** 9.62 µm

		2	Detailed of previous photo 1		/	Considered in the photo 1
		3	Detailed of previous photo 1		/	Considered in the photo 1
		4			Few framboidal structures with altered surface. Few undefined larger forms (up to ~85 µm).	**Total amount of framboids (S):** 2 **Mean framboid diameter (md):** 10.86 µm **Maximum framboid diameter (MFD):** 15.06 µm **Minimum framboid diameter:** 6.66 µm **Standard deviation (SD):** 5.94 µm
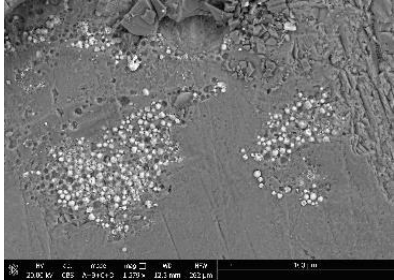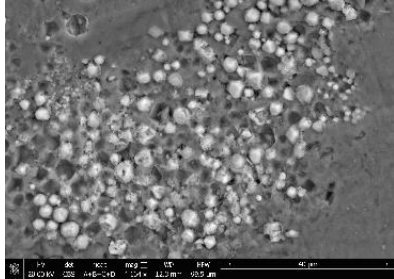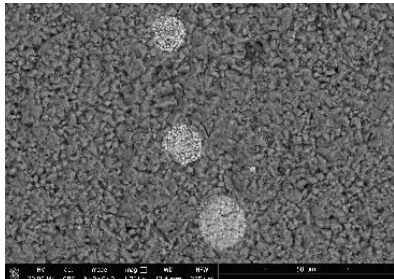
	5	Iron oxides		Few framboidal structures with altered surface. Rare not well-defined euhedral crystals (from ~2 µm to ~29 µm).	**Total amount of framboids (S):** 5 **Mean framboid diameter (md):** 15.71 µm **Maximum framboid diameter (MFD):** 21.35 µm **Minimum framboid diameter:** 5.70 µm **Standard deviation (SD):** 4.53 µm

Considering all the framboids
Total amount of framboids (S): 15
Mean framboid diameter (md): 16.03 µm
Maximum framboid diameter (MFD): 29.73 µm
Minimum framboid diameter: 5.70 µm
Standard deviation (SD): 7.73 µm

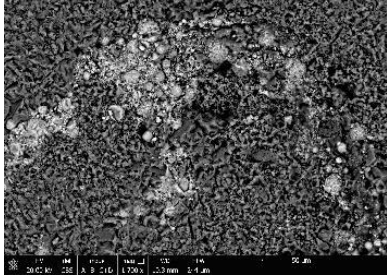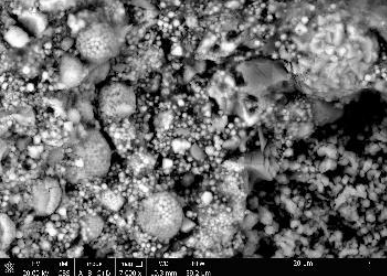| 18a (lower part of block C) | 10 | Pyrite and altered pyrite | | Few framboidal structures with altered surface. Few undefined forms (from ~5 to ~33 µm). | **Total amount of framboids (S):** 14
Mean framboid diameter (md): 18.00 µm
Maximum framboid diameter (MFD): 28.45 µm
Minimum framboid diameter: 8.61 µm
Standard deviation (SD): 5.88 µm |
| | 11 | Detailed of previous photo 10 | | Few framboidal structures with altered surface. One larger undefined form (from ~25 to ~42 µm). | **Total amount of framboids (S):** 6
Mean framboid diameter (md): 14.00 µm
Maximum framboid diameter (MFD): 22.70 µm
Minimum framboid diameter: 8.36 µm
Standard deviation (SD): 5.52 µm |

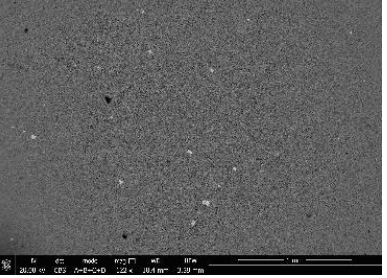|					
				Considering all the framboids **Total amount of framboids (S):** 20 **Mean framboid diameter (md):** 16.75 µm **Maximum framboid diameter (MFD):** 28.45 µm **Minimum framboid diameter:** 8.36 µm **Standard deviation (SD):** 5.92 µm	
				Considering all the framboids of the two samples (photo 1,2,3,4,5,10 and 11) **Total amount of framboids (S):** 35 **Mean framboid diameter (md):** 16.44 µm **Maximum framboid diameter (MFD):** 29.73 µm **Minimum framboid diameter:** 5.70 µm **Standard deviation (SD):** 6.66 µm	
18b (upper part of block C)	6	Iron oxides		Abundant framboidal structures with altered surface. Few undefined forms (from ~4 to ~15 µm). Rare not well-defined euhedral crystals (from ~3 µm to ~10 µm).	**Total amount of framboids (S):** 41 **Mean framboid diameter (md):** 6.89 µm **Maximum framboid diameter (MFD):** 14.32 µm **Minimum framboid diameter:** 2.64 µm **Standard deviation (SD):** 2.59 µm
	7	Detailed of previous photo 6		The size of each crystallite varies from ~0.5 to ~1.7 µm.	Considered in the photo 6
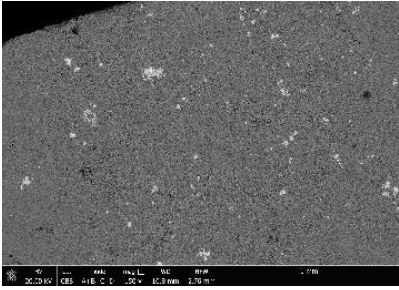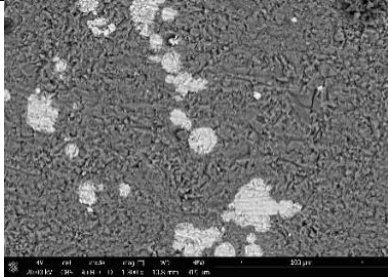
	8	Iron oxides and pyrite		Abundant iron oxides framboidal structures with altered surface. Few undefined forms (from ~4 to ~15 µm). Rare not well-defined euhedral pyrite crystals (~6–7 µm).	**Total amount of framboids (S):** 46 **Mean framboid diameter (md):** 6.25 µm **Maximum framboid diameter (MFD):** 14.30 µm **Minimum framboid diameter:** 2.48 µm **Standard deviation (SD):** 2.50 µm
	9	Detailed of previous photo 8		The size of each crystallite varies from ~0.4 to ~1 µm.	Considered in the photo 8
		Considering all the framboids **Total amount of framboids (S):** 86 **Mean framboid diameter (md):** 6.55 µm **Maximum framboid diameter (MFD):** 14.32 µm **Minimum framboid diameter:** 2.48 µm **Standard deviation (SD):** 2.56 µm			
22a (lower part of block C)	14			No framboidal structures. Several undefined forms that vary in size from ~8 to ~70 µm.	/

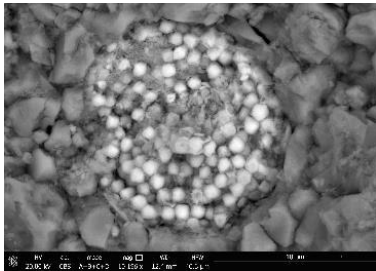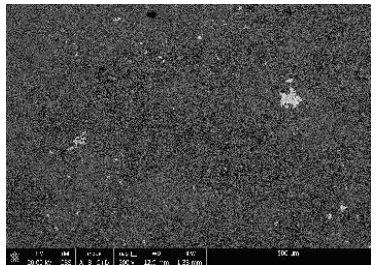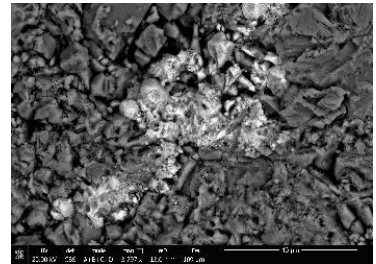|					
	15	Detailed of previous photo 14		/	Considered in the photo 14
22a (upper part of block C)	16			Few framboidal structures with altered surface. Several undefined forms that vary in size from ~6.5 to ~65 µm.	**Total amount of framboids (S):** 9 **Mean framboid diameter (md):** 10.80 m **Maximum framboid diameter (MFD):** 14.63 µm **Minimum framboid diameter:** 7.08 µm **Standard deviation (SD):** 2.86 µm
	17	Detailed of previous photo 16		Few framboidal structures with altered surface.	**Total amount of framboids (S):** 20 **Mean framboid diameter (md):** 7.50 µm **Maximum framboid diameter (MFD):** 12.03 µm **Minimum framboid diameter:** 2.75 µm **Standard deviation (SD):** 2.90 µm
	18	Detailed of previous photo 16		Few framboidal structures with altered surface. Several undefined forms with altered surface (from ~6 to ~65 µm).	**Total amount of framboids (S):** 18 **Mean framboid diameter (md):** 7.64 µm **Maximum framboid diameter (MFD):** 16.14 µm **Minimum framboid diameter:** 2.95 µm **Standard deviation (SD):** 3.46 µm
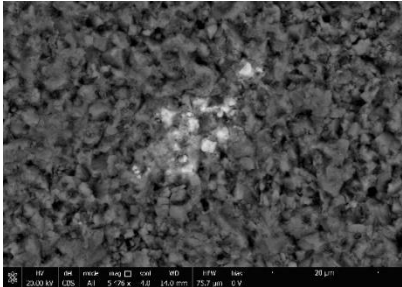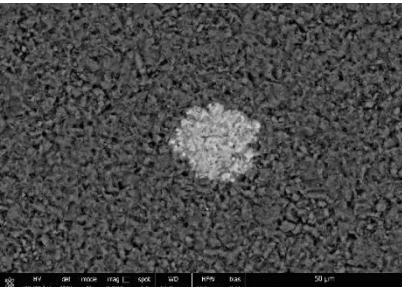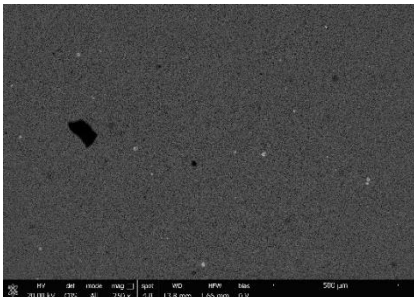
Considering all the framboids **Total amount of framboids (S):** 47 **Mean framboid diameter (md):** 8.17 µm **Maximum framboid diameter (MFD):** 16.14 µm **Minimum framboid diameter:** 2.75 µm **Standard deviation (SD):** 3.31 µm				
marl-22a (upper part of block C)	21			Abundant euhedral crystals with smooth surface which size varies from ~1 to ~7 µm.	/
	22	Limonite or iron oxides		/	Detailed of previous photo, considered in the photo 21
	23	Iron oxides		Three well-defined framboids. The size of each crystallite varies from ~1.5 to ~2.1 µm.	**Total amount of framboids (S):** 3 **Mean framboid diameter (md):** 25.83 µm **Maximum framboid diameter (MFD):** 31.23 µm **Minimum framboid diameter:** 22.76 µm **Standard deviation (SD):** 4.69 µm
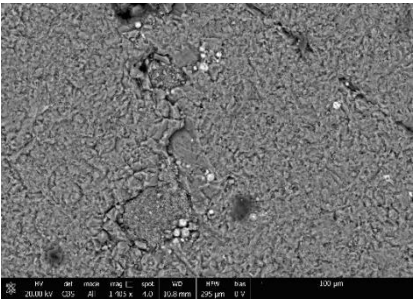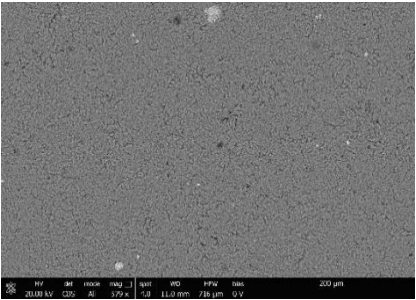
	24			/	Detailed of previous photo, considered in the photo 23
19a (lower part of block A)	19			Euhedral crystals with smooth surface which size varies from ~5 to ~31 µm. Undefined forms with altered surface (from ~4 to ~88 µm). Framboidal structures with altered surface. Iron oxides?	**Total amount of framboids (S):** 5 **Mean framboid diameter (md):** 9.38 µm **Maximum framboid diameter (MFD):** 13.06 µm **Minimum framboid diameter:** 7.28 µm **Standard deviation (SD):** 2.23 µm
	20	Detailed of previous photo 20		Framboidal structures with altered surface. Several isolated small crystallites and undefined (amorphous) forms which vary in size up to ~12 µm. The size of each crystallite is ~0.5 µm. Iron oxides?	**Total amount of framboids (S):** 5 **Mean framboid diameter (md):** 8.36 µm **Maximum framboid diameter (MFD):** 11.36 µm **Minimum framboid diameter:** 6.82 µm **Standard deviation (SD):** 1.81 µm

Considering all the framboids
Total amount of framboids (S): 10
Mean framboid diameter (md): 8.87 µm
Maximum framboid diameter (MFD): 13.06 µm
Minimum framboid diameter: 6.82 µm
Standard deviation (SD): 1.99 µm

139

22a (upper part of block A)	12			Several framboidal structures with altered surface. Several undefined forms that vary in size from ~7 to ~135 µm.	**Total amount of framboids (S):** 74 **Mean framboid diameter (md):** 14.06 µm **Maximum framboid diameter (MFD):** 34.98 µm **Minimum framboid diameter:** 6.46 µm **Standard deviation (SD):** 5.28 µm
	13	Detailed of previous photo 12		/	Considered in the photo 12

TorB (Toraro Mt.): small lithiotid accumulation dominated by *Cochlearites loppianus*
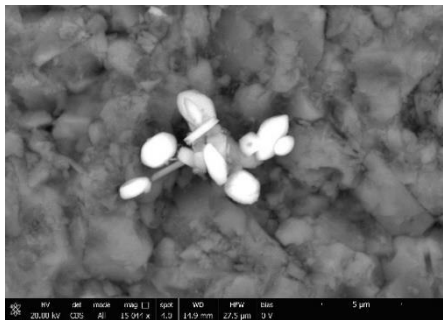
Sample	Photo	Notes SEM Analysis	Image		Measuring
B-1	6-021	Pyrite		Undefined forms (amorphous) with altered surface (no framboids) and rare euhedral crystallites (?). Each crystallite varies from 1 to 4 µm.	/
	6-022	Pyrite		Larger framboid with altered surface (diameter: ~35 µm).	Not considered in the analysis
	6-023	Pyrite		Several framboids with altered surface.	**Total amount of framboids (S):** 22 **Mean framboid diameter (md):** 12.65 µm **Maximum framboid diameter (MFD):** 22.51 µm **Minimum framboid diameter:** 6.68 µm **Standard deviation (SD):** 4.32 µm
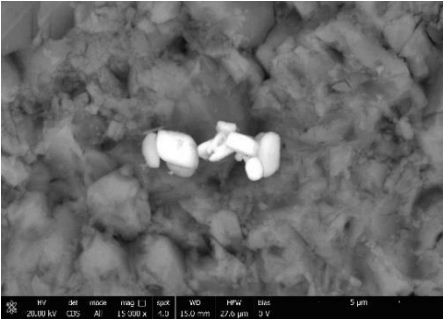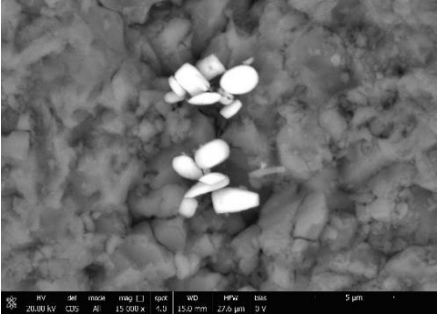
				Only one framboid with altered surface. Each crystallite is ~2 µm large.	Diameter: ~19 µm
	6-024	Pyrite		Only one framboid with altered surface. Each crystallite is ~2 µm large.	Diameter: ~19 µm
	Considering all the pyrite framboids **Total amount of framboids (S):** 23 **Mean framboid diameter (md):** 12.93 µm **Maximum framboid diameter (MFD):** 22.51 µm **Minimum framboid diameter:** 6.68 µm **Standard deviation (SD):** 4.43 µm				
A-2	7-025			Only one framboid with altered surface. Each crystallite varies from ~1 to 2 µm large.	Diameter: ~12.80 µm

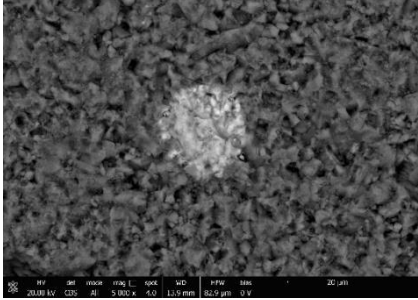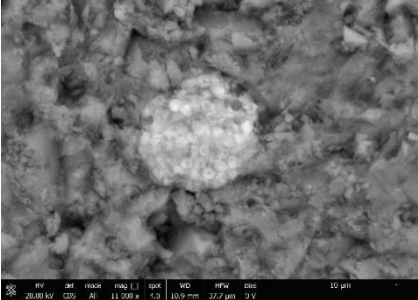|	7-027			Several framboids with altered surface and undefined forms (size: from ~3 up to ~7.5 µm).	**Total amount of framboids (S):** 11 **Mean framboid diameter (md):** 5.81 µm **Maximum framboid diameter (MFD):** 9.93 µm **Minimum framboid diameter:** 2.76 µm **Standard deviation (SD):** 2.01 µm
	7-028	Iron oxides		Several framboids with altered surface (each crystallite is ~2 µm large) and undefined forms (size: from ~2.5 up to ~6.5 µm).	**Total amount of framboids (S):** 9 **Mean framboid diameter (md):** 7.75 µm **Maximum framboid diameter (MFD):** 15.33 µm **Minimum framboid diameter:** 2.59 µm **Standard deviation (SD):** 4.45 µm
	Considering all the pyrite framboids **Total amount of framboids (S):** 21 **Mean framboid diameter (md):** 6.94 µm **Maximum framboid diameter (MFD):** 15.33 µm **Minimum framboid diameter:** 2.59 µm **Standard deviation (SD):** 3.51 µm					

143
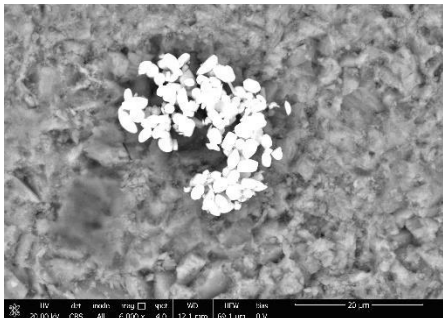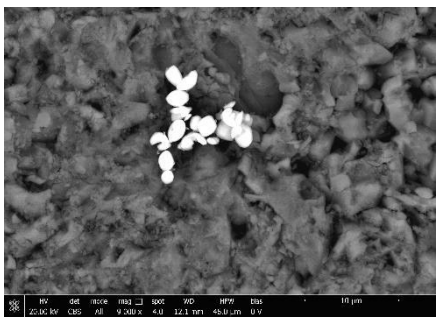
A-3	3-013	Pyrite		Only one framboid with altered surface.	Diameter: ~14.6 µm
	3-014	Pyrite		Disc-shaped pyrite Aggregate of (at least) 9 elements. Each crystallite varies from ~1.39 to 4 µm.	/
	3-015	Altered pyrite		Two framboids with altered surface and altered pyrite with undefined morphology.	**Total amount of framboids (S):** 2 **Mean framboid diameter (md):** 6.45 µm **Maximum framboid diameter (MFD):** 7.82 µm **Minimum framboid diameter:** 5.07 µm **Standard deviation (SD):** 1.94 µm
	Considering all the pyrite framboids **Total amount of framboids (S):** 3 **Mean framboid diameter (md):** 9.05 µm				

144
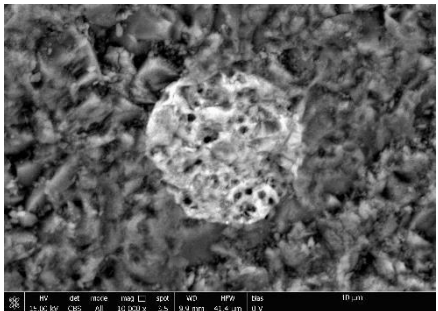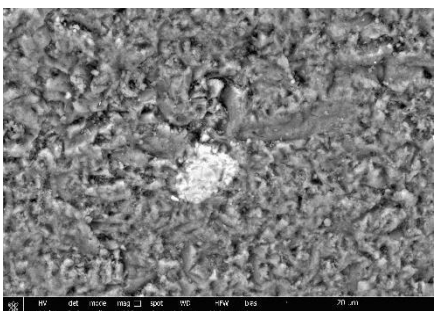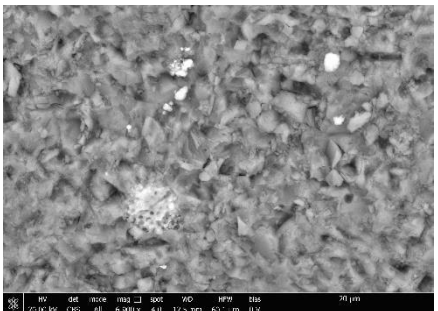
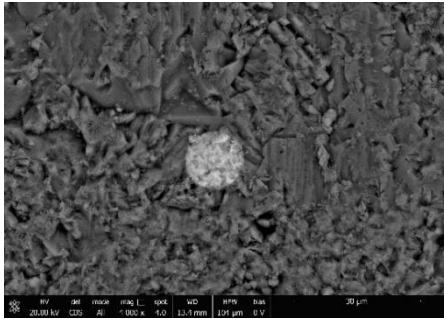|					
			Maximum framboid diameter (MFD): 14.26 µm **Minimum framboid diameter:** 5.07 µm **Standard deviation (SD):** 4.72 µm		
A-4	2-010			Altered pyrite with irregular shape and framboids with altered surface.	**Total amount of framboids (S):** 9 **Mean framboid diameter (md):** 7.06 µm **Maximum framboid diameter (MFD):** 10.07 µm **Minimum framboid diameter:** 4.26 µm **Standard deviation (SD):** 1.93 µm
	2-011			Undefined forms with altered surface (no framboids; size: ~40 µm).	/
	2-012	Limonite and pyrite		Small isolated crystallites (diameter from ~0.7 to ~1.7 µm) and altered pyrite framboids.	**Total amount of framboids (S):** 4 **Mean framboid diameter (md):** 3.87 µm **Maximum framboid diameter (MFD):** 5.07 µm **Minimum framboid diameter:** 3.21 µm **Standard deviation (SD):** 0.83 µm

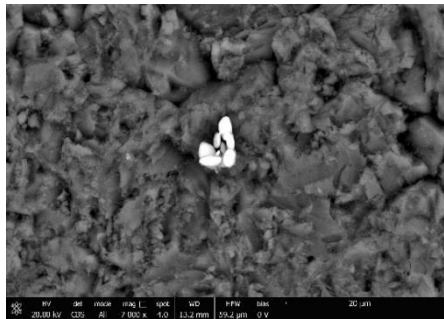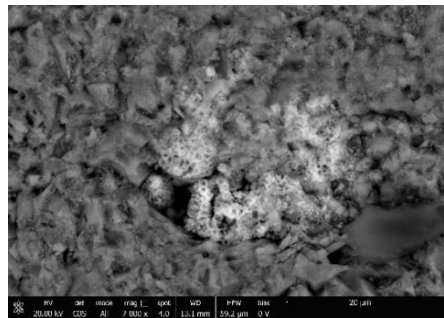|					
			Considering all the pyrite framboids **Total amount of framboids (S):** 13 **Mean framboid diameter (md):** 6.08 µm **Maximum framboid diameter (MFD):** 10.07 µm **Minimum framboid diameter:** 3.21 µm **Standard deviation (SD):** 2.24 µm		
A-5	11-035	Ex-pyrite/ iron oxides		Only one framboid with altered surface.	Diameter of ~6.06 µm
	11-036			Disc-shaped pyrite aggregate of (at least) 12 elements. Each crystallite varies from ~1.7 to 2.8 µm.	/
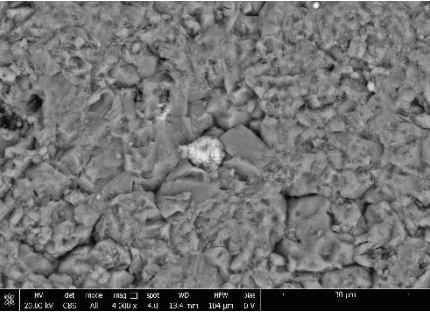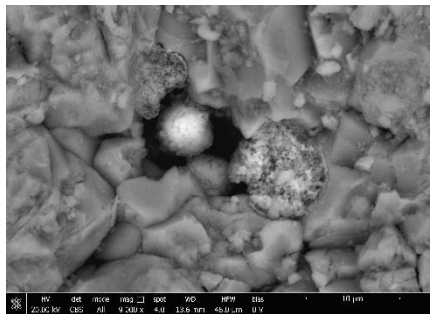
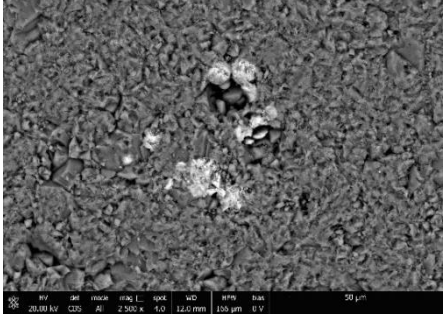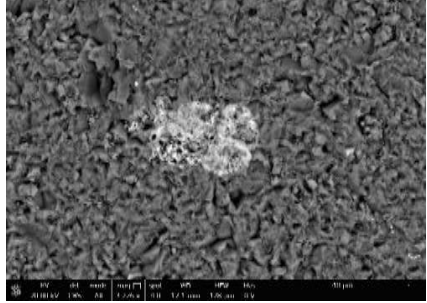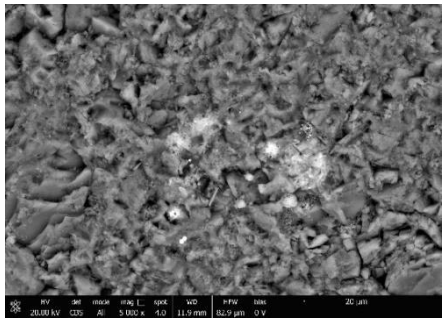| 11-037 | | | Disc-shaped pyrite aggregate of (at least) 8 elements. Each crystallite varies from ~1.4 to 3.4 µm. | / |
| 11-038 | | | Disc-shaped pyrite Aggregate of (at least) 15 elements. Each crystallite varies up to 5 µm. | / |
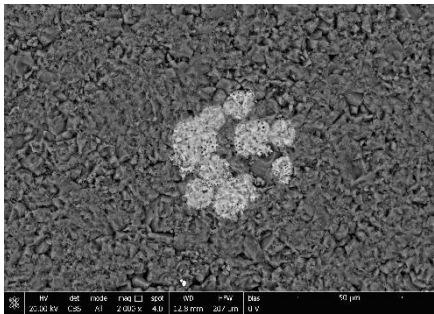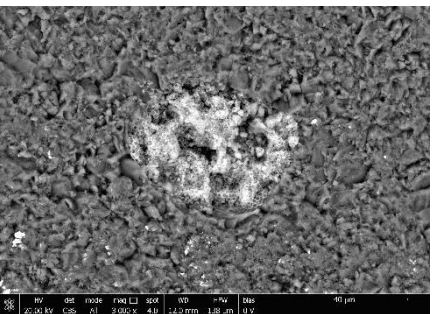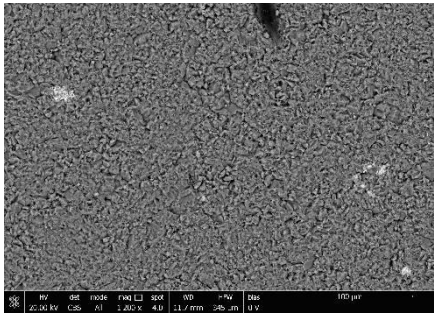
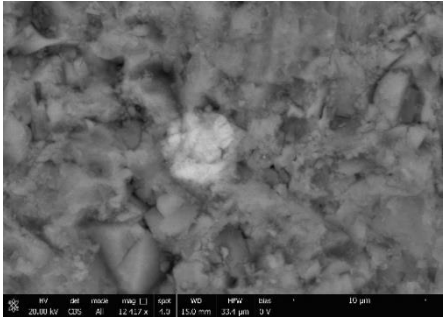**TorC (Toraro Mt.):** Tabular lithiotid accumulation dominated by *Cochlearites loppianus*
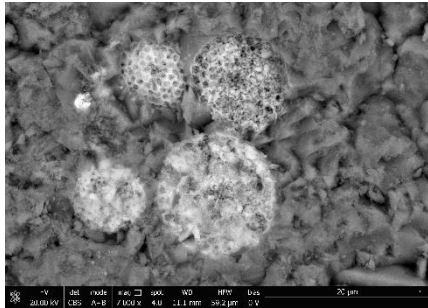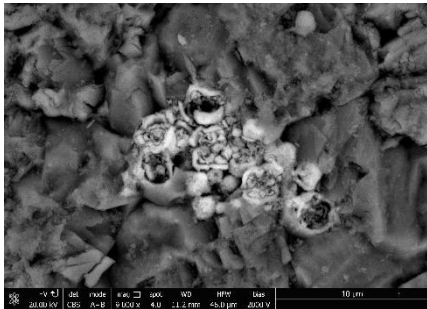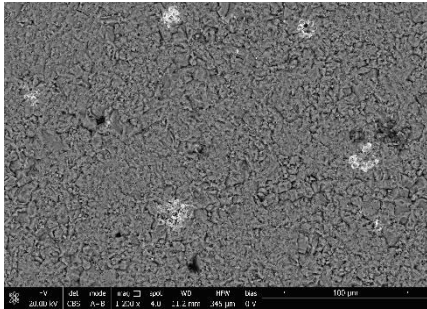
Sample	Photo	Notes SEM Analysis	Image		Measuring
C-1I2	13_040	Pyrite		Disc-shaped pyrite aggregate of (at least) 40 elements. Each crystallite varies from ~1.6 to ~4.5 µm.	/
	13_041	Pyrite		Disc-shaped pyrite aggregate of (at least) 18 elements. Each crystallite varies from ~1 to ~3.5 µm.	/
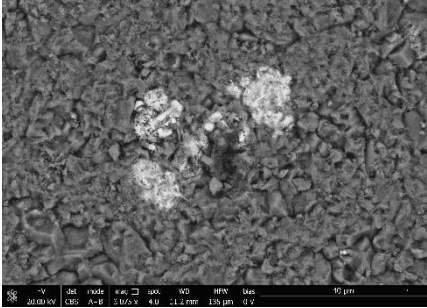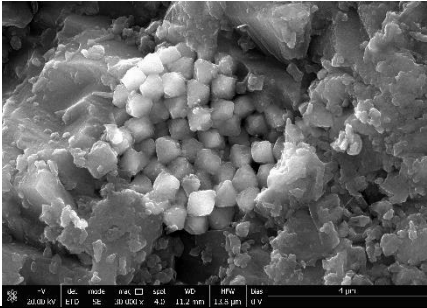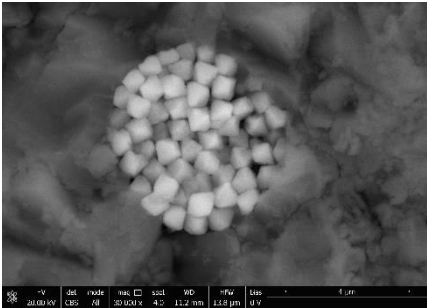
	14_001	No pyrite		Only one framboid (no pyrite) with altered surface (diameter: ~15.9 µm).	/
	14_002	No pyrite		Undefined form with altered surface (no pyrite) which varies from ~11.2 to ~7.3 µm.	/
C-10	12_039			One framboid with altered surface and several undefined forms (amorphous). These elements vary from ~1 to ~3 µm.	Framboid diameter: ~7.89 µm
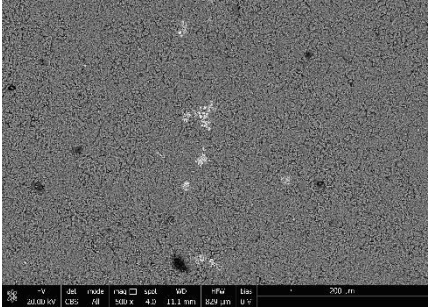
C-1CL	5_019	Iron oxides and goethite		Undefined forms (no framboids) that vary in size up to ~7 µm.	/
	5_020	Altered pyrite		Two framboids with altered surface. The diameter of each crystallite in the smaller framboids is <1 µm.	**Total amount of framboids (S):** 2 **Mean framboid diameter (md):** 6.19 µm **Maximum framboid diameter (MFD):** 8.00 µm **Minimum framboid diameter:** 4.38 µm **Standard deviation (SD):** 2.56 µm
C-1CR	9_032	Iron oxides		Undefined form (no framboidal-shape) which varies from ~33 to ~15.6 µm. Crystallites were recognizable and vary from ~0.9 to ~1.5 µm in size.	/

150

	10_033	Pyrite		One framboid with altered surface. The diameter of each crystallite is <1 µm. There is a small form (diameter: ~1.8 µm).	Framboid diameter: ~9.03 µm
	10_034	Pyrite		Five framboids with altered surface. The diameter of each crystallite in the well-defined framboid is < ~1 µm.	**Total amount of framboids (S):** 4 **Mean framboid diameter (md):** 7.85 µm **Maximum framboid diameter (MFD):** 10.77 µm **Minimum framboid diameter:** 5.65 µm **Standard deviation (SD):** 2.15 µm
			Considering all the studied framboids **Total amount of framboids (S):** 5 **Mean framboid diameter (md):** 8.10 µm **Maximum framboid diameter (MFD):** 10.77 µm **Minimum framboid diameter:** 5.65 µm **Standard deviation (SD):** 2.63 µm			

C-3CL	4_016			Several framboids with altered surface and two undefined forms (coalescent framboids?) which vary in size from ~25 to ~30 µm.	**Total amount of framboids (S):** 7 **Mean framboid diameter (md):** 14.84 µm **Maximum framboid diameter (MFD):** 19.95 µm **Minimum framboid diameter:** 12.60 µm **Standard deviation (SD):** 2.54 µm
	4_017			Two less defined framboids with altered surface and several undefined forms (coalescent framboids?). Crystallites were recognised (their size varies from ~0.9 to ~1.7 µm).	**Total amount of framboids (S):** 2 **Mean framboid diameter (md):** 12.53 µm **Maximum framboid diameter (MFD):** 13.33 µm **Minimum framboid diameter:** 11.72 µm **Standard deviation (SD):** 1.14 µm
	4_018			Few undefined forms (no framboids, altered pyrite?) which vary from ~7.7 to ~16.8 µm).	/
	Considering all the studied framboids **Total amount of framboids (S):** 9 **Mean framboid diameter (md):** 14.33 µm				

			Maximum framboid diameter (MFD): 19.95 µm **Minimum framboid diameter:** 11.72 µm **Standard deviation (SD):** 2.45 µm		
C-5B	1_002	Pyrite		Four framboids (three with altered surface). In better preserved framboids, each crystallite is ~1.1 µm.	**Total amount of framboids (S):** 4 **Mean framboid diameter (md):** 12.33 µm **Maximum framboid diameter (MFD):** 16.88 µm **Minimum framboid diameter:** 9.93 µm **Standard deviation (SD):** 3.28 µm
	1_003	Altered pyrite		No framboids - undefined forms where each crystallite varies from ~2 to ~4.7 µm.	/
	1_004	Limonite		Few undefined forms with altered surface (size from ~10 to ~26 µm). The smaller units/elements vary from ~3.5 to ~7.5 µm.	/

	1_005	Limonite		Few undefined forms with altered surface, included coalescent elements (size from ~3.3 to ~22.2 µm).	/
	1_006	Pyrite		Well-defined pyrite framboid. Each crystallite varies from ~0.7 to ~1 µm.	Diameter: ~5.97 µm
	1_007	Pyrite		Well-defined pyrite framboid. Each crystallite varies from ~0.8 to ~0.9 µm.	Diameter: ~6.19 µm

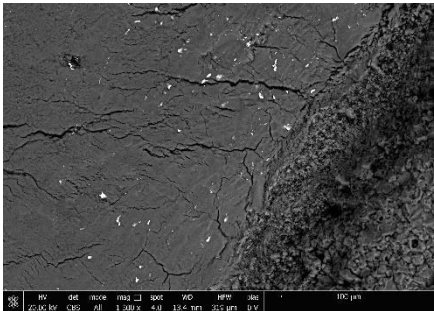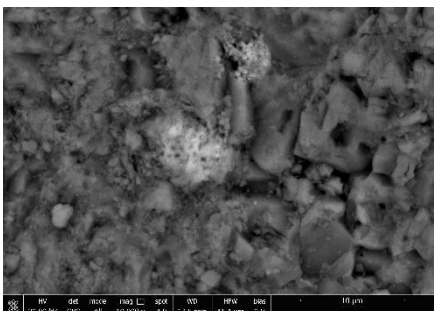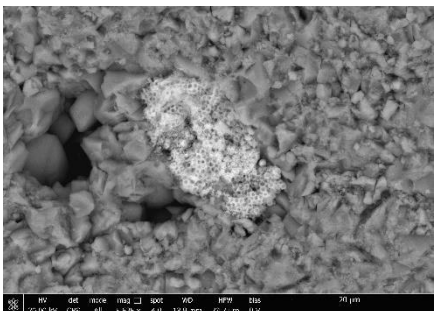| 1_009	Altered pyrite		Few undefined forms (including aggregates) with altered surface (size from ~18 to ~26 µm). The smaller units/elements vary from ~3.5 to ~9 µm.	/
		Considering all the studied framboids **Total amount of framboids (S):** 6 **Mean framboid diameter (md):** 10.14 µm **Maximum framboid diameter (MFD):** 16.88 µm **Minimum framboid diameter:** 5.57 µm **Standard deviation (SD):** 4.24 µm			

Original data of Figure 4.21 (Chapter 4)

Accumulation	Sample	ID	No. of measured samples	Mean diameter (µm)	Standard deviation
TorA1	A1	A1	14	8.95	5.50
	A1-11	A1-11	8	7.89	2.57
TorA2	18 upper part block C	18uC	86	6.55	2.56
	18 lower part block C	18lC	35	16.44	6.66
	22 upper part block C	22uC	47	8.17	3.31
	marl 22 upper part block C	22MuC	3	25.83	4.69
	19 lower part block A	19lA	10	8.87	1.99
	22 upper part block A	22uA	74	14.06	5.28
	22 lower part block C	null			
TorB	B-1	B-1	23	12.93	4.43
	B-2	B-2	21	6.94	3.51
	B-3	B-3	3	9.05	4.72
	B-4	B-4	13	6.08	2.24
TorC	C-1CL	C-1CL	2	6.19	2.56
	C-1CR	C-1CR	5	8.10	2.63
	C-3CL	C-3CL	9	14.33	2.45
	C-5B	C-5B	6	10.14	4.24
TorE	null (see text for further details)				

A.2. Alternative methods to detect pyrite and framboids

The traditional procedure to observed and measure pyrite and framboids includes the scanning electron microscope (SEM) set in backscattered mode (e.g., Wilkin et al., 1996; Wignall and Newton, 1998). Only few works used transmitted and reflected optical light microscopy (e.g., Wang et al., 2012), always joined to SEM analysis.

However, Wilkin et al. (1996) pointed out the limitations of 2D analyses of framboidal pyrite distribution claiming that the estimated measurement error is approximately 10%. Because spherical objects are not uniform in size, the examined surface represents a random section which underestimated of the real diameter of the objects.

Even though SEM constitutes the best method to verify the occurrence of pyrite, it remains a time-consuming procedure and could be not easily accessible. Some alternative methods were tested in order to analyse the pyrite distribution in carbonate rocks. The used methods can be divided into two groups according to the starting samples: thin sections and collected rock blocks.

A.2.1. Thin sections of rock samples

Thin sections were analysed under light-reflected microscope and light-transmitted binocular microscope. For this analysis ultra-polished thin sections were prepared. Under light-reflected microscope, pyrite appears light yellow in colour and distinguished by its morphology, its relatively high reflectance (55) and its hardness (6.0–6.5) verified with "Kalb line" test. Unfortunately, as confirmed by SEM analysis, in the studied samples pyrite occurs in several shapes and a clear distinction of framboids cannot be made.

Few works studied pyrite framboids under light-transmitted binocular microscope (e.g., Wang et al., 2012). In these cases, framboids are abundant and well preserved; they are easily distinguished from the matrix due to the highest colour contrast. Although in the analysed thin sections few dark and/or reddish features were detected, they cannot certainly be identified as pyrite.

A.2.2. Chemical and CT-scan analyses

Few collected samples of TorC (Toraro Mt.) were chosen in order to test different methods to extract pyrite. In literature, pyrite isolation procedure was reported only by

Vallentyne (1963). The aim of this procedure was to obtain the spherules microcrystal components based on heavy mineral centrifugation, flotation of pyrite spherules, and differential sedimentation of pyrite after rupturing spherules into their component microcrystals. This study focused on pyrite spherules-richness sediments of the Little Round Lake, Ontario. This method is quite complex, and the final goal is beyond the scopes of the present thesis.

The followed procedure is here briefly reported. After weight, the samples were immersed in HCl (10%) and H_2O_2 (~10%) in order to dissolve the calcium carbonate and organic fraction and to avoid damages to the framboids. The residue, constituted by insoluble clay terrigenous fraction and other minerals, were filtered over suited paper (pore-size 8 μm) and the collected residue was dried in hoven (ca. two hours at 60 °C). After that, the solid residue was tentatively observed under light-reflected stereo microscope in order to collect the main minerals. Unfortunately, the large amount of mud hampered a clear identification. Only few larger minerals were separated (Fig. 1A). In order to remove the mud, two techniques (i, ii) were performed.

i) The residue was tentatively separated with a centrifuge without success. The few amounts and the reduced size of pyrite hampered a strict separation. A better result could be obtained using an ultra-centrifuge which usually is not easily available in the laboratories.

ii) The solid residue was filtered using a saturated-sugar solution. The sugar solution density, measured with a picnometer, was 1.3517 g/cm^3 while pyrite shows a density of ~5.01 g/cm^3, and mud is ~1.73 g/cm^3. In this case, the separation is due to the high viscosity of sugar solution which allows a slow parting between colloidal muddy fraction from the heavy part, which includes pyrite minerals (Fig. 1C–D). The minerals immersed in the sugar solution were collected and scanned with high resolution scanner (Epson V800 Photo; Fig. 1B). Subsequently, the same samples were also observed with binocular microscope (Leica M50) but the resolution of both devices (scanner and microscope) was not enough.

Finally, considering that the different density between the pyrite and the sugar solution allows the mineral forms reconstruction, the filtered residue was analysed with X-ray tomography (micro-CT scan) at the University of Ferrara. Micro-CT scan is a non-destructive technology which provides high resolution 3D imaging information. Few studies used high resolution X-ray tomography (micro-CT) (e.g., Cárdenes et al., 2016; Merinero et al., 2017). These preliminary works, which verify the micro-CT scan efficiency for the observation of pyrite framboids, are always joined with SEM analysis. SEM is able to determine the morphology and size of pyrite in 2D, while micro-CT scan provides statistically relevant information about the 3D size (Cárdenes et al., 2016).

The micro-computed tomographic system consists of a Hamamatsu L9421-02 tungsten X-ray microfocus tube with an anode voltage of 70 kVp. The used current was 100–110 µA. Rotation step ranges between 0.5° to 1°, with an exposure time of 1 second. The reconstructed voxel size was 5x5x5 µm^3 with the reconstruction algorithm FDK on GPU. The X-ray detector collects hundreds of angular shadow images while the object rotates, thereafter, a computer program (Di Domenico, 2014), developed on CUDA framework and including alignment optimization, uses a modified Feldkamp algorithm allowing the reconstruction of data throughout the full 3D volume. In the resulted images (Fig. 2) the outer morphology of the crystals was observed but their surface was not clear enough to identify them as framboids.
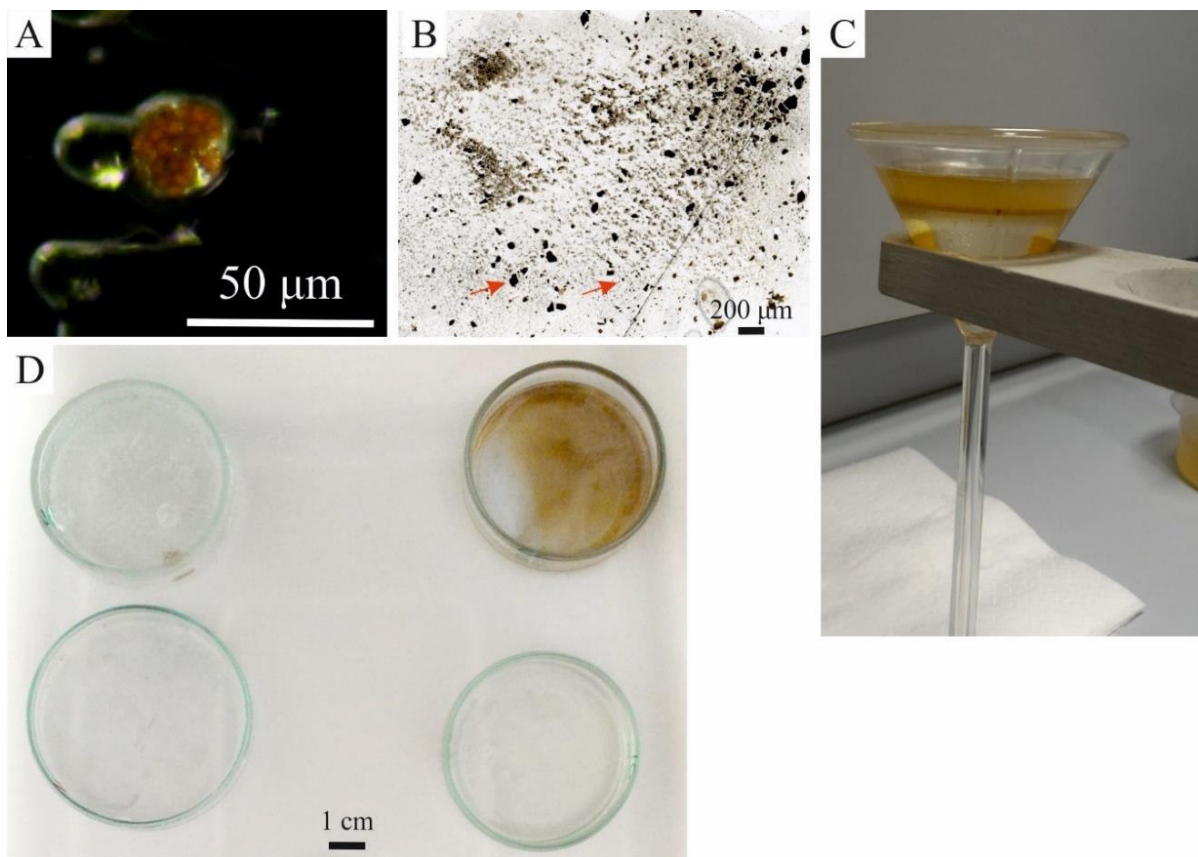
Figure 1. A) Isolated large pyrite framboid viewed under light-reflected stereo microscope (~25 µm in diameter). B) Scanned image of the solid residue; the densest black forms are likely pyrite (red arrows). C) Separated solid residue in saturated sugar solution. D) Petri dishes with the saturated sugar solution and filtered solid residue.

Pyrite is the most abundant sulphide minerals in carbonate rocks, where it occurs in several size and shapes. In paleoredox reconstruction, the most important pyrite forms are constituted by smallest pyrite framboids, whose diameter is less than ~10 µm. Frequently, pyrite framboids are prone to be altered during diagenesis (see Chapter 4 for further details).

As resulted by SEM analysis carried out on the lithiotid accumulation samples, pyrite frequently occurs as altered forms (see Chapter 4 for further details). Unusual morphologies, as

the disc-shaped morphologies, were also recognised. The size of pyrite forms can vary considerably and the well-defined framboids are relatively rare. Even though larger and well-defined pyrite framboids could be isolated and observed under light-reflected stereo microscope (Fig. 1), the most important smallest pyrite framboids, frequently altered, cannot be distinguished.

Primary framboidal morphologies is not distinctive for pyrite (Wilkin and Barnes, 1997). Several authors observed spherical and irregularly shaped aggregates of magnetite, magnesioferrite, marcasite and greigite (see Wilkin and Barnes, 1997 for further details). Other minerals, for example limonite framboids, likely represent oxides or replaced pyrite framboids (e.g., Lougheed and Mancuso, 1973).
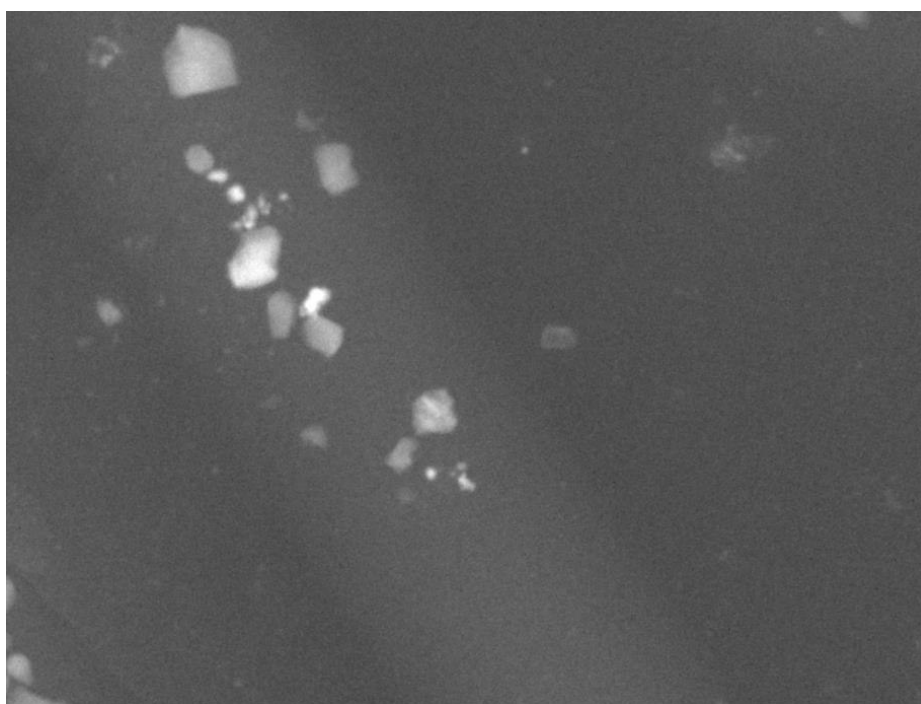
Figure 2. Micro-CT scan image of possible pyrite crystals immersed in the saturated sugar solution after filtration.

In conclusion, SEM analysis is still the most suitable method in order to verify the nature of pyrite framboids and the shapes of the single pyrite crystals, in particular when diagenetic alteration occurs.

A.3. Thin section data elaboration

Lituosepta compressa Zone

Accumulation		Sample	L	Bio	miF	maF	Br	Gas	Ech	*Th.*	*Pal.*	Bac	Onc	Pel	F. P.	Cor	Micrite	Spa.
Ve4	Flanks	Ve4-11	F-RW	R													M	
		Ve4-12	W	R										R			M	
		Ve4-9	W-M	R										C	R		M/MS	
		Ve4-10	FW	R			R										M	
		Ve4-13	F	R													M	
Ve3	Flanks	Ve3-15/1	W	R	R			R				R				R	M/MS	
		Ve3-15/2	W	R	R		R					R		R			M	
		Ve3-7	W-P	R	R							R		R			M	X
		Ve3-8	P-W	R	R									R	R		M	X
Ve2	Core	Ve2-4	M	R								R					M	
		Ve2-5	M-W	R	R							R		R			M	
		Ve2-6	M	R	R							R		R			M/MS	
		Ve2-14	W	R	R					R						R	M/MS	
Ve1	Core	Ve1-1	P-G	A	R	R	R		R			R	C	R	C		M	X
		Ve1-2	FM	R	R		R						R				M	
		Ve1-3	W-M	R	R	R	R					R		R			M/MS	
Ro	Core	Ro-10	W	R	R		R		R		R		R			M/VFGM	
		Ro-3	M	R	R						R		R			M	
		Ro-2	M	R	R				R		R		R			M	
		Ro-6	M-W	C	R		R		R		R		R			M	
		Ro-9	W	R	R		R		R		R		R			M/VFGM	
		Ro-8	W	R	R						R		R			M	
	Flanks	Ro-1	W	R	R		R		R		R		R			M	
		Ro-7	W	R	R		R				R		R			M/VFGM	
		Ro-4	FM	R	R		R				R					M	
		Ro-5	W	R	R			R			R					M	
Cm	Flanks	Cm-1-1	W-P	C	R				R				R	A	R	VFGM/CPM	X
		Cm-1-2	W-P	A				R					R	C		VFGM/CPM	X
		Cm-2	W	C	R								R			VFGM/M	
		Cm-3	W	C									R	R		VFGM/CPM	
		Cm-4	W	C				R					R			VFGM	
TorF	Flanks	F2-1	W-P	A	R			R	R	R			R		R	M/CPM	X
		F2-5	W-P	A	R		R			R		R	R			M/CPM	X
		F2-C	W	A	R	R	R					R	C		R	M	
		F1-1	W	A	R		R	R	R	R		R	C		R	M	
		F1-2	W	A	R	R	R			C		C	C		R	M	
		F1-3	W	A	R		R			C		R	C			M	
		F1-4	W-P	A	R		R	R	R	C		R	R		R	M	X
		F1-C1	FW	A	R		C			R	R	R	R		R	M/MS	
		F1-C2	W	A	C	R			R	R	R		C			M	
		F2-2	W-P	R	R	R	R		R	R		R	C	R	Cor	M	X
		F2-3	W-P	R	R	R		R			R		R			M/CPM	X
		F2-4	W-P	A	R		R	R		R		R	C	R	R	M	X
		F1-B	FP	A	R		R		R	R		R	C		R	M/CPM	X
TorE	Flanks	E-2O3	W	A	R		R			R		R	R			M	X
		E-3O2	FW	C	R		R	R		R		R	R			M	
		E-4O	W	R	R				R	R		R	R			M	
		E-4I	W-P	C	R		R		R	R		C	R			M	X
		E-2O2	W-G	C	R				R	R		C	R			M	X
		E-2I	W-P	A	R		R		R	R		R	R			M	X
		E-1O	W-P	R	R		R			R		C	C			M	X
		E-2OB	W-P	C	R		R		R	R		R	R			M	X
		E-2C	W-P	A	R		R	R		R		R	R	R		M	X
		E-1C	P-G	A	R		C	R		R		C	R			M/CPM	X
		E-5C	P-G	A	C		C			C		R	A			M/CPM	X
		E-3C	W	R	R		R			R		R	R			M	
		E-4C	W	R	R					R		R	R			M/MS	
		E-1B	W-P	R	R		R			R		C	C			M	X
		E-4B	W-P	C	R		R			R		C	C			M	X
		E-3B	FW	R	R		R			R		R	C			M	
		E-5B	FW	A	R		C	R		R		R	R			M	
TorD2	Cover	D2-OB	P-G	A	R	R			R	C	R	R		R		R	VFGM/M	X
		D2-OT	W-G	R	R		R	R	R	R		R	R			VFGM/M	X
	Flanks	D2-U	W	R	R			R	R	R			R			VFGM/M	
		D2-V	W	A	R				R		R		C		C	M/VFGM	
		D2-I	W	A	R			R		R		R		C		C	VFGM/M	X

Zone	Group	Type	Sample	Tex	1	2	3	4	5	6	7	8	9	10	11	12	13	Matrix	
			D2-BT	P-G	A	R	R	R		R	R		R		C	R		M/CPM	X
	TorC	Cover	C-OC	P-W	R	C				A			A	A		R		M	X
			C-1I	M	R													MS/M	
			C-1O	W-P	R	R		R		R	C		R	A	C		R	M	X
			C-5O	M	R													M	
			C-3O	M	R								R		R			M/MS	
			C-4O	M	R			R					R		R	R		MS/M	
			C-6O	FM	R								R		R			MS/M	
			C-OC	P	R	C				A			C	A	A		R	MS/M	
		Core	C-4I	W	R								R					MS/M	
			C-1I2	G-P	C	C	C			R	A				R	R	C	M	X
			C-1B	FM	R										C			MS/M	
			C-2B	M	R								R		R			MS/M	
			C-1CL	FM	R								C		R			M/MS	
			C-3I	M	R			R					R		R			M	
			C-4IS	FM	R			R										MS/M	
			C-5I	M	R													MS/M	
			C-6I	W	R			R					R					MS/M	
			C-1CR	M	R								R					MS/M	
			C-4B	M	R			R					R		R	R		MS/M	
			C-5B	M	R			R							R	R		MS/M	
			C-5C	M	R			R							R	R		MS/M	
	TorB	Cover	B-1	FM	A													VFGM	
		Core	B-3	W	R										C	R		M/MS	
			B-4	M	R			R							R			M/MS	
			B-5	FM	A	R		R	R	R					R		C	VFGM	
		Flanks	B-2	FM	A								R		R	R		M/MS	
?Orbitopsella -Lituosepta compressa Zone	Da	Core	Da-1	W-P	R	R		R			R		R					M/MS	X
			Da-2	FP	R	R		R			R		R		R		R	M	X
			Da-3	W-P	R						R				C			M	X
			Da-4	W	R						R		R		R			M	
			Da-5	W	R			R		R			R		C			M/CPM	
			Da-6	W-P	R						R				R			M	X
			Da-7	W	R	R					R		R					M	
			Da-8	W-G	R				R		R		R		C	C		M/CPM	X
			Da-9	W-P	C			R	R	R	R		R		R			M	X
			Da-10	W-P	C	R			R	R	R		R		R			M	X
			Da-11	FW	R	R					R		R		C	R		M	X
			Da-12	W-P	R						R		R		R			M	X
			Da-13	FW	R				R		R		R		R			M	
			Da-14	W-P	R								R		R			M	S
			Da-15	W	R								R		C			VFGM/M/CPM	
			Da-16	FW	R						R		R		R			M	
			Da-17	W-P	R						R				R			M	X
			Da-18	FP	C			R	R		R		R					M	
			Da-19	W	R	R					R		C		R			M/MS	X
			Da-20	W-P	R			R			R		R		R			M/MS	
			Da-21	W-P	R						R		R		R			M	X
			Da-22	W	R			R			R		R		R			M	
			Da-23	W-P	R						R				R			M/MS	X
			Da-24	W-P	R			R					R		R			M	X
			Da-25	F-RW	R				R	R	R				R		R	VFGM	
			Da-26	W-P	R						R		R		R			M	X
			Da-27	W	R								R		R			M	
			Da-28	W	R						R		R		R			M	
			Da-29	W	R													M	
			Da-30	W-P	R	R		R			R		R		R			M	X
			Da-31	W	R						R		R		R			M	
			Da-32	W-P	R	R		R			R		C		C			M	X
			Da-33	W	R			R			R		R		R			M	
			Da-34	W-P	R			R			R		R		R			M	X
			Da-35	W	R				R		R		R		C			VFGM/M	
Orbitopsella Zone	TorA1	Cover	A1-4	W	R	R		R		R					R			CPM	
			A1-3	W	R	R	R			R					R			M	
			A1-11	W-P	R	R		R							R			M/CPM/MS	
		Core	A1-5	W	R			R					R		R			M	
			A1-6	W	R			R							R			M	
			A1-7	W	C	R		R							R	R		M	
			A1-13	W	R	R		R		R					C	R		M/CPM	
			A1-2	W-P	R	R	R	R		R					R			M/CPM	X
			A1-1	W-P	R	R				R			R		R			M/CPM	X

Orbitopsella Zone				L															
	Flanks		A1-8	W	R	R	R	R		R			R		R			M/CPM	
			A1-9	FW	A	R	C	R		R	R				R		R	CPM	
			A1-10	W-M	R			R		R					R		R	M	
			A1-12	W	R	R	R				R				R			M	
TorA2	**Core**		A2-10	W-P	R	C	R	R							A			M	X

Textural characters, skeletal and non-skeletal components in the analysed lithotid accumulations. TorA1, TorA2 and Contrada Dazio: *Lithiotis*-dominated accumulations; Cm: *Lithioperna*-dominated accumulation; TorB, TorC, TorD2, TorE, TorF, Ro and Ve1–4: *Cochlearites*-dominated accumulations. For each accumulation, samples are grouped according to accumulation geometry (e.g., flank, core and cover). Cover identifies the deposit which overlies the accumulation. The tabular body, TorC is here considered as accumulation core. See text for further details. Non-lithiotid bivalves are rare and are not distinguished in detail. L, lithology; Bio, bioclasts; miF, small benthic foraminifera; maF, larger benthic foraminifera; Br, brachiopods; Gas, gastropods; Ech, echinoderms; *Th.*, *Thaumatoporella parvovesiculifera*; *Pal.*, *Palaeodasycladus* sp.; Bac, bacteria-like structures; Onc, oncoids; Pel, peloids; F. P., fecal pellets; Cor, cortoids; Spa., sparite. R, rare; C, common; A, abundant. X, present. M, mudstone; W, wackestone; P, packstone; G, grainstone; F, floatstone; R, rudstone. Regarding micrite: M, micrite; VFGM, very fine-grained micrite; CPM, clotted peloidal micrite, MS, microsparite. Geographic and stratigraphic locations of the accumulations in Chapter 4 (Tab. 4.1).

Lithiotis -dominated accumulations

		Sample	L	Bio	miF	maF	Br	Gas	Ech	Th.	Pal.	Bac	Pel	F. P.	Cor	Micrite	Spa.
TorA1	Cover	A1-4	W	R	R		R		R				R			CPM	
		A1-3	W	R	R	R				R			R			M	
		A1-11	W-P	R	R		R						R			M/CPM/MS	
	Sum	\	0	0	2	1	3	2	2	3	3	0	3	3	M	1
		R	3	3	1	2	0	1	1	0	0	3	0	0	M/CPM/MS	1
		C	0	0	0	0	0	0	0	0	0	0	0	0	CPM	1
		A	0	0	0	0	0	0	0	0	0	0	0	0	SPARITE	0
	No.	3															
	%	\	0.00	0.00	66.67	33.33	100.00	66.67	66.67	100.00	100.00	0.00	100.00	100.00		
		R	100.00	100.00	33.33	66.67	0.00	33.33	33.33	0.00	0.00	100.00	0.00	0.00		
		C	0.00	0.00	0.00	0.00	0.00	0.00	0.00	0.00	0.00	0.00	0.00	0.00		
		A	0.00	0.00	0.00	0.00	0.00	0.00	0.00	0.00	0.00	0.00	0.00	0.00		

		Sample	L	Bio	miF	maF	Br	Gas	Ech	Th.	Pal.	Bac	Pel	F. P.	Cor	Micrite	Spa.
TorA1	Flanks	A1-13	W	R	R		R		R				C	R		M/CPM	
		A1-2	W-P	R	R	R	R		R				R			M/CPM	X
		A1-1	W-P	R	R				R			R	R			M/CPM	X
		A1-8	W	R	R	R	R		R			R	R			M/CPM	
		A1-9	FW	A	R	C	R		R	R			R		R	CPM	
		A1-10	W-M	R			R		R				R		R	M	
		A1-12	W	R	R	R				R			R			M	
	Sum	\	0	1	3	2	7	1	5	7	5	0	6	5	M	2
		R	6	6	3	5	0	6	2	0	2	6	1	2	VFGM/M	4
		C	0	0	1	0	0	0	0	0	0	1	0	0	CPM	1
		A	1	0	0	0	0	0	0	0	0	0	0	0	SPARITE	2
	No.	7															
	%	\	0.00	14.29	42.86	28.57	100.00	14.29	71.43	100.00	71.43	0.00	85.71	71.43		
		R	85.71	85.71	42.86	71.43	0.00	85.71	28.57	0.00	28.57	85.71	14.29	28.57		
		C	0.00	0.00	14.29	0.00	0.00	0.00	0.00	0.00	0.00	14.29	0.00	0.00		
		A	14.29	0.00	0.00	0.00	0.00	0.00	0.00	0.00	0.00	0.00	0.00	0.00		

Sample	L	Bio	miF	maF	Br	Gas	Ech	Th.	Pal.	Bac	Pel	F. P.	Cor	Micrite	Spa.
Da-1	W-P	R	R		R			R			R			M/MS	X
Da-2	FP	R	R		R			R			R	R	R	M	X
Da-3	W-P	R						R			C			M	X
Da-4	W	R						R		R	R			M	
Da-5	W	R			R		R			R	C			M/CPM	
Da-6	W-P	R						R			R			M	X
Da-7	W	R	R					R			R			M	
Da-8	W-G	R					R	R		R	C		C	M/CPM	X
Da-9	W-P	C			R	R	R	R		R	R			M	X
Da-10	W-P	C	R			R	R	R		R	R			M	X
Da-11	FW	R	R					R		R	C	R		M	X

Data summarised in the Figure 4.13 (Chapter 4). For each accumulation, samples are grouped according to accumulation geometry (e.g., flank, core and cover). L, lithology; Bio, bioclasts; miF, small benthic foraminifera; maF, larger benthic foraminifera; Br, brachiopods; Gas, gastropods; Ech, echinoderms; *Th. Thaumatoporella parvovesiculifera*; *Pal. Paleaodasycladus* sp.; Bac, bacteria-like structures; Onc, oncoids; Pel, peloids; F. P., fecal pellets; Cor, cortoids; Spa., sparite. R, rare; C, common; A, abundant. X, present. M, mudstone; W, wackestone; P, packstone; G, grainstone; F, floatstone; R, rudstone. Regarding micrite: M, micrite; VFGM, very fine-grained micrite; CPM, clotted peloidal micrite, MS, microsparite.

Group	Zone	Sample	L	Bio	miF	maF	Br	Gas	Ech	Th.	Pal.	Bac	Pel	F.P.	Cor	Micrite	Spa.
Dazio	Core	Da-12	W-P	R								R	R			M	X
		Da-13	FW	R				R		R		R	R			M	
		Da-14	W-P	R								R	R			M	S
		Da-15	W	R								R	C			VFGM/M/CPM	
		Da-16	FW	R						R		R	R			M	
		Da-17	W-P	R						R			R			M	X
		Da-18	FP	C			R	R		R		R				M	
		Da-19	W	R	R					R		C	R			M/MS	X
		Da-20	W-P	R			R			R		R	R			M/MS	
		Da-21	W-P	R						R		R	R			M	X
		Da-22	W	R			R			R		R	R			M	
		Da-23	W-P	R									R			M/MS	X
		Da-24	W-P	R			R					R	R			M	X
		Da-25	F-RW	R			R	R		R			R		R	VFGM	
		Da-26	W-P	R						R		R	R			M	X
		Da-27	W	R								R	R			M	
		Da-28	W	R						R			R			M	
		Da-29	W	R												M	
		Da-30	W-P	R	R		R			R		R	R			M	X
		Da-31	W	R						R		R	R			M	
		Da-32	W-P	R	R		R			R		C	C			M	X
		Da-33	W	R			R			R		R	R			M	
		Da-34	W-P	R			R			R		R	R			M	X
		Da-35	W	R				R		R		R	C			VFGM/M	
TorA1	Core	A1-5	W	R			R					R	R			M	
		A1-6	W	R			R						R			M	
		A1-7	W	C	R		R						R	R		M	
TorA2	Core	A2-10	W-P	R	C	R	R						A			M	X

		Sum	\	0	29	38	22	32	36	12	39	10	4	36	37	M	30
			R	35	9	1	17	7	3	27	0	27	27	2	2	M/MS	4
			C	4	1	0	0	0	0	0	0	2	7	1	0	VFGM/M	1
			A	0	0	0	0	0	0	0	0	0	1	0	0	M/CPM	2
			No.	39												VFGM/M/CPM	1
		%	\	0.00	74.36	97.44	56.41	82.05	92.31	30.77	100.00	25.64	10.26	92.31	94.87	SPARITE	19
			R	89.74	23.08	2.56	43.59	17.95	7.69	69.23	0.00	69.23	69.23	5.13	5.13		
			C	10.26	2.56	0.00	0.00	0.00	0.00	0.00	0.00	5.13	17.95	2.56	0.00		
			A	0.00	0.00	0.00	0.00	0.00	0.00	0.00	0.00	0.00	2.56	0.00	0.00		

Cochlearites -dominated accumulations

Group	Zone	Sample	L	Bio	miF	maF	Br	Gas	Ech	Th.	Pal.	Bac	Pel	F. P.	Cor	Micrite	Spa.
TorD2	Flanks	D2U	W	R	R				R	R	R			R			VFGM/M	
		D2-V	W	A	R					R			R	C		C	M/VFGM	
		D2-I	W	A	R				R		R		R	C		C	VFGM/M	X
		D2-BT	P-G	A	R	R	R			R	R		R	C	R		M/CPM	X

Group	Flanks	ID	Code													Desc	X
TorB	Flanks	B-2	FM	A								R	R	R		M/MS	
TorE	Flanks	E-2O2	W-G	C	R				R	R		C	R			M	X
		E-2I	W-P	A	R		R		R	R		R	R			M	X
		E-1O	W-P	R	R		R			R		C	C			M	X
		E-2OB	W-P	C	R		R		R	R		R	R			M	X
		E-2C	W-P	A	R		R	R		R		R	R	R		M	X
		E-1C	P-G	A	R		C	R		R		C	R			M/CPM	X
		E-5C	P-G	A	C		C			C		R	A			M/CPM	X
		E-3C	W	R	R		R			R		R	R			M	
		E-4C	W	R	R					R		R	R			M/MS	
		E-1B	W-P	R	R		R			R		C	C			M	X
		E-2O3	W	A	R		R			R		R	R			M	X
		E-3O2	FW	C	R		R	R		R		R	R			M	
		E-4O	W	R	R				R	R		R	R			M	
		E-4I	W-P	C	R		R		R	R		C	R			M	X
		E-4B	W-P	C	R		R			R		C	C			M	X
		E-3B	FW	R	R		R			R		R	C			M	
		E-5B	FW	A	R		C	R		R		R	R			M	
TorF	Flanks	F2-1	W-P	A	R			R	R	R			R		R	M/CPM	X
		F2-5	W-P	A	R		R			R		R	R			M/CPM	X
		F2-C	W	A	R	R	R					R	C		R	M	
		F1-1	W	A	R		R	R	R	R		R	C		R	M	
		F1-2	W	A	R	R	R			C		C	C		R	M	
		F1-3	W	A	R		R			C		R	C			M	
		F1-4	W-P	A	R		R	R	R	C		R	R		R	M	X
		F1-C1	FW	A	R		C			R	R	R	R		R	M/MS	
		F1-C2	W	A	C	R			R	R		R	C			M	
		F2-2	W-P	R	R	R	R		R	R		R	C	R	R	M	X
		F2-3	W-P	R	R	R			R			R	R			M/CPM	X
		F2-4	W-P	A	R		R	R		R		R	C	R	R	M	X
		F1-B	FP	A	R		R		R	R		R	C		R	M/CPM	X
Ro	Flanks	Ro-1	W	R	R		R		R			R	R			M	
		Ro-7	W	R	R		R					R	R			M/VFGM	
		Ro-4	FM	R	R		R					R				M	
		Ro-5	W	R	R			R				R				M	
Ve3	Flanks	Ve3-15/1	W	R	R			R				R			R	M/MS	
		Ve3-15/2	W	R	R		R					R	R			M	
		Ve3-7	W-P	R	R							R	R			M	X
		Ve3-8	P-W	R	R							R	R			M	X
Ve4	Flanks	Ve4-12	W	R								R				M	
		Ve4-9	W-M	R								C	R			M/MS	
		Ve4-10	FW	R			R									M	
		Ve4-13	F	R												M	
		Ve4-11	F-RW	R												M	
		Sum	\	0	6	42	18	36	33	16	47	8	6	41	36	M	32
			R	22	40	6	26	12	15	28	1	33	25	7	10	M/MS	5

	5	2	0	4	0	0	4	0	7	16	0	2	VFGM/M	4
C														
A	21	0	0	0	0	0	0	0	0	1	0	0	M/CPM	7
No.	48													
% ****	0.00	12.50	87.50	37.50	75.00	68.75	33.33	97.92	16.67	12.50	85.42	75.00		
R	45.83	83.33	12.50	54.17	25.00	31.25	58.33	2.08	68.75	52.08	14.58	20.83		
C	10.42	4.17	0.00	8.33	0.00	0.00	8.33	0.00	14.58	33.33	0.00	4.17		
A	43.75	0.00	0.00	0.00	0.00	0.00	0.00	0.00	0.00	2.08	0.00	0.00		

		Sample	L	Bio	miF	maF	Br	Gas	Ech	*Th.*	*Pal.*	Bac	Pel	F. P.	Cor	Micrite	Spa.
Ve1	**Core**	Ve1-1	P-G	A	R	R	R		R			R	C	R	C	M	X
		Ve1-2	FM	R	R		R						R			M	
		Ve1-3	W-M	R	R	R	R					R	R			M/MS	
Ve2	**Core**	Ve2-4	M	R	R							R				M	
		Ve2-5	M-W	R	R							R	R			M	
		Ve2-6	M	R	R							R	R			M/MS	
		Ve2-14	W	R	R						R				R	M/MS	
Ro	**Core**	Ro-10	W	R	R		R			R		R	R			M/VFGM	
		Ro-3	M	R	R							R	R			M	
		Ro-2	M	R	R					R		R	R			M	
		Ro-6	M-W	C	R		R			R		R	R			M	
		Ro-9	W	R	R		R		R			R	R			M/VFGM	
		Ro-8	W	R	R							R	R			M	
TorC	**Core**	C-4I	W	R									R			MS/M	
		C-1I2	G-P	C	C	C			R	A			R	R	C	M	X
		C-1B	FM	R									C			MS/M	
		C-2B	M	R									R	R		MS/M	
		C-1CL	FM	R									C	R		M/MS	
		C-3I	M	R			R						R	R		M	
		C-4IS	FM	R			R									MS/M	
		C-5I	M	R												MS/M	
		C-6I	W	R			R						R			MS/M	
		C-1CR	M	R								R				MS/M	
		C-4B	M	R			R					R	R	R		MS/M	
		C-5B	M	R									R	R		MS/M	
		C-5C	M	R			R						R	R		MS/M	
TorB	**Core**	B-3	W	R									C	R		M/MS	
		B-4	M	R			R						R			M/MS	
		B-5	FM	A	R		R	R	R				R		C	VFGM	
		Sum ****	0	14	26	16	28	25	25	28	16	5	20	25	M	10
		R	25	14	2	13	1	4	3	1	13	20	9	1	M/MS	16
		C	2	1	1	0	0	0	0	0	0	4	0	3	VFGM/M	2
		A	2	0	0	0	0	0	1	0	0	0	0	0	VFGM	1
		No.	29													
		% ****	0.00	48.28	89.66	55.17	96.55	86.21	86.21	96.55	55.17	17.24	68.97	86.21		
		R	86.21	48.28	6.90	44.83	3.45	13.79	10.34	3.45	44.83	68.97	31.03	3.45		
		C	6.90	3.45	3.45	0.00	0.00	0.00	0.00	0.00	0.00	13.79	0.00	10.34		

A 6.90 0.00 0.00 0.00 0.00 0.00 3.45 0.00 0.00 0.00 0.00 0.00

		Sample	L	Bio	miF	maF	Br	Gas	Ech	*Th.*	*Pal.*	Bac	Onc	Pel	F. P.	Cor	Micrite	Spa.
TorB	Cover	B-1	FM	A										R			VFGM	
TorC	Cover	C-OC	P-W	R	C					A			A	A		R	M	X
		C-1I	M	R										R			MS/M	
		C-1O	W-P	R	R		R		R	C		R	A	C		R	M	X
		C-5O	M	R										R			M	
		C-3O	M	R								R		R			M/MS	
		C-4O	M	R			R					R		R	R		MS/M	
		C-6O	FM	R								R		R			MS/M	
		C-OC	P	R	C					A		C	A	A		R	MS/M	
TorD2	Cover	D2-OB	P-G	A	R	R			R	C	R	R		R		R	VFGM/M	X
		D2-OT	W-G	R	R		R	R	R	R		R		R			VFGM/M	X
		Sum	\	0	6	10	8	10	8	6	10	4	8	1	10	7	M	3
			R	9	3	1	3	1	3	1	1	6	0	7	1	4	VFGM/M	2
			C	0	2	0	0	0	0	2	0	1	0	1	0	0	VFGM	1
			A	2	0	0	0	0	0	2	0	0	3	2	0	0	MS/M	5
			No.	11														
		%	\	0.00	54.55	90.91	72.73	90.91	72.73	54.55	90.91	36.36	72.73	9.09	90.91	63.64		
			R	81.82	27.27	9.09	27.27	9.09	27.27	9.09	9.09	54.55	0.00	63.64	9.09	36.36		
			C	0.00	18.18	0.00	0.00	0.00	0.00	18.18	0.00	9.09	0.00	9.09	0.00	0.00		
			A	18.18	0.00	0.00	0.00	0.00	0.00	18.18	0.00	0.00	27.27	18.18	0.00	0.00		

Lithioperna -dominated accumulations

		Sample	L	Bio	miF	maF	Br	Gas	Ech	*Th.*	*Pal.*	Bac	Pel	F. P.	Cor	Micrite	Sparite
Cm	Flanks	Cm-1-1	W-P	C	R				R				R	A	R	VFGM/CPM	X
		Cm-1-2	W-P	A				R					R	C		VFGM/CPM	X
		Cm-2	W	C	R								R			VFGM/M	
		Cm-3	W	C									R	R		VFGM/CPM	
		Cm-4	W	C				R					R			VFGM	
		Sum	\	0	3	5	5	3	4	5	5	5	0	2	4	VFGM/M	1
			R	0	2	0	0	2	1	0	0	0	5	1	1	VFGM	1
			C	4	0	0	0	0	0	0	0	0	0	1	0	VFGM/CPM	3
			A	1	0	0	0	0	0	0	0	0	0	1	0	SPARITE	2
			No.	5														
		%	\	0	60	100	100	60	80	100	100	100	0	40	80		
			R	0	40	0	0	40	20	0	0	0	100	20	20		
			C	80	0	0	0	0	0	0	0	0	0	20	0		
			A	20	0	0	0	0	0	0	0	0	0	20	0		

A.4. TorA2 accumulation

This low and wide (ca. 20 cm and 4 m, respectively) lithiotid accumulation overlying the TorA1 (green arrow, Fig. 4.14A, Chapter 4), is dominated by *Lithiotis problematica*, characterized by wide and short shells (see Chapter 3 and Brandolese et al., 2019 for further details). The lower part of the accumulation is constituted by marlstone bed (ca. 10 cm thick). This boundary between the marlstone and lithiotid accumulation-bearing bed is irregular. The lithiotid shells, well distinguishable in the upper part, are completely dissolved in the marlstone. In the lithiotid bed, the aragonite is completely replaced by sparry calcite. Only the outer calcitic shell layer seems to be preserved (for further details see Appendix B.6). Most of the shells are still articulated and in life position (i.e., sub-vertical; Chapter 3; Brandolese et al., 2019). Macroscopically, the accumulation included abundant skeletal components such as gastropods, brachiopods, and larger benthic foraminifera.

The Chapter 4 illustrated how the lithiotid accumulations are distinguished by matrix which varies from mudstone to packstone, with peloids and relatively rare skeletal components (e.g., Fig. 4.13, Chapter 4). The TorA2 accumulation differs from the others in having a peloidal grainstone-packstone with abundant skeletal components and only few restricted wackestone occurrence.

A detail analysis on skeletal components along with microtaphonomic features were conducted in order to clarify the bivalve accumulation dynamics.

A.4.1. Materials and methods

The analysis of the biogenic components and microtaphonomic features was carried out on 10 thin sections collected by some rock blocks characterizing the accumulation core (Fig. 4.15, Chapter 4; Appendix A.6). The studied thin sections show different size: two of 6.5×8 cm; two of 4.5×6.5 cm; one of 4.3×4.3 cm; five of 4×4 cm. Microtaphonomic features (i.e., fragmentation, abrasion, micritization, encrustation) were semi-quantitatively evaluated considering bioclasts larger than 1 mm. The effects of the main taphonomic features were reported in percentage based on three classes of alteration: low (little or no effect), moderate (moderate effect) and high (extensive effect) (according to Kowalewski et al., 1995; Fig. 1). The results were plotted using tapho-diagrams as described by Kowalewski et al. (1995).
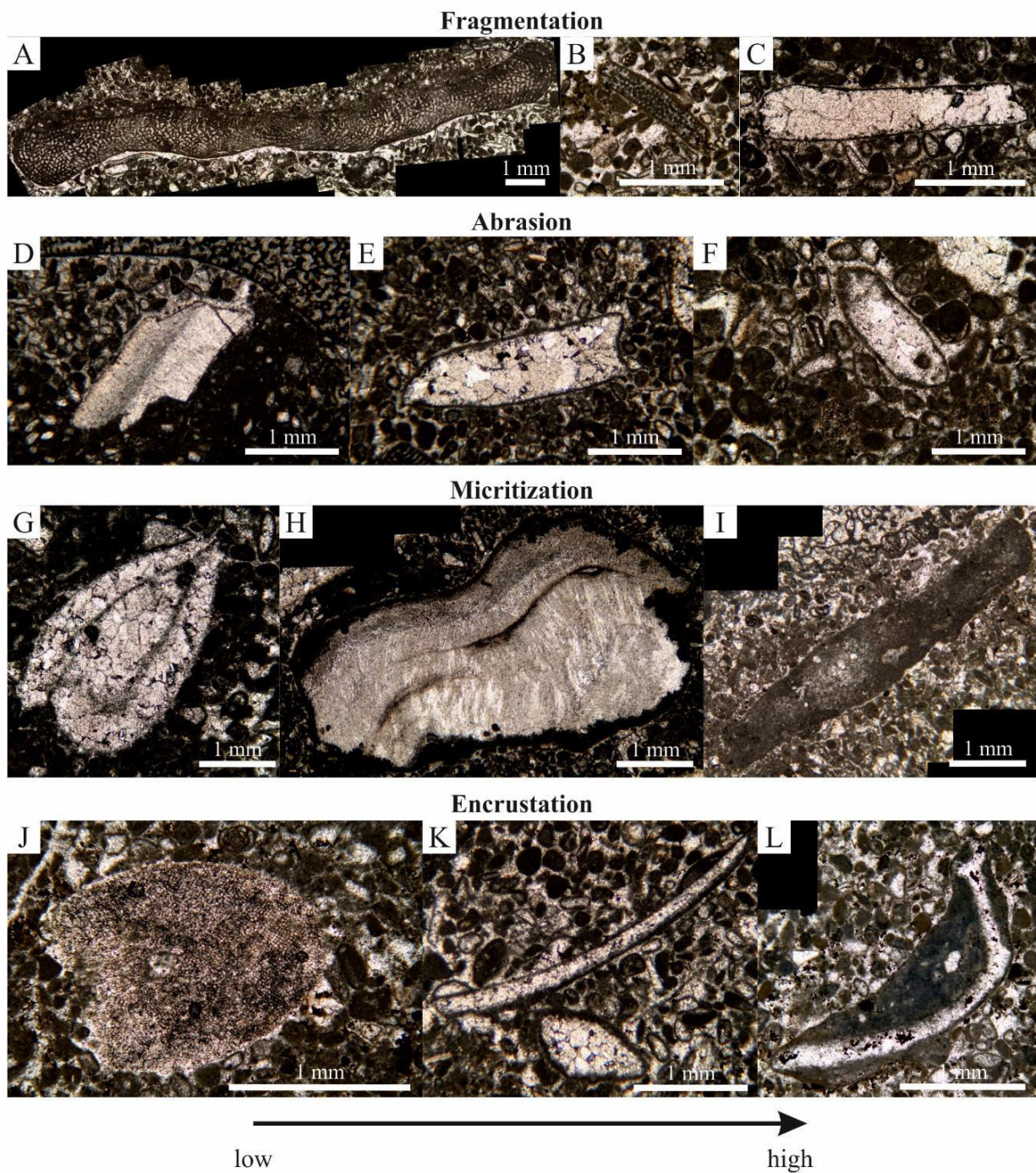
Figure 1. Evaluated main taphonomic features based on three classes of alteration (according to Kowalewski et al., 1995 and Hoffmann et al., 2015). A, D, G, J: low; B, E, H, K: moderate; C, F, I, L: high.

A.4.2. Results

Abundant biogenic components occur in the matrix (Figs. 2–6; see also Supplementary data). Unidentified bioclasts and *Orbitopsella* sp. are abundant along with small benthic foraminifera (textulariids, miliolids). Other larger benthic foraminifera are also present, but the low preservation state hampered their taxonomic identification. Common brachiopods, including articulated specimens, rare gastropods, corals and echinoderms were also distinguished. Rare thin walled thaumatoporellacean algae with irregular ovoidal forms were

170

found inner *Orbitopsella* sp. tests (Fig. 6D). These morphologies might be interpreted as cryptoendolithic forms even if they could occupy pre-exiting cavities so could not be defined as microendolithic forms (Schlagintweit and Velić, 2012). *Thaumatoporella parvovesiculifera* shows also encrusted morphologies and can be found as fragments. Moreover, spheroidal thaumatoporellaceans, interpreted as cyst stages (Schlagintweit et al., 2013; Fig. 3A) also occur. Rare micritic laminae and common fecal pellets aggregates were also identified. The lithology varies from grainstone-packstone with locally rare wackestone. Rare bioturbation traces are recognised by patchy distribution of the components and by variations in packing grain density (Fig. 7; Flügel, 2010).

Fragmentation is high in all the studied samples (Fig. 8; see also Supplementary data). Abrasion is moderate to high, while micritization is fairly low (Fig. 8; see also Supplementary data). Encrustation is relatively low (Fig. 8; see also Supplementary data). Bioerosion is rare.
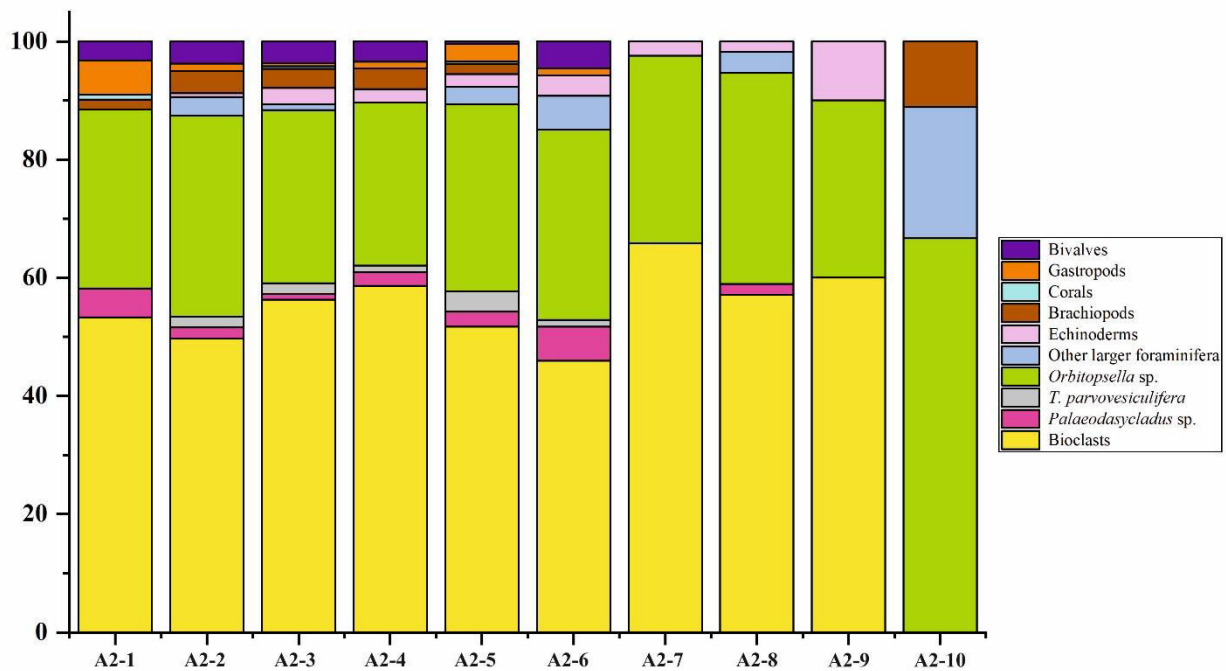
Figure 2. Abundance (%) of the biogenic components in the TorA2 (see Supplementary data). The analysed thin sections are collected from different blocks included in the accumulation core. Bioclasts is referred to undetermined skeletal components.
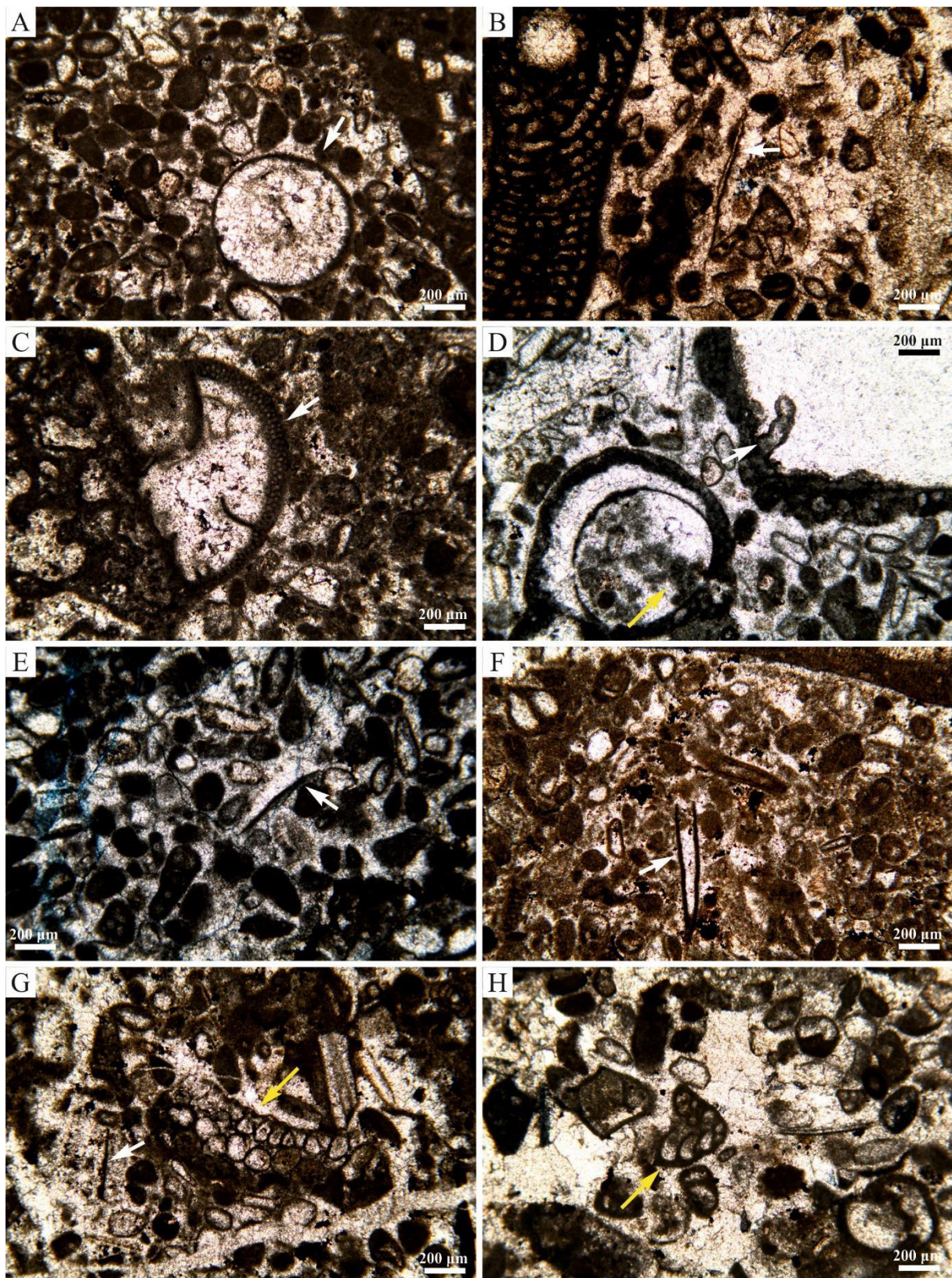
Figure 3. A) *Thaumatoporella parvovesiculifera* (Raineri, 1922), cyst (white arrow) (sample A2-3). B) Peloidal grainstone with bioclasts (e.g., *Orbitopsella* sp. Munier-Chalmas, 1902) (sample A2-2). White arrow points to micritic (?microbial) lamina. C) *T. parvovesiculifera* (Raineri, 1922), irregular roundish specimen with well-defined perforate external wall (white arrow) sample A2-5. D) Bioerosion (white arrow) and microbial clotted peloids with fuzzy outlines in intraskeletal cavity (yellow arrow) (sample A2-2). E) Micritic lamina (white arrow; sample A2-3). F) ?*Earlandia* sp. Plummer, 1930 (white arrow; sample A2-4). G) Fragment of *Palaeodasycladus* sp. (Pia, 1920) Pia, 1927 (yellow arrow) and micritic lamina (white arrow) (sample A2-4). H) *Duotaxis metula* Kristan, 1957 (yellow arrow; sample A2-5).

172
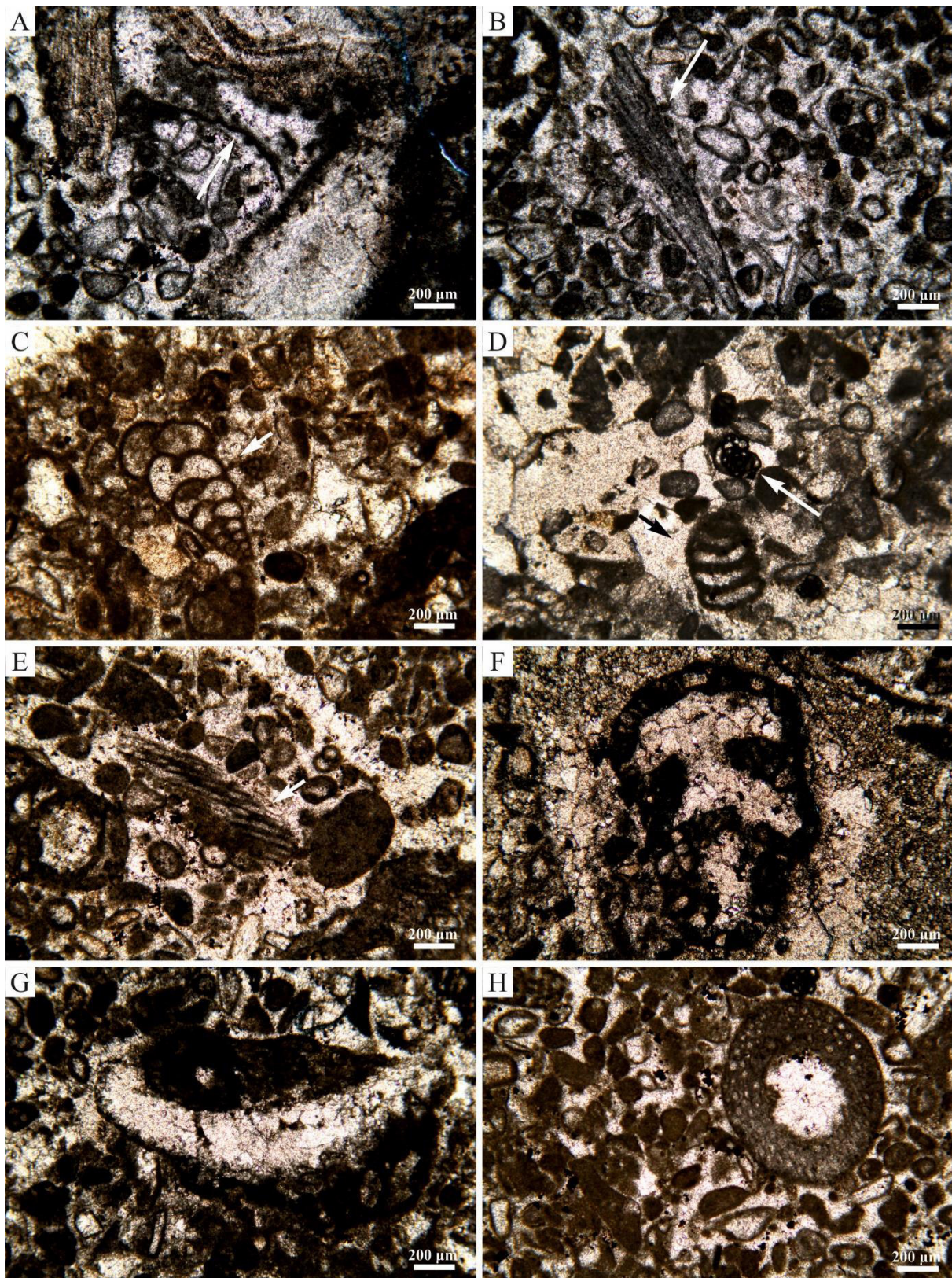
Figure 4. A) Micritic lamina (white arrow; sample A2-3). B) ?*Favreina* sp. Brönnimann, 1955 coprolite longitudinal section (white arrow; sample A2-2). C) Textulariids (white arrow; sample A2-5). D) Undetermined larger benthic foraminifera (black arrow) and porcellanaceous small benthic foraminifera (white arrow) (sample A2-5). E) ?*Favreina* sp. Brönnimann, 1955 coprolite longitudinal section (white arrow; sample A2-5). F) Larger benthic foraminifera (sample A2-5). G) Micritized bioclast with constructive envelope (*sensu* Kobluk and Risk, 1977) (sample A21-5). H) *Palaeodasycladus* sp. (Pia, 1920) Pia, 1927. Transversal section (sample A2-5).
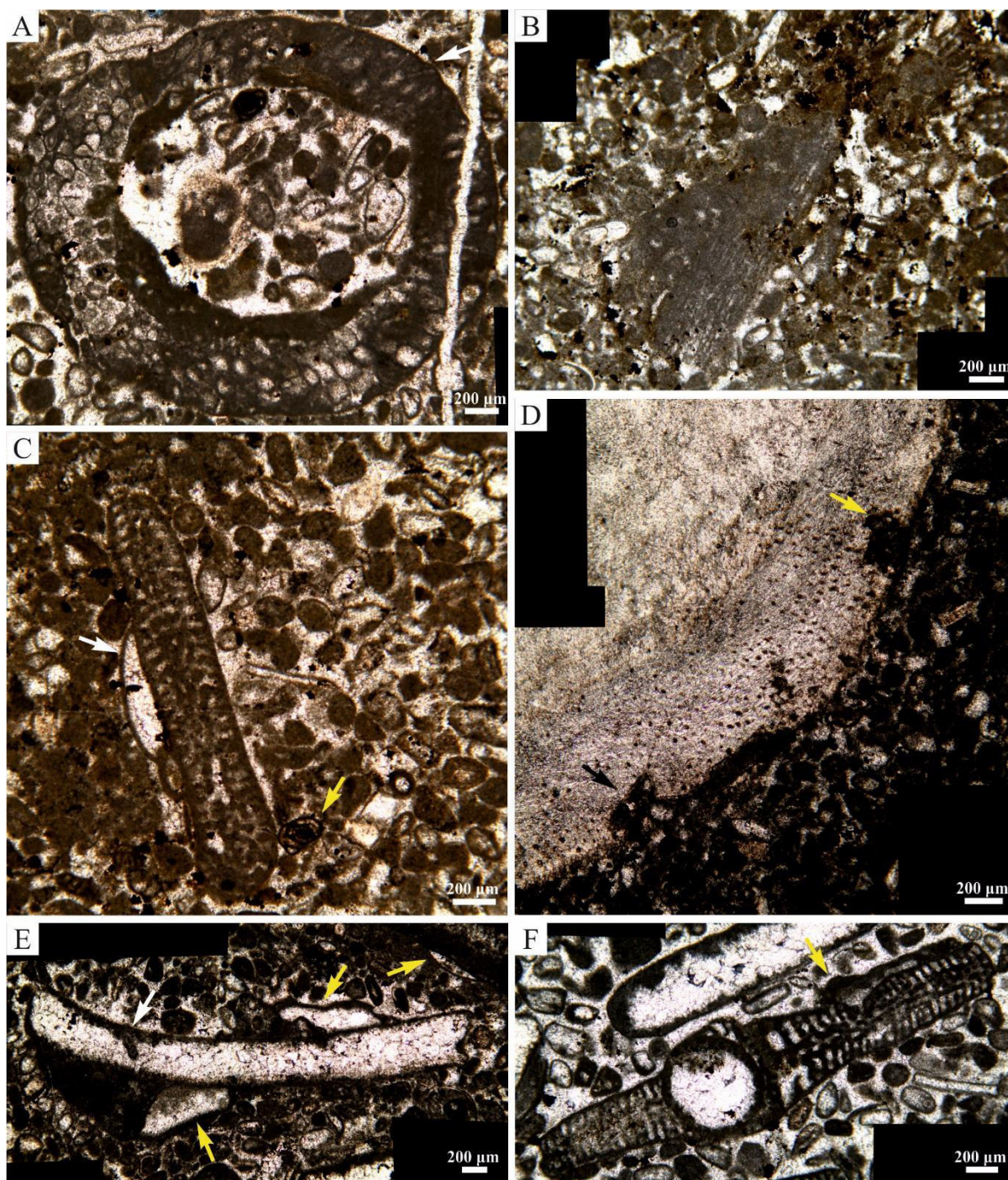
Figure 5. A) *Palaeodasycladus* sp. (Pia, 1920) Pia, 1927. Transversal section (distort stitched microphotograph; sample A2-5). B) ?*Favreina* sp. Brönnimann, 1955 coprolite longitudinal section (distort stitched microphotograph; sample A2-4). C) *Orbitopsella* sp. Munier-Chalmas, 1902 with encrusting thaumatoporelaceans-like structure (white arrow). The yellow arrow indicates small foraminifera likely *Glomospira* sp. Rzehak, 1885 (distort stitched microphotograph) (sample A2-6). D) Brachiopod shell with bioerosion traces (black and yellow arrows; distort stitched microphotograph) (sample A2-4). E) Encrustation (yellow arrows) and bioerosion traces (white arrow) on bioclast with micritic envelope (sample A2-5). F) Encrustation (yellow arrow) and bioerosion traces on larger benthic foraminifera test (*Orbitopsella* sp. Munier-Chalmas, 1902; distort stitched microphotograph) (sample A2-3).

174
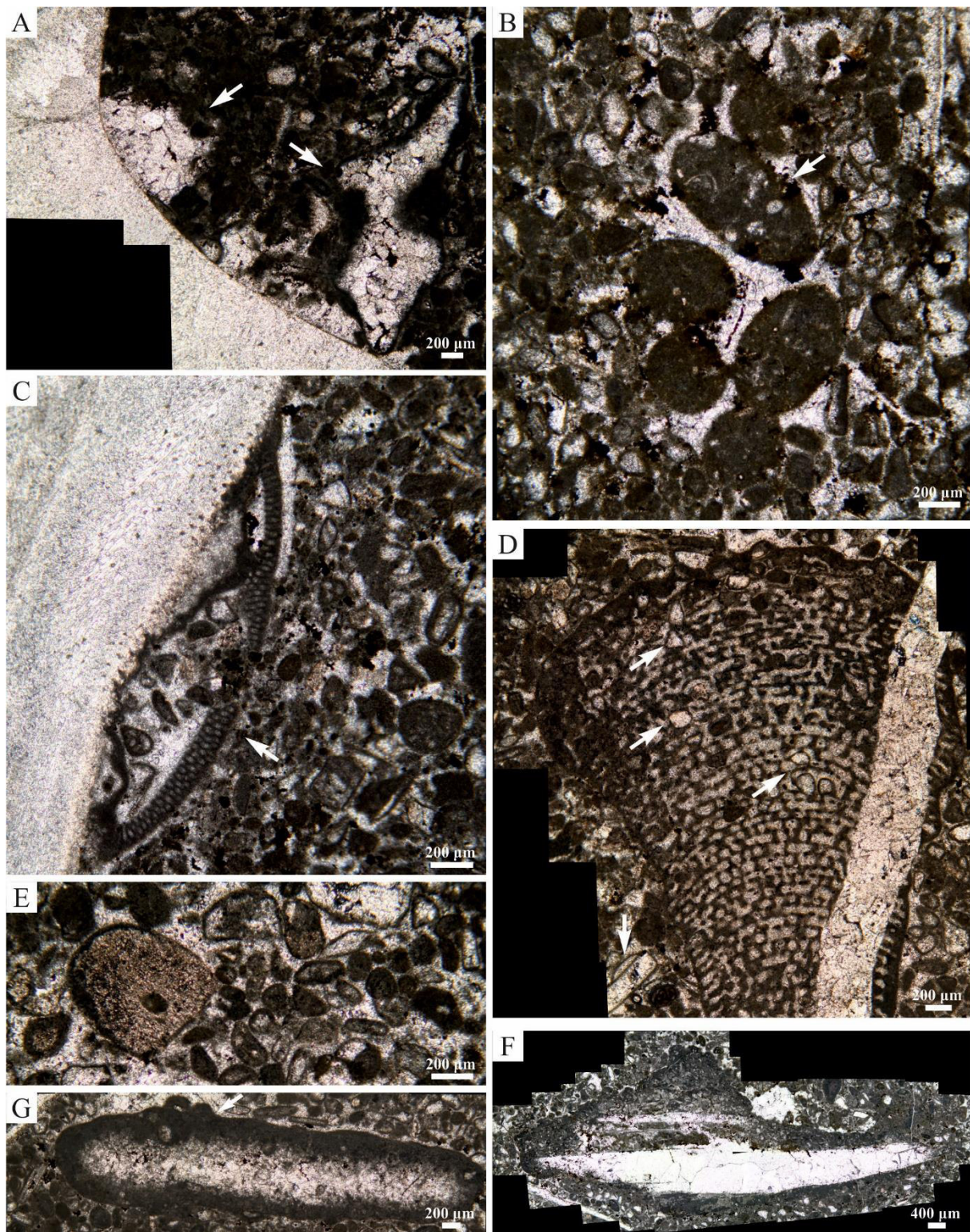
Figure 6. A) ?Encrusted organisms (white arrow; distort stitched microphotograph) (sample A2-5). B) Aggregate of coprolites (transversal sections). White arrow points to internal structures (?canals) (sample A2-4). C) Brachiopod shell with encrusting thaumatoporelaceans-like structure (white arrow; distort stitched microphotograph) (sample A2-4). D) Cryptoendolithic thaumatoporellacean algae (white arrows) inside test of larger benthic foraminifera *Orbitopsella* sp. Munier-Chalmas, 1902 (see text for further details; distort stitched microphotograph) (sample A2-3). E) Echinoderm fragment (sample A2-4). F) Encrustation and micritization on bioclast (distort stitched microphotograph) (sample A2-5). G) Encrustation (white arrow) and micritization on bioclast (distort stitched microphotograph) (sample A2-5).

175
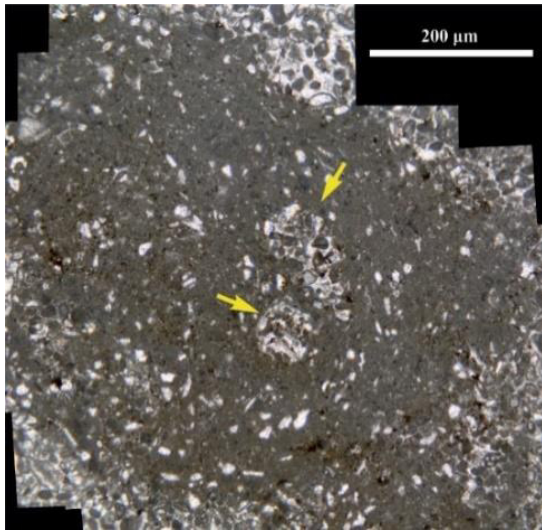
Figure 7. Bioturbation trace in TorA2 accumulation. Yellow arrows point to patchy distribution of the components/structures (sample A2-2).
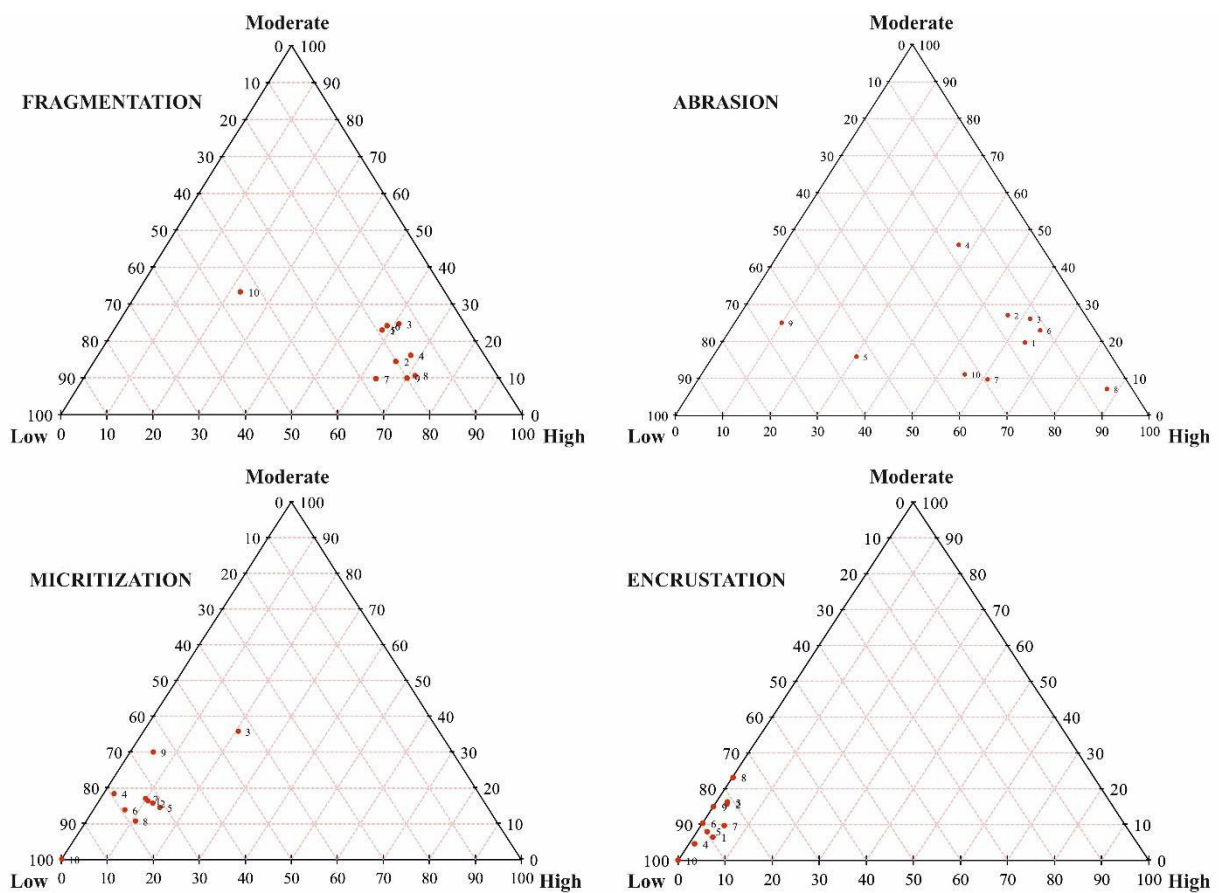
Figure 8. Ternary tapho-diagrams of fragmentation, abrasion, micritization and encrustation in the lithiotid accumulation TorA2 (Toraro Mt.; see Supplementary data). 1, A2-1; 2, A2-2; 3, A2-3; 4, A2-4; 5, A2-5; 6, A2-6; 7, A2-7; 8, A2-8; 9, A2-9; 10, A2-10.

A.4.3. Discussion and Conclusions

In the TorA2, the studied microtaphonomic features provide useful information of the lithiotid accumulation growth stages.

176

Micritization is relatively common, with the occurrence of constructive micrite envelopes due to endolithic algae (e.g., Kobluk and Risk, 1977; e.g., Figs. 4, 6). This process required a low-energy shallow-water setting. Bioerosion traces are absent to rare while encrustation is relatively low, frequently made by thaumatoporellacean forms (e.g., Figs. 5, 6). Encrustation and micritization point to a long residence time before burial. The high percentage of abrasion and fragmentation point to high energy event. Excluding rare articulated brachiopods, which could live close to lithiotids, the disarticulation is relatively high. Moreover, the occurrence of likely thaumatoporellaceans cryptoendolithic forms could be related as protection against hydrodynamic energy (Schlagintweit et al., 2013) even if some authors suggested that these forms could be associated to protection against predation or the need for sheltered microhabitats for reproduction (Cherchi and Schroeder, 1994; Vénec-Peyre, 1996). No features allow to distinguish the timing of micritization, bioerosion and encrustation respect to the transport event. However, the encrustation is well-defined allowing to exclude a subsequently transport (e.g., Figs. 4–6). Other features, such as fecal pellets aggregates along with bioturbation traces (e.g., Figs. 6, 7) point to *in situ* deposition and consequently occur after the transport event. Furthermore, few non-lithiotid bivalve shells show well-preserved ornamentation. *Lithiotis* shells are rarely affected by bioerosion. The rare occurrence of bioerosion traces and the preservation of articulated bivalves in life position suggest a rapid burial (Ngadiuba, 2015).

A complex *pre-* and *post-mortem* history might be delineated for the TorA2 accumulation. Even though the colonization phase cannot be observable in this accumulation, this stage likely occurs on hard/firm substrate represented by storm debris (e.g., Posenato and Masetti, 2012). The up-right development of lithiotid accumulation (aggradation phase) is controlled by relationships between accommodation space, physical, and biological factors (Posenato and Masetti, 2012). The TorA2 overlies TorA1, a higher bivalve accumulation (Fig. 9A). Probably, under constant subsidence/compaction, the TorA2 accommodation space could be reduced due the underlying occurrence of lithiotid accumulation TorA1. During the colonization and aggradation phases, the sedimentation rate must be relatively high, allowing a rapid vertical growth. Temporal or seasonal changes in the sedimentation rate brought about a reduction in the up-right lithiotid growth. Changes in sedimentation rate should be frequent in the lagoon. The analysed lithiotid individuals are distinguished by short shells. In this case, the variations could be caused by the proximity to wave base where sediments are constantly washed. The frequent occurrence of dasycladalean *Palaeodasycladus* sp. and rare *T. parvovesiculifera* confirm this bathymetric setting (e.g., Flügel, 2010). Occasionally, not intense storm events could interest the lithiotid accumulation as attested by small and thin

skeletal layers (Fig. 9D). Considering the mode of life of *Lithiotis* cannot be excluded that they can live close to wave base (e.g., Fraser et al., 2004). The demise of the lithiotid accumulation seem to be related to a more intense storm event which produced a rapid burial, preserving the articulated *Lithiotis* in life position. The reduced height of these individuals could hamper the shell drop and allowing their buried in life position. Moreover, the occurrence of bioclasts in the shell body cavity confirms that the death is caused by the rapid burial (Fig. 9F).

According to the relatively high fragmentation and moderate to high abrasion, duration and intensity of the transport must be high. Skeletal concentrations, dominated by the same bioclasts (i.e., *Orbitopsella* sp. and brachiopods) recognised in the TorA2 matrix, are frequent in the closest areas. Sparse *Orbitopsella* sp. concentrations are common in the middle part of the Rotzo Formation.
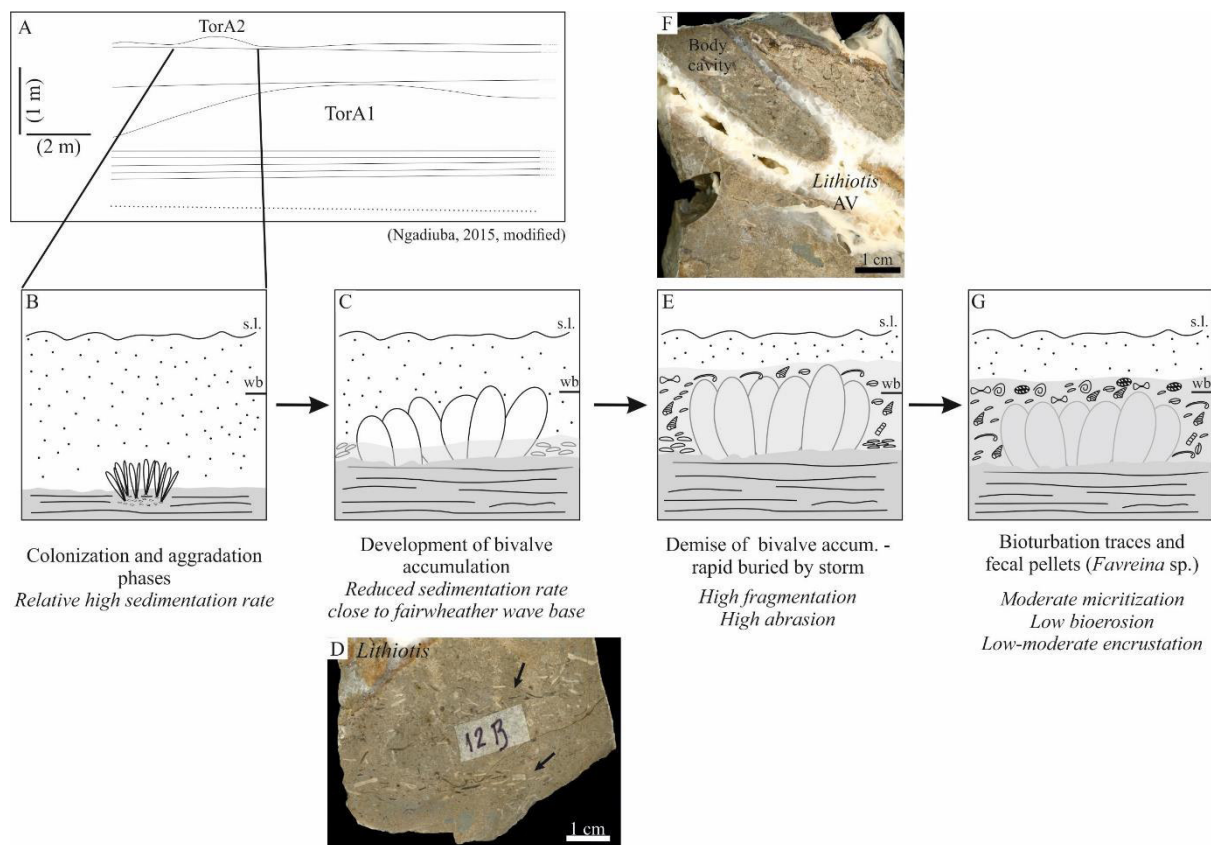
Figure 9. Evolution of the *Lithiotis*-dominated accumulation TorA2. A) Stratigraphic setting of the lithiotid accumulations TorA1 and TorA2 (from Ngadiuba, 2015, modified). B, C, E, G) Dynamics of bivalve accumulation from colonization to burial phases. D) Polished slab, black arrows point to thin skeletal concentrations associated with weaker storm events. F) Polished slab with *Lithiotis* specimen. The shell body cavity is filled with storm deposit. See text for further details. s.l., sea level; wb, wave base; AV, *Lithiotis* attached valve.

Successively, the deposited sediments could be bioturbated and amalgamated. Micritization, bioerosion and encrustation can occur (Fig. 9G).

The preservation state of the *Lithiotis* shells suggests a complex diagenetic path (Fig. 10). The differential diagenesis recorded in the lower part of the TorA2 and in its central area is the product of two different primary materials, marl in the lower portion and packstone-grainstone in the middle one. This is confirmed by the contemporaneous preservation of lithiotid shell mould due to early lithification in the central area and the completely shell dissolution in the lower part (Fig. 10). The higher amount of terrigenous content in the marlstone influenced the early diagenesis which interested the lower bivalve accumulation. The absence of bioclasts in marlstone (thin section A2-10; Fig. 2) can be explained considering the typical matrix content in lithiotid accumulations (see Chapter 4 for further details).

The underlying bed and the lower part of TorA2 are constituted by highly bioturbated marlstone with reduce skeletal contents (Ngadiuba, 2015). After burial, this area is likely included in the taphonomically active zone (TAZ). The TAZ is defined as the upper, bioturbated, mixed zone extending down from the sediment-water interface (Davies et al., 1989; Cherns et al., 2011). In this layer, bioturbation favoured the degradation of organic matter producing an acidic regime which cause the dissolution of aragonite (e.g., Cherns et al., 2011). The reactions which occur in the TAZ are complex resulting from the decay of organic matter and the re-oxidation of by-products producing, for example, H_2S or CO_2. The abundant presence of pyrite forms and in particular of euhedral crystals (i.e., linked to diagenesis; see Chapter 4) could confirm this hypothesis.

In the upper part of the accumulation, the *Lithiotis* shells are immersed in a grain-supported sediment constituted of bioclasts (i.e., storm event deposit) which are interested by early lithification which allowed to preserve the bivalve shell moulds. The rapid burial (i.e., storm deposit) and the early lithification allow to preserve the outer calcitic layer in *Lithiotis* (see Appendix B.6). The upper part of the accumulation is completely truncated due to intense erosion likely associated with subaerial exposure as attests by green marls (e.g., Deconinck and Strasser, 1987; Brady and Bowie, 2017). Locally, marl occurs even as replacing dissolved aragonitic shells. Consequently, the lithification was followed by the completely dissolution of aragonite. In the final stage the dissolved aragonite was completely replaced by calcite (Fig. 10D) and frequently, in the upper part, by marls.
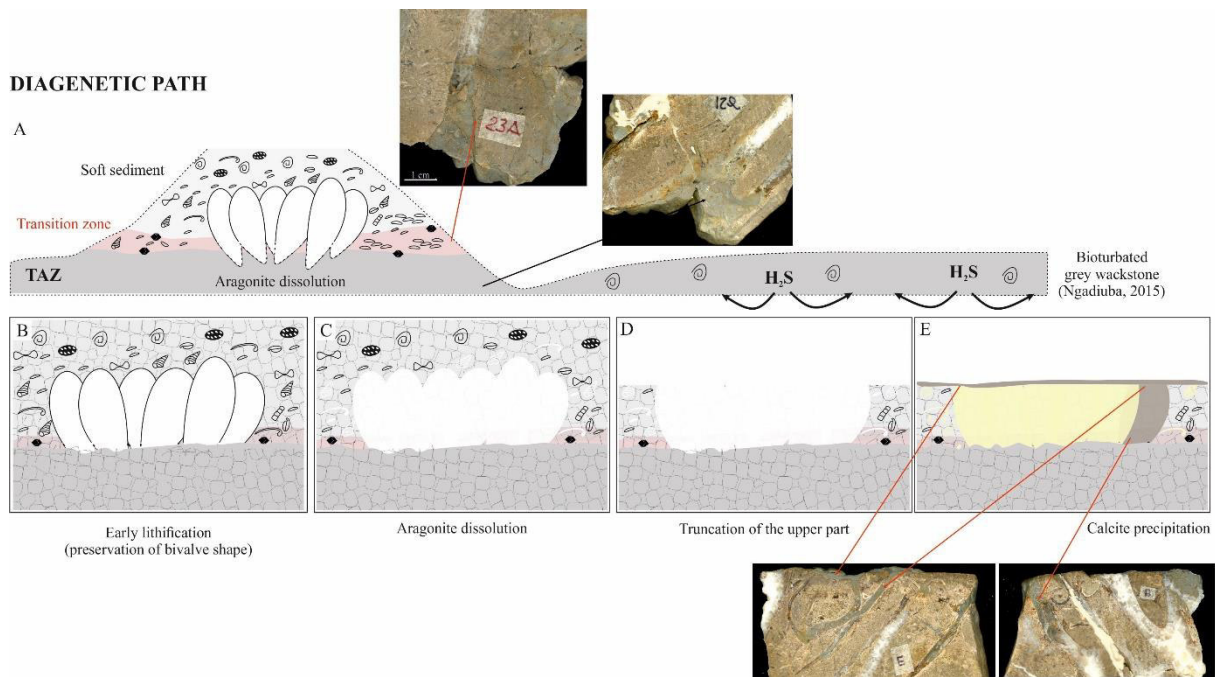
Figure 10. Reconstruction of diagenetic path from soft carbonate mud to lithified limestone. A) After burial, the lower part of *Lithiotis* shells is included in the TAZ (Taphonomically Active Zone) where aragonite is dissolved. B–E) Diagenetic phases recorded in the TorA2 accumulation. See text for further details.

A.4.4. Supplementary data

Original data of Figure 8 (Appendix A.4)

Thin section	Components (in Total)	Fragmentation			Abrasion			Encrustation			Micritization		
		Low	Moderate	High	Low	Moderate	High	Low	Moderate	High	Low	Moderate	High
A2-1	122	23	28	71	20	24	78	109	8	5	89	20	13
A2-2	159	32	23	104	26	43	90	130	25	4	115	25	19
A2-3	215	31	53	131	26	56	133	175	35	5	94	77	44
A2-4	87	14	14	59	15	40	32	82	4	1	69	16	2
A2-5	234	44	54	136	126	37	71	210	19	5	167	34	33
A2-6	87	15	21	51	10	20	57	78	9	0	69	12	6
A2-7	41	11	4	26	12	4	25	35	4	2	30	7	4
A2-8	56	10	6	40	3	4	49	43	13	0	44	6	6
A2-9	20	4	2	14	13	5	2	17	3	0	13	6	1
A2-10	9	4	3	2	3	1	5	9	0	0	9	0	0

Counted components

Thin section	Components (in Total)	Fragmentation			Abrasion			Encrustation			Micritization		
		Low	Moderate	High	Low	Moderate	High	Low	Moderate	High	Low	Moderate	High
A2-1	122	19	23	58	16	20	64	89	7	4	73	16	11
A2-2	159	20	14	65	16	27	57	82	16	3	72	16	12
A2-3	215	14	25	61	12	26	62	81	16	2	44	36	20
A2-4	87	16	16	68	17	46	37	94	5	1	79	18	2
A2-5	234	19	23	58	54	16	30	90	8	2	71	15	14
A2-6	87	17	24	59	11	23	66	90	10	0	79	14	7
A2-7	41	27	10	63	29	10	61	85	10	5	73	17	10
A2-8	56	18	11	71	5	7	88	77	23	0	79	11	11
A2-9	20	20	10	70	65	25	10	85	15	0	65	30	5
A2-10	9	44	33	22	33	11	56	100	0	0	100	0	0

Percentage values

Data summarised in the Figure 8 (Appendix A.4) in the ternary tapho-diagrams of fragmentation, abrasion, micritization and encrustation.
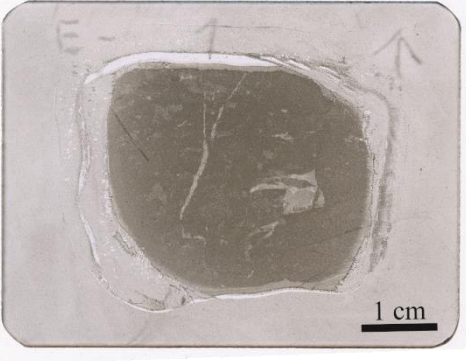
Abundance (%) of the biogenic components in the TorA2 (Figure 2 - Appendix A.4)
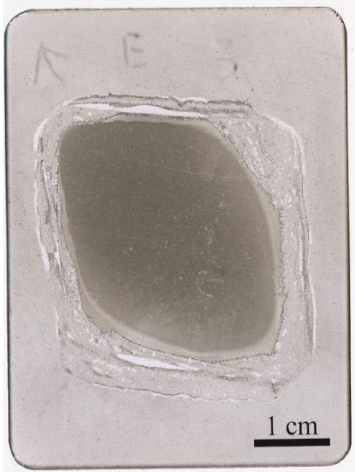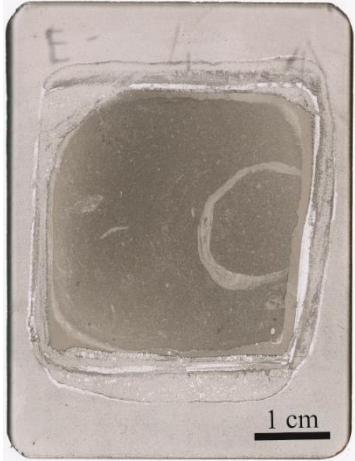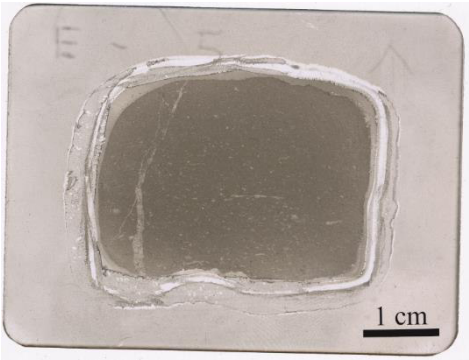
Counted components												
Thin section	Measured area (cm²)	Components (in Total)	Bio	*Pal.*	*Th.*	*Orb.*	Other LBF	Ech	Br	Co	Gas	Biv
A2-1	29.25	122	65	6	0	37	0	0	2	1	7	4
A2-2	29.25	159	79	3	3	54	5	1	6	0	2	6
A2-3	52	215	121	2	4	63	2	6	7	1	1	8
A2-4	18.49	87	51	2	1	24	0	2	3	0	1	3
A2-5	52	234	121	6	8	74	7	5	4	1	7	1
A2-6	20	87	40	5	1	28	5	3	0	0	1	4
A2-7	20	41	27	0	0	13	0	1	0	0	0	0
A2-8	20	56	32	1	0	20	2	1	0	0	0	0
A2-9	6	20	12	0	0	6	0	2	0	0	0	0
A2-10	10.5	9	0	0	0	6	2	0	1	0	0	0
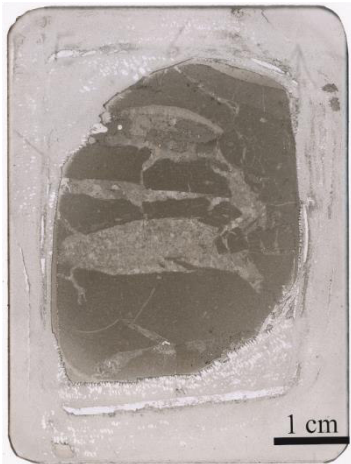
Percentage values												
Thin section	Std area (cm²)	Components (area: 30 cm²)	Bio	*Pal.*	*Th.*	*Orb.*	Other LBF	Ech	Br	Co	Gas	Biv
A2-1	30	125	53.28	4.92	0.00	30.33	0.00	0.00	1.64	0.82	5.74	3.28
A2-2	30	163	49.69	1.89	1.89	33.96	3.14	0.63	3.77	0.00	1.26	3.77
A2-3	30	124	56.28	0.93	1.86	29.30	0.93	2.79	3.26	0.47	0.47	3.72
A2-4	30	141	58.62	2.30	1.15	27.59	0.00	2.30	3.45	0.00	1.15	3.45
A2-5	30	135	51.71	2.56	3.42	31.62	2.99	2.14	1.71	0.43	2.99	0.43
A2-6	30	131	45.98	5.75	1.15	32.18	5.75	3.45	0.00	0.00	1.15	4.60
A2-7	30	62	65.85	0.00	0.00	31.71	0.00	2.44	0.00	0.00	0.00	0.00
A2-8	30	84	57.14	1.79	0.00	35.71	3.57	1.79	0.00	0.00	0.00	0.00
A2-9	30	100	60.00	0.00	0.00	30.00	0.00	10.00	0.00	0.00	0.00	0.00
A2-10	30	26	0.00	0.00	0.00	66.67	22.22	0.00	11.11	0.00	0.00	0.00
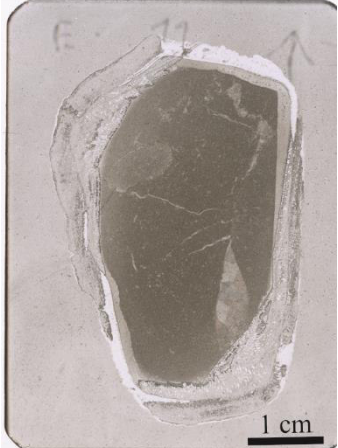
Data summarised in the Figure 2 (Appendix A.4). Percentage values are calculated considering the components respect to a standard area (30 cm²). Bio, bioclasts; *Pal*., *Palaeodasycladus* sp.; *Th*., *Thaumatoporella parvovesiculifera*; *Orb*., *Orbitopsella* sp.; Other LBF, other larger benthic foraminifera; Ech, echinoderms; Br, brachiopods; Co, corals; Gas, gastropods; Biv, bivalves; Std area, standard area.
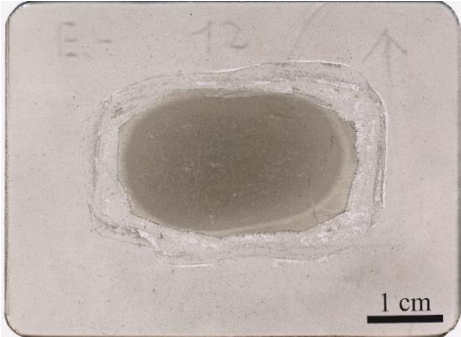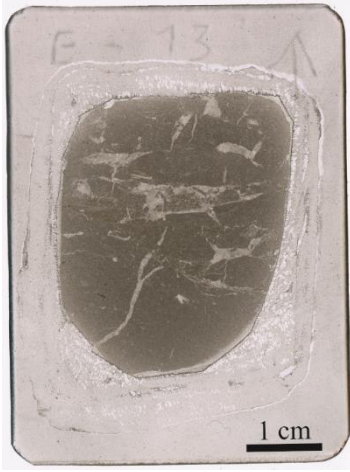
A.5. Toraro Mt. accumulation A1 (TorA1)

No.	Sample	Thin section	Description
1	A1-1	1 cm	**Skeletal components:** rare undefined bioclasts, rare ostracods, rare echinoderms, rare small foraminifera included ?*Glomospira/Planiinvoluta* spp. and ?*Meandrovoluta asiagoensis*, rare *Rivularia*-like structures **Non-skeletal components:** rare undetermined peloids, rare pelletoids, rare dark clotted micritic structures included dendritic forms **Matrix:** micrite/clotted peloidal micrite/sparite **Taphonomical characters:** high fragmentation, high abrasion, no bioerosion, no micritization, no encrustation **Lithology:** wackestone-packstone **Note: /**
2	A1-2	1 cm	**Skeletal components:** rare undefined bioclasts, rare ostracods, rare echinoderms, rare brachiopods, rare small foraminifera included ?*Glomospira/Planiinvoluta* spp., ?*Meandrovoluta asiagoensis* and valvulinids, rare larger foraminifera (*Orbitopsella* sp.) **Non-skeletal components:** rare undetermined peloids, rare pelletoids **Matrix:** micrite/clotted peloidal micrite/sparite in restricted areas **Taphonomical characters:** high fragmentation, high abrasion, low bioerosion (? red circle), low micritization, no encrustation **Lithology:** wackestone-packstone **Note: /**

3	A1-3		**Skeletal components:** rare undefined bioclasts, rare ostracods, rare small foraminifera included *Glomospira/Planiinvoluta* spp. and *Meandrovoluta asiagoensis*, rare larger foraminifera (*Orbitopsella* sp. included *Orbitopsella dubari*), rare micritized ring-shaped bioclasts, rare ?*Thaumatoporella parvovesiculifera* (irregular roundish specimens) **Non-skeletal components:** rare undetermined peloids **Matrix:** micrite **Taphonomical characters:** high fragmentation, high abrasion, no bioerosion, no micritization, no encrustation **Lithology:** wackestone **Note: /**
4	A1-4		**Skeletal components:** rare undefined bioclasts, rare brachiopods, rare echinoderms, rare small foraminifera **Non-skeletal components:** rare undetermined peloids **Matrix:** clotted peloidal micrite **Taphonomical characters:** high fragmentation, high abrasion, no bioerosion, no micritization, no encrustation **Lithology:** wackestone **Note: /**
5	A1-5		**Skeletal components:** rare undefined bioclasts, rare ?*Earlandia* sp., rare micritized ring-shaped bioclasts, rare ostracods, rare brachiopods **Non-skeletal components:** rare undetermined peloids, rare dark micritic clotted structures included dendritic forms **Matrix:** micrite **Taphonomical characters:** high fragmentation, high abrasion, no bioerosion, no micritization, no encrustation **Lithology:** wackestone

			Note: /
6	A1-6	 1 cm	**Skeletal components:** rare undefined bioclasts, rare brachiopods **Non-skeletal components:** rare undetermined peloids **Matrix:** micrite **Taphonomical characters:** high fragmentation, high abrasion, no bioerosion, no micritization, no encrustation **Lithology:** wackestone **Note:** lithiotid shells
7	A1-7	 1 cm	**Skeletal components:** common undefined bioclasts, rare brachiopods, rare bivalves* (bigger skeletal grain), rare small foraminifera **Non-skeletal components:** rare undetermined peloids, rare fecal pellets **Matrix:** micrite **Taphonomical characters:** high fragmentation, high abrasion, no bioerosion, no micritization, no encrustation **Lithology:** wackestone **Note:** bioturbation traces
8	A1-8	 1 cm	**Skeletal components:** rare undefined bioclasts, rare ostracods, rare brachiopods, rare echinoderms, rare ?*Earlandia* sp., rare micritized ring-shaped bioclasts, rare small foraminifera included ?*Glomospira/Planiinvoluta* spp. and ?*Meandrovoluta asiagoensis*, rare larger foraminifera **Non-skeletal components:** rare undetermined peloids, rare pelletoids, rare dark clotted micritic structures included dendritic forms **Matrix:** micrite/clotted peloidal micrite **Taphonomical characters:** high fragmentation, high abrasion, no bioerosion, low micritization, low encrustation **Lithology:** wackestone **Note:** /

9	A1-9		**Skeletal components:** abundant undefined bioclasts, rare ?*Earlandia* sp., rare ostracods, rare brachiopods, rare echinoderms, rare small foraminifera included ?*Meandrovoluta asiagoensis*, common larger foraminifera (*Orbitopsella* sp.), rare *Thaumatoporella parvovesiculifera* (encrusted morphologies) **Non-skeletal components:** rare undetermined peloids, rare cortoids with destructive envelope **Matrix:** clotted peloidal micrite **Taphonomical characters:** high fragmentation, high abrasion, no bioerosion, low micritization, low encrustation **Lithology:** floatstone with wackestone matrix **Note: /**
10	A1-10		**Skeletal components:** rare undefined bioclasts, rare brachiopods, rare ostracods, rare echinoderms **Non-skeletal components:** rare undetermined peloids, rare cortoids with destructive envelope **Matrix:** micrite **Taphonomical characters:** high fragmentation, high abrasion, no bioerosion, low micritization, no encrustation **Lithology:** wackestone-mudstone in restricted areas **Note: /**
11	A1-11		**Skeletal components:** rare undefined bioclasts, rare small foraminifera included ?*Meandrovoluta asiagoensis*, rare brachiopods, rare ostracods **Non-skeletal components:** rare undetermined peloids **Matrix:** micrite/clotted peloidal micrite/microsparite in a restricted area **Taphonomical characters:** high fragmentation, high abrasion, low bioerosion, no micritization, no encrustation

			Lithology: wackestone-packstone **Note:** lithiotid shells
12	A1-12		**Skeletal components:** rare undefined bioclasts, rare small foraminifera included ?*Glomospira/Planiinvoluta* spp., ?*Meandrovoluta asiagoensis* and textulariids, rare larger foraminifera (*Orbitopsella* sp.), rare *Thaumatoporella parvovesiculifera* (irregular roundish specimens) **Non-skeletal components:** rare undetermined peloids **Matrix:** micrite **Taphonomical characters:** high fragmentation, high abrasion, no bioerosion, no micritization, no encrustation **Lithology:** wackestone **Note: /**
13	A1-13		**Skeletal components:** rare undefined bioclasts, rare brachiopods, rare echinoderms, rare small foraminifera included ?*Meandrovoluta asiagoensis*, rare ?*Earlandia* sp., rare micritized ring-shaped bioclasts **Non-skeletal components:** common undetermined peloids, rare pelletoids, rare fecal pellets **Matrix:** micrite/clotted peloidal micrite **Taphonomical characters:** high fragmentation, high abrasion, no bioerosion, low micritization, no encrustation **Lithology:** wackestone **Note: /**
Semi-quantitative analysis of components: (absent), rare, common, abundant Semi-quantitative analysis of taphonomic features: no, low, moderate, high * "bivalves" are referred to non-lithiotid bivalves /: absent			

A.6. Toraro Mt. accumulation A2 (TorA2)
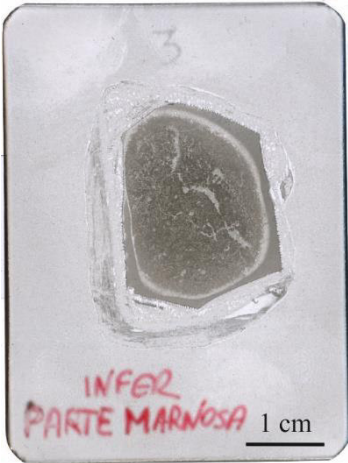
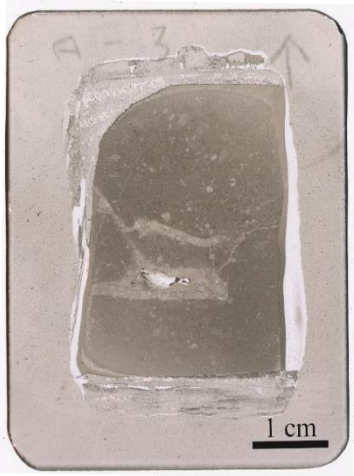| No.	Sample	Thin section	Description
1	A2-1		**Skeletal components:** abundant bioclasts, rare *Palaeodasycladus* sp., rare bivalves*, abundant larger benthic foraminifera (only *Orbitopsella* sp.), rare gastropods, rare echinoderms, rare brachiopods, rare corals, rare ?*Earlandia* sp., abundant small benthic foraminifera (textulariids, ?*Planinvoluta*/*Glomospira*, porcellanaceous foraminifera) **Non-skeletal components:** abundant peloids, rare microbial peloids, rare fecal pellets aggregates, rare pelletoids, abundant cortoids (with destructive and rare with constructive envelope), rare oncoids type I/II **Matrix**: micrite/sparite **Taphonomical characters:** see the text for further details **Lithology:** packstone – grainstone – wackestone in restricted areas **Note:** micritic laminae, silt in restricted areas, bioturbation traces, thin section size: 4,5*6,5 cm
2	A2–2		**Skeletal components:** abundant bioclasts, rare *Palaeodasycladus* sp., rare bivalves*, rare gastropods, abundant larger benthic foraminifera (abundant *Orbitopsella* sp. and rare undefined other larger foraminifera), rare echinoderms, rare brachiopods, rare ?*Earlandia* sp., abundant small benthic foraminifera (textulariids, valvulinids,?*Planiinvoluta*/*Glomospira*, porcellanaceous foraminifera, *Siphovalvulina variabilis*, ?*Meandrovoluta asiagoensis*), rare *Thaumatoporella parvovesiculifera* (fragments and encrusted morphologies) **Non-skeletal components:** abundant peloids, rare isolated ?fecal pellets, rare pelletoids, abundant cortoids (with destructive and rare with constructive envelope), rare oncoids type I/II

188

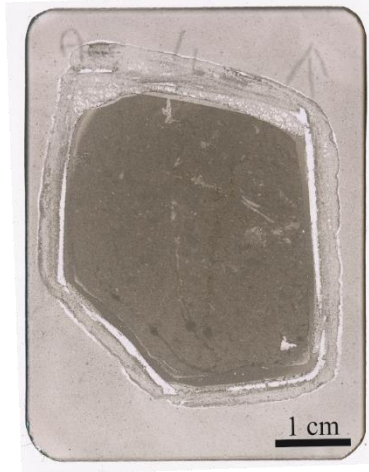|			
			Matrix: micrite/sparite **Taphonomical characters:** see the text for further details **Lithology:** packstone – grainstone – wackestone in restricted areas **Note:** Lithiotid shell, silt in restricted areas, thin section size: 4,5*6,5 cm
3	A2-3	 1 cm	**Skeletal components:** abundant bioclasts, rare *Palaeodasycladus* sp., rare bivalves*, rare gastropods, abundant larger benthic foraminifera (abundant *Orbitopsella* sp. and undefined other larger foraminifera), rare echinoderms, rare corals, rare ostracods, rare brachiopods, rare ?*Earlandia* sp., abundant small benthic foraminifera (textulariids, valvulinids,?*Planiinvoluta*/*Glomospira*, porcellanaceous foraminifera, *Siphovalvulina variabilis*, ?*Meandrovoluta asiagoensis*), rare *Thaumatoporella parvovesiculifera* (fragments, encrusted morphologies and ?microendolithic forms), rare ?Bacteria-like structures **Non-skeletal components:** abundant peloids, rare microbial peloids, rare fecal pellets aggregates, rare pelletoids, abundant cortoids (with destructive and rare with constructive envelope), rare oncoids type I/II **Matrix**: micrite/sparite **Taphonomical characters:** see the text for further details **Lithology:** packstone – grainstone – wackestone in restricted areas **Note:** Lithiotid shell, micritic laminae, ?bioturbation traces, silt in restricted areas, thin section size: 6,5*8 cm

189

| 4 | A2-4 | | **Skeletal components:** abundant bioclasts, rare *Palaeodasycladus* sp., rare bivalves*, rare gastropods, abundant larger benthic foraminifera (only *Orbitopsella* sp.), rare echinoderms, rare brachiopods (one articulated), rare ?*Earlandia* sp., abundant small benthic foraminifera (textulariids, valvulinids,?*Planiinvoluta/Glomospira*, porcellanaceous foraminifera, *Siphovalvulina variabilis*, ?*Meandrovoluta asiagoensis*), rare *Thaumatoporella parvovesiculifera* (fragments, encrusted morphologies and microendolithic forms)

Non-skeletal components: abundant peloids, rare microbial peloids, rare fecal pellets aggregates, rare pelletoids, abundant cortoids (with destructive and rare with constructive envelope), rare oncoids type I/II

Matrix: micrite/sparite

Taphonomical characters: see the text for further details

Lithology: packstone – grainstone

Note: thin section size: 4,3*4,3 cm |
| 5 | A2-5 | | **Skeletal components:** abundant bioclasts, rare *Palaeodasycladus* sp., rare bivalves*, rare gastropods, abundant larger benthic foraminifera (*Orbitopsella* sp. and undefined larger foraminifera), rare echinoderms, rare corals, rare brachiopods, rare ?*Earlandia* sp., rare ostracods, abundant small benthic foraminifera (textulariids, valvulinids,?*Planiinvoluta/Glomospira*, porcellanaceous foraminifera, *Siphovalvulina variabilis*, ?*Meandrovoluta asiagoensis*), rare *Thaumatoporella parvovesiculifera* (fragments, irregular roundish morphologies microendolithic forms)

Non-skeletal components: abundant peloids, rare microbial peloids, rare fecal pellets aggregates, rare pelletoids, abundant cortoids (with destructive and rare with constructive envelope), rare oncoids type I/II |

			Matrix: micrite/sparite **Taphonomical characters:** see the text for further details **Lithology:** packstone – grainstone in restricted areas **Note:** bioturbation traces, silt in restricted areas, thin section size: 5,5*8 cm
6	A2-6	 1 cm	**Skeletal components:** abundant bioclasts, rare *Palaeodasycladus* sp., rare bivalves*, rare gastropods, abundant larger benthic foraminifera (*Orbitopsella* sp. and rare other undefined larger foraminifera), rare echinoderms, rare brachiopods, rare ?*Earlandia* sp., rare ostracods, abundant small benthic foraminifera (included textulariids, valvulinids and porcellanaceous foraminifera) **Non-skeletal components:** abundant peloids, rare pelletoids, rare microbial peloids, rare fecal pellets, abundant cortoids (with destructive and rare with constructive envelope) **Matrix**: micrite/sparite **Taphonomical characters:** see the text for further details **Lithology:** packstone – grainstone – wackestone in restricted areas **Note:** bioturbation traces, silt in restricted areas, thin section size: 4*5 cm
7	A2-7	 1 cm	**Skeletal components:** abundant bioclasts, abundant larger benthic foraminifera (*Orbitopsella* sp.), rare echinoderms, rare ?*Earlandia* sp., rare ostracods, common small benthic foraminifera (included textulariids, valvulinids and porcellanaceous foraminifera) **Non-skeletal components:** abundant peloids, rare fecal pellets aggregate, abundant cortoids (with destructive and rare with constructive envelope), rare oncoids type I/II **Matrix**: micrite/sparite

			Taphonomical characters: see the text for further details **Lithology:** packstone – grainstone in restricted areas **Note:** silt in restricted areas, thin section size: 4*5 cm
8	A2-8	 1 cm	**Skeletal components:** abundant bioclasts, rare *Palaeodasycladus* sp., abundant larger benthic foraminifera (abundant *Orbitopsella* sp. and rare undefined larger foraminifera), rare ?*Earlandia* sp., rare echinoderms, common small benthic foraminifera (included textulariids, valvulinids, porcellanaceous foraminifera) **Non-skeletal components:** abundant peloids, abundant cortoids (with destructive and rare with constructive envelope) **Matrix**: micrite/sparite **Taphonomical characters:** see the text for further details **Lithology:** packstone – grainstone **Note:** bioturbation traces, thin section size: 4*5 cm
9	A2-9	 1 cm	**Skeletal components:** abundant bioclasts, abundant larger benthic foraminifera (abundant *Orbitopsella* sp. and rare undefined larger foraminifera), rare ?*Earlandia* sp., rare echinoderms, common small benthic foraminifera (included textulariids, valvulinids, porcellanaceous foraminifera), rare micritized ring-shaped bioclasts **Non-skeletal components:** abundant peloids, abundant cortoids (with destructive and rare with constructive envelope) **Matrix**: micrite/sparite **Taphonomical characters:** see the text for further details **Lithology:** packstone – grainstone **Note:** thin section size: 4*5 cm

| 10 | A2-10 | | **Skeletal components:** rare brachiopods, rare larger benthic foraminifera (included *Orbitopsella* sp. and rare undefined larger foraminifera), rare ?*Earlandia* sp., common small benthic foraminifera (included textulariids, valvulinids, porcellanaceous foraminifera), rare micritized ring-shaped bioclasts, rare ostracods

Non-skeletal components: abundant peloids

Matrix: micrite/sparite

Taphonomical characters: see the text for further details

Lithology: wackestone – packstone

Note: thin section size: 4*5 cm |

Results of semi-quantitative analysis of taphonomical characters are plotted in the taphodiagrams (details in the text).
Semi-quantitative analysis (%) of skeletal components are explain in the text.
* "bivalves" are referred to non-lithiotid bivalves
/: absent

A.7. Toraro Mt. accumulation B (TorB)
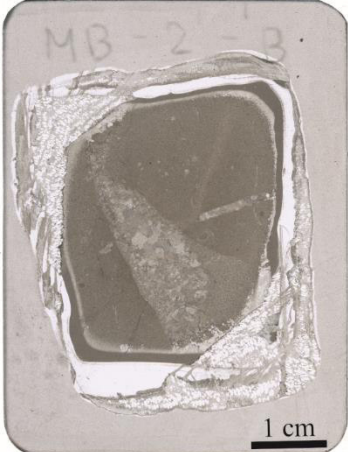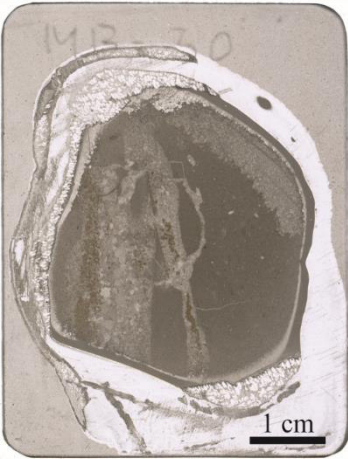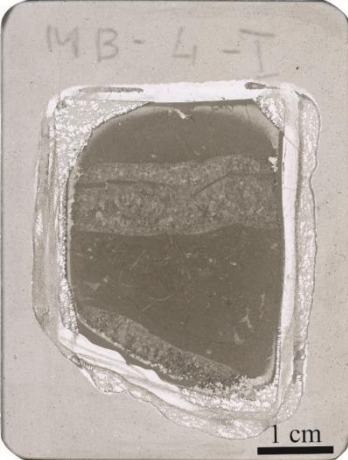
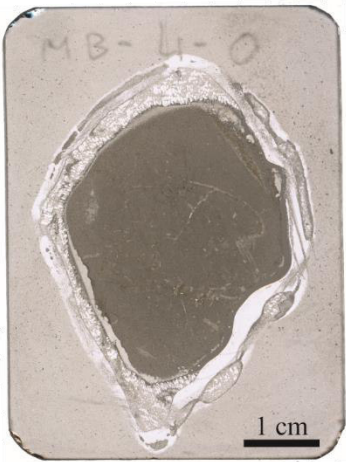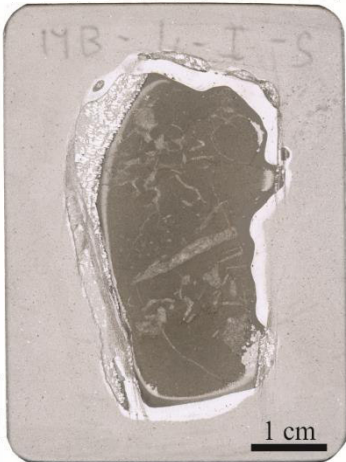| No.	Sample	Thin section	Description
1	B-1	1 cm	**Skeletal components:** abundant undefined bioclasts, rare bivalves* **Non-skeletal components: /** **Matrix:** very fine-grained micrite **Taphonomical characters:** high fragmentation, moderate abrasion, no bioerosion, no micritization, no encrustation **Lithology:** floatstone with mudstone matrix **Note:** bioturbation traces
2	B-2	1 cm	**Skeletal components:** abundant undefined bioclasts **Non-skeletal components:** rare undetermined peloids, rare fecal pellets, rare dark micritic clotted structures **Matrix:** micrite/microsparite **Taphonomical characters:** high fragmentation, high abrasion, no bioerosion, moderate micritization, no encrustation **Lithology:** floatstone with mudstone matrix **Note: /**
3	B-3	1 cm	**Skeletal components:** rare undefined bioclasts **Non-skeletal components:** common undetermined peloids, rare fecal pellets, rare pelletoids **Matrix:** micrite/microsparite **Taphonomical characters:** high fragmentation, high abrasion, no bioerosion, no micritization, no encrustation **Lithology:** wackestone **Note: /**

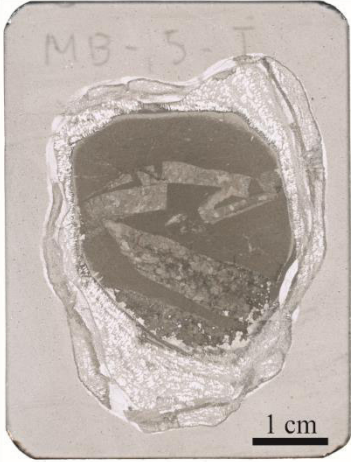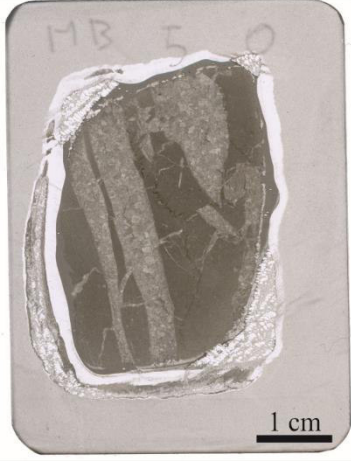|			
4	B-4		**Skeletal components:** rare undefined bioclasts, rare brachiopods **Non-skeletal components:** rare undetermined peloids **Matrix:** micrite/microsparite **Taphonomical characters:** high fragmentation, high abrasion, no bioerosion, low micritization, no encrustation **Lithology:** mudstone **Note: /**
5	B-5		**Skeletal components:** abundant undefined bioclasts, rare brachiopods, rare echinoderms, rare gastropods, rare ostracods, rare ?*Earlandia* sp., rare micritized ring-shaped bioclasts, rare small foraminifera included textulariids, valvulinids, ?*Siphovalvulina variabilis* and *Meandrovoluta asiagoensis* **Non-skeletal components:** rare undetermined peloids, common microbial peloids, common cortoids with constructive and destructive envelope **Matrix:** very fine-grained micrite **Taphonomical characters:** high fragmentation, high abrasion, low bioerosion, moderate micritization, low encrustation **Lithology:** floatstone with mudstone matrix **Note: /**
Semi-quantitative analysis of components: (absent), rare, common, abundant Semi-quantitative analysis of taphonomic features: no, low, moderate, high * "bivalves" are referred to non-lithiotid bivalves /: absent			

A.8. Toraro Mt. accumulation C (TorC)
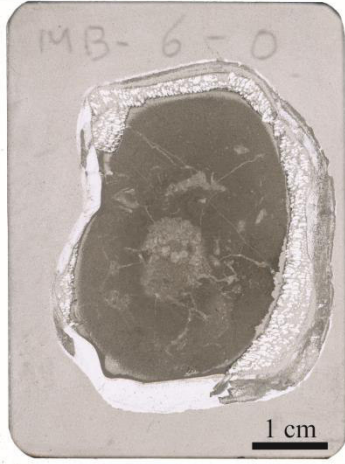
No.	Sample	Thin section	Description
1	C-1O	 1 cm	**Skeletal components:** rare undefined bioclasts included *Tubiphites* like-organism, rare brachiopods, rare echinoderms, rare small foraminifera included ?*Siphovalvulina variabilis*, ?*Meandrovoluta asiagoensis*, valvulinids and textulariids, rare micritized ring-shaped bioclasts, common *Thaumatoporella parvovesiculifera* (irregular roundish specimens, daughter colonies forms, encrusted morphologies within oncoids) **Non-skeletal components:** common undetermined peloids, abundant oncoids type 3/type 4, rare small cortoids with destructive envelope **Matrix:** micrite/sparite **Taphonomical characters:** high fragmentation, moderate abrasion, no bioerosion, no micritization, high encrustation **Lithology:** wackestone – packstone **Note:** /
2	C-1I	 1 cm	**Skeletal components:** rare undefined bioclasts **Non-skeletal components:** rare undetermined peloids **Matrix:** microsparite/micrite **Taphonomical characters:** high fragmentation, high abrasion, no bioerosion, no micritization, no encrustation **Lithology:** mudstone **Note:** lithiotid shells
3	C-1I2	 1 cm	**Skeletal components:** common undefined bioclasts, rare echinoderms, common larger foraminifera included ?*Bosniella* sp. and ?*Everticyclammina* sp., common small foraminifera included *Siphovalvulina variabilis*, textulariids and valvulinids, common micritized ring-shaped bioclasts, rare *Earlandia* sp., abundant *Thaumatoporella parvovesiculifera* (fragments, irregular roundish specimens, daughter colonies forms, encrusted morphologies within cortoids) **Non-skeletal components:** rare undetermined peloids, rare ?pelletoids, rare microbial peloids, rare isolated coprolite (longitudinal

5	C-1CL		section), common cortoids with destructive and constructive envelope **Matrix:** sparite/micrite **Taphonomical characters:** high fragmentation, high abrasion, moderate micritization, no encrustation **Lithology:** grainstone – packstone **Note:** /
4	C-1CR	 1 cm	**Skeletal components:** rare undefined bioclasts **Non-skeletal components:** rare dark micritic clotted structures **Matrix:** microsparite/micrite **Taphonomical characters:** high fragmentation, high abrasion, no bioerosion, low micritization, no encrustation **Lithology:** mudstone **Note:** /
5	C-1CL	 1 cm	**Skeletal components:** rare undefined bioclasts **Non-skeletal components:** common undetermined peloids, rare fecal pellets (isolated and aggregates), rare pelletoids (?) **Matrix:** micrite/microsparite in a restricted area **Taphonomical characters:** high fragmentation, high abrasion, no bioerosion, low micritization, no encrustation **Lithology:** floatstone with mudstone matrix **Note:** lithiotid shells
6	C-1B	 1 cm	**Skeletal components:** rare undefined bioclasts, rare bivalves* **Non-skeletal components:** common undetermined peloids, rare ?pelletoids **Matrix:** microsparite/micrite **Taphonomical characters:** / **Lithology:** floatstone with mudstone matrix **Note:** /

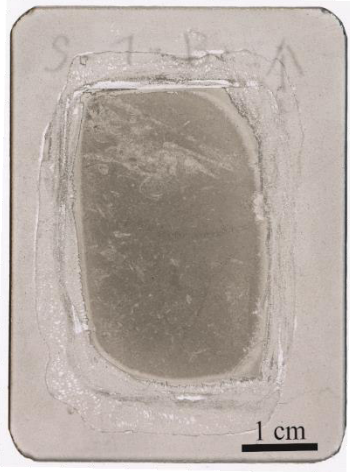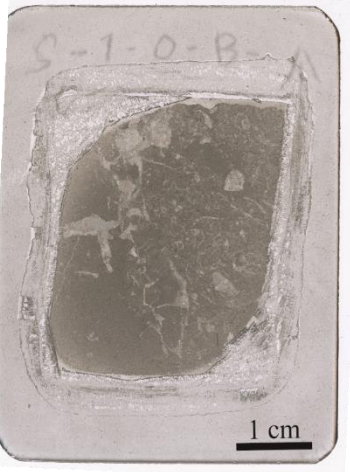| 7 | C-2B | | **Skeletal components:** rare undefined bioclasts

Non-skeletal components: rare undetermined peloids, rare pelletoids

Matrix: microsparite/micrite

Taphonomical characters: high fragmentation, high abrasion, no bioerosion, no micritization, no encrustation

Lithology: mudstone

Note: lithiotid shells |
8	C-3O		**Skeletal components:** rare undefined bioclasts **Non-skeletal components:** rare undetermined peloids, rare dark micritic clotted structures **Matrix:** micrite/microsparite **Taphonomical characters:** high fragmentation, high abrasion, no bioerosion, no micritization, no encrustation **Lithology:** mudstone **Note:** lithiotid shells
9	C-4I		**Skeletal components:** rare undefined bioclasts **Non-skeletal components:** rare undetermined peloids **Matrix:** microsparite/micrite **Taphonomical characters:** high fragmentation, high abrasion, no bioerosion, no micritization, low encrustation **Lithology:** wackestone **Note:** lithiotid shells
10	C-4B		**Skeletal components:** rare undefined bioclasts, rare brachiopods **Non-skeletal components:** rare undetermined peloids, rare fecal pellets (?), rare dark micritic clotted structures **Matrix:** microsparite/micrite **Taphonomical characters:** high fragmentation, high abrasion, no bioerosion, no micritization, no encrustation **Lithology:** mudstone

			Note: lithiotid shells
11	C-4O		**Skeletal components:** rare undefined bioclasts, rare brachiopods, rare bivalves* **Non-skeletal components:** rare undetermined peloids, rare pelletoids, rare dark micritic clotted structures **Matrix:** microsparite/micrite **Taphonomical characters:** high fragmentation, high abrasion, no bioerosion, no micritization, no encrustation **Lithology:** mudstone **Note:** /
12	C-4IS		**Skeletal components:** rare undefined bioclasts, rare brachiopods (one articulated) **Non-skeletal components:** / **Matrix:** microsparite/micrite **Taphonomical characters:** high fragmentation, moderate abrasion, no bioerosion, no micritization, no encrustation **Lithology:** floatstone with mudstone matrix **Note:** lithiotid shells
13	C-BT		**Skeletal components:** common undefined bioclasts, rare brachiopods, rare echinoderms, common small foraminifera included ?*Meandrovoluta asiagoensis*, *Glomospira/Planiinvoluta* spp., textulariids, ?*Ammobaculites* sp. *Siphovalvulina variabilis*, ?*Duotaxis metula*, rare larger foraminifera included ?*Haurania* sp., ?*Lituosepta* sp. and ?*Everticyclammina* sp., rare ?*Earlandia* sp., rare ?*Palaeodasycladus* sp., rare micritized ring-shaped bioclasts, abundant *Thaumatoporella parvovesiculifera* (included ladders, daughter colonies forms, irregular roundish specimens, fragments and encrusted morphologies) **Non-skeletal components:** abundant undetermined peloids, common mud peloids (?), common microbial peloids (in restricted areas), rare cortoids with destructive and constructive envelope, common dark micritic clotted structures included dendritic forms **Matrix:** micrite/sparite **Taphonomical characters:** high fragmentation, moderate abrasion, low

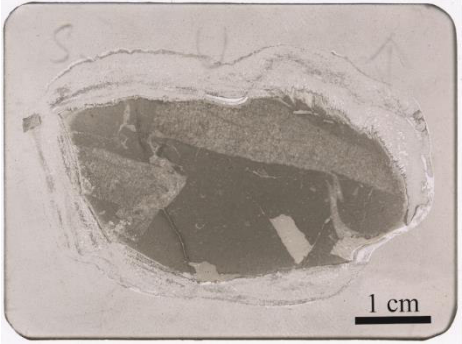|			
			bioerosion, moderate micritization, high encrustation **Lithology:** packstone – grainstone **Note:** lithiotid shells, micritic laminae
14	C-5I		**Skeletal components:** rare undefined bioclasts **Non-skeletal components:** / **Matrix:** microsparite/micrite **Taphonomical characters:** high fragmentation, high abrasion, no bioerosion, no micritization, no encrustation **Lithology:** mudstone **Note:** lithiotid shells
15	C-5O		**Skeletal components:** rare undefined bioclasts **Non-skeletal components:** rare undetermined peloids **Matrix:** micrite **Taphonomical characters:** high fragmentation, high abrasion, low bioerosion, no micritization, no encrustation **Lithology:** mudstone **Note:** lithiotid shells
16	C-5B		**Skeletal components:** rare undefined bioclasts **Non-skeletal components:** rare undetermined peloids, rare fecal pellets (aggregates), rare pelletoids **Matrix:** microsparite/micrite **Taphonomical characters:** high fragmentation, high abrasion, no bioerosion, no micritization, no encrustation **Lithology:** mudstone **Note:** /

17	C-6I		**Skeletal components:** rare undefined bioclasts, rare bivalves*, rare brachiopods (one articulated) **Non-skeletal components:** rare undetermined peloids, rare ?pelletoids **Matrix:** microsparite/micrite **Taphonomical characters:** moderate fragmentation, moderate abrasion, no bioerosion, no micritization, low encrustation **Lithology:** wackestone **Note:** lithiotid shells
18	C-6O		**Skeletal components:** rare undefined bioclasts **Non-skeletal components:** rare undetermined peloids, rare dark micritic clotted structures **Matrix:** microsparite/micrite **Taphonomical characters:** high fragmentation, high abrasion, no bioerosion, no micritization, no encrustation **Lithology:** floatstone with mudstone matrix **Note:** /
19	C5		**Skeletal components:** rare undefined bioclasts, rare brachiopods **Non-skeletal components:** rare undetermined peloids, rare fecal pellets (aggregates) **Matrix:** microsparite/micrite **Taphonomical characters:** high fragmentation, high abrasion, no bioerosion, no micritization, no encrustation **Lithology:** mudstone **Note:** /

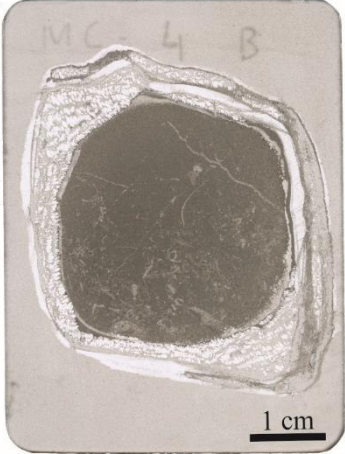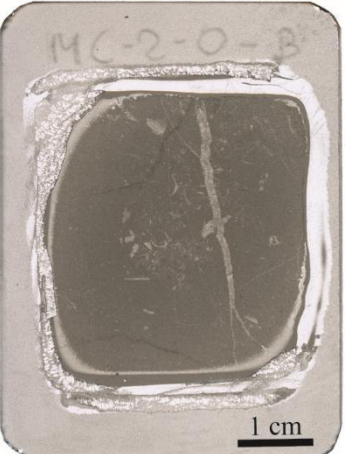| 20 | C-OC | | **Skeletal components:** rare undefined bioclasts, common small foraminifera included *Siphovalvulina variabilis*, ?*Meandrovoluta asiagoensis*, *Glomospira/Planiinvoluta* spp., *Duotaxis metula,* valvulinids and textulariids, common micritized ring-shaped bioclasts, rare ?*Earlandia* sp., abundant *Thaumatoporella parvovesiculifera* (fragments, irregular roundish specimens, daughter colonies forms, encrusted morphologies within oncoids)

Non-skeletal components: abundant undetermined peloids, abundant oncoids type3/type 4, rare cortoids with destructive envelope, common dark micritic clotted structures

Matrix: micrite/sparite

Taphonomical characters: moderate fragmentation, moderate abrasion, low bioerosion, moderate micritization, high encrustation

Lithology: packstone

Note: / |
| Semi-quantitative analysis of components: (absent), rare, common, abundant
Semi-quantitative analysis of taphonomic features: no, low, moderate, high
* "bivalves" are referred to non-lithiotid bivalves
/: absent ||||

A.9. Toraro Mt. accumulation D2 (TorD2)

No.	Sample	Thin section	Description
1	D2-BT	 1 cm	**Skeletal components:** abundant undefined bioclasts, rare brachiopods, rare echinoderms, rare larger foraminifera, rare small foraminifera included *Duotaxis metula*, ?*Meandrovoluta asiagoensis*, ?*Glomospira/Planiinvoluta* spp., textulariids and valvulinids, rare micritized ring-shaped bioclasts, common *Thaumatoporella parvovesiculifera* (fragments), rare encrusted organisms (?foraminifera) **Non-skeletal components:** common undetermined peloids, rare pelletoids, rare fecal pellets aggregates, rare dark micritic clotted structures included dendritic forms **Matrix:** micrite/clotted peloidal micrite/sparite **Taphonomical characters:** high fragmentation, high abrasion, no bioerosion, moderate micritization, low encrustation **Lithology:** packstone – grainstone in restricted area **Note**: /
2	D2-OB	 1 cm	**Skeletal components:** abundant undefined bioclasts, rare ?*Earlandia* sp., rare micritized ring-shaped bioclasts, rare *Palaeodasycladus* sp., rare small foraminifera included textulariids, valvulinids, ?*Meandrovoluta asiagoensis* and ?*Glomospira/Planiinvoluta* spp., rare larger foraminifera included ?*Haurania deserta*, rare echinoderms, common *Thaumatoporella parvovesiculifera* (daughter colonies forms, fragments and irregular roundish specimens) **Non-skeletal components:** rare undetermined peloids, rare cortoids with destructive envelope, rare dark micritic clotted structures included dendritic forms **Matrix:** very fine-grained micrite/micrite/sparite in restricted areas **Taphonomical characters:** high fragmentation, high abrasion, no bioerosion, moderate micritization, no encrustation

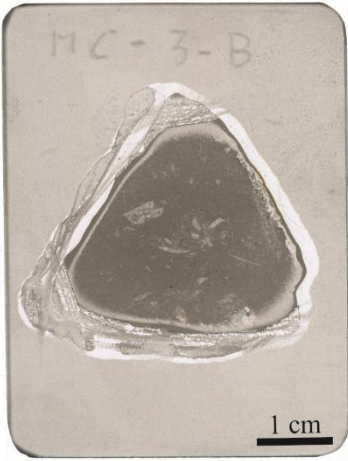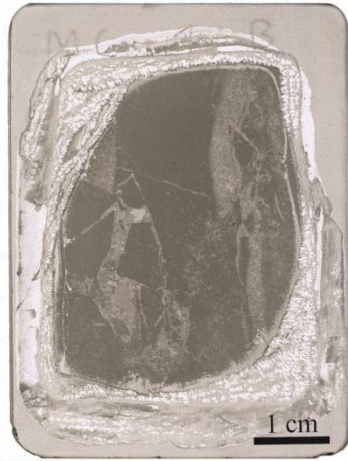|			
			Lithology: packstone – grainstone in a restricted area **Note:** bioturbation traces
3	D2-OT		**Skeletal components:** rare undefined bioclasts, rare brachiopods, rare echinoderms, rare ostracods, rare gastropods, rare small foraminifera included ?*Siphovalvulina variabilis* and ?*Glomospira/Planiinvoluta* spp. and vavulinids, rare ?*Earlandia* sp., rare micritized ring-shaped bioclasts, rare *Thaumatoporella parvovesiculifera* (irregular roundish specimens, encrusted morphologies, fragments and cysts) **Non-skeletal components:** rare undetermined peloids, rare pelletoids, rare dark micritic clotted structures included dendritic forms **Matrix:** very fine-grained micrite in a restricted area/micrite/sparite **Taphonomical characters:** high fragmentation, high abrasion, no bioerosion, moderate micritization, low encrustation **Lithology:** wackestone – grainstone in a restricted area **Note:** lithiotid shells
4	D2-I		**Skeletal components:** abundant undefined bioclasts, rare gastropods, rare small foraminifera included valvulinids, rare micritized ring-shaped bioclasts, rare *Thaumatoporella parovesiculifera* (daughter colonies forms, irregular roundish specimens and fragments), rare ?*Earlandia* sp. **Non-skeletal components:** common undetermined peloids, rare pelletoids, common cortoids with destructive envelope, rare dark micritic clotted structures **Matrix:** very fine-grained micrite/micrite **Taphonomical characters:** high fragmentation, high abrasion, no bioerosion, moderate micritization, no encrustation **Lithology:** wackestone **Note:** lithiotid shells

| 5 | D2-V | | **Skeletal components:** abundant undefined bioclasts, rare small foraminifera included ?*Meandrovoluta asiagoensis*, ?*Glomospira* sp. and textulariids, rare micritized ring-shaped bioclasts, rare *Thaumatoporella parvovesiculifera* (daughter colonies forms and irregular roundish specimens)

Non-skeletal components: common undetermined peloids, rare pelletoids, common cortoids with destructive envelope, rare dark micritic clotted structures included dendritic forms

Matrix: micrite/very fine-grained micrite

Taphonomical characters: high fragmentation, high abrasion, no bioerosion, moderate micritization, no encrustation

Lithology: wackestone

Note: lithiotid shells |
| 6 | D2-U | | **Skeletal components:** rare undefined bioclasts, rare gastropods, rare ostracods, rare echinoderms, rare small foraminifera included valvulinids, ?*Meandrovoluta asiagoensis* and ?*Glomospira* sp., rare micritized ring-shaped bioclasts, rare *Thaumatoporella parvovesiculifera* (daughter colonies forms, cysts and irregular roundish specimens), rare ?*Earlandia* sp.

Non-skeletal components: rare undetermined peloids

Matrix: very fine-grained micrite/micrite in restricted areas

Taphonomical characters: high fragmentation, high abrasion, no bioerosion, no micritization, no encrustation

Lithology: wackestone

Note: lithiotid shells |

Semi-quantitative analysis of components: (absent), rare, common, abundant
Semi-quantitative analysis of taphonomic features: no, low, moderate, high
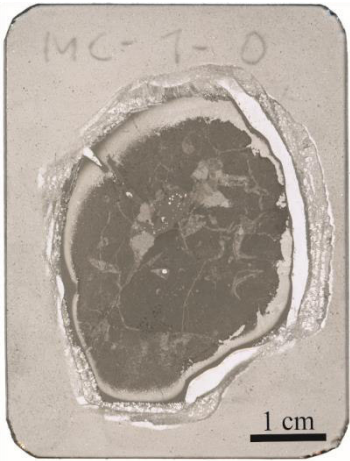* "bivalves" are referred to non-lithiotid bivalves
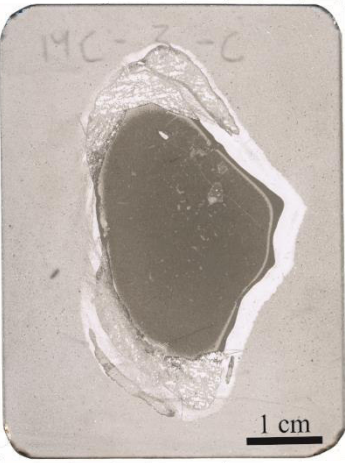/: absent

A.10. Toraro Mt. accumulation E (TorE)

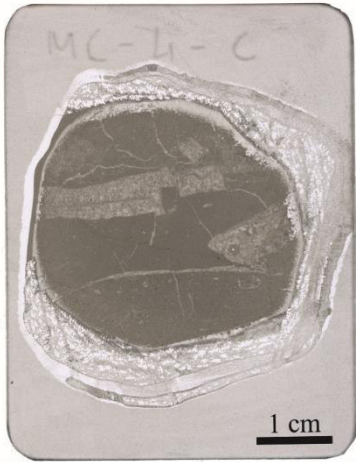| No.	Sample	Thin section	Description
1	E-1C		**Skeletal components:** abundant undefined bioclasts, common brachiopods, rare gastropods, rare small foraminifera included textulariids, rare *Renalcis*-like structures, rare ?*Earlandia* sp., rare micritized ring-shaped bioclasts, rare *Thaumatoporella parvovesiculifera* (irregular roundish specimens, encrusted morphologies, daughter colonies forms and fragments) **Non-skeletal components:** rare undetermined peloids, common dark micritic clotted structures included dendritic forms **Matrix:** micrite/clotted peloidal micrite in a restricted area/sparite in restricted areas **Taphonomical characters:** high fragmentation, high abrasion, no bioerosion, moderate micritization, low encrustation **Lithology:** packstone – grainstone **Note:** bioturbation traces
2	E-2O2		**Skeletal components:** common undefined bioclasts, rare echinoderms, rare small foraminifera included textulariids, valvulinids and ?*Siphovalvulina variabilis*, rare ?*Glomospira/Planiinvoluta* spp., rare ?*Earlandia* sp., rare micritized ring-shaped bioclasts, rare *Thaumatoporella parvovesiculifera* (irregular roundish specimens, ladders, daughter colonies forms and fragments) **Non-skeletal components:** rare undetermined peloids, common dark micritic clotted structures included dendritic forms **Matrix:** micrite/sparite in restricted areas **Taphonomical characters:** high fragmentation, high abrasion, no bioerosion, low micritization, no encrustation **Lithology:** wackestone – grainstone in a restricted area

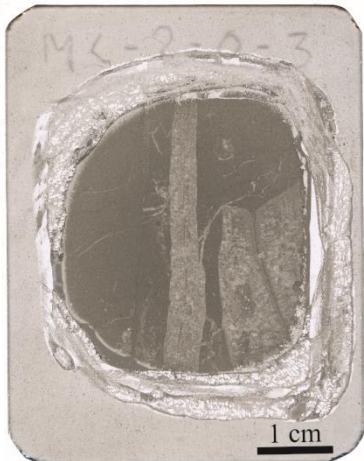|			
			Note: bioturbation traces
3	E-4B	1 cm	**Skeletal components:** common undefined bioclasts, rare brachiopods, one articulated bivalve*, rare small foraminifera included textulariids and valuvlinids, rare micritized ring-shaped bioclasts, rare *Thaumatoporella parvovesiculifera* (irregular roundish specimens, fragments and daughter colonies forms) **Non-skeletal components:** common undetermined peloids, common dark micritic clotted structures included dendritic forms **Matrix:** micrite/sparite in restricted areas **Taphonomical characters:** high fragmentation, high abrasion, no bioerosion, moderate micritization, low encrustation **Lithology:** wackestone – packstone and mudstone in a restricted area **Note:** /
4	E-2OB	1 cm	**Skeletal components:** common undefined bioclasts, rare echinoderms, rare brachiopods, rare bivalves*, rare small foraminifera included *Meandrovoluta asiagoensis*, *Siphovalvulina variabilis*, valvulinids and textulariids, rare micritized ring-shaped bioclasts, rare *Thaumatoporella parvovesiculifera* (fragments) **Non-skeletal components:** rare undetermined peloids, rare dark micritic clotted structures **Matrix:** micrite/sparite **Taphonomical characters:** high fragmentation, moderate abrasion, no bioerosion, moderate micritization, no encrustation **Lithology:** wackestone – packstone in restricted areas **Note:** bioturbation traces
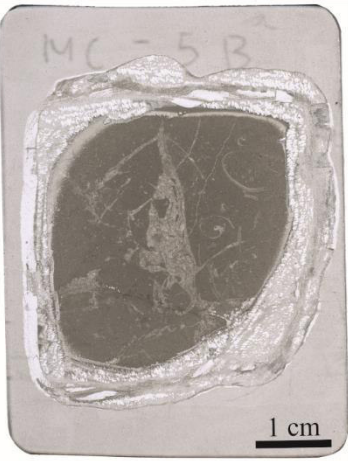
| 5 | E-3O2 | | **Skeletal components:** common undefined bioclasts, rare brachiopods included articulated specimens, rare gastropods, rare small foraminifera included valvulinids and *Siphovalvulina variabilis*, rare micritized ring-shaped bioclasts, rare *Thaumatoporella parvovesiculifera* (irregular roundish specimens, fragments and cysts, daughter colonies forms)

Non-skeletal components: rare undetermined peloids, rare dark micritic clotted structures

Matrix: micrite

Taphonomical characters: high fragmentation, high abrasion, no bioerosion, low micritization, no encrustation

Lithology: floatstone with wackestone matrix

Note: / |
| 6 | E-4O | | **Skeletal components:** rare undefined bioclasts, rare echinoderms, rare small foraminifera included textulariids, ?*Meandrovoluta asiagoensis* and ?*Glomospira/Planiinvoluta* spp., rare ?*Earlandia* sp., rare micritized ring-shaped bioclasts, rare *Thaumatoporella parvovesiculifera* (?cysts, irregular roundish specimens, fragments and daughter colonies forms)

Non-skeletal components: rare undetermined peloids, rare dark micritic clotted structures

Matrix: micrite

Taphonomical characters: high fragmentation, high abrasion, no bioerosion, low micritization, no encrustation

Lithology: wackestone

Note: / |

7	E-3B		**Skeletal components:** rare undefined bioclasts, rare brachiopods, ?*Earlandia* sp., rare small foraminifera included *Siphovalvulina variabilis* and valvulinids, rare micritized ring-shaped bioclasts, rare *Thaumatoporella parvovesiculifera* (fragments and irregular roundish specimens) **Non-skeletal components:** common undetermined peloids, rare dark micritic clotted structures included dendritic forms **Matrix:** micrite **Taphonomical characters:** high fragmentation, high abrasion, no bioerosion, low micritization, no encrustation **Lithology:** floatstone with wackestone matrix **Note:** bioturbation traces
8	E-1B		**Skeletal components:** rare undefined bioclasts, rare brachiopods, rare small foraminifera included rare ?*Glomospira/Planiinvoluta* spp., textulariids and valvulinids, rare micritized ring-shaped bioclasts, rare *Thaumatoporella parvovesiculifera* (fragments and irregular roundish specimens) **Non-skeletal components:** common undetermined peloids, common dark micritic clotted structures included dendritic forms **Matrix:** micrite/sparite in restricted areas **Taphonomical characters:** high fragmentation, high abrasion, no bioerosion, low micritization, no encrustation **Lithology:** wackestone – packstone **Note:** ?lithiotid shells, bioturbation traces

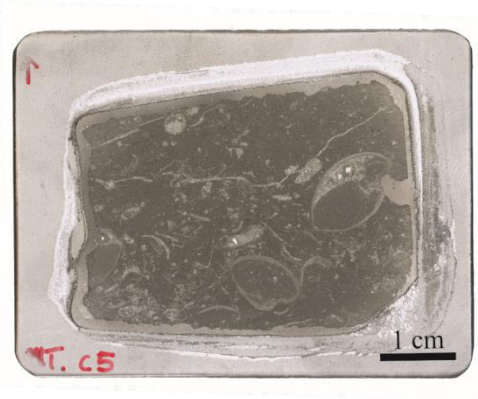| 9	E-1O		**Skeletal components:** rare undefined bioclasts, rare brachiopods, rare small foraminifera included *Planiinvoluta* sp., *Meandrovoluta asiagoensis* and valvulinids, rare *?Earlandia* sp., rare micritized ring-shaped bioclasts, rare *Thaumatoporella parvovesiculifera* (fragments, daughter colonies forms and irregular roundish specimens), rare encrusted organisms (?foraminifera) **Non-skeletal components:** common undetermined peloids, common dark micritic clotted structures included dendritic forms **Matrix:** micrite/sparite **Taphonomical characters:** high fragmentation, high abrasion, no bioerosion, low micritization, low encrustation **Lithology:** wackestone – packstone **Note: /**
10	E-2I		**Skeletal components:** abundant undefined bioclasts, rare brachiopods, rare echinoderms, rare ostracods, rare small foraminifera included *Siphovalvulina variabilis*, valvulinids and *Glomospira* sp., rare micritized ring-shaped bioclasts, rare *Thaumatoporella parvovesiculifera* (fragments and irregular roundish specimens) **Non-skeletal components:** rare undetermined peloids, rare micritic clotted structures included dendritic forms **Matrix:** micrite/sparite in restricted areas **Taphonomical characters:** high fragmentation, high abrasion, no bioerosion, low micritization, no encrustation **Lithology:** wackestone – packstone **Note:** bioturbation traces

11	E-2C		**Skeletal components:** abundant undefined bioclasts, rare brachiopods, rare gastropods, rare small foraminifera included *Siphovalvulina variabilis*, textulariids and valvulinids, rare ?*Earlandia* sp., rare micritized ring-shaped bioclasts, rare *Thaumatoporella parvovesiculifera* (irregular roundish morphologies, ?cysts, fragments and encrusted specimens), rare encrusted organisms **Non-skeletal components:** rare undetermined peloids, rare fecal pellets aggregate (?), rare dark micritic clotted structures included dendritic forms **Matrix:** micrite/sparite in restricted areas **Taphonomical characters:** high fragmentation, high abrasion, no bioerosion, low micritization, low encrustation **Lithology:** wackestone – packstone **Note: /**
12	E-3C		**Skeletal components:** rare undefined bioclasts, rare brachiopods, rare small foraminifera included valvulinids, rare micritized ring-shaped bioclasts, rare *Thaumatoporella parvovesiculifera* (irregular roundish specimens and/or ?cysts) **Non-skeletal components:** rare undetermined peloids, rare dark micritic clotted structures **Matrix:** micrite **Taphonomical characters:** high fragmentation, high abrasion, no bioerosion, low micritization, no encrustation **Lithology:** wackestone **Note: /**

13	E-4C		**Skeletal components:** rare undefined bioclasts, rare small foraminifera included valvulinids, rare micritized ring-shaped bioclasts, rare *Thaumatoporella parvovesiculifera* (fragments), rare encrusted organisms **Non-skeletal components:** rare undetermined peloids, rare dark micritic clotted structures **Matrix:** micrite/microsparite in a restricted area **Taphonomical characters:** high fragmentation, high abrasion, low bioerosion, low micritization, no encrustation **Lithology:** wackestone **Note:** lithiotid shells
14	E-2O3		**Skeletal components:** abundant undefined bioclasts, rare brachiopods, rare small foraminifera included textulariids, valvulinids, ?*Planiinvoluta* sp. and ?*Meandrovoluta asiagoensis*, rare micritized ring-shaped bioclasts, rare *Thaumatoporella parvovesiculifera* (fragments), rare encrusted organisms (?foraminifera) **Non-skeletal components:** rare undetermined peloids, rare dark micritic clotted structures included dendritic forms **Matrix:** micrite/sparite in restricted areas **Taphonomical characters:** high fragmentation, high abrasion, low bioerosion, low micritization, low encrustation **Lithology:** wackestone **Note:** lithiotid shells

15	E-4I		**Skeletal components:** common undefined bioclasts, rare echinoderms, rare brachiopods, rare small foraminifera included textulariids and valvulinids and ?*Meandrovoluta asiagoensis*, rare ?*Earlandia* sp., rare *Thaumatoporella parvovesiculifera* (irregular roundish specimens, ?cysts, fragments and daughter colonies forms) **Non-skeletal components:** rare undetermined peloids, common dark micritic clotted structures **Matrix:** micrite/sparite in restricted areas **Taphonomical characters:** high fragmentation, high abrasion, no bioerosion, low micritization, no encrustation **Lithology:** wackestone – packstone **Note:** micritic laminae
16	E-5B		**Skeletal components:** abundant undefined bioclasts, common brachiopods, rare gastropods, rare small foraminifera included ?*Glomospira/Planiinvoluta* spp., valvulinids, and textulariids, rare ?*Earlandia* sp., rare micritized ring-shaped bioclasts, rare *Thaumatoporella parvovesiculifera* (irregular roundish specimens, fragments and daughter colonies forms) **Non-skeletal components:** rare undetermined peloids, rare dark micritic clotted structures **Matrix:** micrite **Taphonomical characters:** high fragmentation, high abrasion, no bioerosion, low micritization, no encrustation **Lithology:** floatstone with wackestone matrix **Note:** /

17	E-C5		**Skeletal components:** abundant undefined bioclasts, common brachiopods included articulated specimens, common small foraminifera included ?*Meandrovoluta asiagoensis*, *Glomospira/Planiinvoluta* spp., textulariids and valvulinids, rare micritized ring-shaped bioclasts, common *Thaumatoporella parvovesiculifera* (irregular roundish specimens, fragments, daughter colonies forms and cysts), rare encrusted organisms (?foraminifera) **Non-skeletal components:** abundant undetermined peloids, rare microbial peloids, rare dark micritic clotted structures included dendritic forms **Matrix:** micrite/clotted peloidal micrite in restricted areas/sparite in restricted areas **Taphonomical characters:** high fragmentation, moderate abrasion, no bioerosion, low micritization, low encrustation **Lithology:** packstone – grainstone in restricted areas **Note:** /
Semi-quantitative analysis of components: (absent), rare, common, abundant Semi-quantitative analysis of taphonomic features: no, low, moderate, high * "bivalves" are referred to non-lithiotid bivalves /: absent			
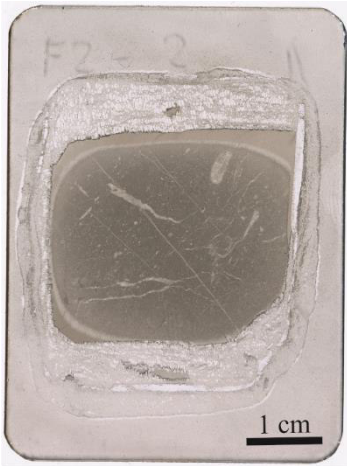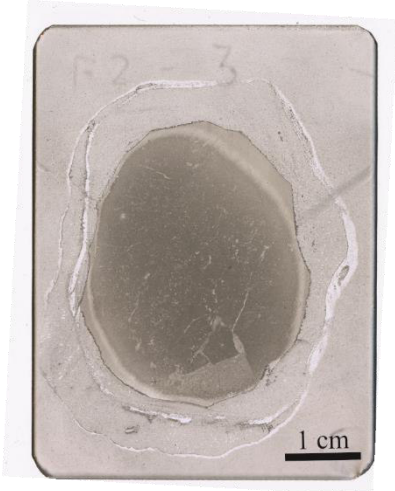
A.11. Toraro Mt. accumulation F (TorF)

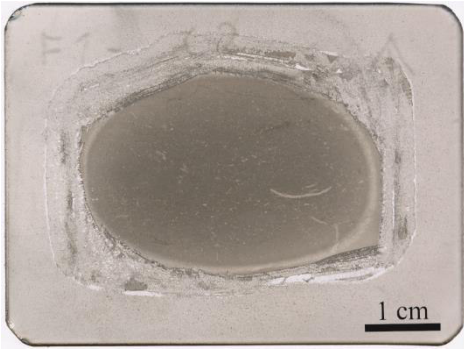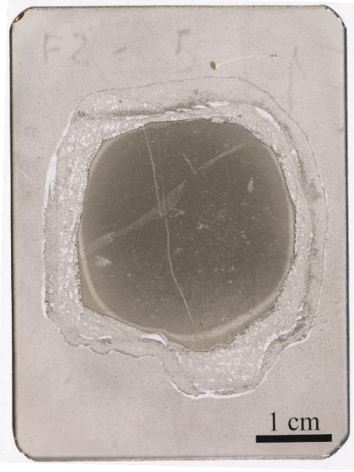| No.	Sample	Thin section	Description
1	F1-1		**Skeletal components:** abundant undefined bioclasts, rare brachiopods, rare ostracods, rare gastropods, rare echinoderms, rare small foraminifera included valvulinids and textulariids, rare *Palaeodasycladus* sp., rare ?*Earlandia* sp., rare micritized ring-shaped bioclasts, rare *Thaumatoporella parvovesiculifera* (daughter colonies forms, irregular roundish specimens, fragments, encrusted morphologies), rare encrusted organisms **Non-skeletal components:** common undetermined peloids (included rare microbial peloids), rare cortoids with destructive envelope, common dark micritic clotted structures included dendritic forms **Matrix:** micrite **Taphonomical characters:** high fragmentation, high abrasion, no bioerosion, low micritization, low encrustation **Lithology:** wackestone **Note:** bioturbation traces
2	F1-2		**Skeletal components:** abundant undefined bioclasts, rare brachiopods, rare larger foraminifers, rare small foraminifera included textulariids, valvulinids and *Meandrovoluta asiagoensis*, rare ?*Earlandia* sp., rare micritized ring-shaped bioclasts, common *Thaumatoporella parvovesiculifera* (daughter colonies forms, fragments and irregular roundish specimens) **Non-skeletal components:** common undetermined peloids, rare cortoids with destructive envelope, common dark micritic clotted structures included dendritic forms **Matrix:** micrite **Taphonomical characters:** high fragmentation, high abrasion, no bioerosion, low micritization, low encrustation **Lithology:** wackestone **Note:** /

| 3 | F1-3 | | **Skeletal components:** abundant undefined bioclasts, rare brachiopods, rare small foraminifera included valvulinids, rare ?*Earlandia* sp., rare micritized ring-shaped bioclasts, *Thaumatoporella parvovesiculifera* (daughter colonies forms, irregular roundish specimens, fragments and encrusted morphologies)

Non-skeletal components: common undetermined peloids, rare dark micritic clotted structures

Matrix: micrite

Taphonomical characters: high fragmentation, high abrasion, no bioerosion, no micritization, no encrustation

Lithology: wackestone

Note: / |
| 4 | F1-4 | | **Skeletal components:** abundant undefined bioclasts, rare echinoderms, rare gastropods, rare brachiopods, rare small foraminifera included ?*Meandrovoluta asiagoensis*, rare micritized ring-shaped bioclasts, common *Thaumatoporella parvovesiculifera* (fragments, daughter colonies forms, irregular roundish specimens)

Non-skeletal components: rare undetermined peloids, rare microbial peloids, rare cortoids with destructive envelope, rare dark micritic clotted structures included dendritic forms

Matrix: micrite/sparite

Taphonomical characters: high fragmentation, high abrasion, low bioerosion, low micritization, low encrustation

Lithology: wackestone – packstone

Note: lithiotid shells, bioturbation traces |

| 5 | F1-B | | **Skeletal components:** abundant undefined bioclasts, rare brachiopods, rare small foraminifera, rare echinoderms, , rare micritized ring-shaped bioclasts, rare *Thaumatoporella parvovesiculifera* (fragments, cysts, daughter colonies forms and irregular roundish specimens)

Non-skeletal components: common undetermined peloids, rare cortoids with destructive envelope, rare dark micritic clotted structures

Matrix: micrite/clotted peloidal micrite/sparite

Taphonomical characters: high fragmentation, high abrasion, no bioerosion, moderate micritization, low encrustation

Lithology: floatstone with packstone matrix

Note: bioturbation traces |
| 6 | F1-C1 | | **Skeletal components:** abundant undefined bioclasts, common brachiopods, rare ostracods, rare small foraminifera included valvulinids and textulariids, rare *Palaeodasycladus* sp., rare micritized ring-shaped bioclasts, rare *Thaumatoporella parvovesiculifera* (fragments, daughter colonies forms, cysts and irregular roundish specimens)

Non-skeletal components: rare undetermined peloids, rare cortoids with destructive envelope, rare dark micritic clotted structures

Matrix: micrite/microsparite in restricted areas

Taphonomical characters: high fragmentation, moderate abrasion, moderate bioerosion, low micritization, no encrustation

Lithology: floatstone with wackestone matrix
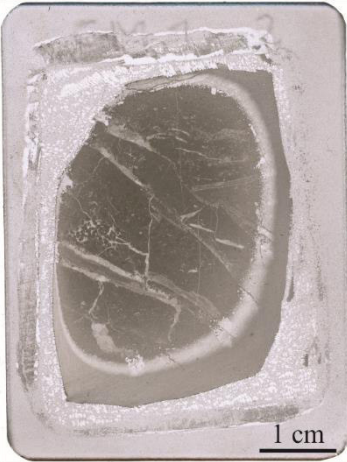
Note: / |

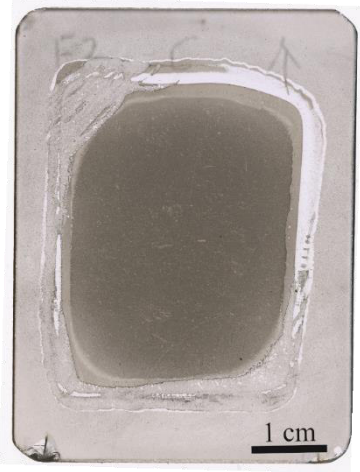| 7 | F1-C2 | | **Skeletal components:** abundant undefined bioclasts, rare echinoderms, rare ostracods, common small foraminifera included *Siphovalvulina variabilis*, textulariids and valvulinids, rare larger foraminifera included *?Amijiella amijii*, rare *Thaumatoporella parvovesiculifera* (fragments, encrusted morphologies and irregular rounded specimens)

Non-skeletal components: common undetermined peloids, rare dark micritic clotted structures

Matrix: micrite

Taphonomical characters: high fragmentation, high abrasion, moderate bioerosion, no micritization, low encrustation

Lithology: wackestone

Note: / |
| 8 | F2-1 | | **Skeletal components:** abundant undefined bioclasts, rare ostracods, rare gastropods, rare echinoderms, rare small foraminifera included textulariids, valvulinids, *?Glomospira/Planiinvoluta* spp. and *Meandrovoluta asiagoensis*, rare *?Earlandia* sp., rare micritized ring-shaped bioclasts, rare *Thaumatoporella parvovesiculifera* (irregular roundish specimens, fragments and cysts)

Non-skeletal components: rare undetermined peloids, rare cortoids with destructive envelope

Matrix: micrite/sparite/clotted peloidal micrite in restricted areas

Taphonomical characters: high fragmentation, high abrasion, no bioerosion, low micritization, no encrustation

Lithology: wackestone – packstone

Note: / |

218

| 9 | F2-2 | | **Skeletal components:** rare undefined bioclasts, rare echinoderms, rare brachiopods, rare small foraminifera included ?*Meandrovoluta asiagoensis*, rare larger foraminifera, rare *Thaumatoporella parvovesiculifera* (fragments and irregular roundish specimens), rare ?*Earlandia* sp., rare micritized ring-shaped bioclasts

Non-skeletal components: common undetermined peloids, rare fecal pellets, rare cortoids with destructive envelope, rare dark micritic clotted structures included dendritic forms

Matrix: micrite/sparite

Taphonomical characters: high fragmentation, high abrasion, no bioerosion, low micritization, no encrustation

Lithology: wackestone – packstone

Note: / |
| 10 | F2-3 | | **Skeletal components:** rare undefined bioclasts, rare echinoderms, rare ?larger foraminifera, rare small foraminifera included valvulinids and ?*Meandrovoluta asiagoensis*, rare ?*Earlandia* sp., rare micritized ring-shaped bioclasts, *Rivularia*-like organisms, *Girvanella*-like structures

Non-skeletal components: rare undetermined peloids, rare dark micritic clotted structures

Matrix: micrite/clotted peloidal micrite in restricted area/sparite

Taphonomical characters: high fragmentation, high abrasion, no bioerosion, no micritization, no encrustation

Lithology: wackestone – packstone

Note: / |

| 11 | F2-4 | | **Skeletal components:** abundant undefined bioclasts, rare brachiopods, rare gastropods, rare small foraminifera included textulariids and *Siphovalvulina variabilis*, rare *Thaumatoporella parvovesiculifera* (irregular roundish specimens, fragments and encrusted morphologies), rare micritized ring-shaped bioclasts

Non-skeletal components: common undetermined peloids, rare microbial peloids, rare fecal pellets, rare cortoids with constructive and destructive envelope, rare dark micritic clotted structures

Matrix: micrite/sparite in restricted areas

Taphonomical characters: high fragmentation, high abrasion, low bioerosion, low micritization, low encrustation

Lithology: wackestone – packstone

Note: / |
| 12 | F2-5 | | **Skeletal components:** abundant undefined bioclasts, rare brachiopods, rare small foraminifera included textulariids, valvulinids and ?*Meandrovoluta asiagoensis*, rare *Thaumatoporella parvovesiculifera* (fragments and cysts), rare ?*Earlandia* sp., rare micritized ring-shaped bioclasts

Non-skeletal components: rare undetermined peloids, rare microbial peloids, rare dark micritic clotted structures

Matrix: micrite/clotted peloidal micrite/sparite in restricted areas

Taphonomical characters: high fragmentation, high abrasion, low bioerosion, no micritization, low encrustation

Lithology: wackestone – packstone

Note: / |

| 13 | F2-C | | **Skeletal components:** abundant undefined bioclasts, rare ostracods, rare brachiopods, rare small foraminifera, rare larger foraminifera included ?*Amijiella amiji*

Non-skeletal components: common undetermined peloids, rare cortoids with destructive envelope, rare dark micritic clotted structures

Matrix: micrite

Taphonomical characters: high fragmentation, high abrasion, no bioerosion, low micritization, no encrustation

Lithology: wackestone

Note: / |
| --- | --- | --- | --- |
| Semi-quantitative analysis of components: (absent), rare, common, abundant
Semi-quantitative analysis of taphonomic features: no, low, moderate, high
/: absent | | | |

A.12. Campoluzzo Mt. accumulation (Cm)

No.	Sample	Thin section	Description
1	Cm-1-1	1 cm	**Skeletal components:** common undefined bioclasts, rare small foraminifera, rare echinoderms **Non-skeletal components:** rare undetermined peloids, rare pelletoids, abundant fecal pellets aggregates, rare cortoids with destructive and constructive envelope **Matrix:** very fine-grained micrite/clotted peloidal micrite in restricted areas/sparite in restricted areas **Taphonomical characters:** high fragmentation, high abrasion, low bioerosion, low micritization, low encrustation **Lithology:** wackestone-packstone **Note:** lithiotid shells
2	Cm-1-2	1 cm	**Skeletal components:** abundant undefined bioclasts, rare gastropods, rare ostracods, rare ?*Earlandia* sp. **Non-skeletal components:** rare undetermined peloids, common fecal pellets included one aggregate **Matrix:** very fine-grained micrite/clotted peloidal micrite in restricted areas/sparite in restricted areas **Taphonomical characters:** high fragmentation, moderate abrasion, low bioerosion, no micritization, low encrustation **Lithology:** wackestone-packstone **Note:** lithiotid shells
3	Cm-2	1 cm	**Skeletal components:** common undefined bioclasts, rare small foraminifera, rare ostracods **Non-skeletal components:** rare undetermined peloids **Matrix:** very fine-grained micrite/micrite **Taphonomical characters:** high fragmentation, high abrasion, low bioerosion, no micritization, no encrustation **Lithology:** wackestone **Note:** lithiotid shells

4	Cm-3		**Skeletal components:** common undefined bioclasts, rare ?*Earlandia* sp. **Non-skeletal components:** rare undetermined peloids, rare isolated fecal pellets **Matrix:** very fine-grained micrite/clotted peloidal micrite in a restricted area **Taphonomical characters:** high fragmentation, moderate abrasion, no bioerosion, no micritization, no encrustation **Lithology:** wackestone **Note:** lithiotid shells
5	Cm-4		**Skeletal components:** common undefined bioclasts, rare gastropods **Non-skeletal components:** rare undetermined peloids **Matrix:** very fine-grained micrite **Taphonomical characters:** high fragmentation, moderate abrasion, low bioerosion, low micritization, no encrustation **Lithology:** wackestone **Note:** lithiotid shells

Semi-quantitative analysis of components: (absent), rare, common, abundant
Semi-quantitative analysis of taphonomic features: no, low, moderate, high

A.13. Rotzo accumulation (Ro)

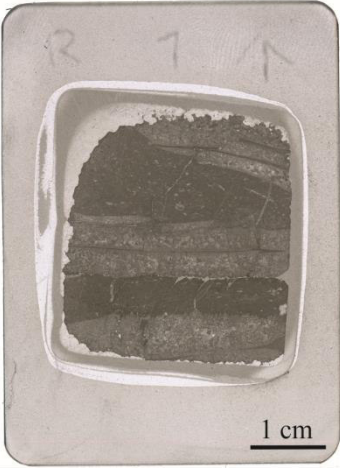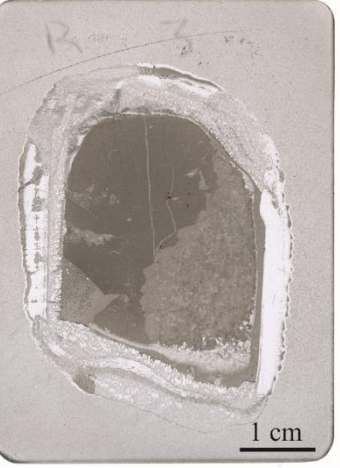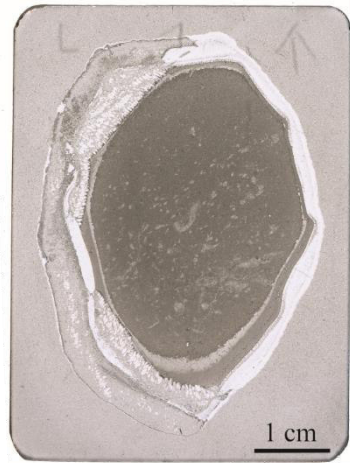| No.	Sample	Thin section	Description
1	Ro-1	 1 cm	**Skeletal components:** rare undefined bioclasts, rare ostracods, rare brachiopods, rare echinoderms, rare small foraminifera, rare micritized ring-shaped bioclasts **Non-skeletal components:** rare undetermined peloids, rare dark clotted micritic structures **Matrix:** micrite **Taphonomical characters:** high fragmentation, moderate abrasion, low bioerosion, no micritization, low encrustation **Lithology:** wackestone **Note:** lithiotid shells
2	Ro-2	 1 cm	**Skeletal components:** rare undefined bioclasts, rare ostracods, rare small foraminifera included *Meandrovoluta asiagoensis*, rare micritized ring-shaped bioclasts, rare *Thaumatoporella parvovesiculifera* (fragments), rare encrusted organisms (foraminifera?) **Non-skeletal components:** rare undetermined peloids **Matrix:** micrite **Taphonomical characters:** high fragmentation, moderate abrasion, low bioerosion, no micritization, low encrustation **Lithology:** mudstone **Note:** lithiotid shells
3	Ro-3	 1 cm	**Skeletal components:** rare undefined bioclasts, rare ostracods, rare small foraminifera **Non-skeletal components:** rare undetermined peloids, rare dark micritic clotted structures **Matrix:** micrite **Taphonomical characters:** high fragmentation, high abrasion, no bioerosion, no micritization, no encrustation **Lithology:** mudstone **Note:** lithiotid shells

#	Sample	Image	Description
4	Ro-4	 1 cm	**Skeletal components:** rare undefined bioclasts, rare ?brachiopods, rare ?bivalves*, rare ostracods, rare small foraminifera, rare micritized ring-shaped bioclasts, rare encrusted organisms (foraminifera?) **Non-skeletal components:** / **Matrix:** micrite **Taphonomical characters:** high fragmentation, moderate abrasion, low bioerosion, no micritization, moderate encrustation **Lithology:** floatstone with mudstone matrix **Note:** lithiotid shells
5	Ro-5	 1 cm	**Skeletal components:** rare undefined bioclasts, rare gastropods, rare bivalves*, rare ostracods, rare small foraminifera included valvulinids, ?*Meandrovoluta asiagoensis* and *Duotaxis metula*, rare micritized ring-shaped bioclasts **Non-skeletal components:** rare dark micritic clotted structures **Matrix:** micrite **Taphonomical characters:** high fragmentation, moderate to high abrasion, low bioerosion, no micritization, low encrustation **Lithology:** wackestone **Note:** lithiotid shells
6	Ro-6	 1 cm	**Skeletal components:** common undefined bioclasts, rare ostracods, rare brachiopods, rare small foraminifera, rare micritized ring-shaped bioclasts, rare ?*Thaumatoporella parvovesiculifera* (fragments) **Non-skeletal components:** rare undetermined peloids, rare dark micritic clotted structures **Matrix:** micrite **Taphonomical characters:** high fragmentation, high abrasion, no bioerosion, no micritization, no encrustation **Lithology:** mudstone-wackestone **Note:** lithiotid shells

7	Ro-7		**Skeletal components:** rare undefined bioclasts, rare brachiopods, rare small foraminifera included *Duotaxis metula*, rare micritized ring-shaped bioclasts, rare encrusted organisms (foraminifera?) **Non-skeletal components:** rare undetermined peloids, rare dark micritic clotted structures **Matrix:** micrite/very fine-grained micrite in restricted areas **Taphonomical characters:** high fragmentation, moderate abrasion, low bioerosion, low micritization, low encrustation **Lithology:** wackestone **Note:** lithiotid shells, bioturbation trace
8	Ro-8		**Skeletal components:** rare undefined bioclasts, rare micritized ring-shaped bioclasts, rare small foraminifera included ?*Meandrovoluta asiagoensis* **Non-skeletal components:** rare undetermined peloids, rare dark micritic clotted structures included dendritic forms **Matrix:** micrite **Taphonomical characters:** high fragmentation, moderate abrasion, low bioerosion, no micritization, low encrustation **Lithology:** wackestone **Note:** lithiotid shells
9	Ro-9		**Skeletal components:** rare undefined bioclasts, rare ostracods, rare brachiopods, rare small foraminifera included textulariids, valvulinids, rare micritized ring-shaped bioclasts, ?*Meandrovoluta asiagoensis* and ?*Glomospira/Planiinvoluta* spp., rare echinoderms, rare encrusted organisms (foraminifera?) **Non-skeletal components:** rare undetermined peloids, rare dark micritic clotted structures included dendritic forms **Matrix:** micrite/very fine-grained micrite in restricted areas **Taphonomical characters:** high fragmentation, high abrasion, low bioerosion, no micritization, low encrustation **Lithology:** wackestone **Note:** lithiotid shells

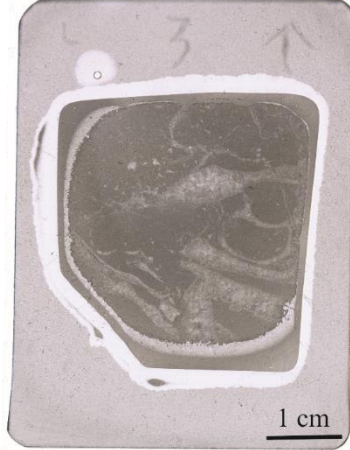| 10 | Ro-10 | | **Skeletal components:** rare undefined bioclasts, rare brachiopods, rare small foraminifera, rare encrusted organisms (?foraminifera), rare micritized ring-shaped bioclasts, rare *?Thaumatoporella parvovesiculifera* (fragments)

Non-skeletal components: rare undetermined peloids, rare dark micritic clotted structures

Matrix: micrite/very fine-grained micrite in a restricted area

Taphonomical characters: high fragmentation, high abrasion, no bioerosion, no micritization, low encrustation

Lithology: wackestone

Note: lithiotid shells |
| Semi-quantitative analysis of components: (absent), rare, common, abundant
Semi-quantitative analysis of taphonomic features: no, low, moderate, high
* "bivalves" are referred to non-lithiotid bivalves
/: absent | | | |

1 cm

A.14. Contrada Dazio accumulation (Da)
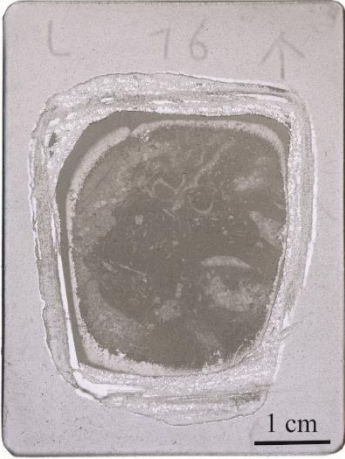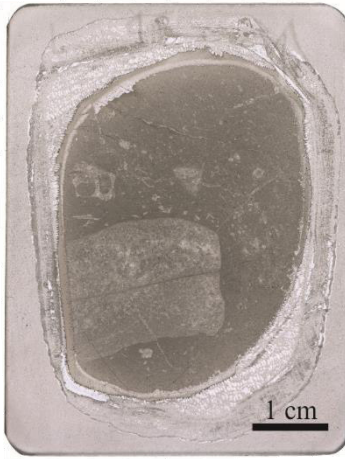
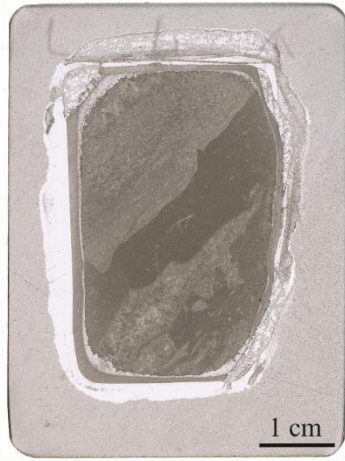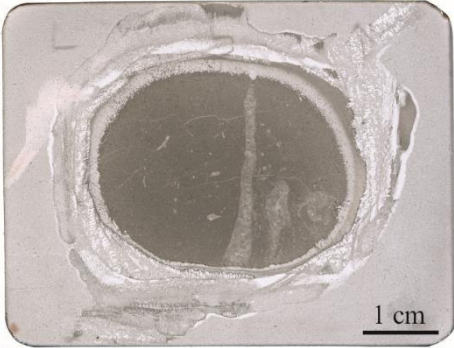| No.	Sample	Thin section	Description
1	Da-1	1 cm	**Skeletal components:** rare undefined bioclasts, rare brachiopods, rare small foraminifera included valvulinids and textulariids, rare *Thaumatoporella parvovesiculifera* (fragments) **Non-skeletal components:** rare dark micritic clotted structures **Matrix:** micrite/microsparite/sparite in a restricted area **Taphonomical characters:** high fragmentation, high abrasion, no bioerosion, low micritization, no encrustation **Lithology:** wackestone-packstone in a restricted area **Note:** /
2	Da-2	1 cm	**Skeletal components:** rare undefined bioclasts, rare brachiopods, rare small foraminifera included ?*Meandrovoluta asiagoensis* and *Glomospira/Planiinvoluta* spp., rare micritized ring-shaped bioclasts, rare *Thaumatoporella parvovesiculifera* (fragments, daughter colonies forms) **Non-skeletal components:** rare undetermined peloids, rare cortoids with destructive envelope, rare dark micritic clotted structures included dendritic forms **Matrix:** micrite/sparite in restricted areas **Taphonomical characters:** high fragmentation, high abrasion, no bioerosion, low micritization, low encrustation **Lithology:** floatstone with packstone matrix **Note:** lithiotid shell
3	Da-3	1 cm	**Skeletal components:** rare undefined bioclasts, rare *Thaumatoporella parvovesiculifera* (fragments and irregular roundish specimens) **Non-skeletal components:** rare undetermined peloids, common microbial peloids **Matrix:** micrite/sparite **Taphonomical characters:** high fragmentation, high abrasion, no bioerosion, low micritization, no encrustation **Lithology:** wackestone-packstone

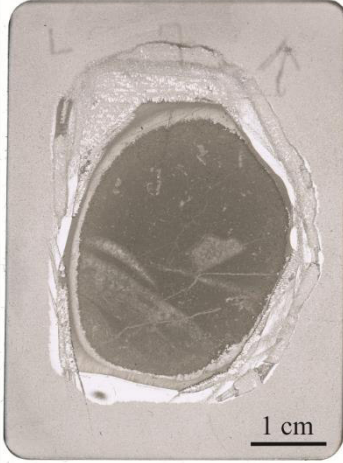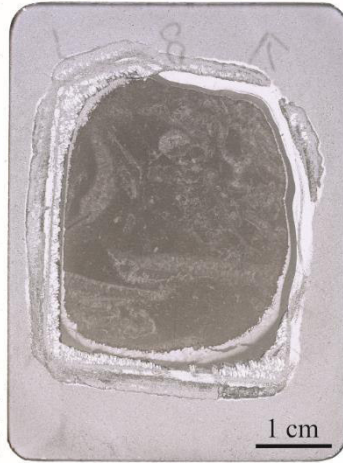|			**Note:** lithiotid shell
4	Da-4		**Skeletal components:** rare undefined bioclasts, rare brachiopods, rare *Thaumatoporella parvovesiculifera* (fragments) **Non-skeletal components:** rare undetermined peloids, rare microbial peloids, rare dark micritic clotted structures **Matrix:** micrite **Taphonomical characters:** high fragmentation, high abrasion, low bioerosion, no micritization, no encrustation **Lithology:** wackestone **Note:** lithiotid shell
5	Da-5		**Skeletal components:** rare undefined bioclasts, rare brachiopods, rare echinoderms **Non-skeletal components:** common undetermined peloids, rare dark micritic clotted structures **Matrix:** micrite/clotted peloidal micrite in a restricted area **Taphonomical characters:** high fragmentation, high abrasion, no bioerosion, low micritization, no encrustation **Lithology:** wackestone **Note:** /
6	Da-6		**Skeletal components:** rare undefined bioclasts, rare *Thaumatoporella parvovesiculifera* (fragments) **Non-skeletal components:** rare undetermined peloids, rare microbial peloids, rare pelletoids **Matrix:** micrite/sparite in a restricted area **Taphonomical characters:** high fragmentation, high abrasion, no bioerosion, no micritization, no encrustation **Lithology:** wackestone-packstone in a restricted area **Note:** lithiotid shell

7	Da-7		**Skeletal components:** rare undefined bioclasts, rare small foraminifera, rare micritized ring-shaped bioclasts, rare *Thaumatoporella parvovesiculifera* (fragments and irregular roundish specimens) **Non-skeletal components:** rare dark micritic clotted structures included dendritic forms **Matrix:** micrite **Taphonomical characters:** high fragmentation, high abrasion, no bioerosion, low micritization, no encrustation **Lithology:** wackestone **Note:** lithiotid shell
8	Da-8		**Skeletal components:** rare undefined bioclasts, rare gastropods, rare *Thaumatoporella parvovesiculifera* (fragments), rare ?*Earlandia* sp. **Non-skeletal components:** common undetermined peloids, rare pelletoids, common fecal pellets, rare microbial peloids, rare dark micritic clotted structures **Matrix:** micrite/clotted peloidal micrite in restricted area/sparite **Taphonomical characters:** high fragmentation, high abrasion, no bioerosion, low micritization, no encrustation **Lithology:** wackestone-peloidal grainstone in a restricted area **Note:** lithiotid shells
9	Da-9		**Skeletal components:** common undefined bioclasts, rare bivalves*, rare echinoderms, rare brachiopods included articulated specimens, rare gastropods, rare *Thaumatoporella parvovesiculifera* (fragments and irregular roundish specimens) **Non-skeletal components:** rare microbial peloids, rare dark micritic clotted structures included dendritic forms **Matrix:** micrite/sparite in restricted areas **Taphonomical characters:** high fragmentation, high abrasion, no bioerosion, no micritization, no encrustation **Lithology:** wackestone-packstone **Note:** /

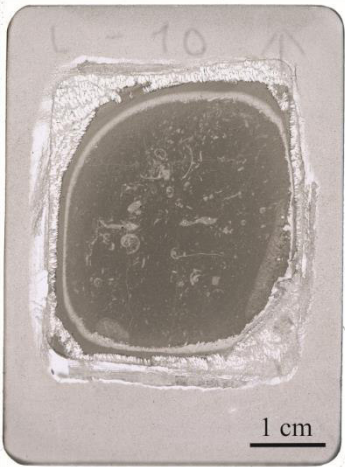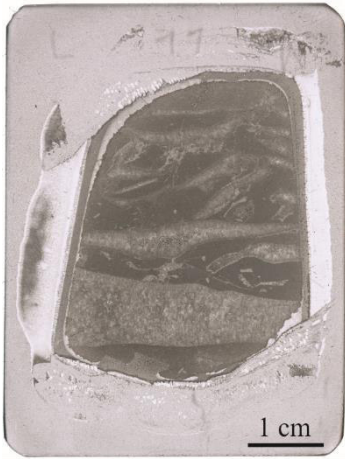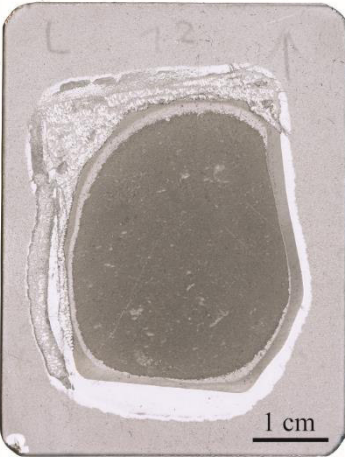| 10	Da-10		**Skeletal components:** common undefined bioclasts, rare ostracods, rare gastropods, rare echinoderms, rare small foraminifera included valvulinids, rare micritized ring-shaped bioclasts, rare *Thaumatoporella parvovesiculifera* (daughter colonies forms, fragments and irregular roundish specimens) **Non-skeletal components:** rare undetermined peloids, rare microbial peloids, rare dark micritic clotted structures included dendritic forms **Matrix:** micrite/sparite **Taphonomical characters:** high fragmentation, high abrasion, no bioerosion, low micritization, no encrustation **Lithology:** wackestone-packstone **Note:** bioturbation traces
11	Da-11		**Skeletal components:** rare undefined bioclasts, rare small foraminifera included ?valvulinids, rare micritized ring-shaped bioclasts, rare *Thaumatoporella parvovesiculifera* (fragments) **Non-skeletal components:** common undetermined peloids, rare fecal pellets aggregates, rare microbial peloids, rare dark micritic clotted structures **Matrix:** micrite/sparite **Taphonomical characters:** high fragmentation, high abrasion, low bioerosion, low micritization, low encrustation **Lithology:** floatstone with wackestone matrix **Note:** lithiotid shell
12	Da-12		**Skeletal components:** rare undefined bioclasts **Non-skeletal components:** rare undetermined peloids, rare dark micritic clotted structures **Matrix:** micrite/sparite in restricted areas **Taphonomical characters:** high fragmentation, high abrasion, no bioerosion, low micritization, no encrustation **Lithology:** wackestone-packstone **Note: /**

13	Da-13	 1 cm	**Skeletal components:** rare undefined bioclasts, rare gastropods, rare bivalves*, rare *Thaumatoporella parvovesiculifera* (fragments and irregular roundish specimens) **Non-skeletal components:** rare undetermined peloids, rare microbial peloids, rare dark micritic clotted structures included dendritic forms **Matrix:** micrite **Taphonomical characters:** high fragmentation, high abrasion, low bioerosion, low micritization, no encrustation **Lithology:** floatstone with wackestone matrix **Note:** /
14	Da-14	 1 cm	**Skeletal components:** rare undefined bioclasts **Non-skeletal components:** rare undetermined peloids, rare dark micritic clotted structures **Matrix:** micrite/sparite **Taphonomical characters:** high fragmentation, high abrasion, low bioerosion, no micritization, no encrustation **Lithology:** wackestone-packstone **Note:** lithiotid shells
15	Da-15	 1 cm	**Skeletal components:** rare undefined bioclasts **Non-skeletal components:** rare undetermined peloids, common microbial peloids, rare dark micritic clotted structures **Matrix:** very fine grained micrite/micrite/clotted peloidal micrite in restricted areas **Taphonomical characters:** high fragmentation, high abrasion, no bioerosion, low micritization, no encrustation **Lithology:** wackestone **Note:** lithiotid shells

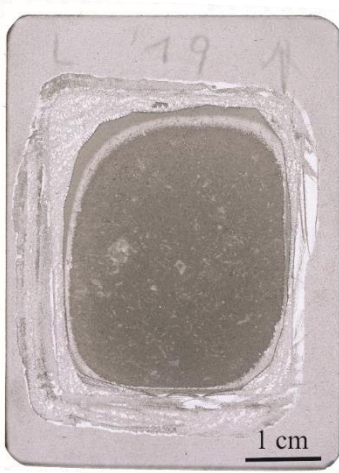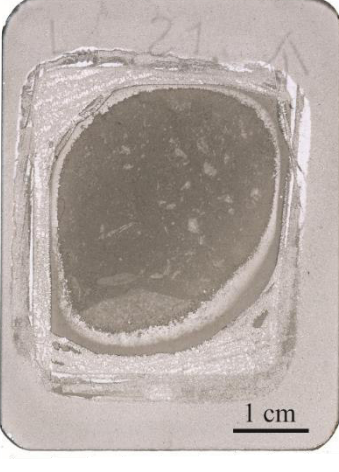| 16 | Da-16 | | **Skeletal components:** rare undefined bioclasts, rare *Rivularia*-like structures, rare *Thaumatoporella parvovesiculifera* (fragments)

Non-skeletal components: rare undetermined peloids

Matrix: micrite

Taphonomical characters: high fragmentation, high abrasion, no bioerosion, no micritization, no encrustation

Lithology: floatstone with wackestone matrix

Note: lithiotid shells |
| 17 | Da-17 | | **Skeletal components:** rare undefined bioclasts, rare *Thaumatoporella parvovesiculifera* (fragments)

Non-skeletal components: rare undetermined peloids

Matrix: micrite/sparite in restricted areas

Taphonomical characters: high fragmentation, high abrasion, no bioerosion, low micritization, no encrustation

Lithology: wackestone-packstone

Note: lithiotid shells |
| 18 | Da-18 | | **Skeletal components:** common undefined bioclasts, rare gastropods, rare brachiopods, rare *Thaumatoporella parvovesiculifera* (fragments)

Non-skeletal components: rare dark micritic clotted structures

Matrix: micrite

Taphonomical characters: high fragmentation, high abrasion, no bioerosion, no micritization, no encrustation

Lithology: floatstone with packstone matrix

Note: lithiotid shells |

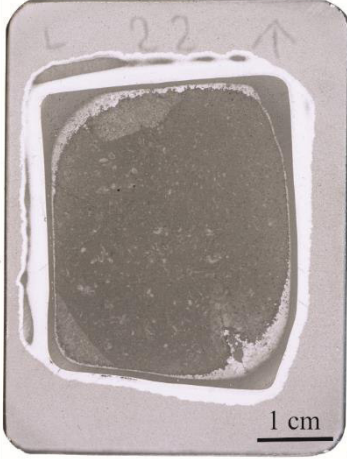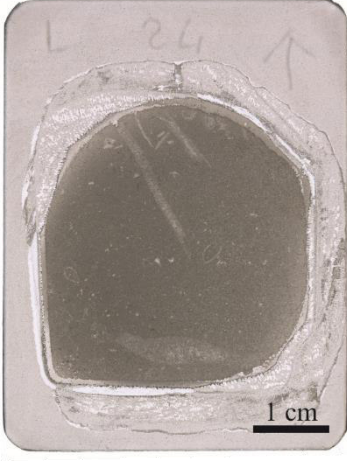|			
19	Da-19		**Skeletal components:** rare undefined bioclasts, rare small foraminifera, rare ?*Rivularia*-like structures, rare *Thaumatoporella parvovesiculifera* (fragments, irregular roundish specimens and daughter colonies forms) **Non-skeletal components:** rare undetermined peloids, common dark micritic clotted structures included dendritic forms **Matrix:** micrite/microsparite and sparite in restricted areas **Taphonomical characters:** high fragmentation, high abrasion, no bioerosion, low micritization, no encrustation **Lithology:** wackestone **Note: /**
20	Da-20		**Skeletal components:** rare undefined bioclasts, rare *Rivularia*-like structures, rare brachiopods, rare *Thaumatoporella parvovesiculifera* (fragments and irregular roundish specimens) **Non-skeletal components:** rare undetermined peloids, common dark micritic clotted structures **Matrix:** micrite/sparite in restricted areas **Taphonomical characters:** high fragmentation, high abrasion, no bioerosion, low micritization, no encrustation **Lithology:** wackestone-packstone **Note:** lithiotid shells
21	Da-21		**Skeletal components:** rare undefined bioclasts, rare *Rivularia*-like structures, rare *Thaumatoporella parvovesiculifera* (fragments and irregular roundish specimens) **Non-skeletal components:** rare undetermined peloids, rare dark micritic clotted structures **Matrix:** micrite/sparite in restricted areas **Taphonomical characters:** high fragmentation, high abrasion, no bioerosion, low micritization, no encrustation **Lithology:** wackestone-packstone **Note:** lithiotid shells

22	Da-22		**Skeletal components:** rare undefined bioclasts, rare brachiopods, rare *Thaumatoporella parvovesiculifera* (fragments) **Non-skeletal components:** rare undetermined peloids, rare dark micritic clotted structures **Matrix:** micrite **Taphonomical characters:** high fragmentation, high abrasion, low bioerosion, low micritization, no encrustation **Lithology:** wackestone **Note:** lithiotid shells
23	Da-23		**Skeletal components:** rare undefined bioclasts **Non-skeletal components:** rare undetermined peloids **Matrix:** micrite/microsparite/sparite in restricted areas **Taphonomical characters:** high fragmentation, high abrasion, no bioerosion, no micritization, no encrustation **Lithology:** wackestone-packstone **Note:** /
24	Da-24		**Skeletal components:** rare undefined bioclasts, rare ostracods, rare brachiopods included articulated specimens **Non-skeletal components:** rare undetermined peloids, rare dark micritic clotted structures **Matrix:** micrite/sparite in restricted areas **Taphonomical characters:** high fragmentation, high abrasion, low bioerosion, low micritization, no encrustation **Lithology:** wackestone-packstone **Note:** lithiotid shells

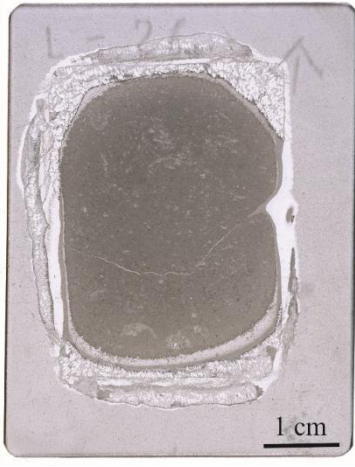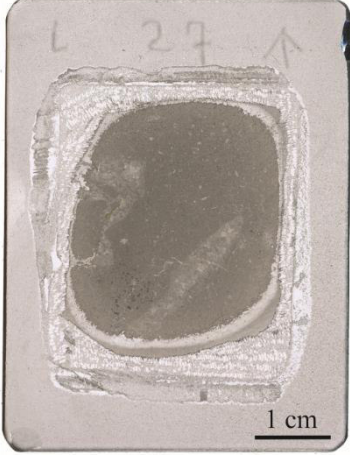| 25	Da-25		**Skeletal components:** rare undefined bioclasts, rare ostracods, rare brachiopods, rare gastropods, rare *Thaumatoporella parvovesiculifera* (fragments and irregular roundish specimens), one coral **Non-skeletal components:** rare microbial peloids **Matrix:** very fine-grained micrite **Taphonomical characters:** high fragmentation, high abrasion, low bioerosion, low micritization, no encrustation **Lithology:** floatstone-rudstone with wackestone matrix **Note:** lithiotid shell
26	Da-26		**Skeletal components:** rare undefined bioclasts, rare *Thaumatoporella parvovesiculifera* (fragments and cysts) **Non-skeletal components:** rare undetermined peloids, rare dark micritic clotted structures **Matrix:** micrite/sparite in restricted areas **Taphonomical characters:** high fragmentation, high abrasion, no bioerosion, no micritization, no encrustation **Lithology:** wackestone-packstone **Note: /**
27	Da-27		**Skeletal components:** rare undefined bioclasts **Non-skeletal components:** rare undetermined peloids, rare dark micritic clotted structures **Matrix:** micrite **Taphonomical characters:** high fragmentation, high abrasion, no bioerosion, low micritization, no encrustation **Lithology:** wackestone **Note:** lithiotid shell

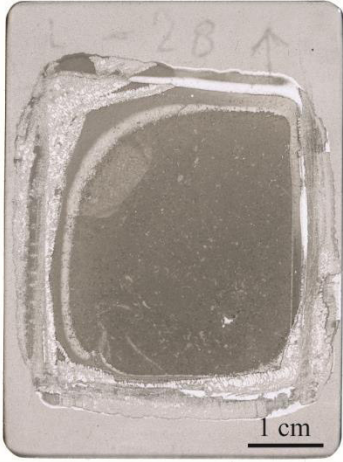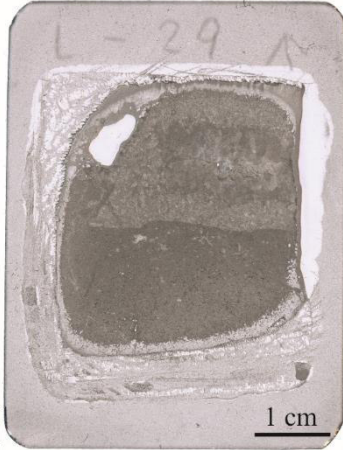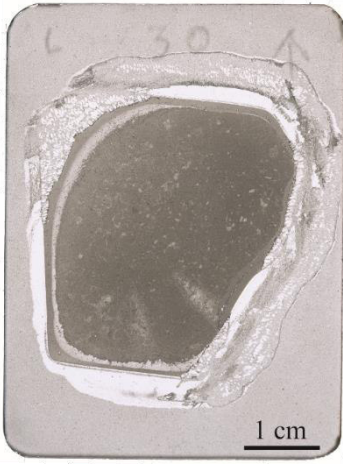| 28	Da-28		**Skeletal components:** rare undefined bioclasts, rare *Thaumatoporella parvovesiculifera* (fragments) **Non-skeletal components:** rare undetermined peloids **Matrix:** micrite **Taphonomical characters:** high fragmentation, high abrasion, no bioerosion, low micritization, no encrustation **Lithology:** wackestone **Note:** lithiotid shell
29	Da-29		**Skeletal components:** rare undefined bioclasts **Non-skeletal components:** / **Matrix:** micrite **Taphonomical characters:** high fragmentation, high abrasion, no bioerosion, no micritization, no encrustation **Lithology:** wackestone **Note:** lithiotid shell
30	Da-30		**Skeletal components:** rare undefined bioclasts, rare ostracods, rare small foraminifera, rare brachiopods, rare *Thaumatoporella parvovesiculifera* (fragments and irregular roundish specimens) **Non-skeletal components:** rare undetermined peloids, rare dark micritic clotted structures **Matrix:** micrite/sparite **Taphonomical characters:** high fragmentation, high abrasion, no bioerosion, low micritization, no encrustation **Lithology:** wackestone-packstone **Note:** /

31	Da-31	 1 cm	**Skeletal components:** rare undefined bioclasts, rare *Thaumatoporella parvovesiculifera* (fragments) **Non-skeletal components:** rare undetermined peloids, rare dark micritic clotted structures **Matrix:** micrite **Taphonomical characters:** high fragmentation, high abrasion, low bioerosion, low micritization, low encrustation **Lithology:** wackestone **Note:** lithiotid shell
32	Da-32	 1 cm	**Skeletal components:** rare undefined bioclasts, rare small foraminifera, rare brachiopods, rare *Thaumatoporella parvovesiculifera* (fragments and irregular roundish specimens) **Non-skeletal components:** common undetermined peloids, common dark micritic clotted structures included dendritic forms **Matrix:** micrite/sparite in restricted area **Taphonomical characters:** high fragmentation, high abrasion, no bioerosion, low micritization, low encrustation **Lithology:** wackestone-packstone **Note: /**
33	Da-33	 1 cm	**Skeletal components:** rare undefined bioclasts, rare brachiopods, rare *Thaumatoporella parvovesiculifera* (fragments and irregular roundish specimens) **Non-skeletal components:** rare undetermined peloids, rare dark micritic clotted structures included dendritic forms **Matrix:** micrite **Taphonomical characters:** high fragmentation, high abrasion, no bioerosion, low micritization, no encrustation **Lithology:** wackestone **Note: /**

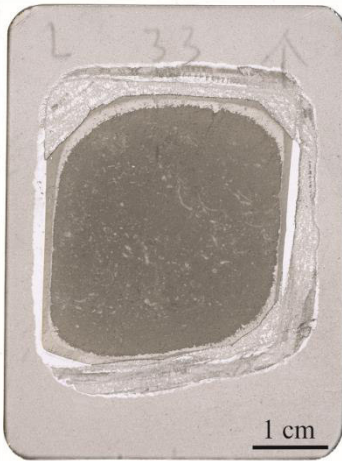| 34	Da-34		**Skeletal components:** rare undefined bioclasts, rare *Thaumatoporella parvovesiculifera* (fragments), rare brachiopods **Non-skeletal components:** rare undetermined peloids, rare dark micritic clotted structures included dendritic forms **Matrix:** micrite/sparite **Taphonomical characters:** high fragmentation, high abrasion, no bioerosion, low micritization, no encrustation **Lithology:** wackestone-packstone **Note: /**
35	Da-35		**Skeletal components:** rare undefined bioclasts, rare gastropods, rare *Thaumatoporella parvovesiculifera* (fragments) **Non-skeletal components:** common peloids, rare microbial peloids, rare dark micritic clotted structures **Matrix:** very fine-grained micrite/micrite **Taphonomical characters:** high fragmentation, high abrasion, low bioerosion, low micritization, low encrustation **Lithology:** wackestone **Note:** lithiotid shells

Semi-quantitative analysis of components: (absent), rare, common, abundant
Semi-quantitative analysis of taphonomic features: no, low, moderate, high
* "bivalves" are referred to non-lithiotid bivalves
/: absent

239
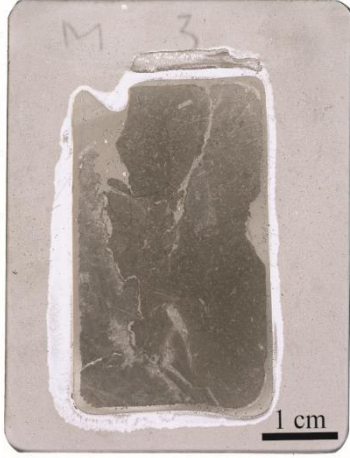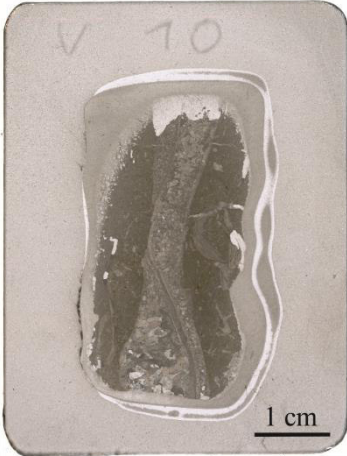
A.15. Passo Vezzena accumulations (Ve)
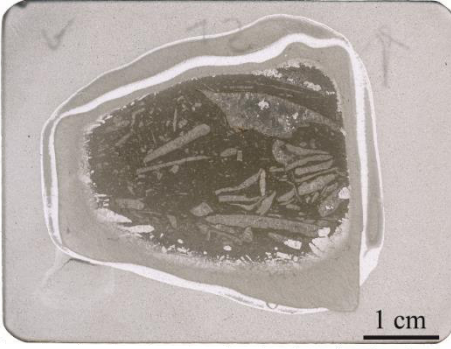
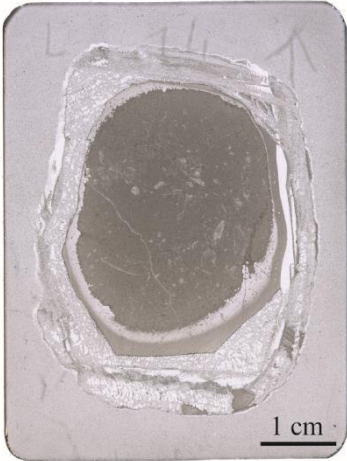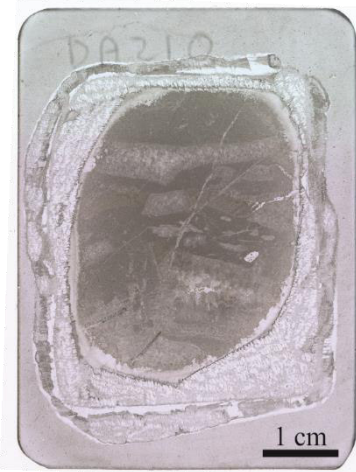| No.	Sample	Thin section	Description
1	Ve1-1	1 cm	**Skeletal components:** abundant undefined bioclasts, rare echinoderms, rare brachiopods, rare bivalves*, rare small foraminifera included valvulinids, textulariids, ?*Meandrovoluta asiagoensis*, *Glomospira*/*Planiinvoluta* spp., ?*Duotaxis metula* and ?*Ammobaculites* sp., rare larger foraminifera included ?*Amijiella amiji* or ?*Haurania deserta* **Non-skeletal components:** common undetermined peloids, rare pelletoids, rare fecal pellets, common cortoids with constructive and destructive envelope, rare dark micritic clotted structures **Matrix:** micrite/sparite **Taphonomical characters:** high fragmentation, high abrasion, low bioerosion, moderate micritization, moderate encrustation **Lithology:** packstone – grainstone **Note:** /
2	Ve1-2	1 cm	**Skeletal components:** rare undefined bioclasts, rare ostracods, rare brachiopods, rare small foraminifera **Non-skeletal components:** rare undetermined peloids **Matrix:** micrite **Taphonomical characters:** high fragmentation, moderate abrasion, low bioerosion, no micritization, no encrustation **Lithology:** floatstone with mudstone matrix **Note:** lithiotid shells, stilolaminated fabric

3	Ve1-3		**Skeletal components:** rare undefined bioclasts, rare ostracods, rare brachiopods, rare small foraminifera included valvulinids and textulariids, rare micritized ring-shaped bioclasts, rare larger foraminifera included ?*Pseudocyclammina liassica* and ?*Evertyciclammina* sp. **Non-skeletal components:** rare undetermined peloids, rare pelletoids, rare dark micritic clotted structures included dendritic forms **Matrix:** micrite/microsparite **Taphonomical characters:** high fragmentation, high abrasion, no bioerosion, low micritization, no encrustation **Lithology:** wackestone – mudstone in restricted areas **Note:** lithiotid shells, bioturbation traces
4	Ve2-4		**Skeletal components:** rare undefined bioclasts, rare ostracods, rare micritized ring-shaped bioclasts, rare small foraminifera included ?valvulinids **Non-skeletal components:** rare dark micritic clotted structure (included one big dendritic form) **Matrix:** micrite **Taphonomical characters:** high fragmentation, high abrasion, no bioerosion, no micritization, no encrustation **Lithology:** mudstone **Note:** lithiotid shell
5	Ve2-5		**Skeletal components:** rare undefined bioclasts, rare micritized ring-shaped bioclasts, rare small foraminifera **Non-skeletal components:** rare undetermined peloids, rare dark micritic clotted structures **Matrix:** micrite **Taphonomical characters:** high fragmentation, high abrasion, no bioerosion, no micritization, no encrustation **Lithology:** mudstone – wackestone

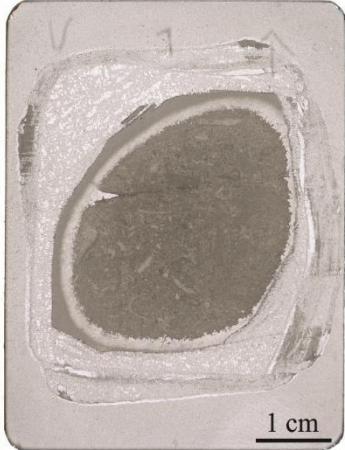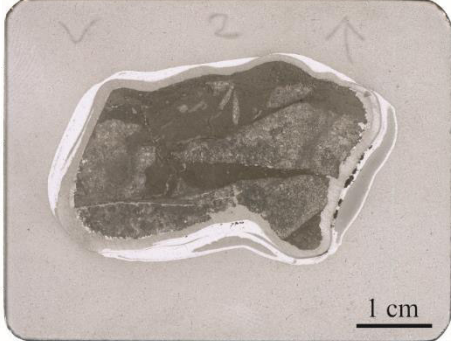|			
			Note: lithiotid shells, stilolaminated fabric
6	Ve2-6		**Skeletal components:** rare undefined bioclasts, rare micritized ring-shaped bioclasts, rare small foraminifera included valvulinids **Non-skeletal components:** rare undetermined peloids, rare dark micritic clotted structures **Matrix:** micrite/microsparite in restricted areas **Taphonomical characters:** high fragmentation, high abrasion, no bioerosion, no micritization, no encrustation **Lithology:** mudstone **Note:** lithiotid shells
7	Ve2-14		**Skeletal components:** rare undefined bioclasts, rare *Palaeodasycladus* sp., rare micritized ring-shaped bioclasts, rare small foraminifera **Non-skeletal components:** rare cortoids with destructive and constructive envelope **Matrix:** micrite/microsparite in restricted areas **Taphonomical characters:** high fragmentation, moderate abrasion, low bioerosion, low micritization, low encrustation **Lithology:** wackestone **Note:** lithiotid shells
8	Ve3-7		**Skeletal components:** rare undefined bioclasts, rare ostracods, rare small foraminifera **Non-skeletal components:** rare undetermined peloids, rare dark micritic clotted structures **Matrix:** micrite/sparite **Taphonomical characters:** high fragmentation, high abrasion, no bioerosion, no micritization, no encrustation **Lithology:** wackestone – packstone **Note:** lithiotid shells, stilolaminated fabric

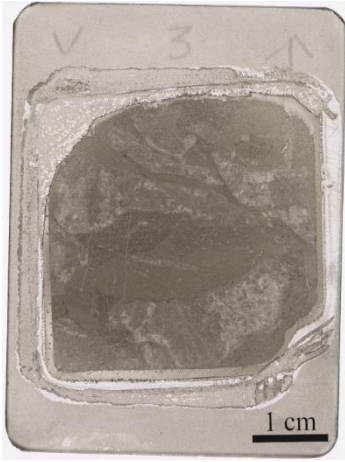|			
9	Ve3-8		**Skeletal components:** rare undefined bioclasts, rare small foraminifera included *Duotaxis metula*, ?*Meandrovoluta asiagoensis* and valvulinids, rare micritized ring-shaped bioclasts, rare encrusted organisms (foraminifera?), rare ostracods **Non-skeletal components:** rare undetermined peloids, rare fecal pellets (?) **Matrix:** micrite/sparite **Taphonomical characters:** high fragmentation, high abrasion, no bioerosion, no micritization, low encrustation **Lithology:** packstone – wackestone **Note:** lithiotid shells, concavo-convex contacts, bioturbation traces
10	Ve3-15/1		**Skeletal components:** rare undefined bioclasts, rare gastropods, rare ostracods, rare small foraminifera included ?*Duotaxis metula,* textulariids and ?*Meandrovoluta asiagoensis*, rare ?*Earlandia* sp., rare micritized ring-shaped bioclasts, rare encrusted organisms (foraminifera?), rare *Rivularia*-like organisms **Non-skeletal components:** rare undetermined peloids, rare pelletoids, rare cortoids with destructive envelope, rare dark micritic clotted structures included dendritic forms **Matrix:** micrite/microsparite **Taphonomical characters:** high fragmentation, high abrasion, no bioerosion, no micritization, low encrustation **Lithology:** wackestone **Note:** /

11	Ve3-15/2		**Skeletal components:** rare undefined bioclasts, rare brachiopods, rare ostracods, rare small foraminifera included ?*Meandrovoluta asiagoensis*, ?*Duotaxis metula* and valvulinids, rare micritized ring-shaped bioclasts **Non-skeletal components:** rare undetermined peloids, common dark micritic clotted structures **Matrix:** micrite **Taphonomical characters:** high fragmentation, moderate abrasion, no bioerosion, no micritization, no encrustation **Lithology:** wackestone **Note:** lithiotid shells
12	Ve4-9		**Skeletal components:** rare undefined bioclasts **Non-skeletal components:** common undetermined peloids, rare fecal pellets (isolated and aggregates) **Matrix:** micrite/microsparite in restricted areas **Taphonomical characters:** high fragmentation, high abrasion, no bioerosion, no micritization, no encrustation **Lithology:** wackestone – mudstone in a restricted area **Note:** lithiotid shells, bioturbation traces
13	Ve4-10		**Skeletal components:** rare undefined bioclasts, rare brachiopods **Non-skeletal components:** / **Matrix:** micrite **Taphonomical characters:** high fragmentation, high abrasion, low bioerosion, no micritization, no encrustation **Lithology:** floatstone with wackestone matrix **Note:** lithiotid shells

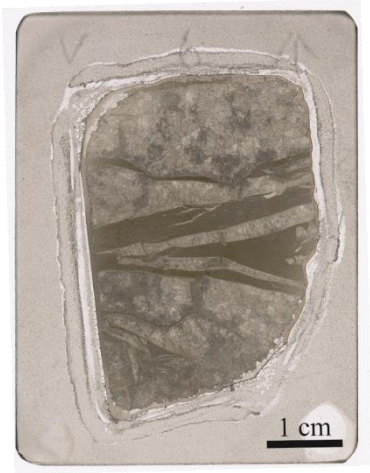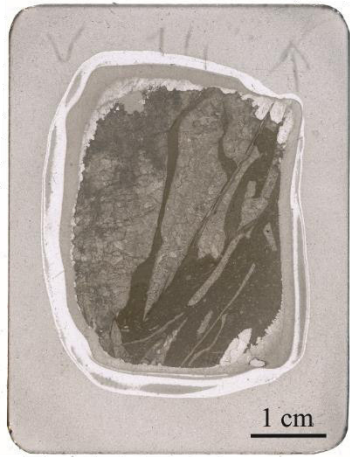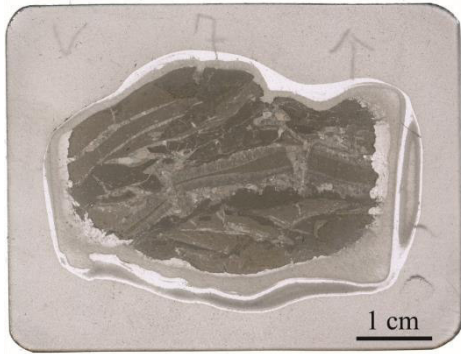|			
14	Ve4-11		**Skeletal components:** rare undefined bioclasts, rare ostracods **Non-skeletal components:** / **Matrix:** micrite (very dark in restricted areas) **Taphonomical characters:** high fragmentation, high abrasion, low bioerosion, low micritization, low encrustation **Lithology:** floatstone – rudstone with wackestone matrix **Note:** lithiotid shells, concave-convex contacts, bioturbation traces
15	Ve4-12		**Skeletal components:** rare undefined bioclasts **Non-skeletal components:** rare undetermined peloids **Matrix:** micrite **Taphonomical characters:** high fragmentation, high abrasion, no bioerosion, no micritization, no encrustation **Lithology:** wackestone **Note:** lithiotid shells, concave-convex/sutured contacts
16	Ve4-13		**Skeletal components:** rare undefined bioclasts **Non-skeletal components:** / **Matrix:** micrite **Taphonomical characters:** high fragmentation, moderate abrasion, low bioerosion, no micritization, no encrustation **Lithology:** floatstone **Note:** lithiotid shells

Semi-quantitative analysis of components: (absent), rare, common, abundant
Semi-quantitative analysis of taphonomic features: no, low, moderate, high
* "bivalves" are referred to non-lithiotid bivalves
/: absent

Appendix B

B.1. The analysed taxa

Taxon	Specimen ID	Sclerochronology	Diagenetic screening			Isotopic Analysis
			SEM	XRD	CL	$\delta^{13}C$ and $\delta^{18}O$
Lithiotis problematica	LT1	**x**				
	LT2	x				
	LT3	x				
	LT6	x	x	x	x	x
	LT7	x	x	x	x	x
Lithioperna scutata	LP1	x				
	LP2	x				
	LP3	x	x	x	x	x
	LP4	x				
Cochlearites loppianus	CO1	x	x	x	x	x
	CO2	x	x	x	x	x
	CO3	x				
Opisoma excavatum	O1		x	x	x	x
Pachyrisma (Durga) crassa	P1	x	x	x	x	x
	P2	x				

Table 1. List of the studied bivalve specimens for geochemical and sclerochronological analyses. The evaluation of growth pattern in the shell surface was conducted on several specimens deposited in the "Piero Leonardi" Museum at the University of Ferrara. They are not reported in this table.
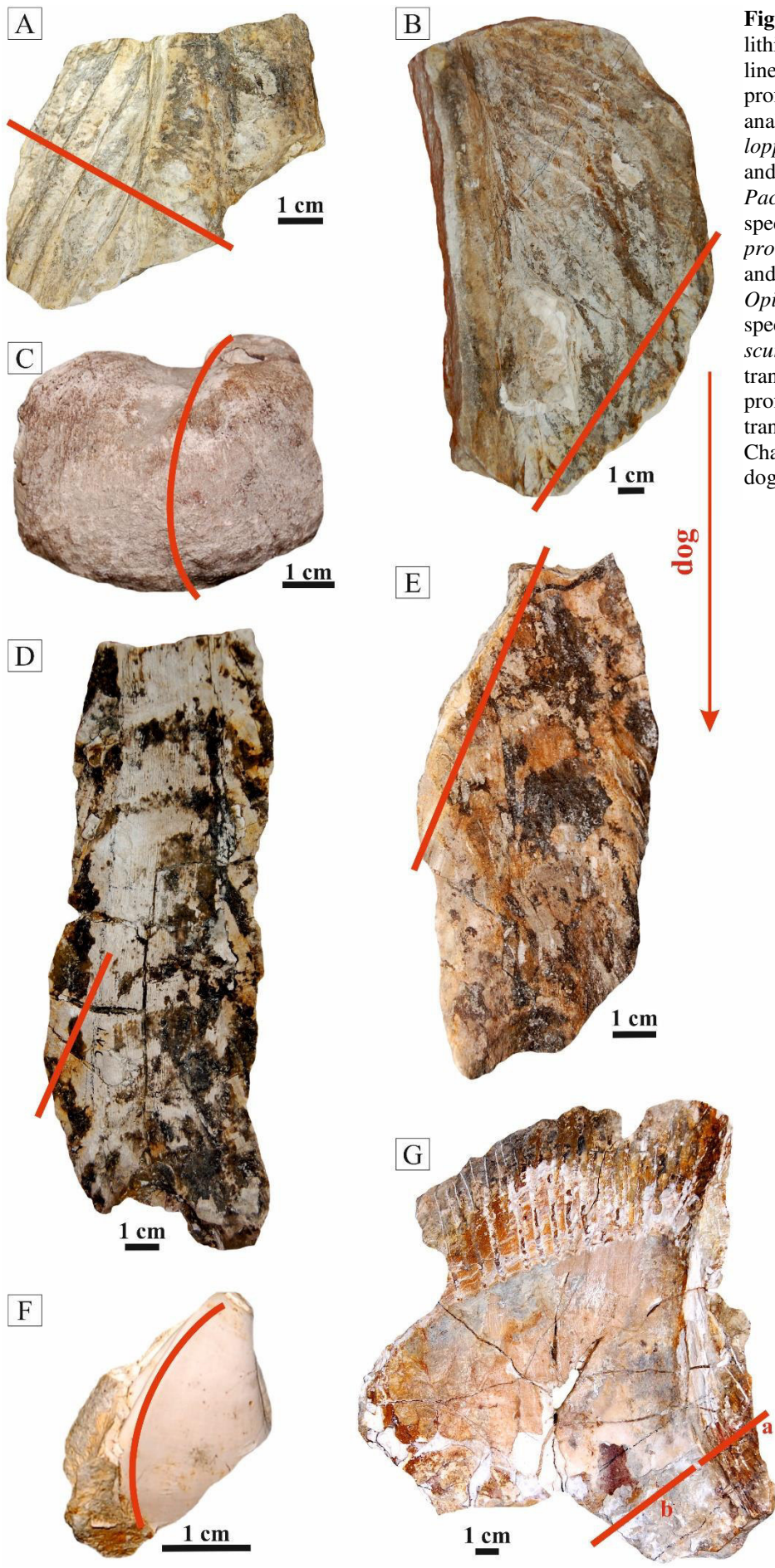
Figure 1. Main analysed lithiotid bivalves. The red lines indicate the cutting profiles used for geochemical analyses. A, B) *Cochlearites loppianus*, specimen CO1 and CO2, respectively. C) *Pachyrisma* (*Durga*) *crassa*, specimen P1. D, E) *Lithiotis problematica*, specimen LT6 and LT7, respectively. F) *Opisoma excavatum*, specimen O1. G) *Lithioperna scutata,* specimen LP3. The *a* transect is referred to wing profile while *b* is the nearly transversal section (see Chapter 5 for further details). dog, direction of growth.

248
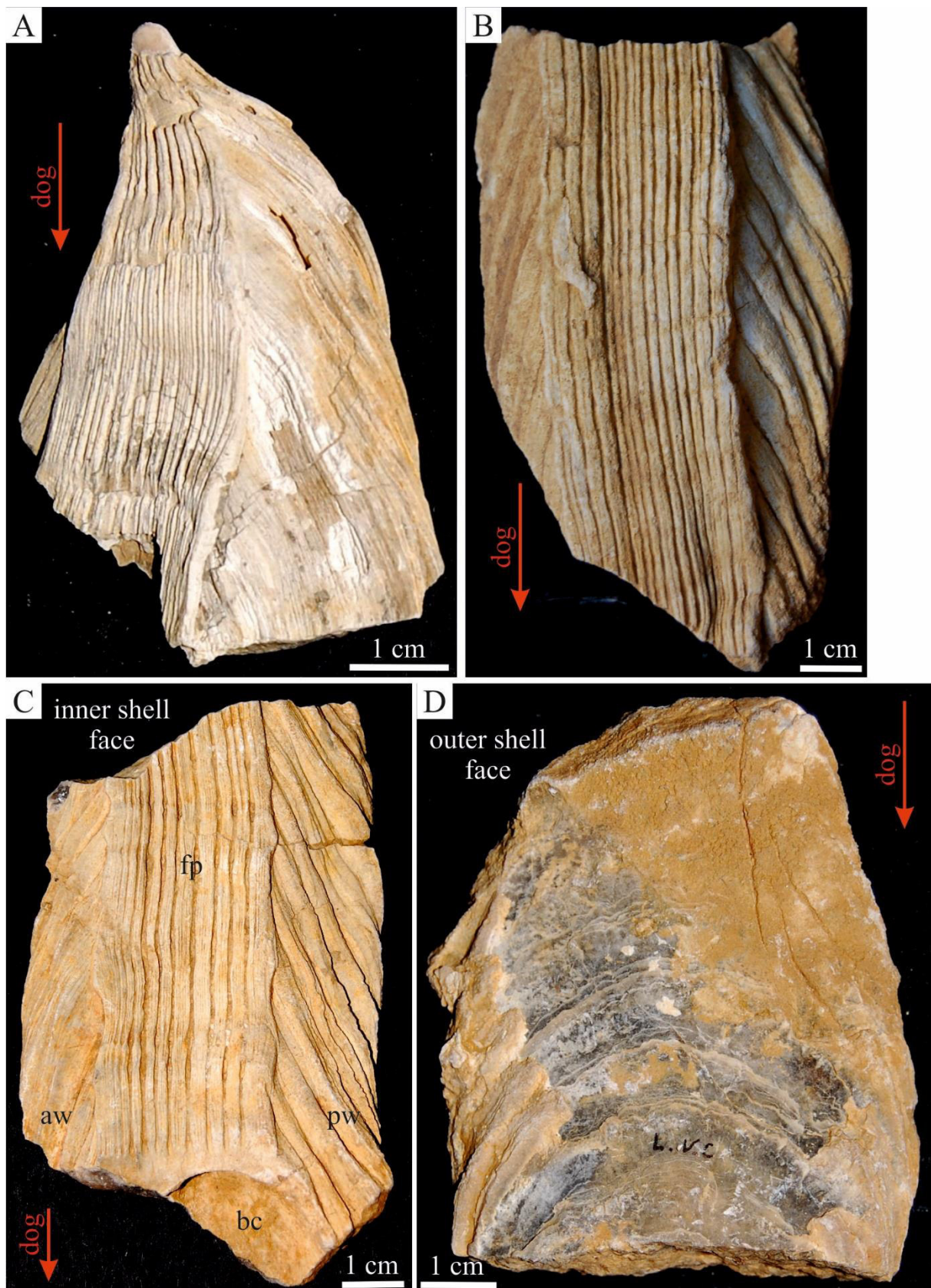
Figure 2. Some of the studied *Lithiotis problematica* specimens. The growth pattern in the anterior and posterior wings are particularly well detectable (A, B, C). Rarely, growth lines are also recognizable in the outer shell surface (D). aw, anterior wing; pw, posterior wing; fp, furrowed plate (also called central platform; see Chinzei, 1982); bc, body cavity; dog, direction of growth.
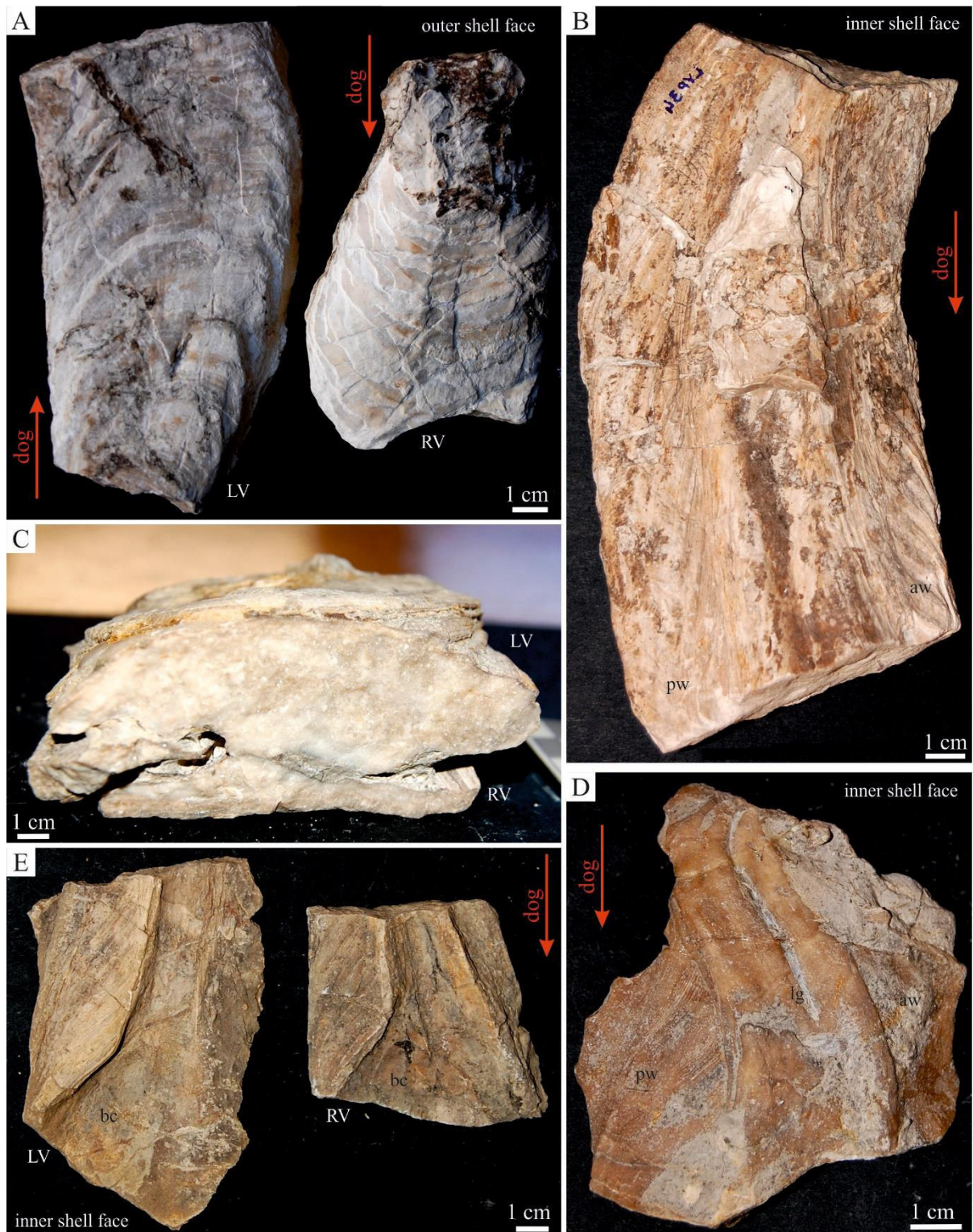
Figure 3. Some of the studied *Cochlearites loppianus* specimens. A) Articulated specimen, outer shell surface. Rarely, growth lines are also recognizable in the outer shell surface. The valve orientation is opposite. Note the growth pattern in the anterior and posterior wings (B, D, E). C) Articulated individual; transverse section. Note the different valve thickness. aw, anterior wing; pw, posterior wing; lg, ligamental groove (in the central platform; see Chinzei, 1982 for further details); bs, body space; rv, right valve; lv, left valve; dog, direction of growth.
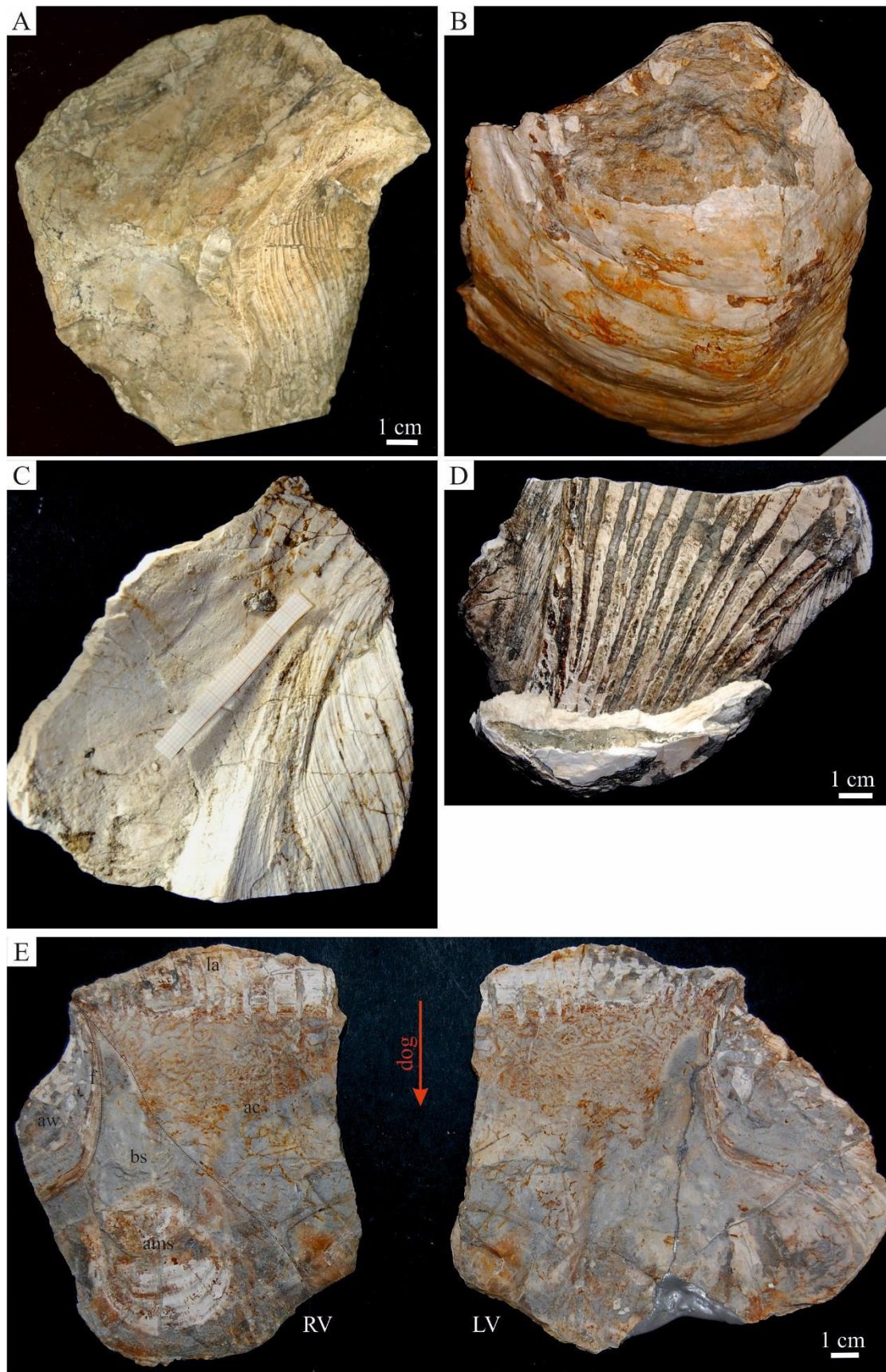
Figure 4. Photographs of some of the *Lithioperna scutata* specimens showing the highly variability in the feather-like wings (A–E). Well-development ligamental area (F). RV, right valve; LV, left valve; la, ligamental area; ams, adductor muscle scar; bs, body space; ac, area of contact; dog, direction of growth.
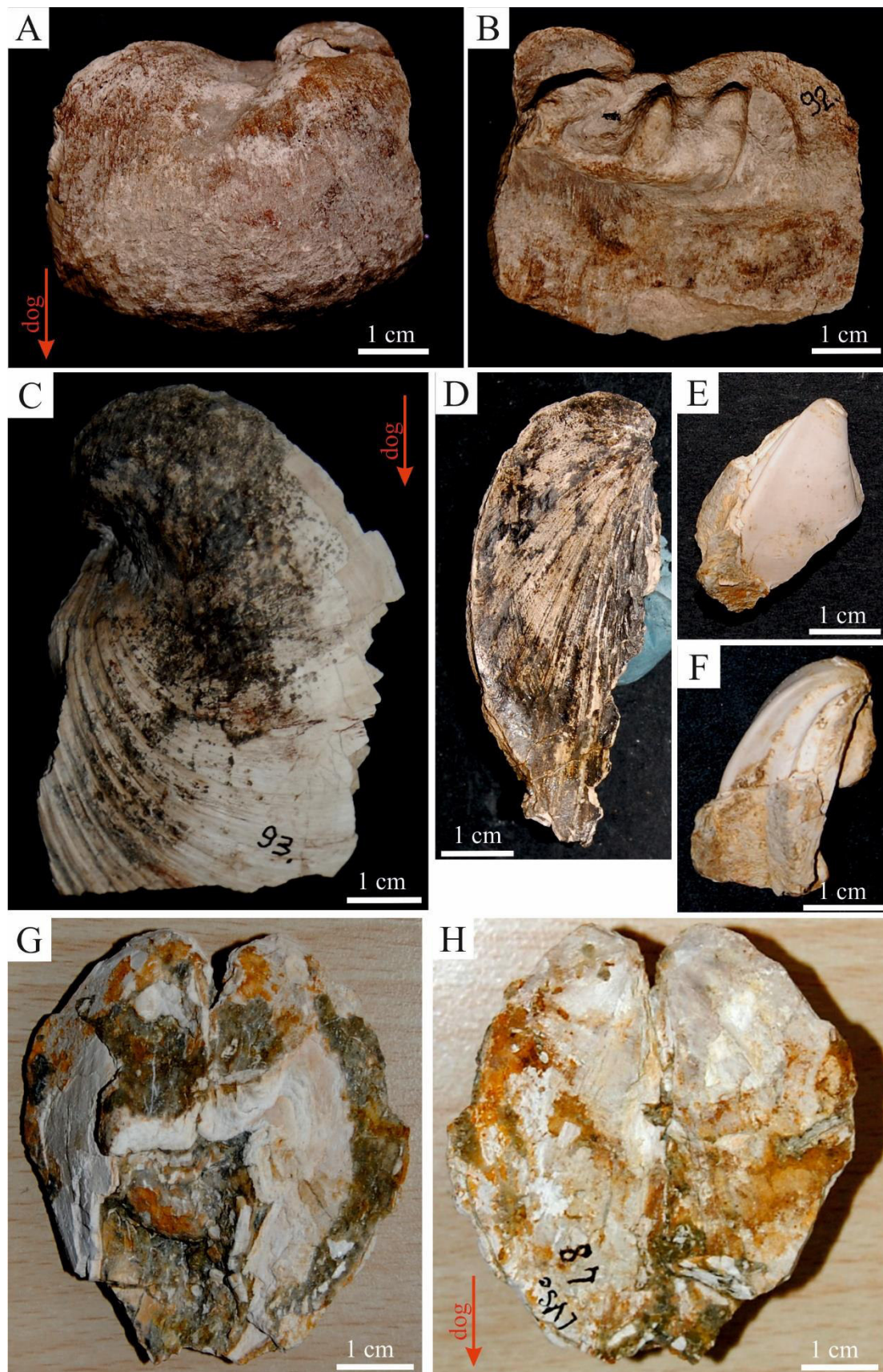
Figure 5. A, B, C) *Pachyrisma* (*Durga*) *crassa*. A) Outer shell view. B) Inner shell view. C) Weakly growth lines recognizable in the outer shell surface. D–H) *Opisoma excavatum*. D) Note the weakly growth lines recognizable in the outer shell surface. E, F) The analysed specimen O1. G, H) Articulated individual, apical and basal shell views, respectively. dog, direction of growth.

252

B.2. SEM results

Scanning electron microscope images showing the ultrastructure of the studied bivalve shells.
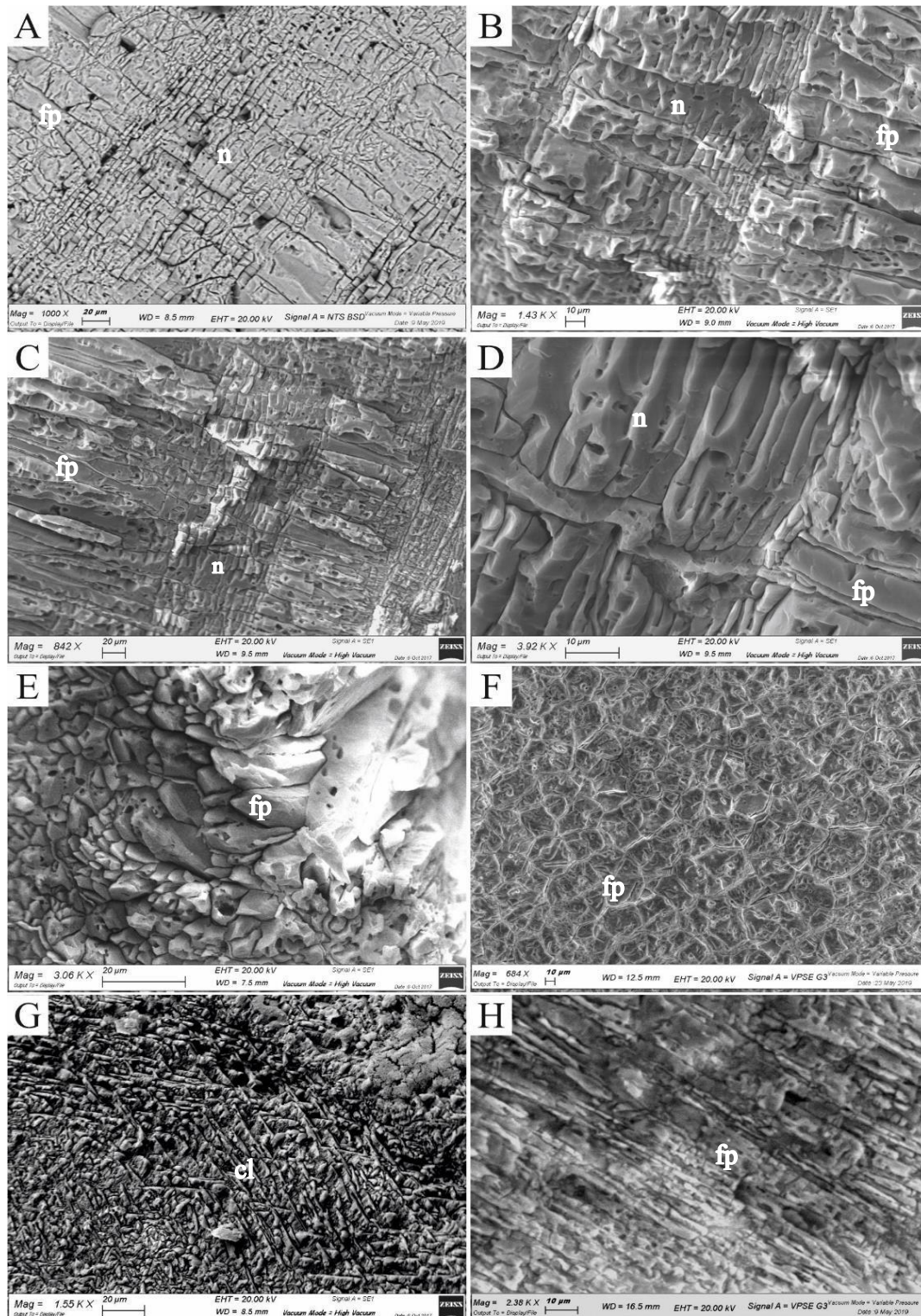
Figure 1. A–F) *Lithioperna scutata*, specimen LP3. Aragonitic irregular fibrous prismatic layer and nacreous sublayers. D) Detail of the previous nacreous alternations. E, F) Oblique and sub-horizontal sections of irregular fibrous prismatic layer. G) *Opisoma excavatum*, specimen O1. Aragonitic cross-lamellar microstructure. H) *Lithiotis problematica*, specimen LT1. Aragonitic irregular fibrous prismatic layer occurring in the inner surface of the feather-like wings (longitudinal section). fp, fibrous prismatic; cl, cross-lamellar; n, nacre. See Chapter 5 for further details.

253
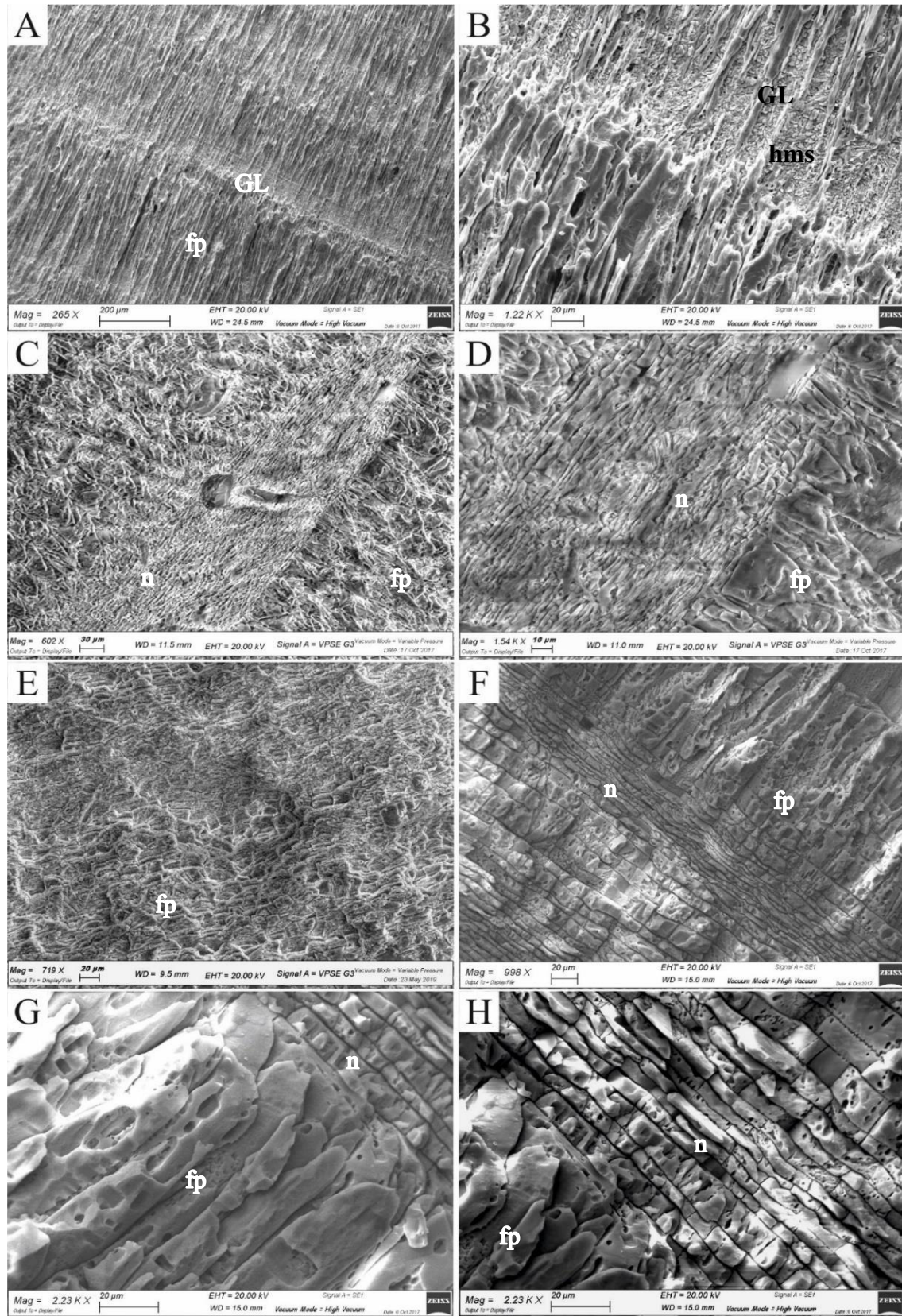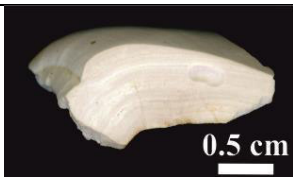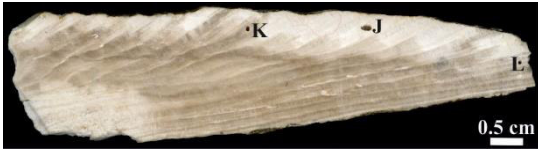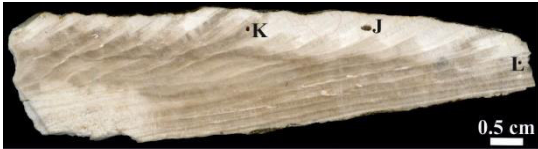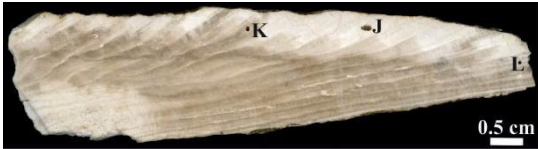
Figure 2. A, B) *Pachyrisma* (*Durga*) *crassa*, specimen P1. Inner irregular fibrous prismatic layer with growth increments highlighted by changes in size and shape of aragonitic crystals (homogeneous microstructure). C–E) *Cochlearites loppianus*, specimen CO2. C, D) Well-defined nacreous layer intercalated in the aragonitic irregular fibrous prismatic layer. E) Oblique/sub-transversal section of the nacreous layer. F–H) *Cochlearites loppianus*, specimen CO1. F) Nacreous and aragonitic irregular fibrous prismatic layers. G) Aragonitic irregular fibrous prismatic layer occurring in the inner surface of the feather-like wings (longitudinal section). H) Well-defined nacreous layer intercalated in the aragonitic irregular fibrous prismatic layer. fp, fibrous prismatic; n, nacre; hms, homogeneous microstructure; GL, growth line. See Chapter 5 for further details.

B.3. XRD results

XRD results and relatives diffractograms of the studied bivalve specimens. See Chapter 5 for further details.

Taxon	Specimen		Sampled area and respective spectrum	Results
Lithioperna scutata	LP3		White area (Fig. A)	Aragonite and calcite (ca. 23%)
			Brownish area (Fig. B)	Calcite (ca. 85%) and aragonite
			White area (Fig. C)	Aragonite
Opisoma excavatum	O1		Only one sample (Fig. D)	Aragonite
Lithiotis problematica	LT6		White area (Fig. E)	Aragonite and calcite (ca. 27%)
			Brownish area (Fig. F)	Calcite
	LT7		White area (Fig. G)	Aragonite and calcite (ca. 34%)
			Brownish area (Fig. H)	Calcite
Pachyrisma (*Durga*) *crassa*	P1		Only one sample (Fig. I)	Aragonite
Cochlearites loppianus	CO1		White area (Fig. J)	Aragonite
			Brownish area (Fig. K)	Calcite
			Brownish-white banded area	Calcite

		(Fig. L)	
CO2		White area (Fig. M)	Aragonite
		Brownish area (Fig. N)	Calcite

Table 1. X-ray results of the studied specimens used for isotope analysis. For each analysed specimen the sampled area was reported. When aragonite and calcite occur together, the percentage of the two mineralogical phases is calculated considering the area of mean peaks.
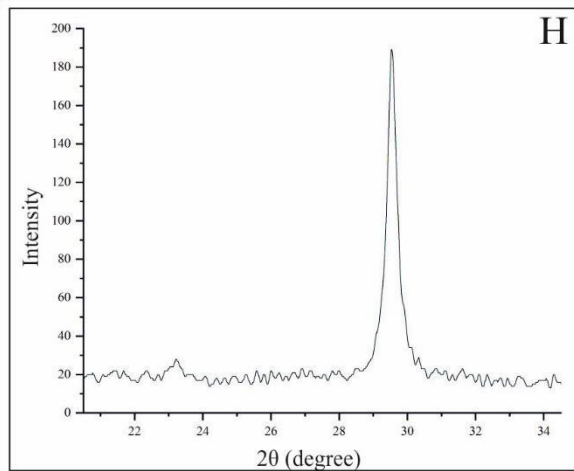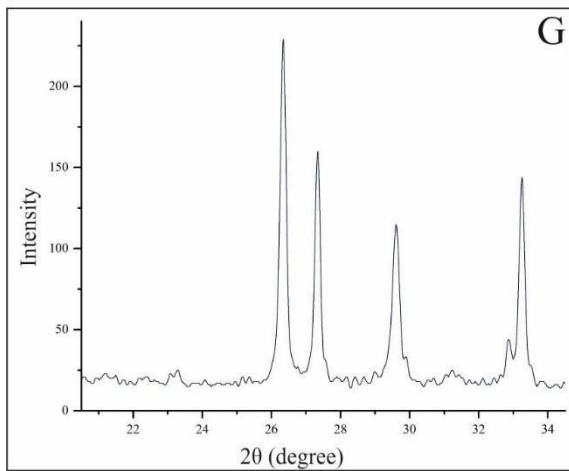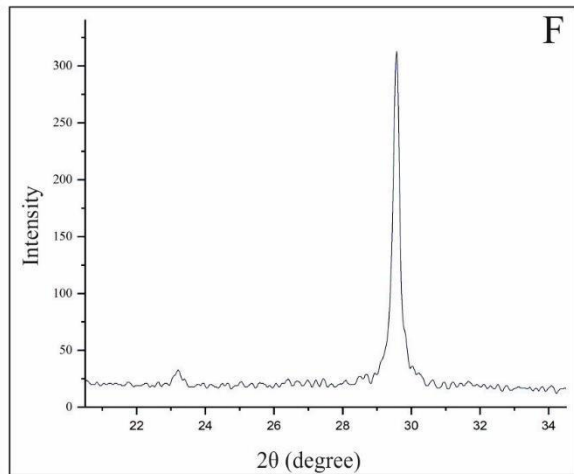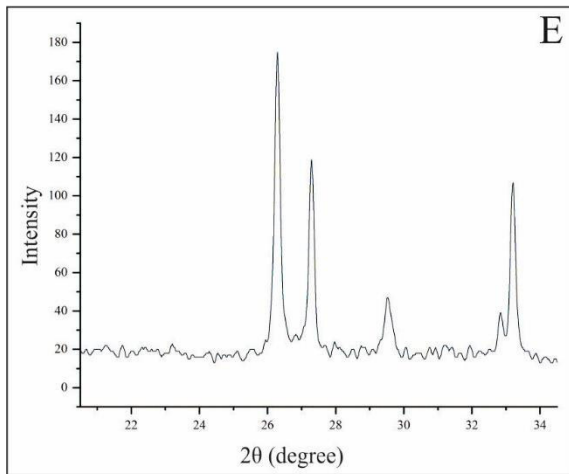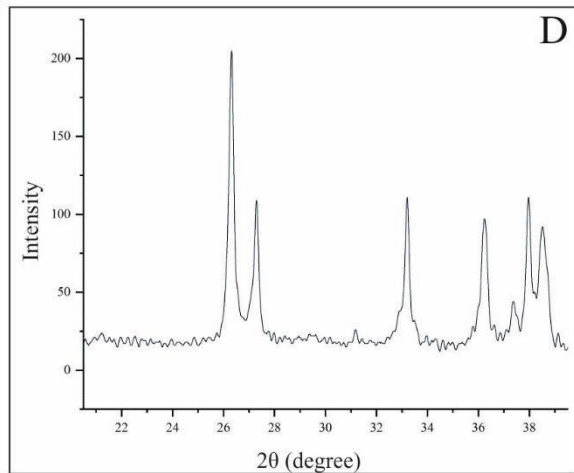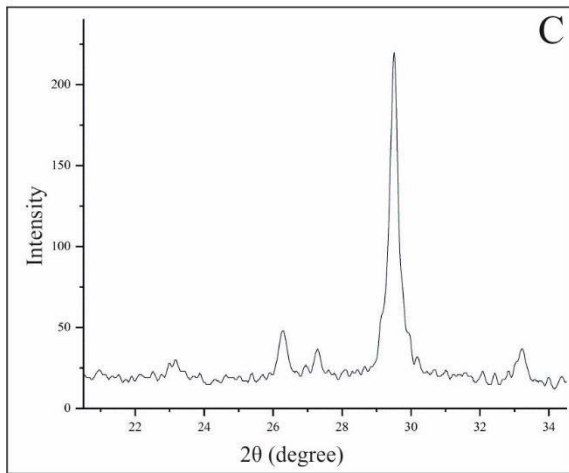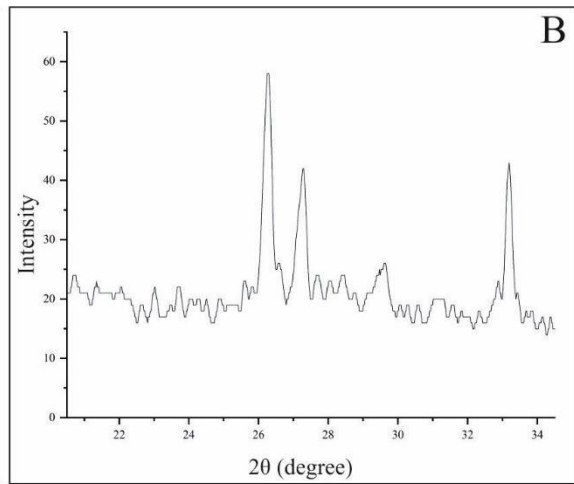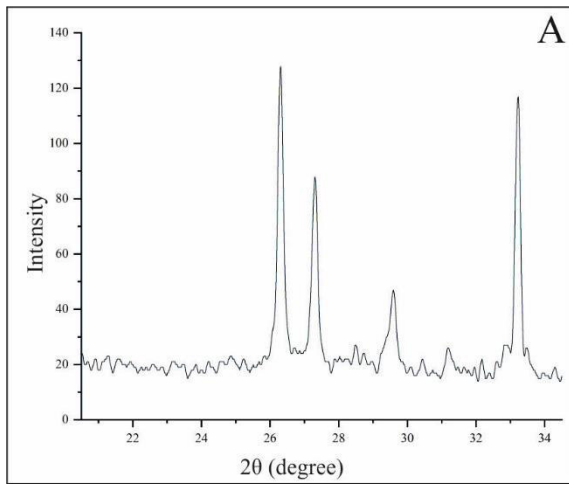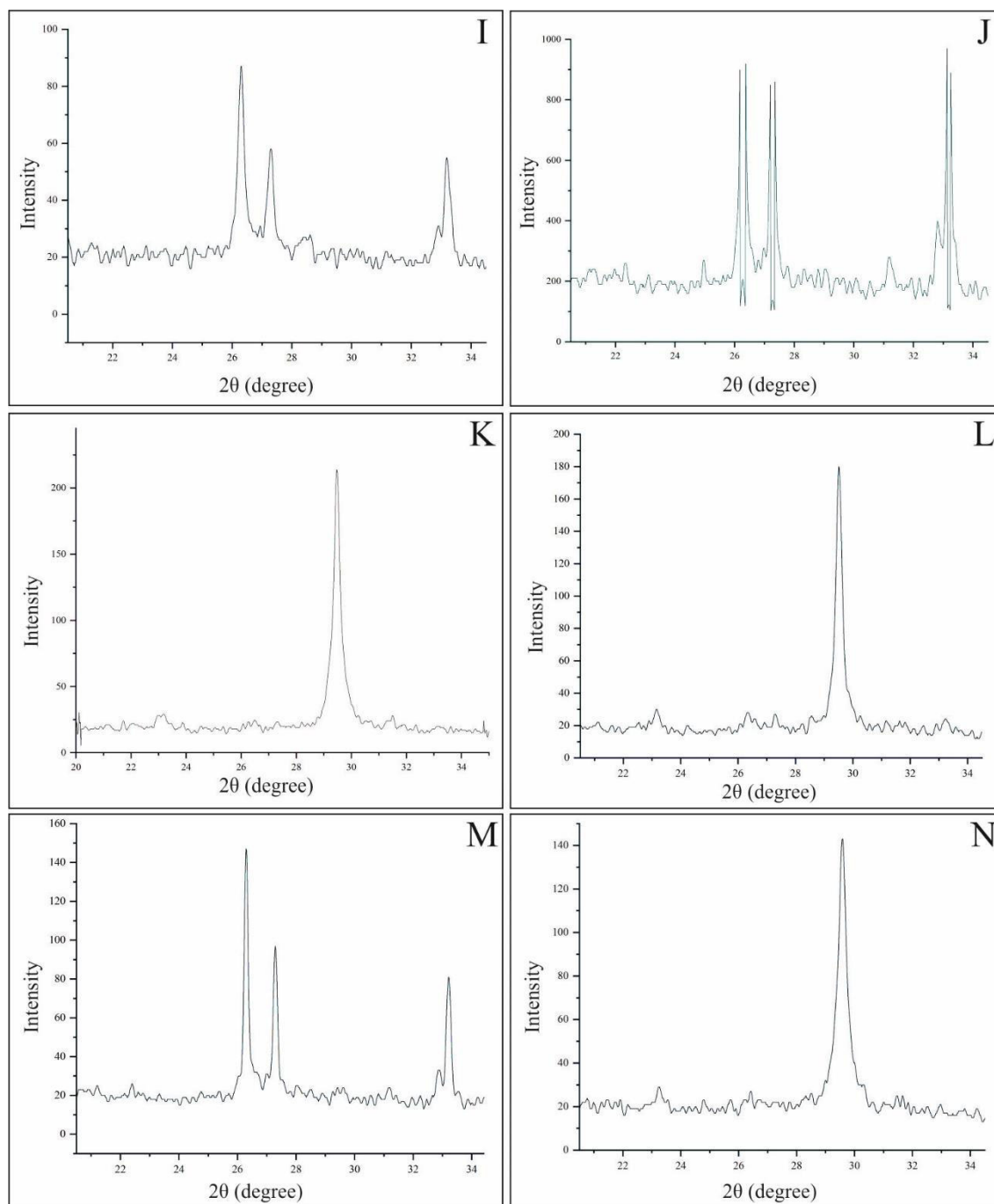
Figure 1. A–C) *Lithioperna scutata*, specimen LP3. D) *Opisoma excavatum*, specimen O1. E, F) *Lithiotis problematica*, specimen LT6. G, H) *Lithiotis problematica*, specimen LT7. I) *Pachyrisma* (*Durga*) *crassa*, specimen P1. J–L) *Cochlearites loppianus*, specimen CO1. M, N) *Cochlearites loppianus*, specimen CO2. The characteristics peaks for aragonite are: 26.2 > 27.2 > 33.1 > 37.8, 36.1, 38.4. Calcite peaks are: 29.4 > 36.0, 23.0, 39.3 > 31.3.

B.4. $\delta^{13}C$ and $\delta^{18}O$ results and inferred paleotemperatures

Stable oxygen and carbon isotope values of the studied bivalves with the inferred paleotemperatures calculated for three $\delta^{18}O_{water}$ values (VSMOW): -1‰ (according to Shackleton and Kennett, 1975), -1.2‰ (according to Martin-Garin et al., 2010) and 0‰ using the equation of Grossman and Ku (1986) for "all skeletal data" with a scale correction of -0.27‰ (Dettman et al., 1999). In the specimens LT1, LT2, CO1 and CO2 the bold and underlined values indicate lower oxygen isotope value (<-4‰) which should not be considered in the final analysis of paleotemperatures (due to influence of diagenesis). The reported paleotemperatures were calculated considering normal marine salinity conditions (see Chapter 5 for further details).

Lithioperna scutata (specimen LP3a - wing profile)

No.	Sample	Distance (mm)	$\delta^{13}C$ (‰ VPDB)	$\delta^{18}O$ (‰ VPDB)	Temperature calculated for $\delta^{18}O$		
					-1	-1.2	0
1	LP-B1	0	5.41	-0.97	19.3	18.4	23.9
2	LP-B2	0.44	5.21	-1.60	22.0	21.2	26.7
3	LP-B3	0.93	4.98	-1.63	22.2	21.3	26.8
4	LP-B4	1.73	5.26	-1.37	21.0	20.2	25.7
5	LP-B5	2.30	5.75	-1.27	20.6	19.8	25.3
6	LP-B6	2.90	4.96	-1.96	23.6	22.7	28.2
7	LP-B7	3.36	5.25	-1.61	22.1	21.2	26.7
8	LP-B8	3.93	4.98	-2.06	24.0	23.2	28.7
9	LP-B9	4.18	4.93	-1.60	22.0	21.2	26.7
10	LP-B10	4.59	5.84	-1.02	19.5	18.7	24.2
11	LP-B12	5.55	6.21	0.09	14.7	13.8	19.3
12	LP-B13	6.14	5.39	-0.89	19.0	18.1	23.6
13	LP-B14	6.68	5.86	-0.55	17.5	16.6	22.1
14	LP-B15	6.95	5.17	-1.15	20.1	19.2	24.7
15	LP-B16	7.47	5.14	-1.31	20.8	19.9	25.4
16	LP-B17	7.99	5.88	-0.38	16.7	15.9	21.4
17	LP-B18	8.55	5.23	-1.43	21.3	20.4	26.0
18	LP-B19	9.07	5.31	-1.92	23.4	22.6	28.1
19	LP-B20	9.75	5.21	-1.92	23.4	22.5	28.1
20	LP-B21	10.18	5.33	-1.30	20.7	19.9	25.4
21	LP-B22	10.49	5.47	-1.17	20.2	19.3	24.8
22	LP-B24	12.27	5.76	-1.29	20.7	19.8	25.3
23	LP-B25	13.01	5.72	-1.02	19.5	18.7	24.2
24	LP-B26	13.71	4.97	-2.01	23.8	23.0	28.5

No.	Sample	Distance (mm)	δ¹³C	δ¹⁸O			
25	LP-B27	14.77	5.01	-1.79	22.9	22.0	27.5

Average		5.37	-1.33	20.8	20.0	25.5
Minimum		4.93	-2.06	14.7	13.8	19.3
Maximum		6.21	0.09	24.0	23.2	28.7
Standard Deviation		0.35	0.53	2.3	2.3	2.3

Lithioperna scutata (specimen LP3b - nearly transversal profile)

No.	Sample	Distance (mm)	δ¹³C (‰ VPDB)	δ¹⁸O (‰ VPDB)	Temperature calculated for δ¹⁸O		
					-1	-1.2	0
1	LP-A1	0	5.18	-1.19	20.2	19.4	24.9
2	LP-A2	0.30	6.36	-0.46	17.1	16.2	21.7
3	LP-A3	0.61	5.97	-0.94	19.2	18.3	23.8
4	LP-A4	1.19	6.08	-1.12	19.9	19.1	24.6
5	LP-A5	1.80	5.22	-1.68	22.4	21.5	27.0
6	LP-A6	2.28	5.02	-1.43	21.3	20.4	25.9
7	LP-A7	2.92	5.72	-0.86	18.8	18.0	23.5
8	LP-A8	3.30	5.17	-1.26	20.6	19.7	25.2
9	LP-A9	3.62	5.28	-1.63	22.1	21.3	26.8
10	LP-A10	4.16	5.72	-0.78	18.5	17.6	23.1
11	LP-A11	4.79	5.83	-0.99	19.4	18.5	24.0
12	LP-A12	5.40	5.65	-0.79	18.5	17.6	23.2
13	LP-A13	5.99	5.23	-1.63	22.1	21.3	26.8
14	LP-A14	6.29	5.49	-1.21	20.3	19.5	25.0
15	LP-A15	6.59	5.67	-1.21	20.3	19.5	25.0
16	LP-A16	7.03	5.60	-1.65	22.3	21.4	26.9
17	LP-A17	7.56	5.12	-1.83	23.0	22.2	27.7
18	LP-A18	7.92	5.92	-1.01	19.5	18.6	24.1
19	LP-A19	8.09	6.13	-1.00	19.4	18.6	24.1
20	LP-A20	8.41	7.42	-0.73	18.3	17.4	22.9
21	LP-A21	8.90	7.47	-0.58	17.6	16.7	22.3
22	LP-A22	9.57	7.76	-1.27	20.6	19.7	25.3
23	LP-A23	10.31	7.59	-1.97	23.6	22.8	28.3

Average		5.94	-1.18	20.2	19.4	24.9
Minimum		5.02	-1.97	17.1	16.2	21.7
Maximum		7.76	-0.46	23.6	22.8	28.3
Standard Deviation		0.84	0.41	1.8	1.8	1.8

Opisoma excavatum (specimen O1)

No.	Sample	Distance (mm)	δ¹³C (‰ VPDB)	δ¹⁸O (‰ VPDB)	Temperature calculated for δ¹⁸O		
					-1	-1.2	0
1	O - 1 - 2	0.2	4.28	-0.76	18.4	17.5	22.7

2	O - 2	0.6	4.32	-0.52	17.4	16.5	21.7
3	O - 3 - 2	1.0	5.11	0.08	14.7	13.9	19.1
4	O - 4	1.5	5.32	-0.01	15.1	14.7	19.5
5	O - 5	1.9	5.36	-0.37	16.7	15.8	21.0
6	O - 6	2.3	5.24	-0.27	16.3	15.4	20.6
7	O - 7	2.7	4.62	-0.98	19.3	18.5	23.7
8	O - 8	3.1	5.75	-1.10	19.9	19.0	24.2
9	O - 9	3.6	6.01	-0.67	18.0	17.1	22.3
10	O - 10	4.0	5.86	-0.50	17.2	16.4	21.6
11	O - 11	4.4	5.05	-0.11	15.6	14.7	19.9
12	O - 12	4.8	5.68	-0.14	15.7	14.8	20.0
13	O - 13	5.2	5.73	0.48	13.0	12.1	17.3
14	O - 14	5.7	5.74	0.10	14.7	13.8	19.0
15	O - 15	6.1	5.24	-0.60	17.7	16.8	22.0
16	O - 16	6.5	5.23	-1.03	19.6	18.7	23.9
17	O - 17	6.9	6.02	-0.64	17.9	17.0	22.21
18	O - 18	7.3	4.93	-1.19	20.3	19.4	24.6
19	O - 19 - 2	7.8	4.98	-0.64	17.9	17.0	22.2
20	O - 20	8.2	5.03	-0.47	17.1	16.2	21.5
21	O - 21 - 2	8.6	5.18	-0.85	18.8	17.9	23.1
22	O - 22	9.0	5.15	-0.75	18.4	17.5	22.7
23	O - 23	9.4	5.75	-0.06	15.3	14.5	19.7
24	O - 24 - 2	9.9	6.08	-0.34	16.6	15.7	20.9
25	O - 25	10.3	5.21	-0.52	17.3	16.5	21.7
26	O - 26	10.7	5.29	0.02	15.0	14.1	19.3
27	O - 27	11.1	5.53	0.00	15.1	14.2	19.4
28	O - 28	11.5	6.12	0.05	14.9	14.0	19.2
29	O - 29	12.0	5.81	-1.05	19.7	18.8	24.0
30	O - 30	12.4	6.34	-0.95	19.2	18.4	23.6
31	O - 31	12.8	6.04	-1.28	20.7	19.8	25.0
32	O - 32	13.2	5.39	-1.80	23.0	22.0	27.3
33	O - 33	13.6	5.75	-0.46	17.1	16.2	21.4
34	O - 34	14.1	4.94	-0.29	16.4	15.5	20.7
35	O - 35	14.5	5.18	0.06	14.8	14.0	19.2
36	O - 36	14.9	5.77	0.23	14.1	13.2	18.4
37	O - 37	15.3	6.43	-0.12	15.6	14.8	20.0
38	O - 38	15.7	6.37	-0.20	16.0	15.1	20.3
39	O - 39	16.2	6.83	-0.69	18.1	17.2	22.4
40	O - 40	16.6	5.54	-0.85	18.8	18.0	23.1
41	O - 41	17.0	5.72	-0.45	17.0	16.2	21.4
42	O - 42	17.4	5.97	-0.02	15.2	14.3	19.5
43	O - 43	17.8	4.91	0.02	15.0	14.1	19.3
44	O - 44	18.3	6.81	0.37	13.5	12.6	17.8
45	O - 45	18.7	6.59	0.00	15.1	14.2	19.4

46	O - 46	19.1	6.51	-0.37	16.7	15.9	21.1
47	O - 47	19.5	5.71	-0.63	17.8	17.0	22.2
48	O - 48	19.9	5.94	-0.67	18.0	17.1	22.3
49	O - 49	20.4	6.30	-0.90	19.0	18.1	23.3
50	O - 50	20.8	6.20	-0.91	19.0	18.2	23.4
51	O - 51	21.2	6.24	-0.65	17.9	17.1	22.3
52	O - 52	21.6	6.22	-0.53	17.4	16.5	21.7
53	O - 53	22.0	5.82	-0.79	18.5	17.7	22.9
54	O - 54	22.5	5.36	-1.31	20.8	19.9	25.1
55	O - 55	22.9	5.07	-1.59	22.0	21.1	26.4
56	O - 56	23.3	4.92	-1.75	22.7	21.8	27.0

Average			5.62	-0.52	17.4	16.5	21.7
Minimum			4.28	-1.80	13.0	12.1	17.3
Maximum			6.83	0.48	22.9	22.0	27.3
Standard Deviation			0.59	0.51	2.2	2.2	2.2

Lithiotis problematica (specimen LT6)

No.	Sample	Distance (mm)	δ¹³C (‰ VPDB)	δ¹⁸O (‰ VPDB)	Temperature calculated for δ¹⁸O		
					-1	-1.2	0
1	**LT1-56**	**0**	**2.55**	**-4.34**	**33.9**	**33.1**	**38.3**
2	LT1-55	0.44	2.32	-3.22	29.1	28.2	33.4
3	LT1-54	0.98	2.24	-3.22	29.1	28.2	33.4
4	LT1-53	1.48	2.33	-3.24	29.1	28.3	33.5
5	LT1-52	1.78	2.40	-3.23	29.1	28.3	33.5
6	LT1-51	2.24	2.46	-3.04	28.3	27.4	32.6
7	LT1-50	2.71	3.14	-2.55	26.1	25.3	30.5
8	LT1-49	3.30	3.77	-2.02	23.9	23.0	28.2
9	LT1-48	3.58	4.10	-1.88	23.2	22.4	27.6
10	LT1-47	3.83	4.74	-2.01	23.8	23.0	28.2
11	LT1-46	4.34	5.24	-1.80	22.9	22.0	27.2
12	LT1-45	4.34	5.08	-2.00	23.8	22.9	28.1
13	LT1-44	4.61	4.61	-2.33	25.2	24.3	29.5
14	LT1-43	5.05	4.37	-2.38	25.4	24.5	29.7
15	LT1-42	5.33	3.76	-2.50	25.9	25.1	30.3
16	LT1-41	5.72	3.21	-2.74	27.0	26.1	31.3
17	LT1-40	5.99	2.92	-3.43	30.0	29.1	34.3
18	**LT1-39**	**6.35**	**2.79**	**-4.27**	**33.6**	**32.8**	**38.0**
19	**LT1-38**	**6.88**	**2.71**	**-4.50**	**34.6**	**33.7**	**39.0**
20	**LT1-36**	**7.45**	**2.87**	**-5.45**	**38.7**	**37.9**	**43.1**
21	**LT1-35**	**7.78**	**2.98**	**-6.30**	**42.4**	**41.6**	**46.8**
22	**LT1-34**	**8.34**	**3.00**	**-6.14**	**41.8**	**40.9**	**46.1**
23	**LT1-33**	**8.96**	**3.06**	**-6.61**	**43.8**	**42.9**	**48.1**

24	**LT1-32**	**9.42**	**2.87**	**-6.13**	**41.7**	**40.8**	**46.0**
25	**LT1-30**	**9.81**	**2.89**	**-6.03**	**41.3**	**40.4**	**45.6**
26	**LT1-29**	**10.31**	**3.00**	**-6.25**	**42.2**	**41.4**	**46.6**
27	**LT1-28**	**11.01**	**3.07**	**-6.40**	**42.8**	**42.0**	**47.2**
28	**LT1-27**	**11.47**	**3.18**	**-6.62**	**43.8**	**43.0**	**48.2**
29	**LT1-26**	**11.94**	**3.32**	**-6.92**	**45.1**	**44.3**	**49.5**
30	**LT1-25**	**12.84**	**3.18**	**-5.92**	**40.8**	**39.9**	**45.1**
31	**LT1-24**	**13.51**	**2.90**	**-4.15**	**33.1**	**32.2**	**37.4**
32	LT1-23	14.40	2.99	-3.52	30.4	29.5	34.7
33	LT1-22	15.29	3.00	-2.99	28.0	27.2	32.4
34	LT1-21	16.34	3.06	-3.59	30.7	29.8	35.0
35	LT1-20	16.90	3.04	-2.95	27.9	27.0	32.3
36	LT1-19	17.46	3.13	-2.66	26.6	25.8	31.0
37	LT1-18	18.53	3.04	-2.30	25.1	24.2	29.4
38	LT1-17	19.19	3.26	-2.29	25.0	24.2	29.4
39	LT1-16	19.71	3.55	-1.88	23.2	22.4	27.6
40	LT1-15	20.14	4.13	-1.92	23.4	22.6	27.8
41	LT1-14	20.67	4.11	-1.67	22.3	21.5	26.7
42	LT1-13	21.12	4.09	-1.94	23.5	22.7	27.9
43	LT1-12	21.71	4.20	-3.35	29.6	28.8	34.0
44	LT1-11	22.31	4.61	-2.50	25.9	25.1	30.3
45	**LT1-10**	**22.85**	**4.10**	**-4.08**	**32.8**	**31.9**	**37.2**
46	**LT1-9**	**23.41**	**4.30**	**-4.02**	**32.5**	**31.7**	**36.9**
47	LT1-8	23.97	4.66	-2.73	26.9	26.1	31.3
48	LT1-7	24.50	4.35	-3.76	31.4	30.5	35.7
49	**LT1-6**	**25.12**	**4.17**	**-4.75**	**35.7**	**34.9**	**40.1**
50	**LT1-5**	**25.52**	**3.74**	**-5.92**	**40.8**	**39.9**	**45.1**
51	**LT1-4**	**25.92**	**3.84**	**-5.85**	**40.5**	**39.6**	**44.8**
52	**LT1-3**	**26.45**	**3.62**	**-6.15**	**41.8**	**40.9**	**46.1**
53	**LT1-2**	**26.95**	**3.29**	**-7.12**	**46.0**	**45.1**	**50.4**
54	**LT1-1**	**27.50**	**3.34**	**-6.86**	**44.8**	**44.0**	**49.2**

Average	3.46	-3.93	32.2	31.3	36.5
Minimum	2.24	-7.12	22.3	21.5	26.7
Maximum	5.24	-1.67	46.0	45.1	50.4
Standard Deviation	0.75	1.72	7.5	7.5	7.5

Without highlighted values

Average	3.61	-2.63	26.5	25.7	30.9
Minimum	2.24	-3.76	22.3	21.5	26.7
Maximum	5.24	-1.67	31.4	30.5	35.7
Standard Deviation	0.87	0.61	2.7	2.7	2.7

263

Lithiotis problematica (specimen LT7)

No.	Sample	Distance (mm)	δ¹³C (‰ VPDB)	δ¹⁸O (‰ VPDB)	Temperature calculated for δ¹⁸O		
					-1	-1.2	0
1	**LT2-1**	**0.00**	**2.11**	**-4.39**	**34.2**	**33.3**	**38.5**
2	LT2-2	0.48	2.20	-3.53	30.4	29.5	34.7
3	LT2-3	1.10	2.33	-3.23	29.1	28.2	33.4
4	LT2-4	1.80	2.57	-3.97	32.3	31.5	36.7
5	**LT2-5**	**2.49**	**2.88**	**-4.08**	**32.8**	**31.9**	**37.1**
6	**LT2-6**	**3.12**	**2.72**	**-4.45**	**34.4**	**33.5**	**38.7**
7	**LT2-7**	**3.71**	**2.70**	**-4.24**	**33.5**	**32.6**	**37.8**
8	**LT2-8**	**3.89**	**2.68**	**-4.30**	**33.7**	**32.9**	**38.1**
9	**LT2-9**	**4.15**	**2.69**	**-4.14**	**33.1**	**32.2**	**37.4**
10	**LT2-10**	**4.70**	**2.52**	**-4.37**	**34.0**	**33.2**	**38.4**
11	**LT2-11**	**5.08**	**2.59**	**-4.60**	**35.0**	**34.2**	**39.4**
12	**LT2-12**	**5.53**	**2.48**	**-5.14**	**37.4**	**36.5**	**41.8**
13	**LT2-13**	**5.95**	**2.74**	**-5.21**	**37.7**	**36.8**	**42.0**
14	**LT2-14**	**6.33**	**2.80**	**-5.40**	**38.5**	**37.6**	**42.8**
15	**LT2-15**	**6.68**	**2.32**	**-5.58**	**39.3**	**38.5**	**43.7**
16	**LT2-16**	**7.13**	**3.03**	**-5.53**	**39.1**	**38.2**	**43.4**
17	**LT2-17**	**7.45**	**3.27**	**-4.74**	**35.7**	**34.8**	**40.0**
18	**LT2-18**	**7.63**	**3.34**	**-4.38**	**34.1**	**33.2**	**38.4**
19	LT2-19	8.20	3.52	-3.82	31.7	30.8	36.0
20	LT2-20	8.66	4.08	-3.14	28.7	27.8	33.0
21	LT2-21	9.13	4.15	-3.28	29.3	28.4	33.6
22	**LT2-22**	**9.65**	**3.91**	**-4.35**	**34.0**	**33.1**	**38.3**
23	LT2-23	10.19	4.59	-3.19	28.9	28.0	33.3
24	LT2-24	10.57	4.07	-3.80	31.6	30.7	35.9
25	**LT2-25**	**11.12**	**3.19**	**-4.42**	**34.3**	**33.4**	**38.6**
26	**LT2-26**	**11.51**	**3.25**	**-4.87**	**36.2**	**35.4**	**40.6**
27	LT2-27	11.97	3.17	-3.91	32.0	31.2	36.4
28	**LT2-28**	**12.64**	**3.13**	**-5.02**	**36.9**	**36.0**	**41.2**
29	**LT2-29**	**13.10**	**2.84**	**-5.80**	**40.2**	**39.4**	**44.6**
30	**LT2-30**	**13.47**	**3.10**	**-6.10**	**41.6**	**40.7**	**45.9**
31	**LT2-31**	**13.75**	**3.26**	**-6.38**	**42.8**	**41.9**	**47.1**
32	**LT2-32**	**14.30**	**3.02**	**-5.40**	**38.5**	**37.6**	**42.8**
33	**LT2-33**	**14.95**	**2.58**	**-5.15**	**37.4**	**36.6**	**41.8**
34	**LT2-34**	**15.58**	**3.22**	**-4.76**	**35.8**	**34.9**	**40.1**
35	**LT2-35**	**16.15**	**3.80**	**-4.42**	**34.3**	**33.4**	**38.6**
36	**LT2-36**	**16.56**	**3.89**	**-4.01**	**32.5**	**31.6**	**36.8**
37	**LT2-37**	**17.06**	**4.12**	**-5.47**	**38.8**	**38.0**	**43.2**
38	LT2-38	17.60	4.77	-2.39	25.5	24.6	29.8
39	LT2-39	18.02	4.01	-2.88	27.6	26.7	31.9
40	**LT2-40**	**18.39**	**3.34**	**-5.86**	**40.5**	**39.6**	**44.9**
41	**LT2-B1**	**18.59**	**3.19**	**-6.47**	**43.2**	**42.3**	**47.5**

42	**LT2-B2**	**18.84**	**3.20**	**-6.68**	**44.1**	**43.2**	**48.4**
43	**LT2-B3**	**19.43**	**3.19**	**-6.19**	**41.9**	**41.1**	**46.3**
44	**LT2-B4**	**19.79**	**3.32**	**-6.25**	**42.2**	**41.3**	**46.6**
45	**LT2-B5**	**20.35**	**3.33**	**-5.79**	**40.2**	**39.3**	**44.5**

Average	3.18	-4.69	35.4	34.6	39.8
Minimum	2.11	-6.68	25.5	24.6	29.8
Maximum	4.77	-2.39	44.1	43.2	48.4
Standard Deviation	0.63	1.04	4.5	4.5	4.5

Without highlighted values

Average	3.59	-3.38	29.7	28.8	34.1
Minimum	2.20	-3.97	25.5	24.6	29.8
Maximum	4.77	-2.39	32.3	31.6	36.7
Standard Deviation	0.90	0.49	2.1	2.1	2.1

Pachyrisma (Durga) crassa (specimen P1)

No.	Sample	Distance (mm)	$\delta^{13}C$ (‰ VPDB)	$\delta^{18}O$ (‰ VPDB)	Temperature calculated for $\delta^{18}O$		
					-1	**-1.2**	**0**
1	P-1	0	5.01	-1.14	20.0	19.2	24.4
2	P-2	0.53	4.21	-1.30	20.7	19.8	25.4
3	P-3	1.00	4.51	-1.12	19.9	19.1	24.6
4	P-4	1.48	3.53	-1.63	22.2	21.3	26.8
5	P-5	2.05	4.17	-1.15	20.1	19.2	24.7
6	P-6	2.45	3.81	-1.19	20.3	19.4	24.9
7	P-7	2.86	4.14	-1.23	20.4	19.6	25.1
8	P-8	3.03	4.66	-0.87	18.9	18.0	23.5
9	P-9	3.53	4.51	-1.18	20.2	19.3	24.8
10	P-10	3.81	4.56	-1.24	20.5	19.6	25.1
11	P-11	4.24	4.70	-1.15	20.1	19.2	24.7
12	P-12	4.59	4.24	-1.33	20.9	20.0	25.5
13	P-13	4.76	4.65	-1.03	19.6	18.7	24.2
14	P-14	5.24	4.44	-0.78	18.5	17.6	23.1
15	P-15	5.66	5.18	-0.91	19.1	18.2	23.7
16	P-16	5.97	4.58	-1.37	21.0	20.2	25.7
17	P-17	6.37	4.38	-1.21	20.3	19.5	25.0
18	P-18	6.86	4.04	-1.59	22.0	21.1	26.6
19	P-19	7.38	4.09	-1.34	20.9	20.0	25.5
20	P-20	7.76	4.20	-1.13	20.0	19.1	24.6
21	P-21	8.34	3.98	-1.78	22.8	22.0	27.5
22	P-22	9.07	3.87	-0.91	19.0	18.2	23.7
23	P-23	9.33	4.12	-1.48	21.5	20.6	26.1
24	P-24	9.78	4.34	-1.15	20.1	19.2	24.7
25	P-25	10.21	4.50	-1.01	19.5	18.6	24.1

No.	Sample	Distance	δ13C	δ18O			
26	P-26	10.62	3.98	-1.86	23.2	22.3	27.8
27	P-27	11.14	4.10	-0.86	18.8	18.0	23.5
28	P-28	11.70	4.24	-0.43	16.9	16.1	21.6
29	P-29	12.06	4.14	-1.83	23.0	22.2	27.7
30	P-30	12.46	4.11	-1.37	21.1	20.2	25.7
31	P-31	13.03	4.89	-0.74	18.3	17.4	23.0
32	P-32	13.48	4.60	-1.71	22.5	21.6	27.1
33	P-33	13.95	4.80	-0.76	18.4	17.5	23.0
34	P-34	14.49	4.89	-0.71	18.2	17.3	22.8
35	P-35	15.03	4.82	-0.71	18.1	17.3	22.8
36	P-36	15.38	4.56	-1.17	20.2	19.3	24.8
37	P-37	15.92	4.69	-1.00	19.4	18.6	24.1
38	P-38	16.37	4.22	-1.27	20.6	19.7	25.2
39	P-39	16.84	4.55	-1.54	21.8	20.9	26.4
40	P-40	17.25	4.38	-1.62	22.1	21.2	26.8
41	P-41	17.63	4.19	-1.16	20.1	19.3	24.8
42	P-42	18.05	4.25	-0.64	17.8	17.0	22.5
43	P-43	18.46	3.97	-0.70	18.1	17.2	22.8
44	P-44	19.09	3.38	-1.39	21.1	20.3	25.8
45	P-45	19.56	3.64	-0.65	17.9	17.1	22.6
46	P-46	20.02	3.60	-1.06	19.7	18.8	24.3
47	P-47	20.39	3.72	-1.08	19.8	18.9	24.4

Average	4.30	-1.16	20.1	19.3	24.8
Minimum	3.38	-1.86	17.0	16.1	21.6
Maximum	5.18	-0.43	23.2	22.3	27.8
Standard Deviation	0.40	0.34	1.5	1.5	1.5

Cochlearites loppianus (specimen CO1)

No.	Sample	Distance (mm)	δ13C (‰ VPDB)	δ18O (‰ VPDB)	Temperature calculated for δ18O		
					-1	-1.2	0
1	CO1 - 1	0.14	3.71	-5.25	37.9	37.0	42.2
2	CO1 - 2	0.43	3.87	-4.71	35.5	34.7	39.9
3	CO1 - 3	0.72	3.90	-5.10	37.2	36.4	41.6
4	CO1 - 4	1.01	4.05	-5.22	37.8	36.9	42.1
5	CO1 - 5	1.29	3.98	-5.06	37.0	36.2	41.4
6	CO1 - 6	1.58	3.83	-4.79	35.9	35.0	40.2
7	CO1 - 7	1.87	3.81	-4.68	35.4	34.5	39.8
8	CO1 - 8	2.16	3.86	-4.93	36.5	35.6	40.8
9	CO1 - 9	2.44	3.92	-4.94	36.5	35.6	40.9
10	CO1 - 10	2.73	3.93	-5.18	37.6	36.7	41.9
11	CO1 - 11	3.02	3.81	-5.13	37.3	36.5	41.7
12	CO1 - 12	3.30	3.68	-4.99	36.7	35.9	41.1

13	**CO1 - 13**	**3.59**	**3.76**	**-4.44**	**34.3**	**33.5**	**38.7**
14	CO1 - 14	3.88	3.97	-3.80	31.6	30.7	35.9
15	CO1 - 15	4.17	3.97	-3.73	31.3	30.4	35.6
16	CO1 - 16	4.45	3.84	-4.00	32.4	31.6	36.8
17	**CO1 - 17**	**4.74**	**3.91**	**-4.96**	**36.6**	**35.7**	**41.0**
18	**CO1 - 18**	**5.03**	**3.86**	**-4.90**	**36.3**	**35.5**	**40.7**
19	**CO1 - 19**	**5.32**	**3.89**	**-4.48**	**34.5**	**33.7**	**38.9**
20	**CO1 - 20**	**5.60**	**3.77**	**-4.13**	**33.0**	**32.2**	**37.4**
21	**CO1 - 21**	**5.89**	**3.68**	**-4.02**	**32.6**	**31.7**	**36.9**
22	**CO1 - 22**	**6.18**	**3.64**	**-4.26**	**33.6**	**32.7**	**37.9**
23	**CO1 - 23**	**6.47**	**3.70**	**-4.54**	**34.8**	**33.9**	**39.1**
24	CO1 - 24	6.75	3.76	-3.95	32.2	31.4	36.6
25	CO1 - 25	7.04	3.62	-3.73	31.3	30.4	35.6
26	CO1 - 26	7.33	3.29	-3.27	29.3	28.4	33.6
27	CO1 - 27	7.62	3.19	-2.56	26.2	25.3	30.5
28	CO1 - 28	7.90	3.11	-1.37	21.1	20.2	25.4
29	CO1 - 29	8.19	3.14	-1.33	20.9	20.0	25.2
30	CO1 - 30	8.48	4.08	-1.17	20.2	19.3	24.5
31	CO1 - 31	8.77	4.00	-0.98	19.3	18.5	23.7
32	CO1 - 32	9.05	3.27	-0.88	18.9	18.0	23.2
33	CO1 - 33	9.34	3.32	-1.31	20.8	19.9	25.1
34	CO1 - 34	9.63	2.84	-3.88	31.9	31.0	36.2
35	**CO1 - 35**	**9.91**	**2.96**	**-4.09**	**32.9**	**32.0**	**37.2**
36	CO1 - 36	10.20	3.15	-3.83	31.7	30.8	36.1
37	CO1 - 37	10.49	3.29	-3.45	30.1	29.2	34.4
38	**CO1 - 38**	**10.78**	**3.40**	**-4.24**	**33.5**	**32.6**	**37.8**
39	**CO1 - 39**	**11.06**	**3.35**	**-5.00**	**36.8**	**35.9**	**41.1**
40	**CO1 - 40**	**11.35**	**3.11**	**-4.93**	**36.5**	**35.6**	**40.8**
41	**CO1 - 41**	**11.64**	**3.20**	**-4.53**	**34.8**	**33.9**	**39.1**
42	CO1 - 42	11.93	2.99	-3.07	28.4	27.6	32.8
43	CO1 - 43	12.21	3.09	-2.88	27.6	26.7	31.9
44	CO1 - 44	12.50	2.76	-2.25	24.9	24.0	29.2
45	CO1 - 45	12.79	2.82	-2.01	23.8	22.9	28.1
46	CO1 - 46	13.08	3.10	-2.05	24.0	23.1	28.3
47	CO1 - 47	13.36	3.71	-1.43	21.3	20.4	25.6
48	CO1 - 48	13.65	3.80	-2.32	25.2	24.3	29.5
49	CO1 - 49	13.94	4.45	-0.70	18.1	17.3	22.5
50	CO1 - 50	14.23	3.58	-1.23	20.4	19.5	24.8
51	CO1 - 51	14.51	3.22	-1.88	23.3	22.4	27.6
52	CO1 - 52	14.80	4.08	-1.37	21.0	20.2	25.4
53	CO1 - 53	15.09	3.44	-2.84	27.4	26.6	31.8
54	**CO1 - 54**	**15.38**	**2.47**	**-4.25**	**33.5**	**32.7**	**37.9**
55	**CO1 - 55**	**15.66**	**2.78**	**-4.66**	**35.3**	**34.4**	**39.6**
56	**CO1 - 56**	**15.95**	**2.40**	**-4.61**	**35.1**	**34.2**	**39.4**

57	**CO1 - 57**	**16.24**	**2.29**	**-4.05**	**32.7**	**31.8**	**37.0**
58	**CO1 - 58**	**16.52**	**2.37**	**-4.37**	**34.0**	**33.2**	**38.4**
59	**CO1 - 59**	**16.81**	**2.46**	**-4.24**	**33.5**	**32.6**	**37.8**
60	CO1 - 60	17.10	2.51	-3.80	31.6	30.7	35.9
61	CO1 - 61	17.39	2.32	-3.85	31.8	30.9	36.1
62	CO1 - 62	17.67	2.50	-3.85	31.8	30.9	36.1
63	CO1 - 63	17.96	2.32	-2.85	27.5	26.6	31.8
64	CO1 - 64	18.25	2.35	-2.65	26.6	25.7	30.9
65	CO1 - 65	18.54	2.79	-1.88	23.2	22.4	27.6
66	CO1 - 66	18.82	2.75	-1.94	23.5	22.6	27.8
67	CO1 - 67	19.11	3.02	-2.69	26.8	25.9	31.1
68	CO1 - 68	19.40	3.21	-2.12	24.3	23.4	28.6
69	CO1 - 69	19.69	3.26	-1.42	21.3	20.4	25.6
70	CO1 - 70	19.97	3.35	-0.91	19.0	18.2	23.4
71	CO1 - 71	20.26	3.18	-1.09	19.8	19.0	24.2
72	CO1 - 72	20.55	2.45	-2.20	24.6	23.8	29.0
73	CO1 - 73	20.84	2.53	-1.57	21.9	21.0	26.2
74	CO1 - 74	21.12	2.50	-2.14	24.4	23.5	28.7
75	CO1 - 75	21.41	2.54	-2.57	26.2	25.4	30.6
76	**CO1 - 76**	**21.70**	**2.24**	**-4.07**	**32.8**	**31.9**	**37.1**
77	CO1 - 77	21.98	2.87	-3.72	31.2	30.4	35.6
78	CO1 - 78	22.27	2.42	-3.51	30.3	29.4	34.7
79	**CO1 - 79**	**22.56**	**2.82**	**-4.72**	**35.6**	**34.7**	**39.9**
80	**CO1 - 80**	**22.85**	**2.63**	**-4.38**	**34.1**	**33.2**	**38.4**
81	CO1 - 81	23.13	2.82	-3.57	30.6	29.7	34.9
82	CO1 - 82	23.42	3.37	-2.99	28.0	27.2	32.4
83	CO1 - 83	23.71	3.02	-2.85	27.5	26.6	31.8
84	CO1 - 84	24.00	2.75	-2.54	26.1	25.3	30.5
85	CO1 - 85	24.28	2.83	-2.39	25.5	24.6	29.8
86	CO1 - 86	24.57	2.94	-2.15	24.4	23.6	28.8
87	CO1 - 87	24.86	3.80	-1.26	20.6	19.7	24.9
88	CO1 - 88	25.15	3.39	-0.83	18.7	17.8	23.0
89	CO1 - 89	25.43	3.23	-0.86	18.8	17.9	23.1
90	CO1 - 90	25.72	3.85	-0.92	19.1	18.2	23.4
91	CO1 - 91	26.01	3.62	-1.18	20.2	19.3	24.6
92	CO1 - 92	26.30	3.28	-1.22	20.4	19.5	24.7
93	CO1 - 93	26.58	3.26	-1.23	20.4	19.6	24.8
94	CO1 - 94	26.87	3.30	-1.32	20.8	20.0	25.2
95	CO1 - 95	27.16	3.12	-1.46	21.4	20.6	25.8
96	CO1 - 96	27.45	3.24	-1.38	21.1	20.2	25.4
97	CO1 - 97	27.73	2.89	-2.07	24.1	23.2	28.4
98	CO1 - 98	28.02	2.85	-2.54	26.1	25.3	30.5
99	CO1 - 99	28.31	3.00	-2.73	26.9	26.1	31.3
100	CO1 - 100	28.59	2.62	-3.71	31.2	30.3	35.5

101	CO1 - 101	28.88	2.90	-3.11	28.6	27.7	32.9
102	CO1 - 102	29.17	2.43	-2.68	26.7	25.9	31.1
103	CO1 - 103	29.46	2.85	-3.09	28.5	27.6	32.9
104	CO1 - 104	29.74	2.76	-3.00	28.1	27.2	32.4
105	CO1 - 105	30.03	2.85	-3.04	28.3	27.4	32.6
106	CO1 - 106	30.32	2.78	-2.95	27.9	27.0	32.2
107	CO1 - 107	30.61	2.62	-3.01	28.2	27.3	32.5
108	CO1 - 108	30.89	2.49	-2.99	28.1	27.2	32.4
109	CO1 - 109	31.18	2.74	-2.76	27.1	26.2	31.4
110	CO1 - 110	31.47	2.84	-2.44	25.7	24.8	30.0
111	CO1 - 111	31.76	2.91	-1.80	22.9	22.0	27.2
112	CO1 - 112	32.04	3.14	-1.40	21.2	20.3	25.5
113	CO1 - 113	32.33	3.46	-1.22	20.4	19.5	24.7
114	CO1 - 114	32.62	4.19	-1.30	20.7	19.9	25.1
115	CO1 - 115	32.91	4.46	-1.30	20.7	19.8	25.1
116	CO1 - 116	33.19	4.37	-1.72	22.5	21.7	26.9
117	CO1 - 117	33.48	4.21	-1.32	20.8	20.0	25.2
118	CO1 - 118	33.77	3.91	-0.86	18.8	17.9	23.2
119	CO1 - 119	34.05	3.82	-0.80	18.5	17.7	22.9
120	CO1 - 120	34.34	3.63	-0.85	18.8	17.9	23.1
121	CO1 - 121	34.63	3.06	-1.34	20.9	20.0	25.3
122	CO1 - 122	34.92	2.68	-2.01	23.8	23.0	28.2
123	CO1 - 123	35.20	2.41	-2.29	25.0	24.1	29.4
124	CO1 - 124	35.49	2.47	-2.91	27.7	26.9	32.1
125	CO1 - 125	35.78	2.71	-2.85	27.5	26.6	31.8
126	CO1 - 126	36.07	3.58	-3.31	29.4	28.6	33.8
127	CO1 - 127	36.35	3.65	-3.29	29.4	28.5	33.7
128	CO1 - 128	36.64	3.43	-3.42	29.9	29.1	34.3
129	CO1 - 129	36.93	3.12	-3.41	29.9	29.0	34.2
130	CO1 - 130	37.22	2.94	-3.36	29.7	28.8	34.0
131	CO1 - 131	37.50	2.91	-3.03	28.2	27.4	32.6
132	CO1 - 132	37.79	2.90	-2.95	27.9	27.0	32.2
133	CO1 - 133	38.08	2.96	-2.38	25.4	24.6	29.8
134	CO1 - 134	38.37	3.21	-1.91	23.4	22.5	27.7
135	CO1 - 135	38.65	3.47	-1.66	22.3	21.4	26.6
136	CO1 - 136	38.94	3.44	-1.48	21.5	20.6	25.8
137	CO1 - 138	39.52	3.74	-1.43	21.3	20.4	25.6
138	CO1 - 139	39.80	4.47	-1.15	20.1	19.2	24.4
139	CO1 - 140	40.09	5.02	-0.89	18.9	18.1	23.3
140	CO1 - 141	40.38	5.10	-0.96	19.3	18.4	23.6
141	CO1 - 142	40.66	4.55	-0.79	18.5	17.6	22.9
142	CO1 - 143	40.95	3.80	-0.80	18.5	17.7	22.9
143	CO1 - 144	41.24	3.32	-0.96	19.3	18.4	23.6
144	CO1 - 145	41.53	3.05	-1.27	20.6	19.7	24.9

145	CO1 - 146	41.81	2.70	-1.58	22.0	21.1	26.3
146	CO1 - 147	42.10	2.57	-1.81	22.9	22.1	27.3
147	CO1 - 148	42.39	2.67	-2.19	24.6	23.7	28.9
148	CO1 - 149	42.68	2.77	-2.16	24.5	23.6	28.8
149	CO1 - 150	42.96	2.79	-2.07	24.1	23.2	28.4
150	CO1 - 151	43.25	2.69	-2.21	24.7	23.8	29.0
151	CO1 - 152	43.54	2.62	-2.47	25.8	25.0	30.2
152	CO1 - 153	43.83	2.66	-2.88	27.6	26.7	31.9
153	CO1 - 154	44.11	2.81	-3.13	28.7	27.8	33.0
154	CO1 - 155	44.40	3.36	-2.95	27.9	27.0	32.2
155	CO1 - 156	44.69	3.57	-2.87	27.5	26.7	31.9
156	CO1 - 157	44.98	3.66	-2.78	27.2	26.3	31.5
157	CO1 - 158	45.26	3.24	-2.61	26.4	25.5	30.7
158	CO1 - 159	45.55	3.54	-2.13	24.3	23.4	28.7
159	CO1 - 160	45.84	3.72	-1.72	22.6	21.7	26.9
160	CO1 - 161	46.12	3.97	-1.33	20.8	20.0	25.2
161	CO1 - 162	46.41	3.96	-1.19	20.2	19.4	24.6
162	CO1 - 163	46.70	4.09	-1.07	19.7	18.8	24.1
163	CO1 - 164	46.99	4.01	-0.95	19.2	18.3	23.5
164	CO1 - 165	47.27	3.56	-0.96	19.3	18.4	23.6
165	CO1 - 166	47.56	3.04	-1.06	19.7	18.8	24.0
166	CO1 - 167	47.85	2.92	-1.11	19.9	19.0	24.3
167	CO1 - 168	48.14	2.87	-1.19	20.2	19.4	24.6
168	CO1 - 169	48.42	2.77	-1.28	20.7	19.8	25.0
169	CO1 - 170	48.71	2.98	-1.60	22.0	21.2	26.4
170	CO1 - 171	49.00	3.89	-2.25	24.8	24.0	29.2
171	CO1 - 172	49.29	3.73	-2.03	23.9	23.0	28.2
172	CO1 - 173	49.57	4.24	-2.76	27.1	26.2	31.4
173	CO1 - 174	49.86	3.99	-2.78	27.2	26.3	31.5
174	CO1 - 176	50.44	3.34	-2.62	26.5	25.6	30.8
175	CO1 - 177	50.72	2.74	-2.46	25.8	24.9	30.1
176	CO1 - 178	51.01	2.63	-2.30	25.1	24.2	29.4
177	CO1 - 179	51.30	2.74	-1.97	23.6	22.7	28.0
178	CO1 - 180	51.59	2.91	-1.64	22.2	21.4	26.6
179	CO1 - 181	51.87	3.27	-1.69	22.4	21.6	26.8
180	CO1 - 182	52.16	4.15	-1.11	19.9	19.0	24.2
181	CO1 - 183	52.45	4.24	-1.41	21.2	20.3	25.5
182	CO1 - 184	52.73	3.76	-1.98	23.7	22.8	28.0
183	CO1 - 185	53.02	3.05	-1.55	21.8	20.9	26.2
184	CO1 - 186	53.31	2.52	-1.37	21.0	20.2	25.4
185	CO1 - 187	53.60	2.51	-0.95	19.2	18.3	23.5
186	CO1 - 188	53.88	2.66	-1.03	19.6	18.7	23.9
187	CO1 - 189	54.17	2.43	-1.34	20.9	20.0	25.2
188	CO1 - 190	54.46	2.48	-1.49	21.6	20.7	25.9

189	CO1 - 191	54.75	2.99	-1.93	23.4	22.6	27.8
190	CO1 - 192	55.03	3.27	-2.73	26.9	26.1	31.3
191	CO1 - 193	55.32	3.28	-3.62	30.8	29.9	35.2
192	CO1 - 194	55.61	3.28	-3.34	29.6	28.7	33.9
193	CO1 - 195	55.90	3.40	-3.10	28.5	27.7	32.9
194	CO1 - 196	56.18	3.52	-2.89	27.6	26.8	32.0
195	CO1 - 197	56.47	3.29	-2.13	24.3	23.4	28.7
196	CO1 - 198	56.76	3.05	-1.72	22.5	21.7	26.9
197	CO1 - 199	57.05	3.34	-1.55	21.8	21.0	26.2
198	CO1 - 200	57.33	4.35	-0.96	19.2	18.4	23.6
199	CO1 - 201	57.62	4.67	-0.85	18.8	17.9	23.1
200	CO1 - 202	57.91	4.59	-0.75	18.3	17.5	22.7
201	CO1 - 203	58.20	4.07	-0.79	18.5	17.7	22.9
202	CO1 - 204	58.48	3.53	-1.48	21.5	20.6	25.8
203	CO1 - 205	58.77	3.26	-1.98	23.7	22.8	28.0
204	CO1 - 206	59.06	3.56	-2.49	25.9	25.0	30.2
205	CO1 - 207	59.34	4.05	-2.53	26.1	25.2	30.4
206	CO1 - 208	59.63	4.46	-1.87	23.2	22.3	27.5
207	CO1 - 209	59.92	4.73	-1.46	21.4	20.6	25.8
208	CO1 - 210	60.21	4.85	-0.73	18.2	17.4	22.6
209	CO1 - 211	60.49	3.84	-0.80	18.6	17.7	22.9
210	CO1 - 212	60.78	3.44	-0.88	18.9	18.0	23.2
211	CO1 - 213	61.07	3.25	-1.35	21.0	20.1	25.3
212	CO1 - 214	61.36	3.89	-3.76	31.4	30.5	35.7

Average	3.31	-2.49	25.9	25.0	30.2
Minimum	2.24	-5.25	18.1	17.3	22.5
Maximum	5.10	-0.70	37.9	37.0	42.2
Standard Deviation	0.61	1.27	5.5	5.5	5.5

Without highlighted values

Average	3.30	-2.08	24.1	23.3	28.5
Minimum	2.32	-4.00	18.1	17.3	22.5
Maximum	5.10	-0.70	32.4	31.6	36.8
Standard Deviation	0.61	0.92	4.0	4.0	4.0

Cochlearites loppianus (specimen CO2)

No.	Sample	Distance (mm)	δ¹³C (‰ VPDB)	δ¹⁸O (‰ VPDB)	Temperature calculated for δ¹⁸O		
					-1	-1.2	0
1	CO2 - 1	0.2	3.44	-3.08	28.5	27.6	32.8
2	CO2 - 2	0.5	3.11	-3.70	31.1	30.3	35.5
3	**CO2 - 3**	**0.8**	**2.70**	**-4.14**	**33.1**	**32.2**	**37.4**
4	**CO2 - 4**	**1.1**	**2.43**	**-4.33**	**33.9**	**33.0**	**38.2**
5	CO2 - 5	1.4	3.15	-3.80	31.6	30.7	35.9
6	CO2 - 6	1.7	4.39	-2.85	27.5	26.6	31.8
7	CO2 - 7	2.0	4.60	-2.67	26.7	25.8	31.0
8	CO2 - 8	2.3	4.76	-2.40	25.5	24.6	29.8
9	CO2 - 9	2.6	4.59	-2.73	26.9	26.1	31.3
10	CO2 - 10	2.9	4.47	-3.43	30.0	29.1	34.3
11	CO2 - 11	3.2	4.37	-3.84	31.8	30.9	36.1
12	CO2 - 12	3.5	4.36	-3.39	29.8	28.9	34.2
13	CO2 - 13	3.8	4.59	-2.63	26.5	25.6	30.9
14	CO2 - 14	4.1	5.24	-1.01	19.5	18.6	23.8
15	CO2 - 15	4.4	5.72	-0.94	19.2	18.3	23.5
16	CO2 - 16 - 2	4.7	4.66	-1.39	21.1	20.2	25.5
17	CO2 - 17	5.0	3.65	-1.98	23.7	22.8	28.0
18	CO2 - 18	5.4	4.19	-1.49	21.6	20.7	25.9
19	CO2 - 19	5.7	4.01	-1.32	20.8	19.9	25.2
20	CO2 - 20	6.0	4.41	-0.84	18.8	17.9	23.1
21	CO2 - 21	6.3	4.27	-1.58	22.0	21.1	26.3
22	CO2 - 22	6.6	4.48	-0.55	17.5	16.6	21.8
23	CO2 - 23	6.9	3.84	-0.83	18.7	17.8	23.0
24	CO2 - 24	7.2	3.79	-1.44	21.4	20.5	25.7
25	CO2 - 25	7.5	3.68	-1.67	22.3	21.5	26.7
26	CO2 - 26	7.8	3.80	-2.75	27.0	26.2	31.4
27	CO2 - 27	8.1	3.66	-3.52	30.4	29.5	34.7
28	**CO2 - 28**	**8.4**	**3.45**	**-4.09**	**32.8**	**32.0**	**37.2**
29	CO2 - 29	8.7	3.44	-2.98	28.0	27.2	32.4
30	CO2 - 30	9.0	3.51	-2.00	23.8	22.9	28.1
31	CO2 - 31	9.3	3.53	-2.64	26.6	25.7	30.9
32	CO2 - 32	9.6	4.34	-0.98	19.4	18.5	23.7
33	CO2 - 33	9.9	4.76	-0.76	18.4	17.5	22.7
34	CO2 - 34	10.2	5.02	-0.77	18.4	17.6	22.8
35	CO2 - 35	10.6	4.49	-0.55	17.5	16.6	21.8
36	CO2 - 36	10.9	3.96	-0.90	19.0	18.1	23.3
37	CO2 - 37	11.2	3.52	-2.11	24.2	23.4	28.6
38	CO2 - 38	11.5	3.35	-3.17	28.9	28.0	33.2
39	CO2 - 39	11.8	3.26	-3.93	32.1	31.3	36.5
40	CO2 - 40	12.1	3.38	-3.42	29.9	29.1	34.3
41	CO2 - 41	12.4	3.47	-2.91	27.7	26.9	32.1

42	CO2 - 42	12.7	3.80	-2.20	24.6	23.8	29.0
43	CO2 - 43	13.0	3.90	-2.35	25.3	24.4	29.6
44	CO2 - 44	13.3	3.96	-2.25	24.9	24.0	29.2
45	CO2 - 45	13.6	3.97	-2.23	24.7	23.9	29.1
46	CO2 - 46	13.9	4.16	-2.31	25.1	24.3	29.5
47	CO2 - 47	14.2	4.50	-2.59	26.3	25.5	30.7
48	CO2 - 48 - 2	14.5	4.17	-2.22	24.7	23.9	29.1
49	CO2 - 49	14.8	3.78	-2.55	26.7	25.3	30.5
50	CO2 - 50	15.1	3.59	-2.16	24.5	23.6	28.8
51	CO2 - 51	15.4	3.76	-1.92	23.4	22.5	27.8
52	CO2 - 52	15.8	4.08	-1.35	21.0	20.1	25.3
53	CO2 - 53	16.1	4.54	-0.87	18.8	18.0	23.9
54	CO2 - 54	16.4	4.69	-0.53	17.4	16.5	21.7
55	CO2 - 55	16.7	4.32	-0.27	16.3	15.4	20.6
56	CO2 - 56	17.0	4.24	-0.89	19.0	18.1	23.3
57	CO2 - 57	17.3	4.20	-0.77	18.4	17.6	22.8
58	CO2 - 58	17.6	4.07	-0.97	19.3	18.4	23.6
59	CO2 - 59	17.9	4.35	-1.27	20.6	19.7	24.9
60	CO2 - 60 - 2	18.2	4.31	-1.50	21.6	20.7	25.9
61	CO2 - 61	18.5	4.44	-2.18	24.6	23.7	28.9
62	CO2 - 62 - 2	18.8	4.44	-1.92	23.4	22.6	27.8
63	CO2 - 63	19.1	4.63	-1.06	19.7	18.8	24.0
64	CO2 - 64	19.4	4.59	-0.95	20.0	18.3	23.5
65	CO2 - 65	19.7	4.44	-1.07	19.7	18.9	24.1
66	CO2 - 66	20.0	3.99	-0.35	16.6	15.7	21.0
67	CO2 - 67	20.3	4.24	-0.90	19.0	18.1	23.4
68	CO2 - 68	20.6	4.55	-1.58	21.9	21.1	26.3
69	CO2 - 69	21.0	4.21	-1.92	23.4	22.5	27.8
70	CO2 - 70	21.3	4.64	-2.35	25.3	24.4	29.6
71	CO2 - 71	21.6	4.05	-1.90	23.3	22.5	27.7
72	CO2 - 72	21.9	4.54	-0.92	19.1	18.2	23.4
73	CO2 - 73	22.2	4.18	-0.97	19.3	18.5	23.7
74	CO2 - 74	22.5	4.32	-0.74	18.3	17.4	22.6
75	CO2 - 75	22.8	4.02	-0.79	18.5	17.7	22.9
76	CO2 - 76	23.1	4.10	-0.88	18.9	18.0	23.2
77	CO2 - 77	23.4	3.73	-1.65	22.3	21.4	26.6
78	CO2 - 78	23.7	4.32	-2.68	26.7	25.8	31.1
79	CO2 - 79	24.0	3.55	-2.75	27.0	26.1	31.3
80	CO2 - 80	24.3	3.51	-2.44	25.7	24.8	30.0
81	CO2 - 81	24.6	3.93	-1.72	22.6	21.7	26.9
82	CO2 - 82	24.9	4.35	-1.03	19.5	18.7	23.9
83	CO2 - 83	25.2	4.46	-1.51	21.6	20.8	26.0
84	CO2 - 84	25.5	3.47	-3.53	30.4	29.5	34.7
85	**CO2 - 85**	**25.9**	**3.24**	**-4.54**	**34.8**	**33.9**	**39.1**

86	CO2 - 86	26.2	3.53	-3.96	32.3	31.4	36.6
87	CO2 - 87	26.5	4.36	-3.30	29.4	28.5	33.7
88	CO2 - 88	26.8	3.96	-1.70	22.5	21.6	26.8
89	CO2 - 89	27.1	4.04	-1.30	20.7	19.9	25.1
90	CO2 - 90	27.4	4.16	-1.15	20.1	19.2	24.4
91	CO2 - 91	27.7	4.47	-0.96	19.3	18.4	23.6
92	CO2 - 92	28.0	4.66	-0.89	19.0	18.1	23.3
93	CO2 - 93	28.3	4.53	-0.40	16.8	16.0	21.2
94	CO2 - 94	28.6	3.79	-0.31	16.5	15.6	20.8
95	CO2 - 95	28.9	3.05	-0.91	19.1	18.2	23.4
96	CO2 - 96	29.2	2.97	-1.37	21.1	20.2	25.4
97	CO2 - 97	29.5	3.46	-2.37	25.4	24.5	29.7
98	CO2 - 98	29.8	3.95	-2.65	26.6	25.7	30.9
99	CO2 - 99	30.1	4.24	-3.52	30.4	29.5	34.7
100	CO2 - 100	30.4	5.28	-3.93	32.2	31.3	36.5
101	CO2 - 101	30.7	5.75	-1.56	21.9	21.0	26.2
102	CO2 - 102	31.0	5.98	-0.82	18.6	17.8	23.0

Average	4.10	-1.96	23.6	22.7	27.9
Minimum	2.43	-4.54	16.3	15.4	20.6
Maximum	5.98	-0.27	34.8	33.9	39.1
Standard Deviation	0.60	1.10	4.8	4.8	4.8

Without highlighted values

Average	4.15	-1.87	23.2	22.3	27.5
Minimum	2.97	-3.96	16.3	15.4	20.6
Maximum	5.98	-0.27	32.3	31.4	36.6
Standard Deviation	0.56	1.01	4.4	4.4	4.4

B.5. *Trichites* sp. and *Gervilleioperna* sp.

In addition to the previous taxa discussed in Chapter 5 other two bivalves, which frequently occur in the Rotzo Formation (Trento Platform), were analysed from sclerochronological point of view: *Trichites* sp. and *Gervilleioperna* sp. (2 and 3 specimens, respectively).

Trichites sp. specimens were collected from Toraro Mt. (Vicenza; Fig. 1) whilst *Gervilleioperna* sp. come from the Lessini Mts. (Verona; Fig. 1).
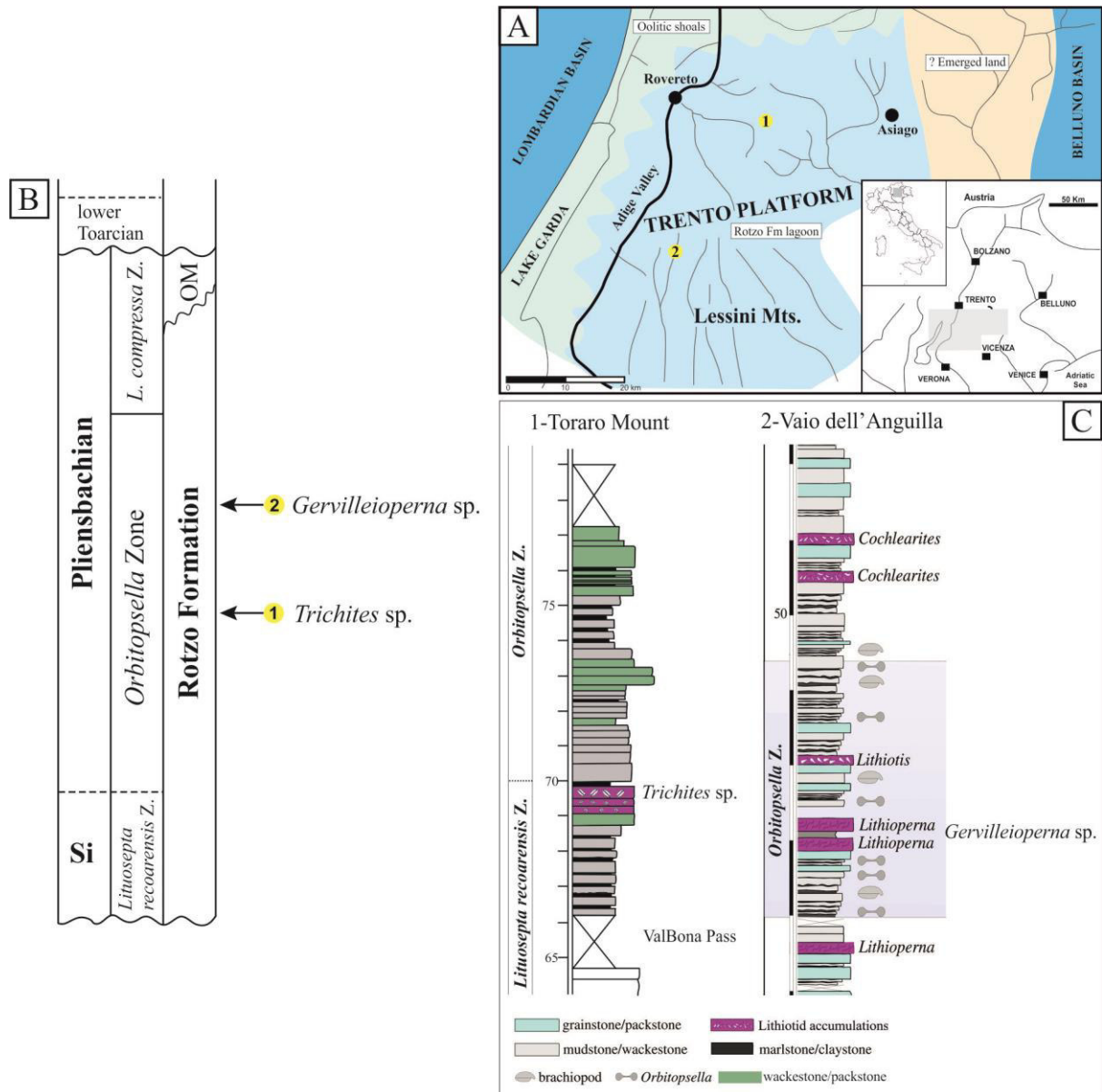
Figure 1. Geographical (A) and stratigraphic location (B, C) of the collected specimens in the Trento Platform (north-eastern of Italy). 1, Toraro Mt. (Vicenza); 2, Ponte dell'Anguillara (Vaio dell'Anguilla, Verona). Palaeogeographic map modified from Posenato and Masetti (2012). The stratigraphic sections (C) are modified from Coletta (2012; Toraro Mt.) and Posenato and Masetti (2012; Vaio dell'Anguilla). Z., Zone; *L. compressa* Z., *Lituosepta compressa* Zone; OM, Oolite di Massone; Si, upper Sinemurian.

Diagenetic screening was conducted using scanning electron microscope at the University of Ferrara (Italy). For sclerochronological studies, *Gervilleioperna* sp. were cut along the direction of maximum growth. All the collected *Trichites* sp. specimens are incomplete hampering a usual sclerochronological analysis (along the direction of maximum growth). Therefore, the growth pattern was tentatively observed on transversal sections. In these taxa, the growth pattern in the outer shell surface is less developed, therefore will not considered in the results. For further information see the paragraph 5.5 (Materials and methods) in Chapter 5.

Trichites sp. Voltz in Thurmann, 1832

Trichites sp. is distinguished by thick calcitic shell with well-defined simple prisms. SEM analysis confirms the good preservation of the analysed specimens (Fig. 2). In restricted areas, daily microgrowth increments were also recognised. Their thickness varies from ~3 to ~6 µm. Rarely, groups of 13 to 16 consecutive microgrowth increments formed distinct bundles.
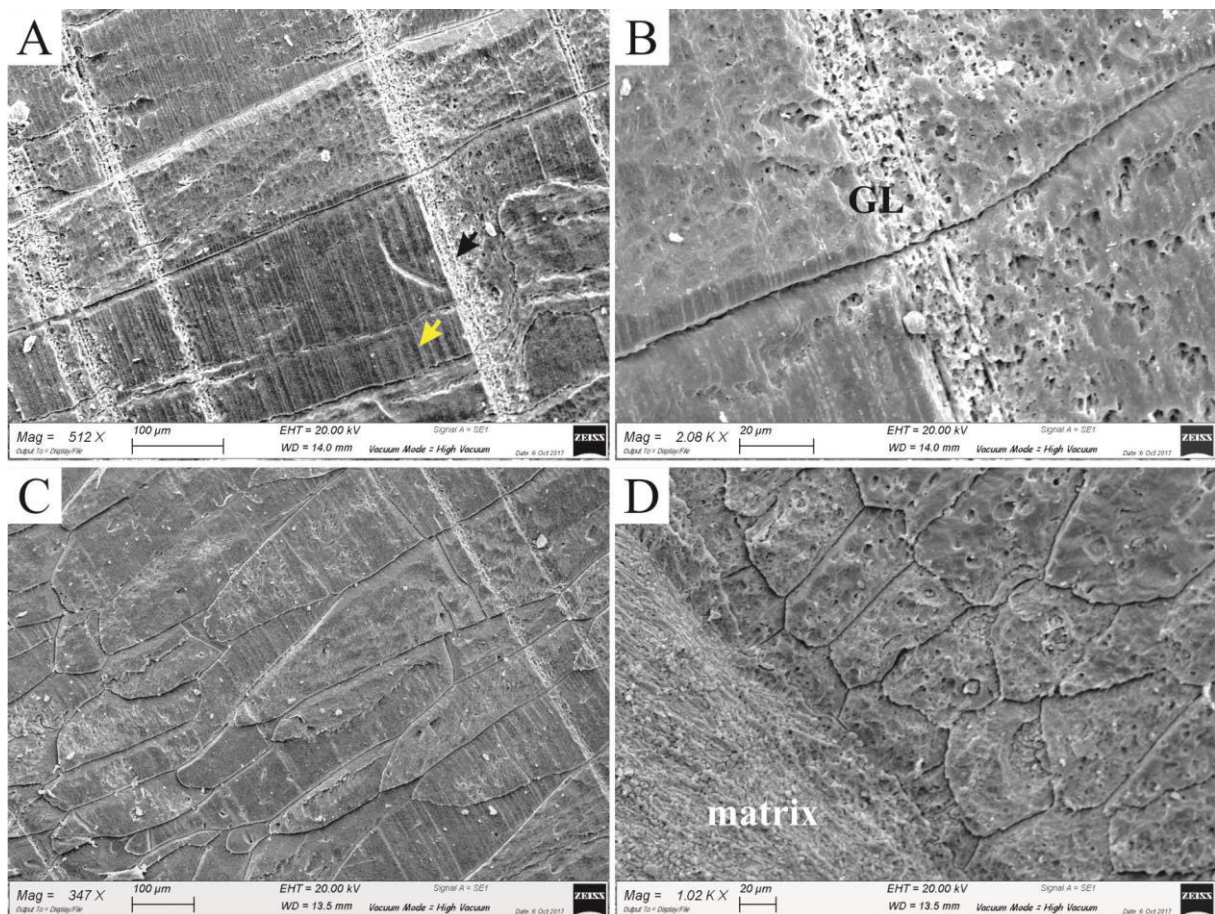
Figure 2. *Trichites* sp., specimen TR1. A–D) Simple prismatic layer with well-defined major (black arrow) and minor growth lines (yellow arrow). GL, growth lines.

A similar growth pattern was observed also in thin sections under transmitted light microscope. Daily increments (range from ~2.5 to ~6.5 μm in thick; average: ~4 μm) and fortnightly bundles were identified only in restricted shell portions (Fig. 3). The possible annual growth increments were not easy recognizable due to the unclear distinction of the annual growth lines (usually, more marked). Therefore, it's not possible to outline the bivalve life span even if the analysed specimens might not live more than few years.
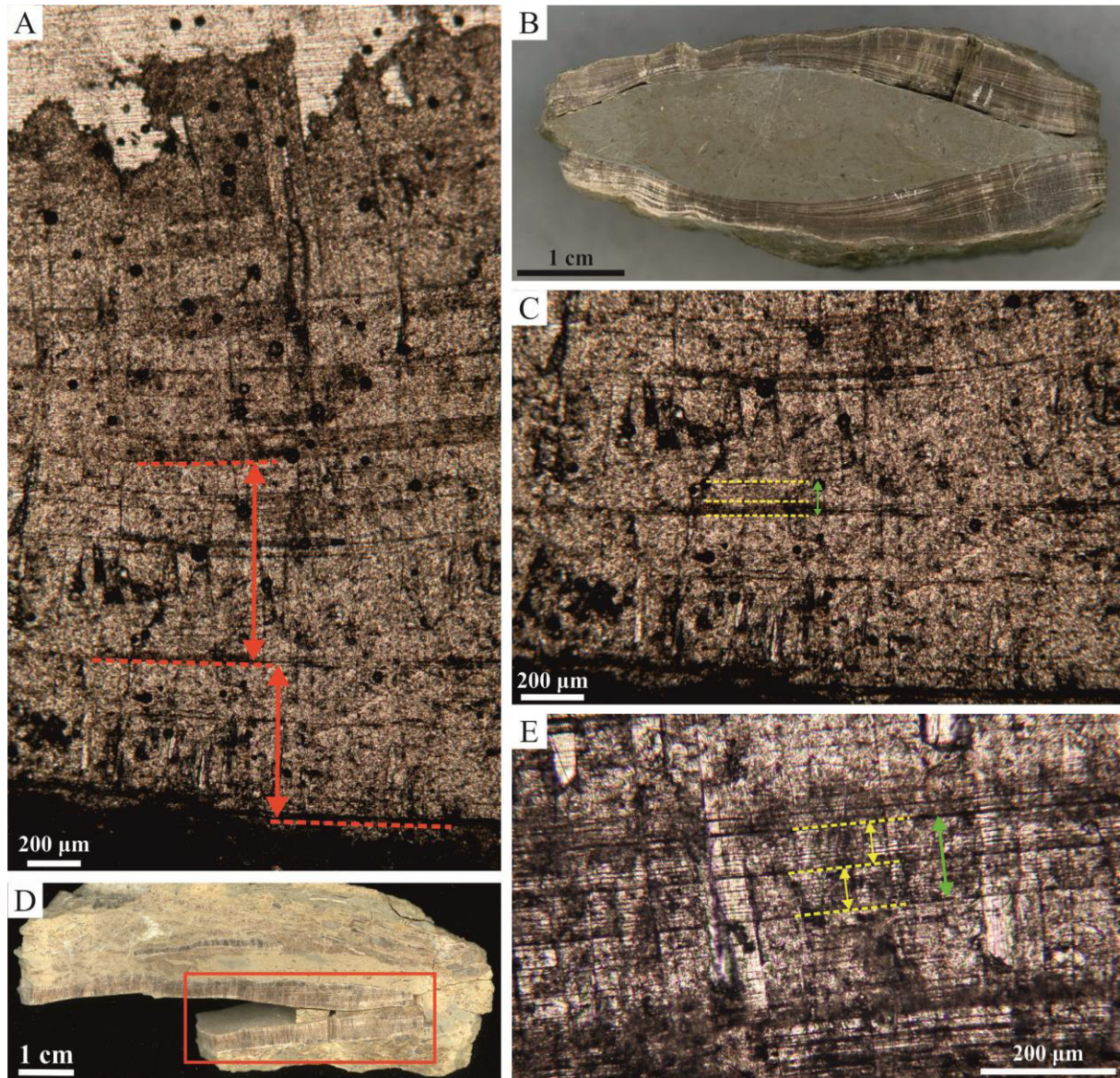
Figure 3. Growth pattern in *Trichites* sp. A–C) Specimen TR1. A) Stitched microphotographs of thin section showing the entire shell thickness with not well-defined growth pattern. The red lines highlight likely annual growth increments. B) Scanned image of the analysed articulated specimen TR1. C) Detailed microphotograph of likely monthly (green arrow) and fortnightly bundles (yellow lines). D, E) Specimen TR2. D) Scanned image of the analysed articulated specimen TR2. The red rectangle shows the analysed area. E) Detailed microphotograph of daily growth increments grouped in fortnightly bundles (~14 increments/bundle; yellow lines). The green arrow points to a monthly bundle.

Gervilleioperna sp. Krumbeck, 1923

Gervilleioperna sp. is distinguished by calcitic prismatic outer layer (frequently not preserved), a middle nacreous layer and an inner aragonitic fibrous prismatic layer. The calcitic and nacreous layers contribute to the growth increments recognizable in the shell surface (Tasselli, 1982; Accorsi Benini and Broglio Loriga, 1982). SEM analysis confirms the good preservation of the analysed specimens (Fig. 4).

The growth pattern was recognisable only in one of the three studied specimens (e.g., Fig. 5). It is better recorded in the thinner right valve since the thicker valve seems to be more prone to diagenetic alteration (Fig. 5A). Shell microgrowth pattern, recognised only in a restricted area, is characterized by daily increments, which vary from ~2 to ~4.5 µm in thick (average: ~3 µm), arranged in fortnightly bundles (~14 increments/bundle). Annual increments were tentatively recognised in the polished sections (Fig. 5A). About ~430 daily microgrowth increments were counted constituting a sufficiently long chronology in order to conduct spectral analysis (Fig. 5C).
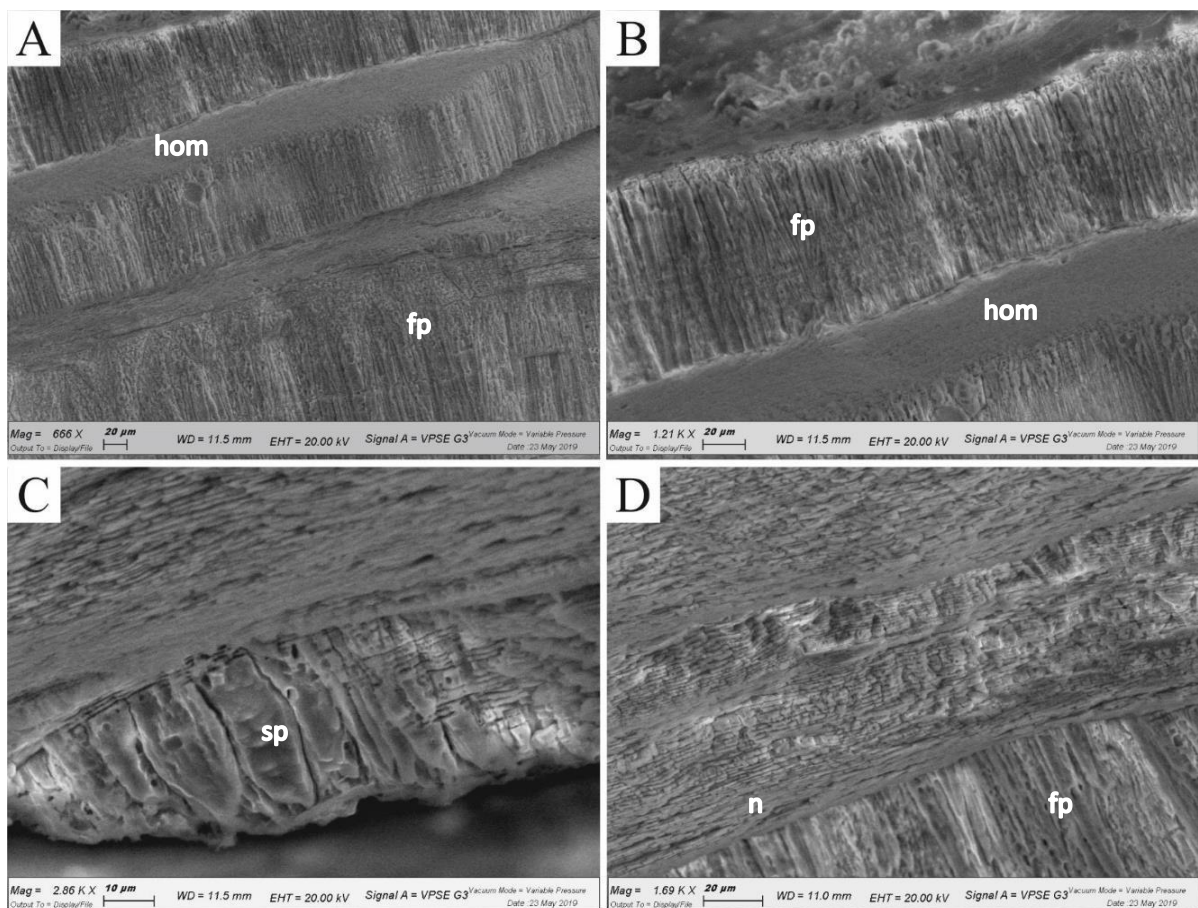
Figure 4. *Gervilleioperna* sp., specimen GP2. A) Inner shell layer with fibrous prismatic aragonitic layer intercalated with homogenous aragonite. This microstructure derived from degradation of prims (Accorsi Benini and Broglio Loriga, 1982). B) Detail of fibrous prismatic aragonite. C) Outer calcitic shell layer, simple prisms. D) Detail of nacreous layer occurring in the outer shell layer. For further details see Accorsi Benini and Broglio Loriga (1982). fp, fibrous prismatic; n, nacre; sp, simple prismatic; hom, homogenous microstructure.
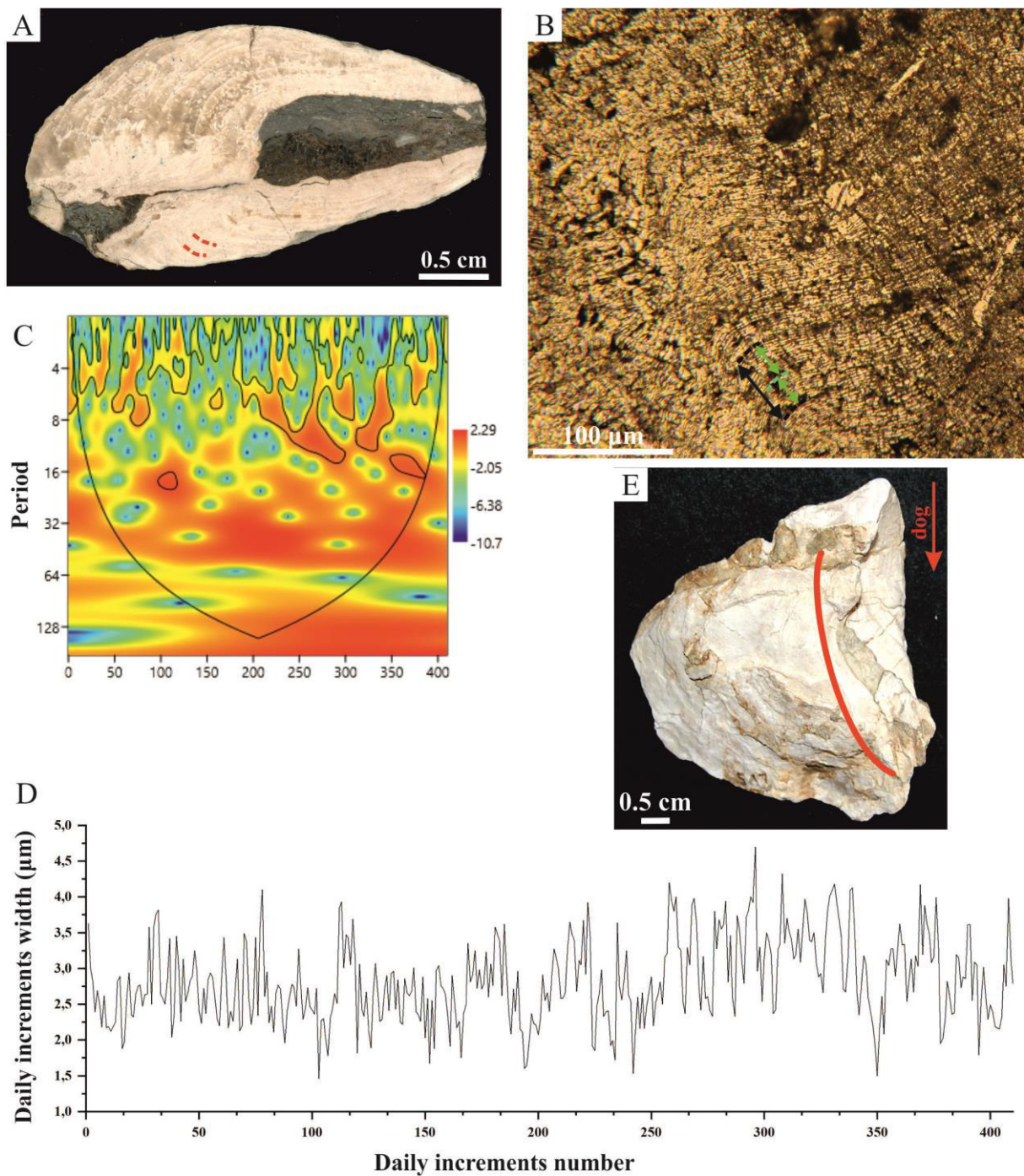
Figure 5. *Gervilleioperna* sp., specimen GP2. A) Scanned polished section with recognizable annual growth increments (red lines). B) Microphotographs of acetate peel with well-defined daily microgrowth increments. Dotted black lines indicate a monthly bundle while the green ones delimit fortnightly bundles. C) Continuous wavelet transformation analysis. Thick black contour lines display significant power (above the 5% significance level). The "cone of influence" shows the region where boundary effects are present (Hammer et al., 2001). D) Microgrowth increment width chronology. Assuming tide-controlled growth cycles, the chronologies represent 430 days. E) Articulated individual. Red line indicates the cutting direction. dog, direction of growth.

Continuous wavelet transformation spectra showed a signal at period of ~16 increments (Fig. 5C). The annual growth increments observed in polished slabs are ~1.5 mm in thickness. Considering the studied specimens, the taxon could live up to ~10–15 years.

Both taxa show a clear tidal influence (i.e., fortnightly bundles). *Trichites* sp. was likely semi-infaunal and usually inhabited moderate soft sediments in brackish lagoon (Fürsich, 1980; 1981). *Gervilleioperna* sp. shows a well-defined fortnightly growth pattern since this bivalve lived in the intertidal zone (e.g., Gambarin, 1986).

B.6. New data on *Lithiotis problematica* shell microstructures

B.6.1. Introduction

Lithiotis problematica Gümbel, 1871 was the first lithiotid taxon described in literature. Morphological and systematic studies were conducted by Böhm (1891), Reis (1903), Cox (1971), Accorsi Benini and Broglio Loriga (1977) and Chinzei (1982). The mode of life was discussed by Chinzei (1982), Seilacher (1984; 1985) and Savazzi (1996).

Lithiotis is characterized by a dorso-ventrally elongated and inequivalve shell. The thicker valve, usually defined as attached valve, is up to ~0.5 m height and up to 2 cm thick, whilst the other valve is thinner and defined as free valve (only few mm thick). In literature, the attached valve was alternatively considered as the right or the left (Accorsi Benini and Broglio Loriga, 1977; Chinzei, 1982). The individual was cemented at early life stage and mud-supported during the adult phase (e.g., Chinzei, 1982).

The inner face of the attached valve is divided in two parts: the umbonal or cardinal region and the body cavity (Accorsi Benini and Broglio Loriga, 1977; Chinzei, 1982). The body cavity located at the ventral end of the shell, is reduced respect to the whole shell size. It is distinguished by a spoon-like cavity with one large muscle scar located in central-posterior area. The shell is particularly thin and flat close to the ventral margin, likely due to weakly calcification or the occurrence of higher organic content of shell margins (e.g., Chinzei, 1982). The umbonal region is distinguished by central platform with several ridges and grooves and two lateral feather-like wings recording the growth increments. Reis (1903) observed rare articulated specimens. The free valve was represented by a thin calcareous lamina. He suggested that the thinner valve of *Lithiotis* is as high as the thick valve and the cardinal area should occur on the both valves. Accorsi Benini and Broglio Loriga (1977), observing rare specimens with the same calcareous lamina, proposed that the thin valve should be shorter, lid-like (opercular) and mostly restricted to the body cavity of the thick valve. Moreover, they reported that the outer face of the free valve was smooth and lacking, in the inner surface, of the typical features of the cardinal area of the attached valve.

Chinzei (1982) suggested that the ligament became non-functional after the juvenile stage and in the adult individuals the mechanism of opening and closing shell was based on elasticity of the thin free valve. Study conducted on well preserved articulated *L. problematica* specimens allow to clarify the occurrence of multivincular ligament placed in the ligamental grooves of the cardinal area (Savazzi, 1996). The latter author concluded that

the occurrence of a long ligament means that the free valve had the same height of the attached one (as reported also by Nauss and Smith, 1988) and the closure mechanism was based on flexibility of the free valve. On contrary, describing some articulated *Lithiotis* specimens studied in polished slabs, Nauss and Smith (1988) suggested that the thin and flat free valve closed by articulating.

Cox (1971, p. 1199) stated that *Lithiotis* shell is "*formed of lamellar calcite together with prismatic calcite*". Subsequently, other authors demonstrated that *Lithiotis* shell is essentially composed by aragonitic fibrous prisms, frequently alternated by nacreous wedges in the feather-like wings (e.g., Accorsi Benini and Broglio Loriga, 1977; Chinzei, 1982). In well preserved specimens generally occurring in marlstones, the original aragonitic structures are detectable only in the outer part of the shell. The inner part of the shell is always recrystallized. This alteration is likely due to the occurrence of highly porous aragonitic chalky deposit (Chinzei, 1982). Only Chinzei (1982) provided some information on the microstructure of the free valve. He considered the free valve as composed by "*alternating prismatic and nacreous aragonitic layers interbedded with granular and prismatic calcitic layers*" (Chinzei, 1982, p. 188). However, he did not figure this architecture or demonstrated the mineralogical composition (his description also included *Cochlearites*) and the relationship between calcitic and aragonitic layers was not clearly defined.

The diagnosis of the family Lithiotidae lacks a clear documentation on the shell structure and composition of *Lithiotis* inducing Carter (1990) to describe with uncertainty the occurrence of an outer layer of calcitic prisms.

The finding of well-preserved and articulated specimens of *L. problematica* allows to clarify the occurrence and structure of the outer calcitic layer in this species. Moreover, the preservation of these lithiotid specimens allows to improve the knowledge of the free valve shell morphology. Additionally, the corroboration that *Lithiotis* is distinguished by bi-mineralic nacroprismatic shell could give new information on its systematic position.

B.6.2. Materials and methods

The studied materials were collected from a small lithiotid accumulation (Toraro Mt., Vicenza, Italy) dominated by *Lithiotis problematica*. Its stratigraphic position is illustrated in the Chapter 3 and in Brandolese et al. (2019; TorA2). The shell accumulation is ~4 m wide and ~30 cm high. The *L. problematica* shells are included in hard limestone which precluded to isolate specimens from the matrix. In this lithology the aragonitic portions are always recrystallized. Two collected rock blocks (here referred to as block A and block C; Fig. 1)

were cut perpendicular to the bedding surface in serial slabs about 1 cm in thickness (see Supplementary data). Each slab was polished and scanned with high resolution scanner (Epson Perfection V800 Photo) in order to reconstruct the lithiotid shells arrangement (for further details see Chapter 3 and Brandolese et al., 2019) and bivalve morphology.
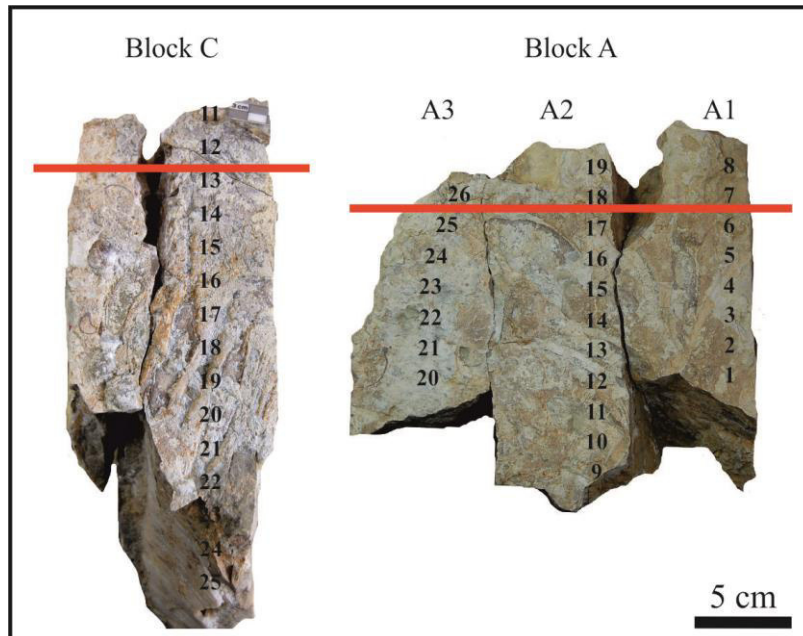
Figure 1. The studied blocks of TorA2, surface view (modified from Posenato et al., 2014). The red lines indicate the cutting direction. The bold numbers show the location of polished slices.

The most representative slabs were selected for further analyses in order to characterize the calcitic layer both in free valve (FV) and attached valve (AV) of *Lithiotis problematica*. The analysis was conducted by acetate peels, thin sections, SEM-EDS (Energy Dispersive X-ray Spectrometry), cathodoluminescence and Raman spectroscopy. Acetate peels and thin sections (4.5x6 cm), made from selected slabs, were observed with optical light microscope in order to assess morphology and shell architecture.

Two polished thin sections (ca. 4.5x3 cm) were observed with cold luminescence microscope (University of Ferrara, Italy) in order to detect the pristine nature of the prismatic layers. Cathodoluminescence (CL) microscopy is a powerful technique to study biominerals and, in particular to asses preservation of carbonate rocks and shells (e.g., Barbin, 2013). Calcite luminescence depends on the molar ratio of iron and manganese (Fe/Mn). High Mn content in the calcite lattice is an activator of luminescence, whereas Fe is a quencher (e.g., Garbelli et al., 2012). Mn is generally low in unaltered recent and fossil calcitic shells (e.g., Brand et al., 2003), where it could be preferentially incorporated during diagenesis (Brand and Veizer, 1980). The analysed thin sections were prepared according to the methodology proposed by Mugridge and Young (1984).

Bivalve samples were analysed for shell microstructure and major trace elements with SEM Zeiss EVO 40 scanning electron microscope coupled with EDS device set in pressure variable mode (University of Ferrara, Italy). Before the analysis, the samples were polished, etching with HCl 1% for about 10 seconds and clean with ultrapure water. They were not covered with gold in order to reuse them for further analyses.

Regarding mineralogy, Raman spectra were acquired at Department of Physics and Earth Science of Ferrara University (Italy) using HORIBA Jobin Yvon LabRam HR800 spectrometer coupled to Olympus BXFM optical microscope, equipped with ×10 and ×50 magnifications. The analysis was conducted on ultra-polished thin sections which allow to obtain better results. The instrument operates with He-Ne laser source with excitation wavelength at 632.81 nm and the laser beam diameter is about 1 mm. The investigated vibration frequencies spanned from 100 to 1600 cm^{-1}, covering all the frequency range both internal (molecular) and external (lattice) vibrations. All Raman spectra were smoothed and elaborated with data analysis and graphing software (further details in Supplementary data). Raman spectroscopy is a useful tool to rapidly and accurately identified sample mineralogy. This analysis easily distinguishes calcium carbonate polymorphs including aragonite, calcite, vaterite and amorphous phases (DeCarlo, 2018, and references therein). All calcium carbonates are distinguished by a strong v1 peak around 1085 cm^{-1} that represents the symmetric stretching of C–O bonds. Another C–O bonds (as in-plane bedding) in the ~700 cm^{-1} region is helpful to discriminate between calcite and aragonite (e.g., Urmos et al., 1991; Behrens et al., 1995). These peaks are called "internal modes" (or "molecular modes") because they are originated from vibrations between the C and O of carbonate (CO_3^{2-}). In addition, the Raman spectra of crystalline calcium carbonates contain other mineral-specific peaks, called "lattice modes" (or "external modes"). These peaks are in the <400 cm^{-1} region and result from vibrations between molecules in the lattice (e.g., Urmos et al., 1991). The Raman shifts available in literature do not perfectly agree each other (see Discussion) therefore the main peaks of calcite and aragonite are reported in Supplementary data.

For SEM-EDS analysis the *Lithiotis* shells were compared with other specimens collected from the Rotzo Formation (Trento Platform, Southern Alps). All the analysed samples are listed in the Supplementary data.

Because of unusual shell morphologies a specific nomenclature was already proposed in the past (e.g., Accorsi Benini and Broglio Loriga, 1977; Chinzei, 1982) and it is adopted also in this study (Fig. 2). In particular, the feather-like wings are distinguished by well-defined growth increments (e.g., Chinzei, 1982), here referred to as major growth increments.

Sometimes, in each major growth increment, weakly minor growth increments can be recognizable (here referred to as minor growth increments; e.g., Accorsi Benini, 1985).
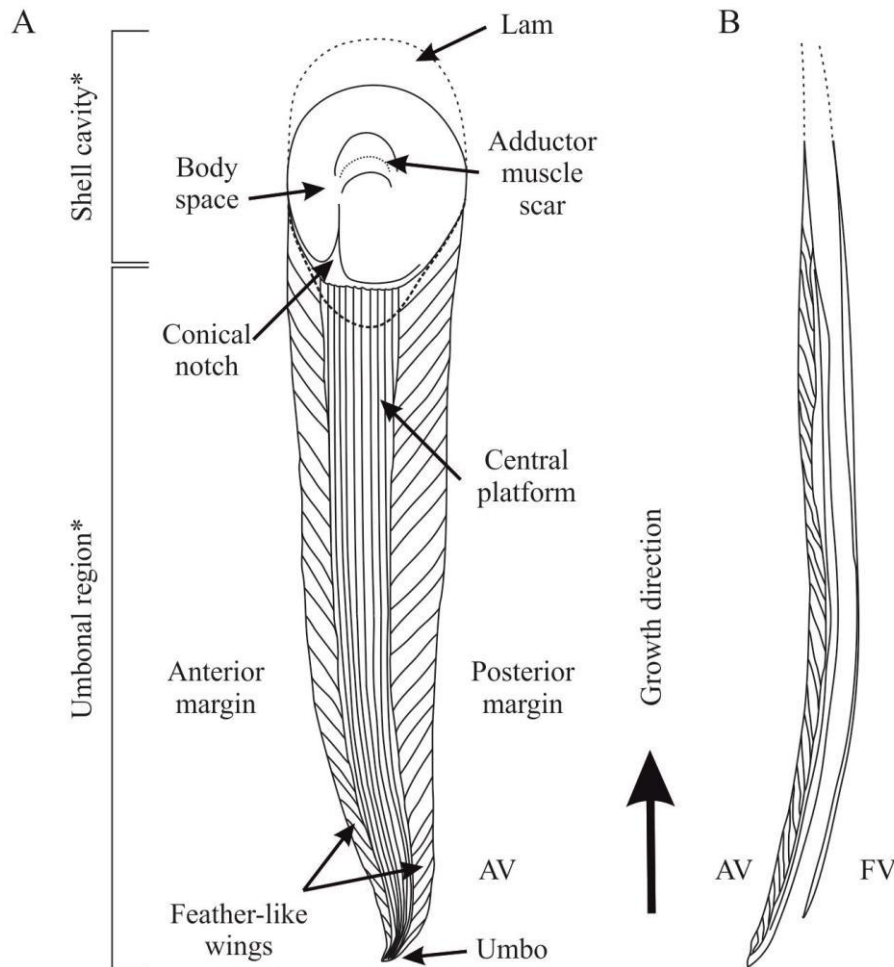
Figure 2. *Lithiotis problematica* and here adopted terminology (from Chinzei, 1982, modified). A) Internal view of attached valve. B) Side view of articulated individual. * Terms used by Accorsi Benini and Broglio Loriga (1977). The umbonal region is also called cardinal or apical area in Chinzei (1982). AV, attached valve; FV, free valve. Lam, conchiolin-rich thin lamellae (Chinzei, 1982). As suggested by Chinzei (1982), the feather-like wings should not be included in the cardinal area. The shell orientation is according to the up-right *L. problematica* mode of life.

B.6.3. Results

In the block A (Fig. 1) five *L. problematica* individuals were recognised (see Supplementary data). All the individuals are short and large (up to 11 cm high and 8.5 cm wide) and inclined between 40° to 50° (Ngadiuba, 2015) in respect to the vertical plane. They are articulated and the FV is well-recognizable. The reduced height can be related to a low sedimentation rate (see Chapter 4 for further details). The shells are dissolved in the umbonal region and the aragonitic layers are completely recrystallized. Frequently, in the upper part, the shell moulds are infilled by marls. Only few thin portions, opaque whitish in colour, correspond to the prismatic layers. These layers occur both in the attached and free valves.

The block C (Fig. 1) includes at least five individuals. The FV cannot always be distinguished. In this block the analysis was focused on the occurrence of prismatic layer in the attached valves.

In the polished slabs, the FV is well-defined towards the ventral area where it is ~1 mm thick. As the AV, the FV is dissolved towards the dorsal margin. In the middle part of the shell, the FV reaches a maximum thickness of ~3 mm. The inner face is smooth and slightly curved (Fig. 3). The outer face is characterized by squamose ornamentations with scales about 1 mm in high and they are more frequent in correspondence of body space (Fig. 3). In the FV the prismatic layers occur in the inner part of the external scales (Fig. 3). In thin sections and acetate peels under optical light microscope, the prisms are well-defined and frequently arranged in sub-layers (Fig. 3). Each prism is short and wide, oriented perpendicular to the inner face (e.g., Fig. 3F). The entire layer measured in longitudinal section is up to ~500 µm in thick. In horizontal section, the prismatic structure shows an irregular, almost polygonal, outlines of the prisms, whose major axes range from ~20 to ~60 µm wide. The completely recrystallization of the inner shell portions hampered to define the geometrical relationship between the outer calcitic layer and the inner aragonitic part. In the FV, in particular in the sample Fv5, the prismatic layer observed in polarized light (cross-light) is characterized by wavy extinction.

One isolated FV specimen was collected from the debris of TorA2. This specimen allows describing the internal surface characters clearly detectable on small shell portions. As supposed by Chinzei (1982), the FV is as high as the AV and shows the same internal features: a central platform with ridge and grooves structure and two feather-like wings with growth increments (Fig. 4). Due to the reduced thickness, the internal features are less prominent than the AV. The growth increments measured in the FV was comparable to those observed in some *Lithiotis* AV (see Chapter 5 for further details). Although the correct thickness is biased by the lower preservation state, the single major increment is ~0.5 cm thick and the lower ones are ~0.2–0.3 mm thick. The well recognizable scales thickness (~0.4–0.5 cm) is almost compatible with the measure of cross-sectioned shell in the polished slabs. The ventral region is distinguished by reddish area, without a calcified layer which could be considered as the end of the ventral region entirely made of organic matter, now oxidized (e.g., Chinzei, 1982; Posenato and Masetti, 2012).

The prismatic layer was recognised also in the outer AV shell face. In this surface the prismatic layer is not continuous (Fig. 3A). Apparently, the prismatic layer occurs also in the feather-like wings towards the inner face where the prisms are organized in thin sub-layers

(Fig. 5). In horizontal sections, the prisms have well defined polygonal outlines, with a maximum axis ranging from ~20 to ~60 µm (Fig. 5E).
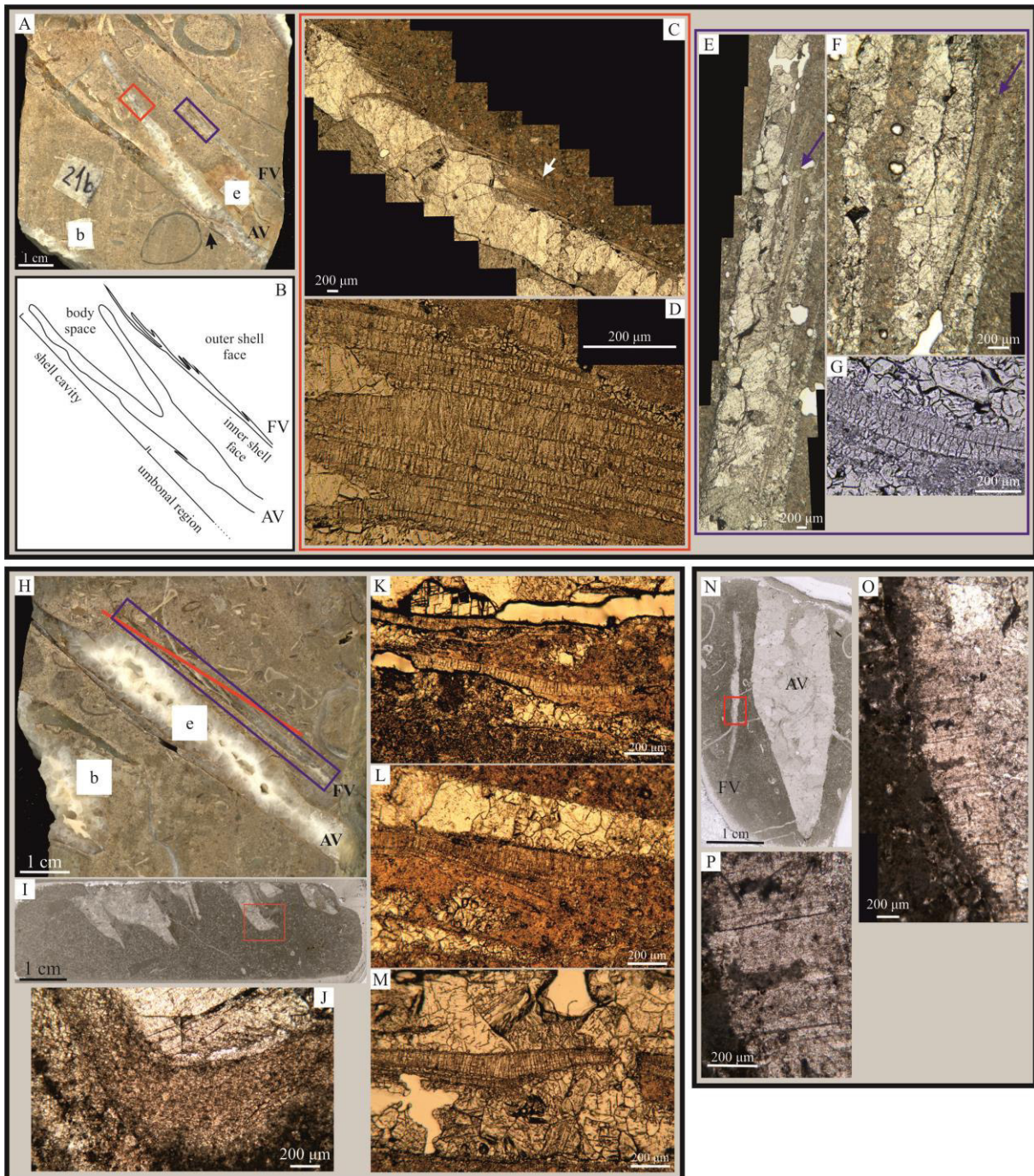
Figure 3. *Lithiotis problematica*, articulated specimen. A) Polished slab (slab 21b, block A3; see Supplementary data). The black arrow points to the outer prismatic layer in the AV. B) Sketch of attached valve (AV) and free valve (FV) showing the terminology used in the text. C, D) Detailed microphotographs of the red rectangle in the polished slab showing the prismatic layers in the AV (white arrow). E, F, G) Detailed microphotographs of the blue rectangle in the polished slab showing the prismatic layer in the FV (blue arrows) with well-defined prisms. H) Another polished slab cutting the same individual towards the umbonal region (slab 23b, block A3; see Supplementary data). I, J) Oblique/sub-horizontal section (red line points to the cutting direction) of outer prismatic layer. K–M) Detailed microphotographs of the blue rectangle in the polished slab showing the prismatic layer in the FV. N–P) Another articulated individual (isolated block). N) Thin section. P, O) Detailed microphotographs (red rectangle in thin section) of the prismatic layer in the FV (Fv5). See text for further details.
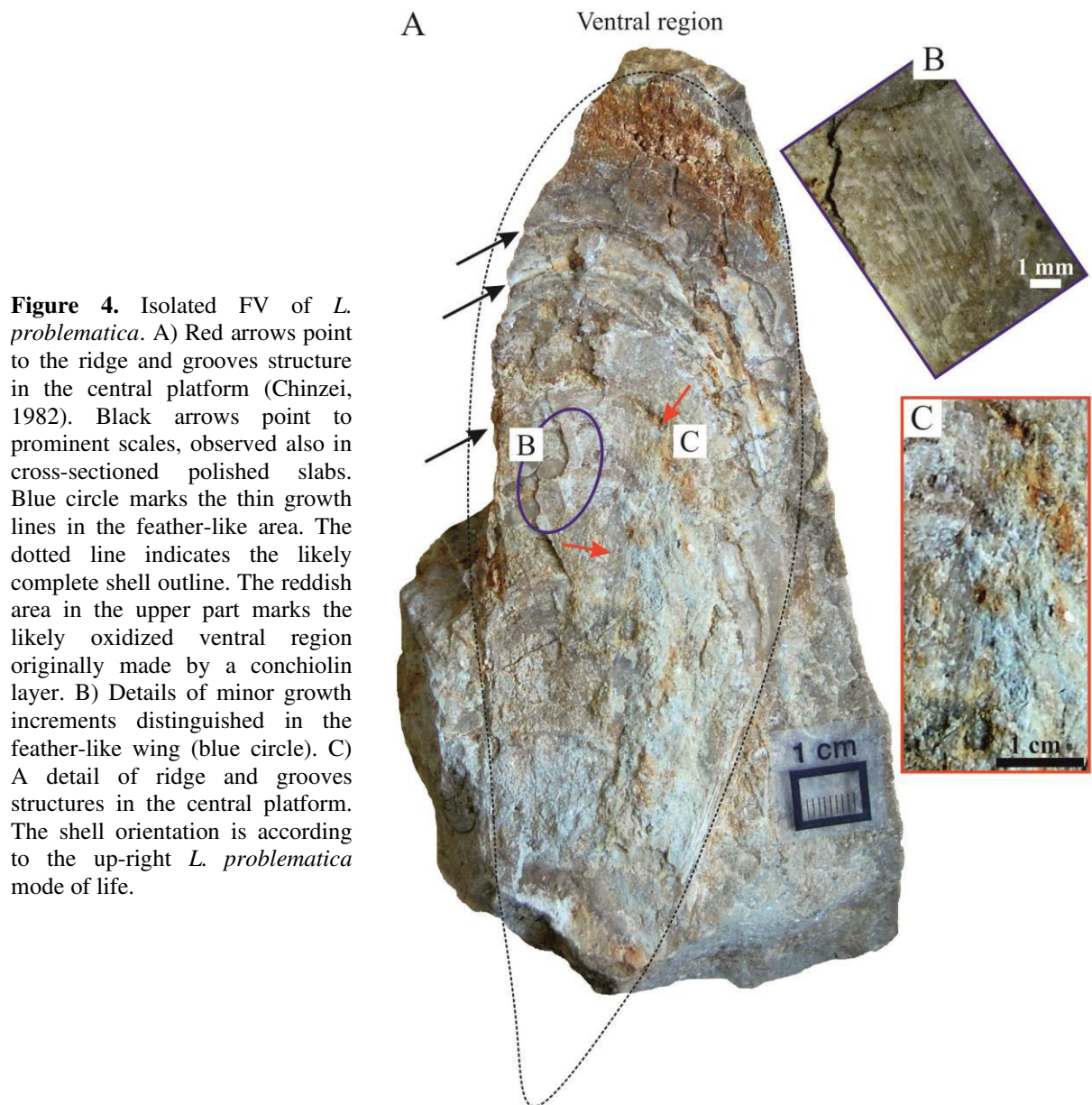
Figure 4. Isolated FV of *L. problematica*. A) Red arrows point to the ridge and grooves structure in the central platform (Chinzei, 1982). Black arrows point to prominent scales, observed also in cross-sectioned polished slabs. Blue circle marks the thin growth lines in the feather-like area. The dotted line indicates the likely complete shell outline. The reddish area in the upper part marks the likely oxidized ventral region originally made by a conchiolin layer. B) Details of minor growth increments distinguished in the feather-like wing (blue circle). C) A detail of ridge and grooves structures in the central platform. The shell orientation is according to the up-right *L. problematica* mode of life.

The prismatic calcitic layer, both of FV and AV, was observed by SEM in longitudinal and oblique/horizontal sections. The size of measured crystals varies from ~10 µm to ~30 µm in wide. Frequently, the prisms are organized in several sub-layers and their height (along c-axis) varies from ~50 µm to ~95 µm (Fig. 6). Small granular crystals are recognizable between two sub-layers whilst the base of the prisms is not recognizable, probably due to not optimal preservation state (e.g., Fig. 6). According to Carter et al. (2012) granular microstructure is defined as "*a variety of homogeneous shell microstructure consisting of more or less equidimensional, first-order structural units generally greater than 5 µm in width*" and is distinguished by homogenous microstructure *sensu stricto* which are distinguished by first-order structural units generally less than 5 µm in width (Carter et al.,

2012). In the analysed samples, each unit varies up to ~15 µm therefore could be defined as granular structures.
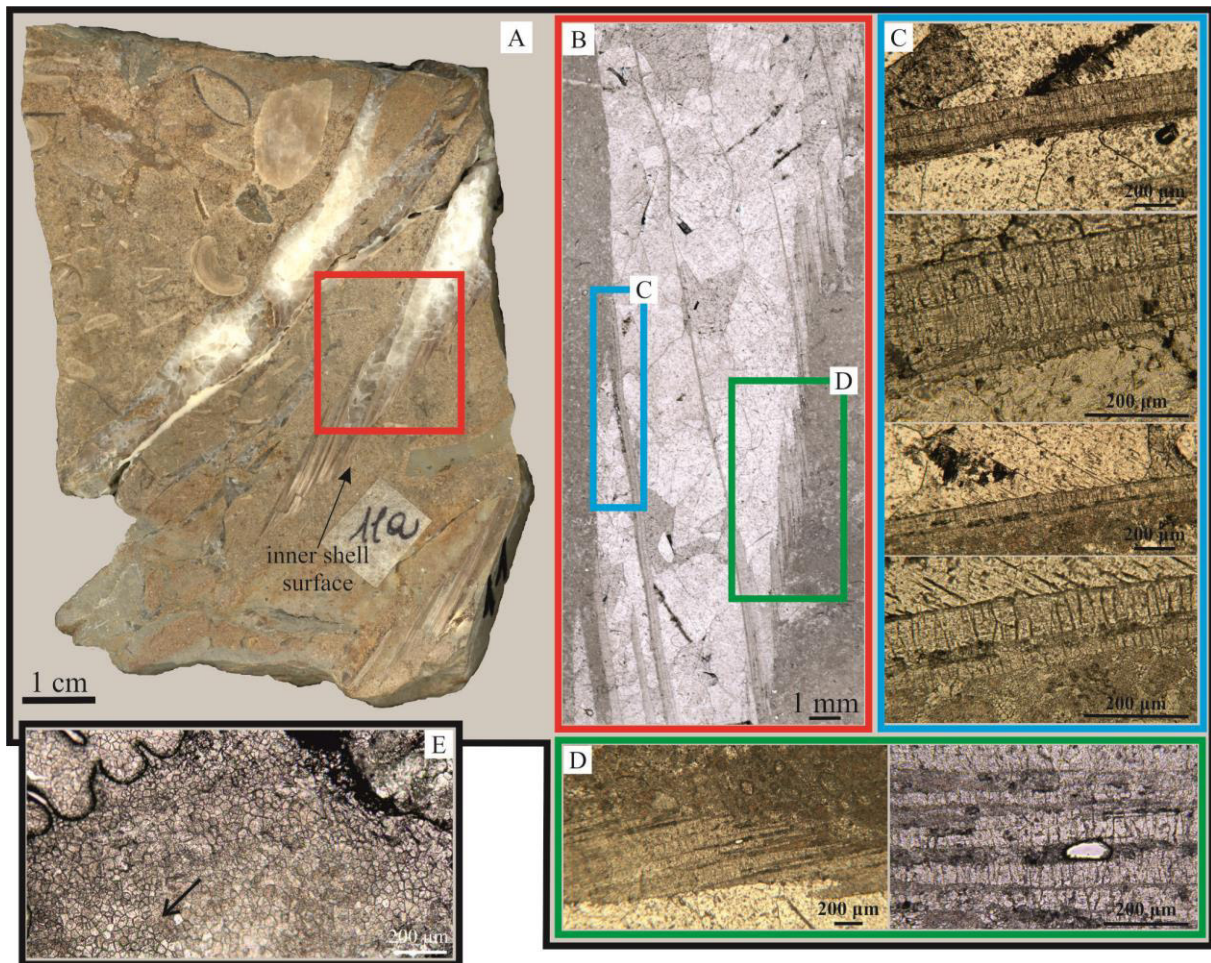
Figure 5. A–D) Attached valve of *L. problematica*, polished slab 11 (block A2). A, B) Polished slab and scanned acetate peel images. C) Acetate peel microphotographs of the outer prismatic layer. D) Detail of previous microphotographs. E) Acetate peel microphotograph with well-defined polygonal prism outlines (AV, slab 16 block C; surface view).

Figure 6 (following page). SEM images of prismatic calcitic layer in *L. problematica* FV and AV. A) Free valve, sample Fv2, slab 24 block A3. B, C) Free valve, sample Fv1, slab 22 block C. C) Horizontal section showing the prism surface. The yellow rectangle delimited well-define prism outlines. D–G) Free valve, sample Fv1, slab 22 block C. H) Attached valve, Sample Av1, slab 22 block C. I, J) Attached valve, sample Av2, slab 11 block A2. SP, simple prismatic microstructure; GM, granular microstructure; R, inner dissolved aragonitic layer replaced by calcite.
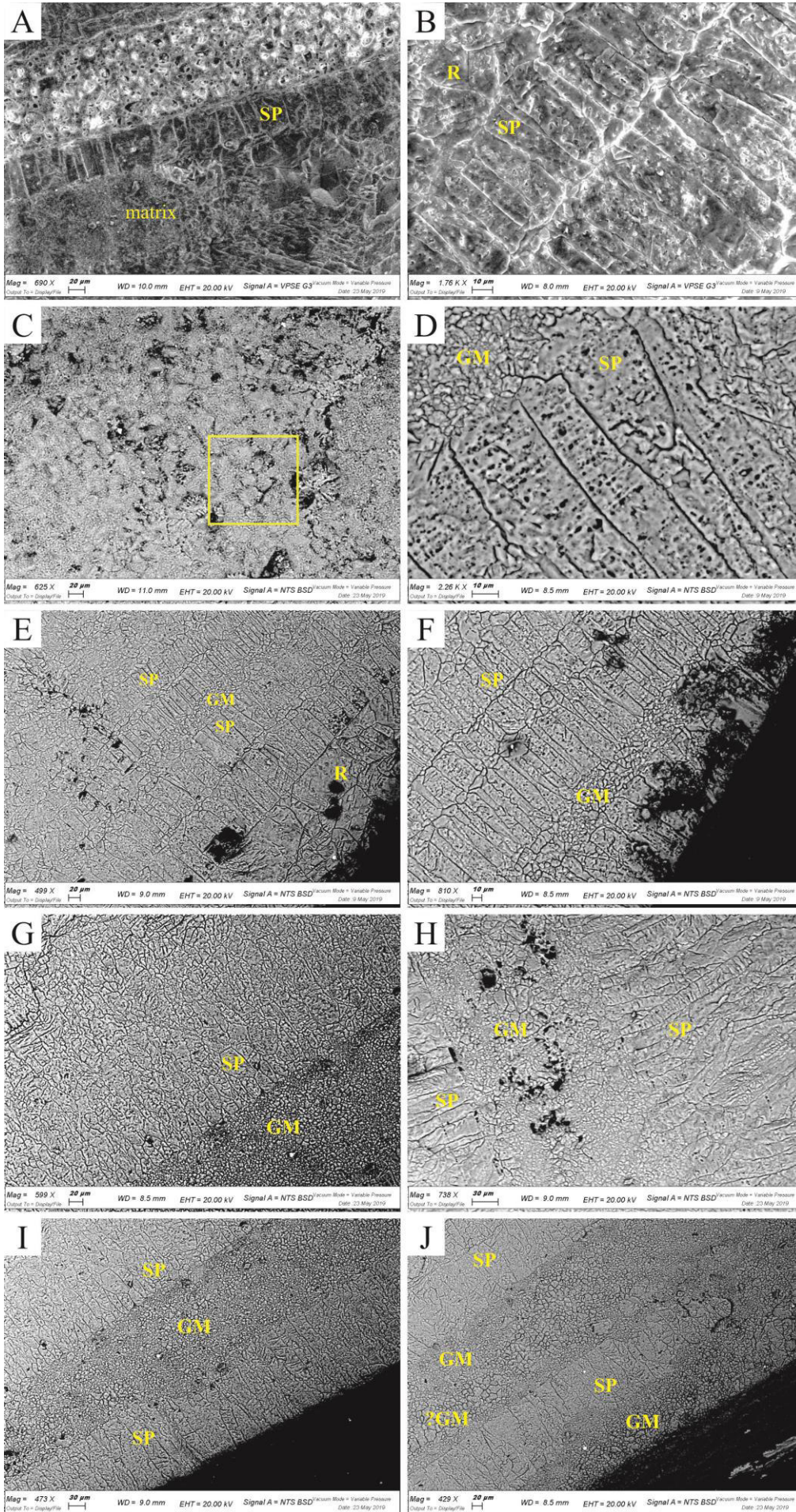
The prisms are different from the irregular fibrous prismatic microstructures (aragonite) which is reported for the inner part of *Lithiotis* shell. The prisms outlines observed in oblique/sub-horizontal sections are less defined (Fig. 6C).

The screened FV shows no luminescence in the prismatic layer as the AV does. The difference with the host rock is remarkable: peloids and surrounding matrix are not well preserved (Figs. 7, 8).
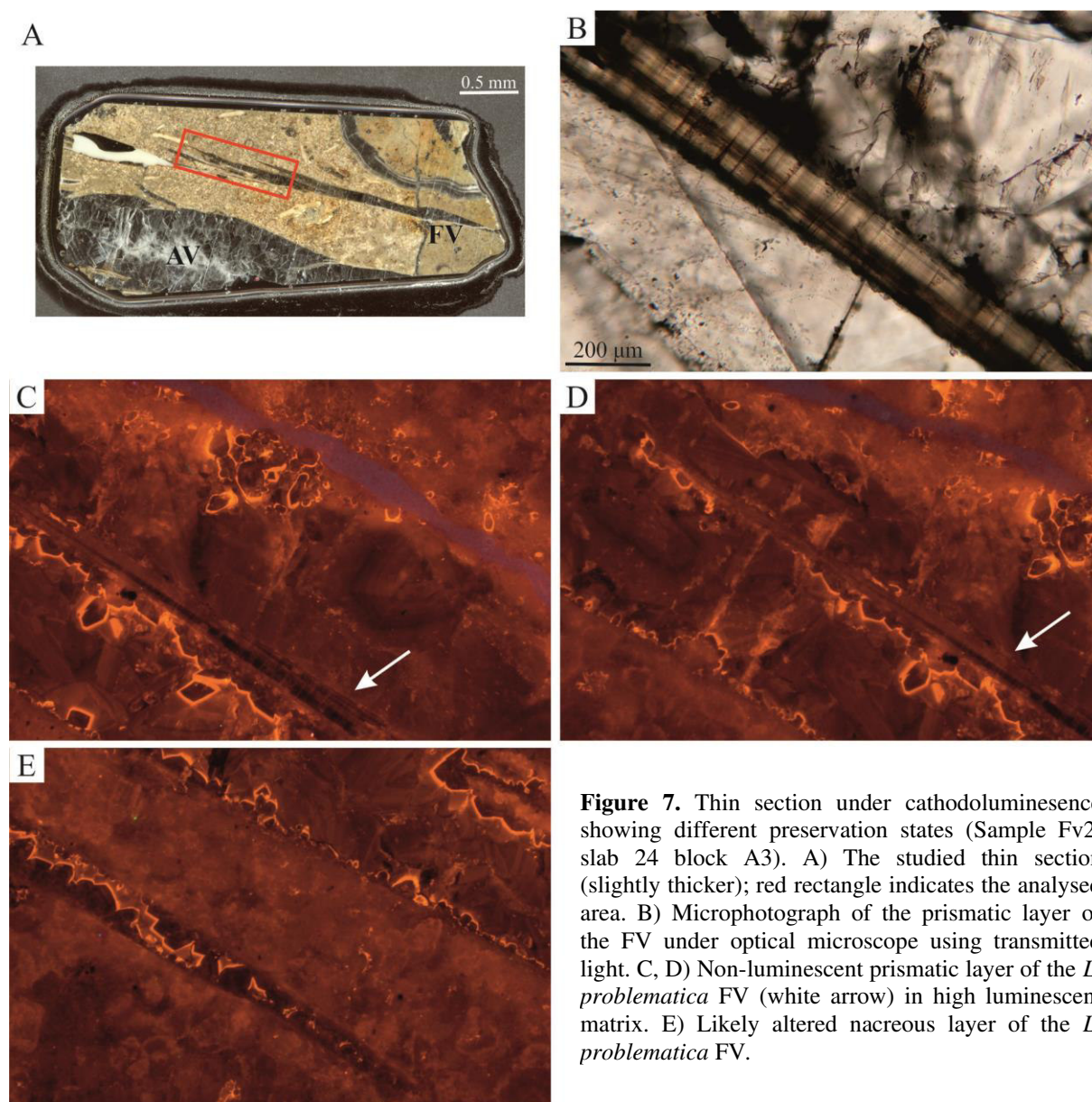
Figure 7. Thin section under cathodoluminesence showing different preservation states (Sample Fv2, slab 24 block A3). A) The studied thin section (slightly thicker); red rectangle indicates the analysed area. B) Microphotograph of the prismatic layer of the FV under optical microscope using transmitted light. C, D) Non-luminescent prismatic layer of the *L. problematica* FV (white arrow) in high luminescent matrix. E) Likely altered nacreous layer of the *L. problematica* FV.

The Raman shifts observed in the studied materials do not perfectly fit with the results available in literature (see Supplementary data). This variance could be due to instrumental differences among laboratories or to the fact that carbonates are solid solutions and their chemical composition importantly influences the Raman mode positions (Borromeo et al., 2017). Raman spectra confirm that calcite occurs in almost all the analysed samples (see

Supplementary data). The distinction with the recrystallized calcite is sharp due to the low fluorescence effect (see Supplementary data).
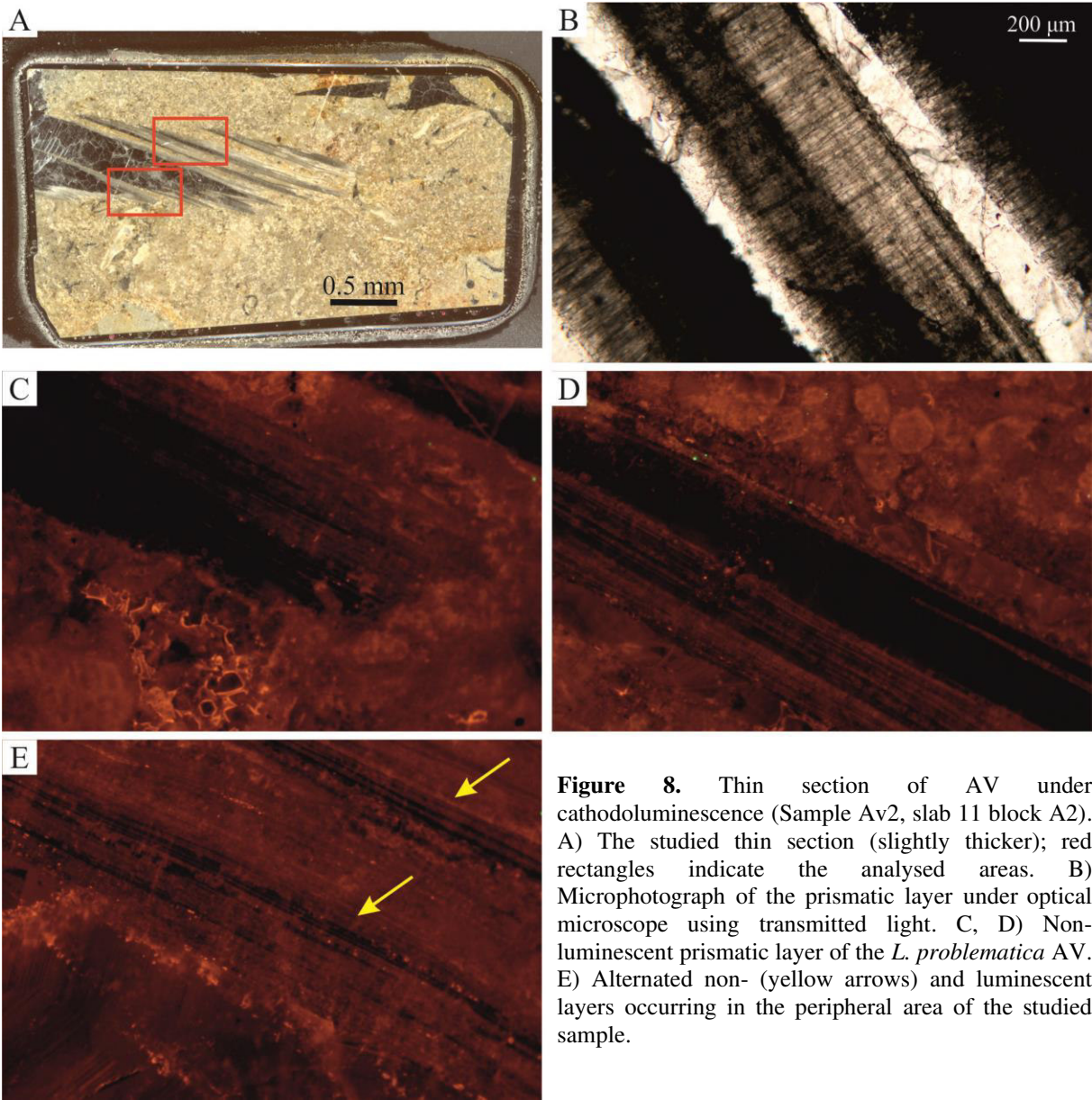
Figure 8. Thin section of AV under cathodoluminescence (Sample Av2, slab 11 block A2). A) The studied thin section (slightly thicker); red rectangles indicate the analysed areas. B) Microphotograph of the prismatic layer under optical microscope using transmitted light. C, D) Non-luminescent prismatic layer of the *L. problematica* AV. E) Alternated non- (yellow arrows) and luminescent layers occurring in the peripheral area of the studied sample.

B.6.4. Discussion

B.6.4.1. Preservation state

Multiple screening tests are highly recommended for the detection of the preservation state. CL was long considered a useful tool to revealed diagenetic modification along with SEM observations. In order to better define the prismatic layer recognised in the *L. problematica* individuals (TorA2, Toraro Mt. section) a comparison with the prismatic microstructure characterizing *Trichites*, another bivalve genus from the Rotzo Formation, was carried out (Fig. 9).

Trichites sp. (Family Pinnidae Leach, 1819) is distinguished by thick shell consisting of an outer shell layer originated by calcitic simple prisms (Carter, 1990; Fig. 9C). In the analysed specimens (collected from Toraro Mt. succession; see Appendix B.5 for further details), each prism varies from 70 to 140 µm wide.

SEM-EDS analysis revealed a reduced magnesium (Mg) content in the *Trichites* sp. and in the prismatic layer of analysed *Lithiotis* AV (TorA2; Fig. 9). In the FV of *L. problematica* the prismatic layer shows a negligible amount of Mg (Fig. 9B). In *Trichites* sp., EDS analysis also revealed the occurrence of sulphur (S) as reported by several author for the prismatic layer in *Pinna nobilis* (e.g., Dauphin and Cuif, 1999; Masuda and Hirano, 1980). Sulphur is associated with the organic content in the shell microstructure therefore its occurrence along with well-preserved prims (as observed with SEM; see Appendix B.2 for further details) confirm that the studied *Trichites* sp. specimen is pristine.

SEM-EDS is not probably the most suitable tool to detect the Mg content due to the low resolution of this technique. Considering that in calcite Mg varies during the diagenesis, the EDS analysis could give information on the enrichment in Mg. Comparing the SEM-EDS analyses carried out on well-preserved calcitic shells (i.e., *Trichites* sp.) along with cathodoluminescence analysis, a neomorphic alteration in the analysed *Lithiotis* specimens can be excluded. The analyses confirm that the observed calcitic prismatic layer in *L. problematica* (TorA2) is pristine. It's might be possible that a gently alteration could interest the prisms as suggested by the less-defined border observable in some samples (e.g., Fig. 6I–J).

Regarding the granular microstructure, it might be possible that slight alteration interested this layer as suggested by the wide size range of units. Moreover, the granular microstructure could be associated with shell dissolution induced by changes in paleoenvironmental conditions (i.e., temperature; e.g., Lutz and Rhoads, 1980). In this case, the microstructural

changes are gradual instead of distinguished by sharp contact as in the analysed *Lithiotis* specimens.
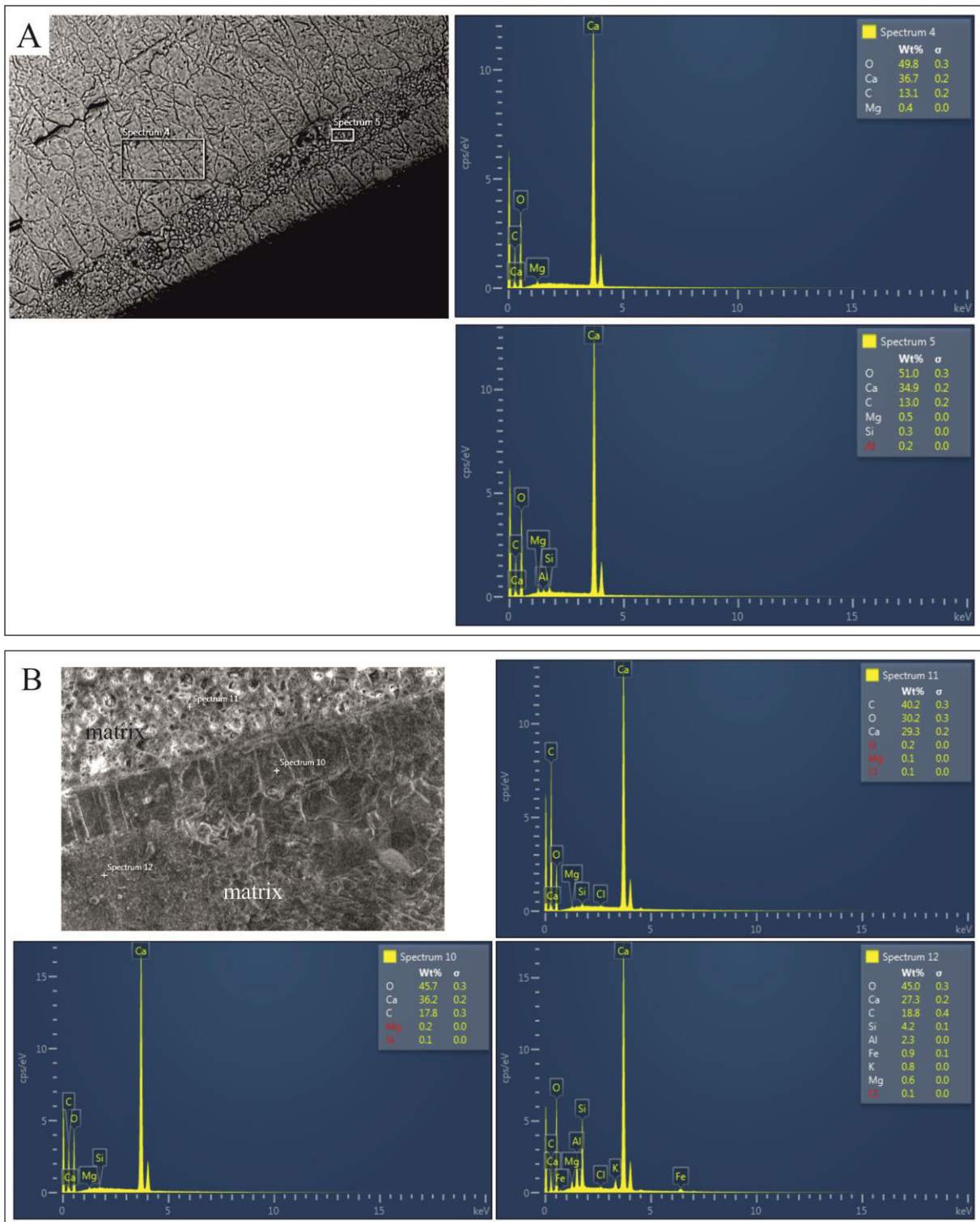
Figure 9. SEM-EDS analysis of *Lithiotis problematica* AV (A) and FV (B). For AV and FV, the chemical composition is compared with the surrounding sediment matrix. Mg was detected in AV while in FV it is below the detection limit (red label).
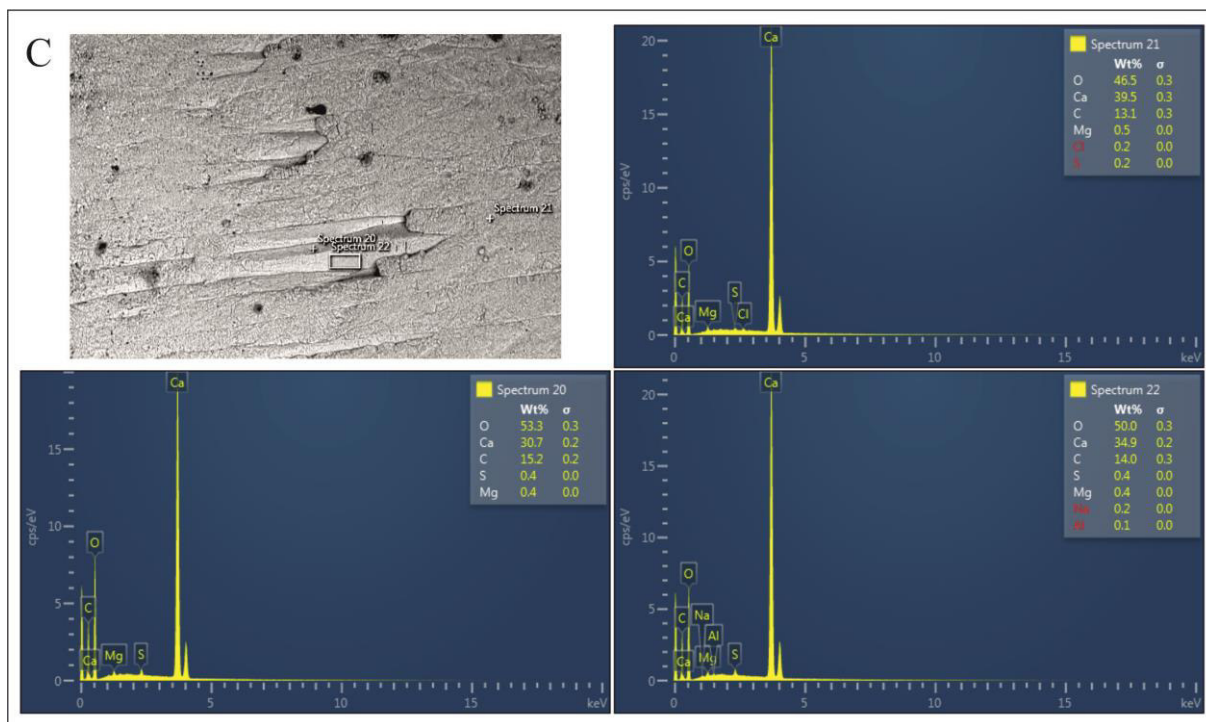
Figure 9. *continued*. C) SEM-EDS analysis of *Trichites* sp. (specimen collected from Toraro Mt. section; see Appendix B.5 for further details) In this taxon, S occurrence is associated with higher organic content in the prismatic layer.

B.6.4.2. *Lithiotis problematica* Free Valve

The bivalve shell is constituted by carbonate mineral and organic matrix. Carbonates could be aragonite or calcite while organic matter is essentially constituted by proteins. The mutual spatial arrangement between carbonates and organic matrix is translate in several type of microstructure which are characterized by specific mechanics proprieties. The shell secretion is essentially controlled by genetic and environmental factors (e.g., temperature).

In the analysed free valves, the aragonitic portion was completely recrystallized hampered the identification of original microstructure and arrangement. Probably, as briefly mentioned by Chinzei (1982), the aragonite occurred as fibrous prismatic and nacre layers.

The combination of higher organic matrix in the periostracum and the simple prismatic layer, which usually occurs as outer layer, provide an enhancing shell-margin flexibility (Carter, 1980). In the lithiotids the flexibility of the FV was already supposed by Chinzei (1982) and confirmed by Savazzi (1996). Their hypothesis was based on shell morphology and ligament function. No specific microstructural data were considered until now.

Considering the growth pattern observed in longitudinal sections, Chinzei (1982) suggested that a conchiolin-rich fringe (not in *sensu* Carter et al., 2012) could characterized the ventral margin of *Lithiotis* (both in AV and FV). The interruptions of growth lines only one or two centimetres beyond the muscle scar indicate the outer shell layer was not so

extended (Chinzei, 1982). This could hamper the accommodation of the gills, so the presence of conchiolin-rich lamellae may be expected along the ventral margin (Chinzei, 1982). The reddish area observed in the isolated FV (Fig. 4), likely derived from oxidation of conchiolin-rich lamellae during the diagenesis.

The calcitic prismatic microstructure in pteriomorphian bivalves contains the highest content in organic matter recorded in molluscs (Checa et al., 2005), prone to diagenetic alteration. The organic content seems to be the main controlling factor involved in the microstructure alteration (e.g., Glover and Kidwell, 1993; Chadwick et al., 2019).

On the outer FV face, the prismatic calcitic layer occurs only in restricted portions and it is arranged in protruding ribs, or as isolated prismatic fragments (Fig. 10). This aspect is likely associated with the maceration process. The maceration is due to the combination of dissolution and degradation of organic phase in shell microstructure which allows the breaking down of carbonate shell into various structural subunits (Alexandersson, 1978; 1979; Fig. 10G). In particular, the prismatic calcitic degradation was more intense in the outer side of the scales whilst the segments sheltered between two scales are more prone to preservation in case of rapid burial (Fig. 10).

A similar process was also recognised in a *Trichites* sp. specimen collected from Toraro Mt. (Fig. 11). This genus is distinguished by organic-rich prismatic calcite as outer layer. The rapid burial occurred in TorA2 probably allowed the preservation of the prismatic calcitic layer both in *Lithiotis* FV and AV.

In *L. problematica* FV, the common occurrence of prismatic layer remains close to shell cavity is due to the upward shift of ventral margin during the bivalve growth. The flexibility requested by the opening shell mechanism is allowed by the ventral region whilst is not necessary towards the umbonal region. Consequently, the loss of the outer layer could also occur before bivalve death and it is not necessarily associated with diagenetic processes.
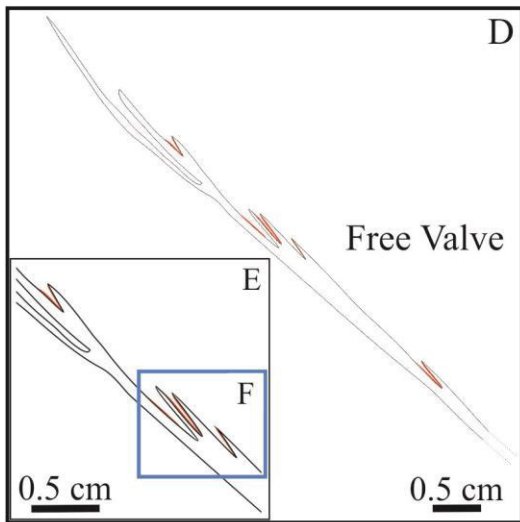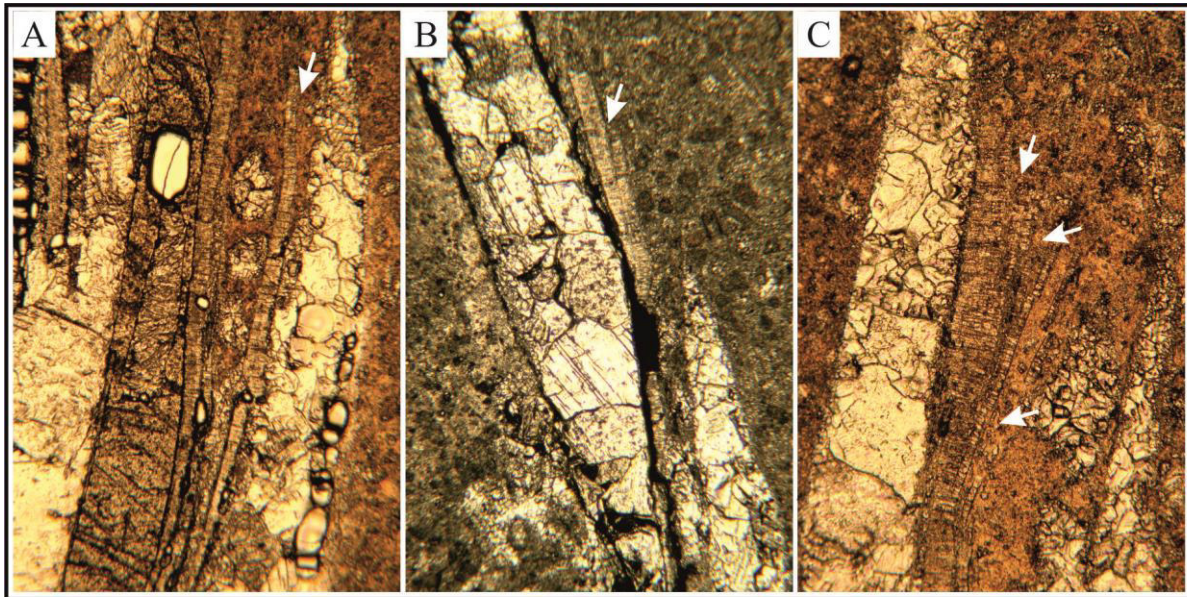
Figure 10. The arrangement of the outer prismatic calcitic layer and the maceration process in *L. problematica* FV.

A–C) Observed prismatic layer in the studied specimens (white arrows). D, E) Sketch illustrating the position of calcitic prismatic layer (red portions) in *L. problematica* FV, as observed in the polished slabs. F) Reconstruction of the original location of the outer calcitic layer (red portions). The light blue rectangle indicates the portions loosed during the pre-diagenetic phase. G) Maceration process which involves the outer prismatic layer. The different prismatic layer thickness observed in the studied specimens is due to the preservation state and the progress of maceration process. See text for further details.

297
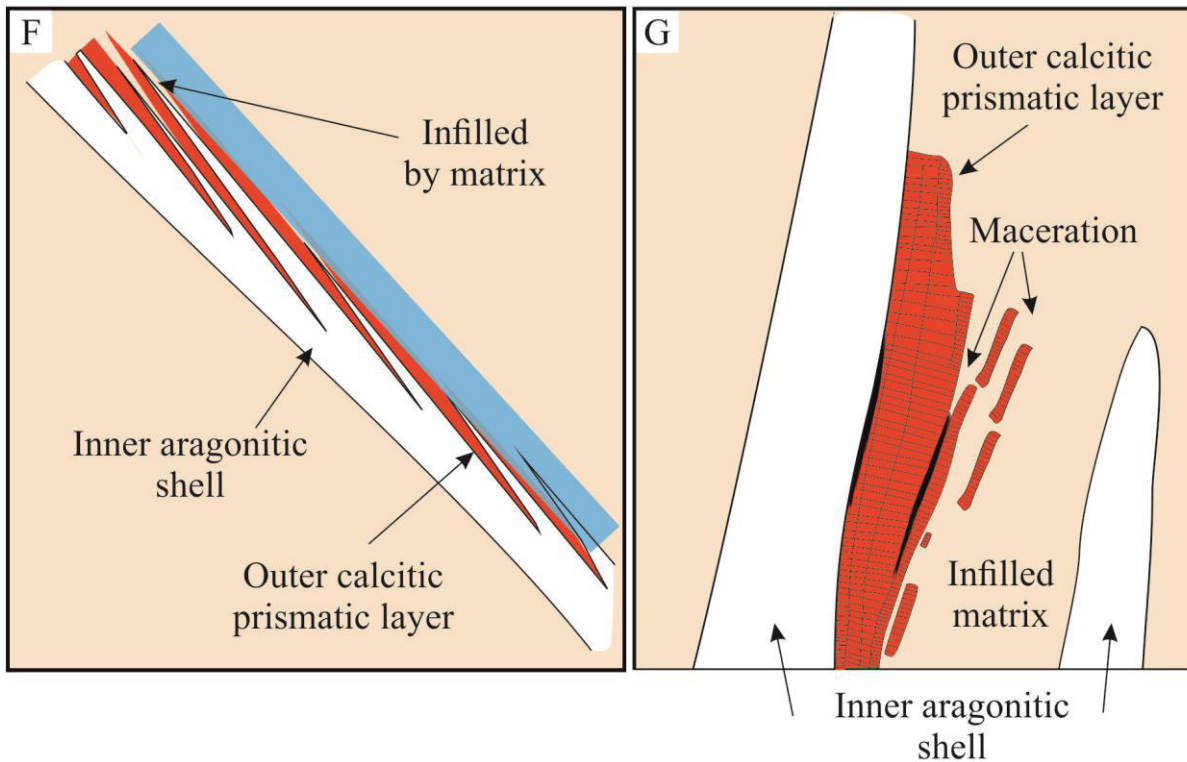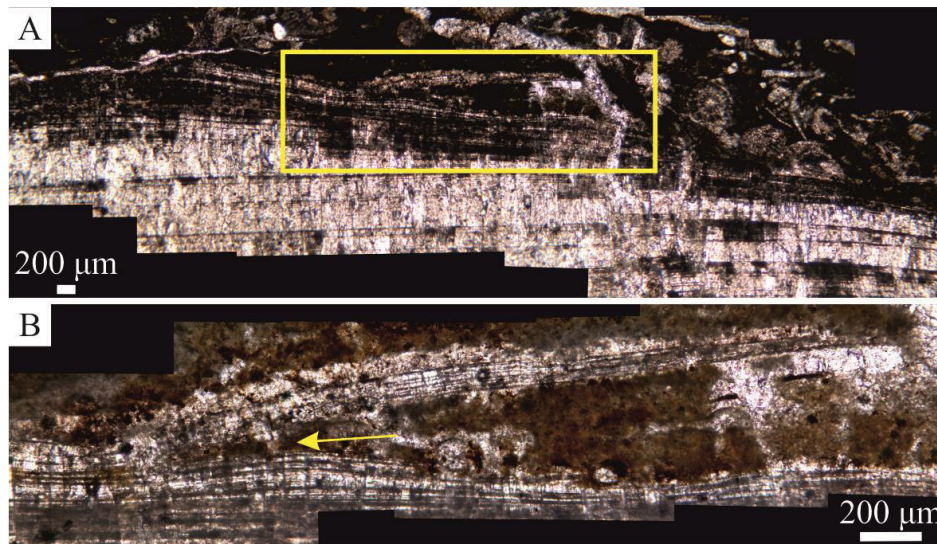
Figure 11. A, B) *Trichites* sp. specimen collected from Toraro Mt. (Vicenza) (distort stitched microphotograph). B) Detail microphotographs of Fig. A (yellow rectangle). The maceration process occurring in the outer calcitic prismatic layer of *L. problematica* is also observable in this genus (yellow arrow). See text for further details.

B.6.4.3. *Lithiotis problematica* Attached Valve

In the *L. problematica* AV, the occurrence of the outer prismatic layer was just presumed (Chinzei, 1982) and in the previous well-studied specimens was never documented. According to the observations on polished slabs and acetate peels, the thin calcitic prismatic layer occurs in the outer shell face extended up to of external border of the feather-like wings (Fig. 12A–C). The outer shell surface is characterized by more or less prominent ribs, which correspond to the main growth increments recognizable in the feather-like areas (e.g., Fig. 12). During the shell growth, the up-right shift of the body cavity leads the adding of new shell materials with the contemporaneous shift of the prismatic layer which never reaches the central platform. Frequently, the outer shell layer is not preserved. Its absence in the ventral region could be due to pre-diagenetic alteration because of the reduced thickness which usually characterised this area. On contrary, the rapid burial which occurred only in the lower part of the accumulation hampered the maceration process which imply the rapid degradation of the outer prismatic layer.

The AV sections observed in the TorA2 slabs are oblique, up-right directed allowing to observe the interdigitate prismatic arrangement in feather-like wings (e.g., Figs. 5, 12). In the observed specimens, the apparently occurrence of prismatic layer towards the inner shell face (e.g., slab 21 block A3; Fig. 3A–C) could be associated with a section-cutting through the area proximal to the end of cardinal area, in the wing-regions (Fig. 12D). The attached valve observed in the polished slabs 11a (block A2; Fig. 5) is instead a tangential section of

the adult bivalve shell (Fig. 12E). Peripheral areas were calcite-rich therefore the occurrence of several calcitic layers are more frequent (Fig. 5).
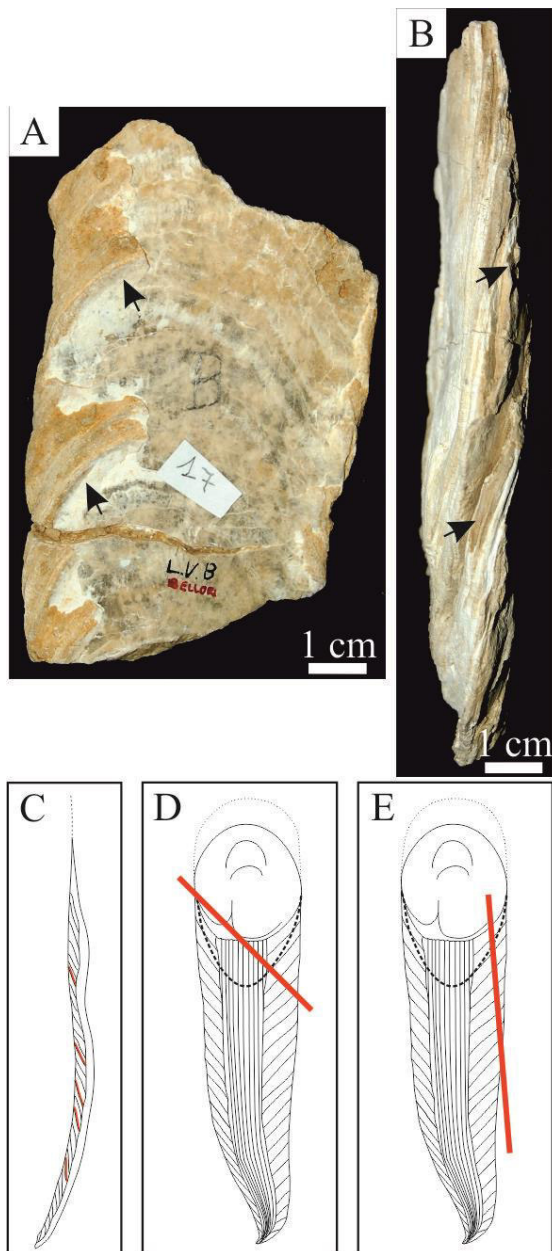
Figure 12. A, B) *Lithiotis problematica* AV (specimens deposited at "Piero Leonardi" Museum, University of Ferrara, Italy). A) Outer face with quite preserved growth increments corresponding to those in the feather-like wings. B) AV of another specimen, lateral view. The growth increments are well-defined along the side. Black arrows point to the prominent ornaments both in profile view and outer shell face. C) Sketch showing the location of prismatic layer remains in the *L. problematica* AV (red portions); side view. D, E) The section-cutting of the specimens in the Figs. 3A and 5, respectively confirm the occurrence of prismatic calcitic layer only in the external portions of the feather-like wings of the AV. In the Fig. D and E, the black dotted lines indicate the umbonal cavity.
The shell orientation is according to the up-right *L. problematica* mode of life.

Considering the large number of collected specimens, the sampling bias can be ruled out for the absence of documented calcitic outer layer in the previous studies. The absence is therefore due to taphonomic alteration. The most studied and well-preserved lithiotid specimens are collected from the Lessini Mounts (see Chapter 5 for further details), from organic-rich marlstones. The high organic content and low/absent permeability of these sediments contribute to the preservation of aragonitic layers. Surprisingly, the higher stability of calcite respect to aragonite should contribute to the preservation of the calcitic layer.

Therefore, the previously discussed maceration process could explain the lack of outer prismatic layer in the specimens collected in the past.

B.6.4.4. Systematic remarks

Originally, *Lithiotis problematica* was included in family Lithiotidae Reis, 1903 (e.g., Accorsi Benini and Broglio Loriga, 1977). Bouchet and Rocroi (2010) invalidated the authorship of Lithiotidae Reis, 1903, because Reis (1903) used the name "Lithiotiden" that is a German vernacular name published after 1900, and thus not available according to the ICZN. The author of Lithiotidae is therefore Cox (1971), and the nomenclatural priority pertains to the Plicatostylidae Lupher & Packard, 1929. Now, the valid *Lithiotis problematica* Gümbel, 1871 classification is the following (Carter et al., 2011):

Class Bivalvia Linnaeus, 1758 in 1758–1759
Clade Eubivalvia Carter, nov.
Subclass Autobranchia Grobben, 1894
Infraclass Pteriomorphia Beurlen, 1944
Cohort Ostreomorphi Férussac, 1822 in 1821–1822
Subcohort Ostreioni Férussac, 1822 in 1821–1822
Megaorder Ostreata Férussac, 1822 in 1821–1822
Order Ostreida Férussac, 1822 in 1821–1822
Suborder Malleidina! J. Gray, 1854
Superfamily Pterioidea! J. Gray, 1847 (Goldfuss, 1820)
Family Plicatostylidae Lupher & Packard, 1929
Genus *Lithiotis* Gümbel, 1871
Lithiotis problematica Gümbel, 1871

In literature, another genus similar to *Lithiotis* was reported: *Plicatostylus* Lupher & Packard, 1929, which is considered a junior synonym of *Lithiotis* Gümbel, 1871 (Grubić, 1961; Buser, 1965; Broglio Loriga and Neri, 1976; Accorsi Benini and Broglio Loriga, 1977; Smith and Tipper, 1986; Nauss and Smith, 1988; Debeljak and Buser, 1998; Aberhan, 1998, 2001; Fraser et al., 2004; Ros-Franch et al., 2014).

In the family Isognomonidae Woodring, 1925, the calcitic prisms show mostly irregular, wavy polycrystalline extinction in crossed polarized light (Carter, 1990). The same extinction is shown in the family Bakevellidae King, 1850 distinguished by outer shell layer,

usually calcitic, with regular prisms in both valves (Carter, 1990). This is completely different from the family Pinnidae Leach, 1819 where the calcitic regular prisms show a perfect, monocrystalline extinction under crossed polarized light due to optically homogenous nature of each crystal (Carter, 1990). The observed extinction in the FV is different from *Trichites* sp. (Pinnidae) distinguished by well-defined monocrystalline extinction and from inoceramids, which show grainy extinction. It is more similar to the wavy extinction characterizing the Bakeveliidae and Isognomonidae families. This phylogenetic relationship confirms the hypothesis so far proposed, on the basis of shell morphology, by Seilacher (1984) and Savazzi (1996).

B.6.5. Conclusions

Studies on some extraordinarily preserved *Lithiotis problematica* shells have allowed to improve the knowledge on the microstructure of the outer shell layer and of the free valve morphology. Multiple screening tests (i.e., SEM, Raman and cathodoluminescence analyses) were carried out for the detection of the preservation state.

- The thin free valve shows the same height and the same internal features (i.e., feather-like wings and central platform with ridge and groove structures) of the attached thicker valve.

- A calcitic prismatic outer layer occurs both in the attached and free valves. The simple prisms are organized in several sub-layers and varies from ~50 µm to ~95 µm in height (along c-axis) and from ~10 µm to ~60 µm in width. The entire calcitic layer is up to ~500 µm thick. In the attached valve, the layer doesn't reach the inner central platform. The calcitic simple prims provide high shell flexibility due to the occurrence of inter-crystalline sheaths made by conchiolin as described in the living *Pinna*. The probable occurrence of conchiolin-rich rim along the ventral region confirm that the shell opening mechanism was based on margin flexibility.

- The rare preservation of outer prismatic calcitic layer is likely due to a very rapid burial which impeded the maceration process.

- The microstructure of the outer calcitic prisms suggests a close phylogenetic relationship of *Lithiotis* with the families Bakevellidae and Isognomonidae.

B.6.6. Supplementary data

The analysed specimens

Method	Sample	Sample ID	Notes
Acetate peels on polished slabs	Attached valve - slab 15b (block A2)		
	Articulated individual - slab 21b (block A3)		
	Articulated individual - slab 23b (block A3)		
	Attached valve - slab 11a (block A2)	Av2	Section
	Attached valve - slab 16b (block C)	Av16	Section and surface
	Attached valve - slab 18a (block C)		
	Attached valve - slab 21b (block C)		
Thin sections	*Trichites* sp. (Toraro Mt.)	Tr	Section and surface
	Free valve - 23 (block A3)	Fv3	Surface
	Free valve - 14 (block A2)	Fv4	Surface
	Free valve - isolated block	Fv5	Section
	Attached valve - 16 (block C)	Av16	Section
	Attached valve - To41.2 (block G)	Av3	Section
	Attached valve - To41.3 (block G)	Av4	Section
Cathodoluminescence (CL)	Attached valve - 11 (block A2)	Av2	Section
	Free valve - 24 (block A3)	Fv2	Section
SEM-EDS	*Trichites* sp. (Toraro Mt.)	Tr	Section and surface
	Free valve - 22 (block C)	Fv1	Section and surface
	Free valve - 24 (block A3)	Fv2	Section Same thin section of CL
	Attached valve - 22 (block C)	Av1	Surface and section
	Attached valve - 11 (block A2)	Av2	Surface and section Same thin section of CL
	Attached valve - To41.2 (block G)	Av3	
	Attached valve - isolated samples	Av5	Surface

Table 1. Summary of the studied specimens. Attached and free valve is always referred to *Lithiotis problematica* individuals. Block G is an isolated block collected from the debris of TorA2. Fv5 and Av5 are not referred to the same articulated individual.
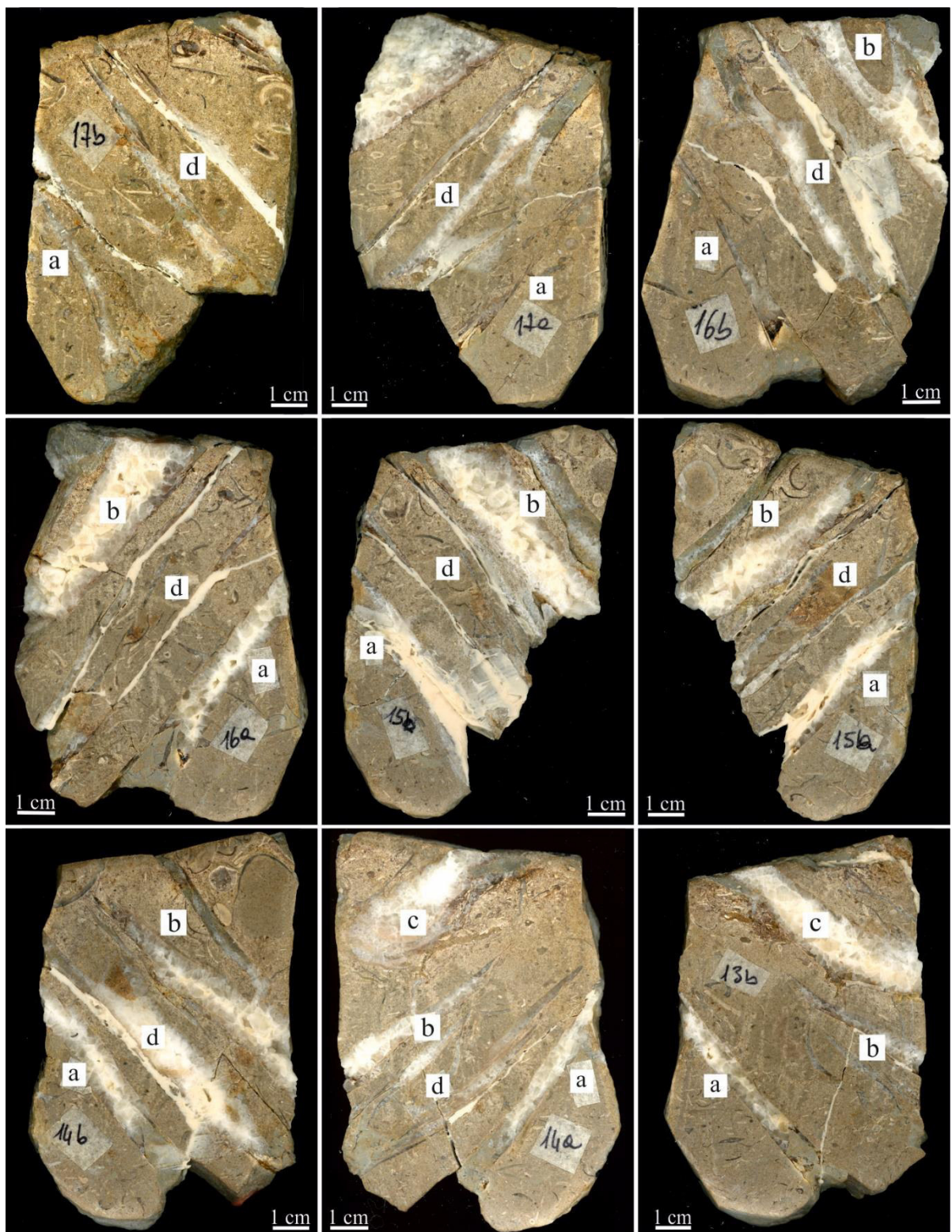
Figure 1. Polished slabs of the block A2 showing several *Lithiotis problematica* individuals (Ngadiuba 2015, modified). In the block A1 the shells are not well-defined (see Appendix B.6, Fig. 1). The respective thickness (mm) are: 0, 14.5, 18.5, 29.2, 33.2, 43.9, 47.9, 59.9.
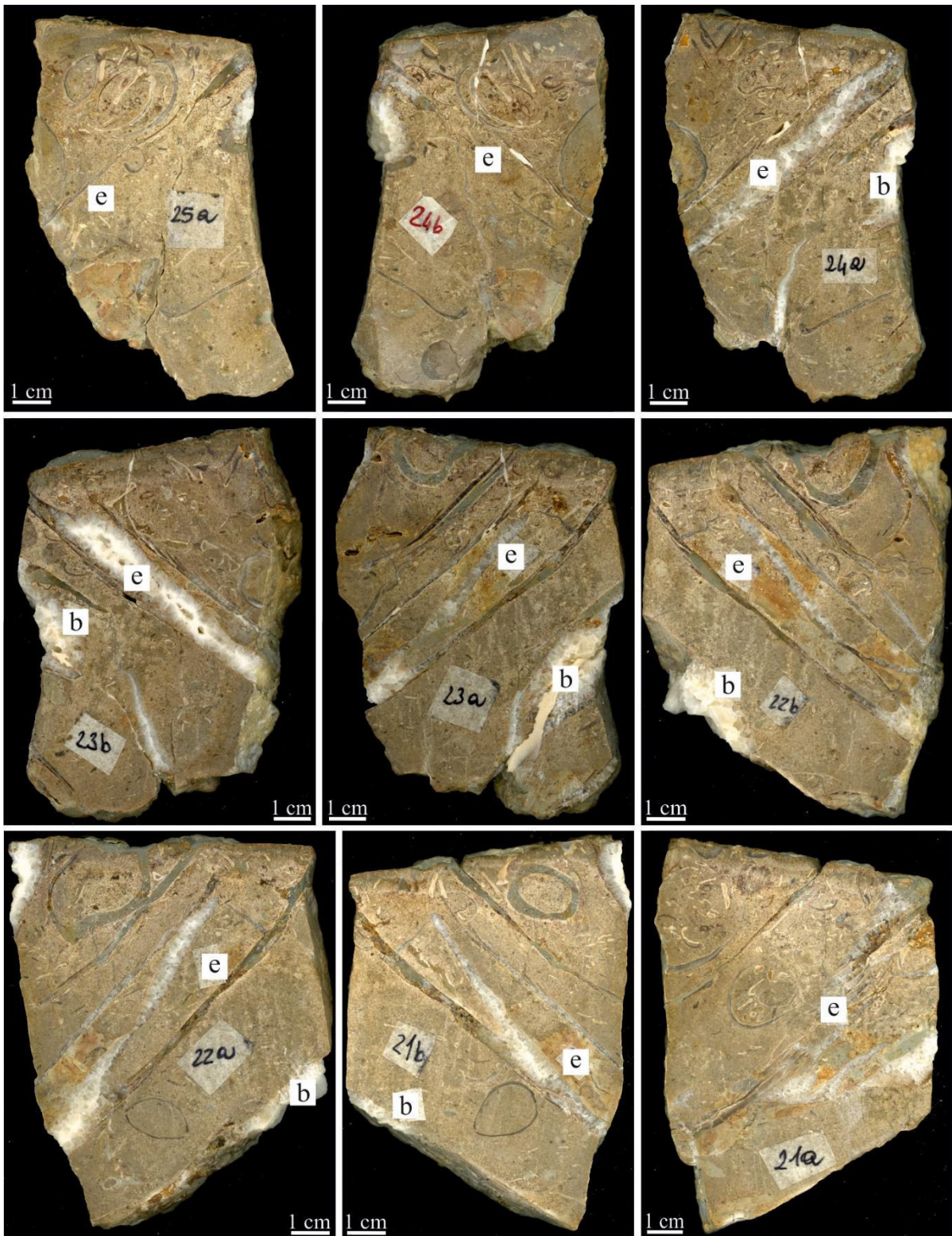
Figure 2. Polished slabs of the block A3 showing several *Lithiotis problematica* individuals (Ngadiuba 2015, modified). The respective thickness (mm) are: 0, 4, 15.6, 19.6, 29.9, 33.9, 45.3, 49.3, 66.3.
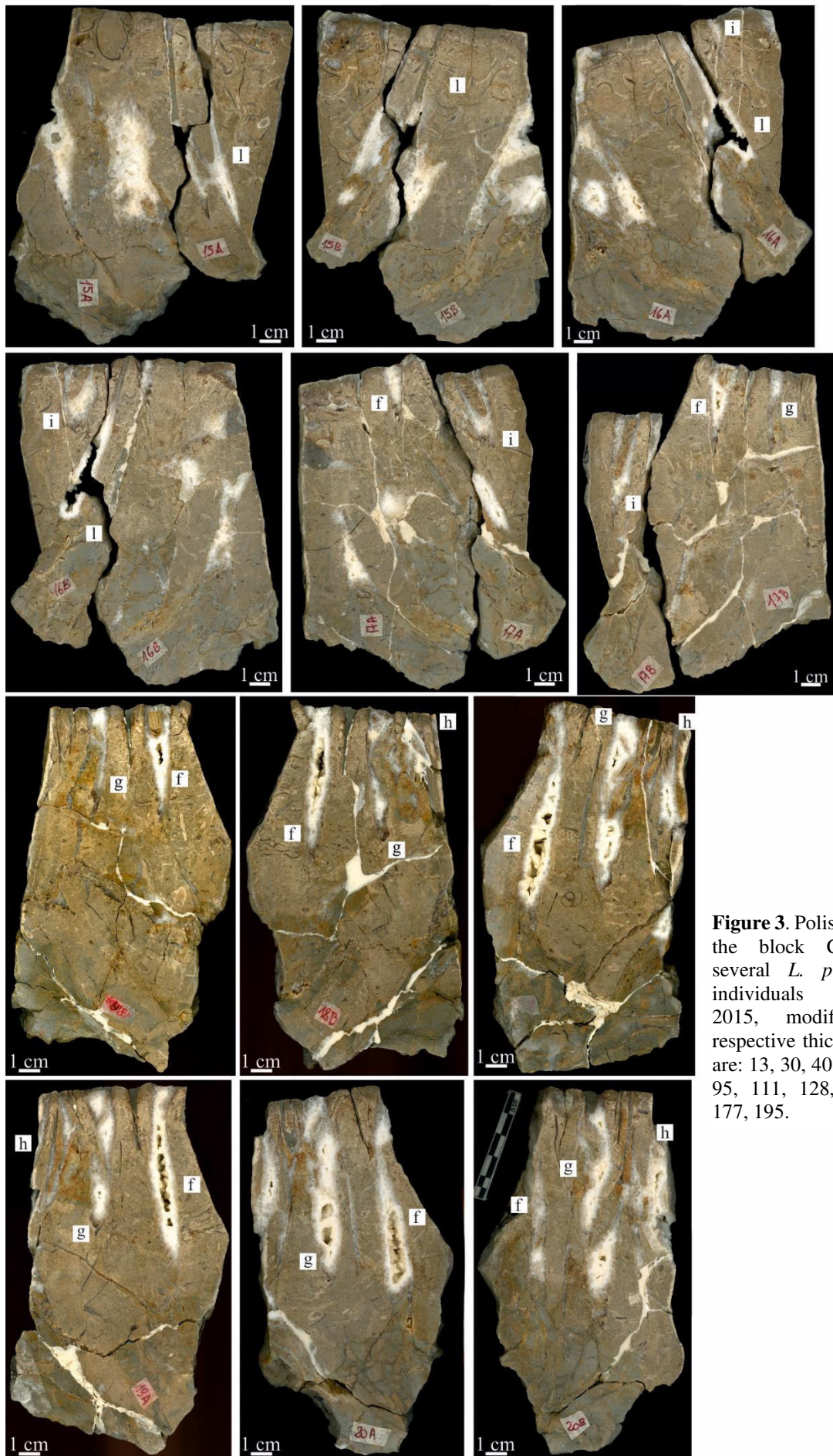
Figure 3. Polished slabs of the block C showing several *L. problematica* individuals (Ngadiuba, 2015, modified). The respective thickness (mm) are: 13, 30, 40, 55, 70, 84, 95, 111, 128, 146, 163, 177, 195.

Raman analyses

Biogenic calcitic and aragonitic samples typically produce noisy spectra because of fluorescence due to the occurrence of organic content (Bischoff et al., 1985). The fluorescence effect (Fig. 4) was not corrected as done by other works (e.g., Perrin and Smith, 2007).

In order to compare the obtained spectra, the data was normalized with data analysis and graphing software (Figs. 5, 6). Afterwards, the spectra were smoothed, and the Raman shift of the main peaks were also reported in the final graphs (Figs. 5, 6; Tab. 2).

Moreover, the main peaks of calcite and aragonite available in literature are reported in Tab. 3 and Tab. 4.
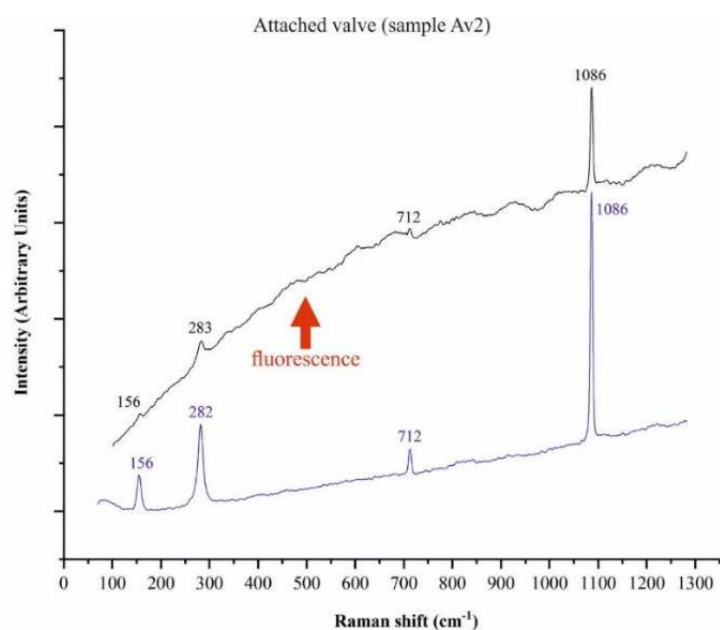
Figure 4. Raman spectra of the attached valve (sample Av2). The black spectrum is related to calcitic prismatic layer while the blue one represents the recrystallized inner calcite. The fluorescence effect is evident in the first spectrum due to the occurrence of organic content in the pristine calcitic microstructure.
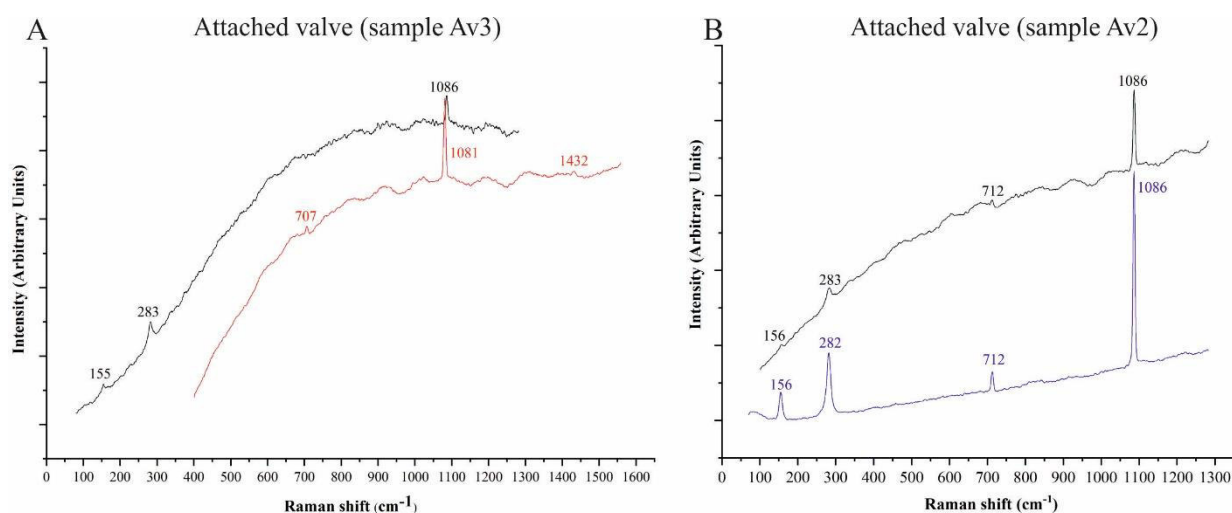
Figure 5. Raman spectra of *Lithiotis problematica* specimens. For the sample acronyms see Tab. 1. A) Both spectra are referred to the same sample. The two colours indicate two different analysed points. B) The black spectrum corresponds to prismatic layer whilst the blue one to recrystalized inner area (calcite).
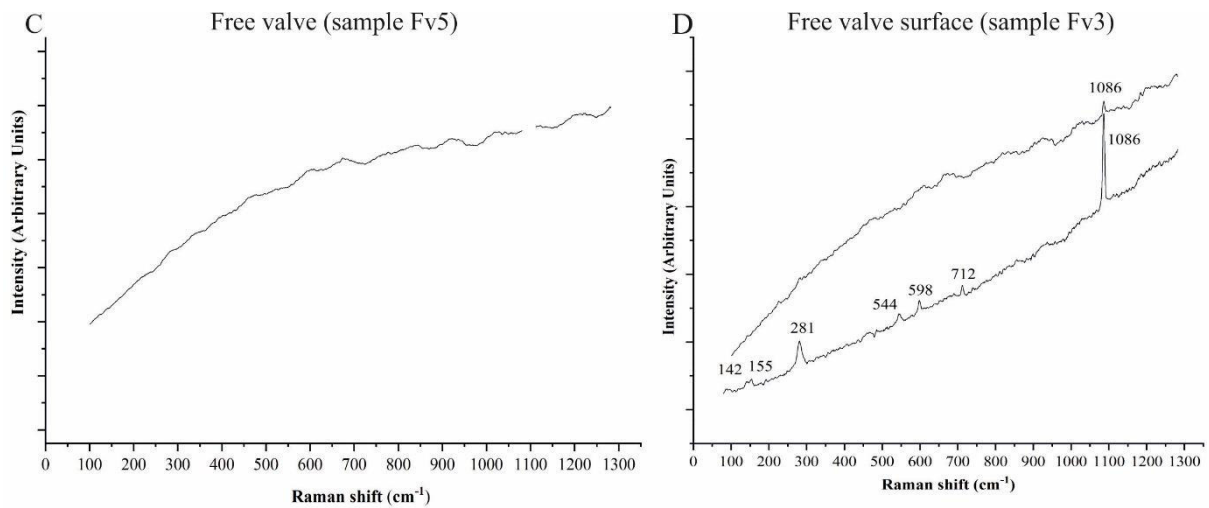
Figure 5. *continued*. Raman spectra of *Lithiotis problematica* specimens. For the sample acronyms see Tab. 1. C) The spectrum of analysed sample Fv5 shows no picks. D) The upper spectrum corresponds to prismatic layer whilst the lower one to recrystalized inner area (calcite).
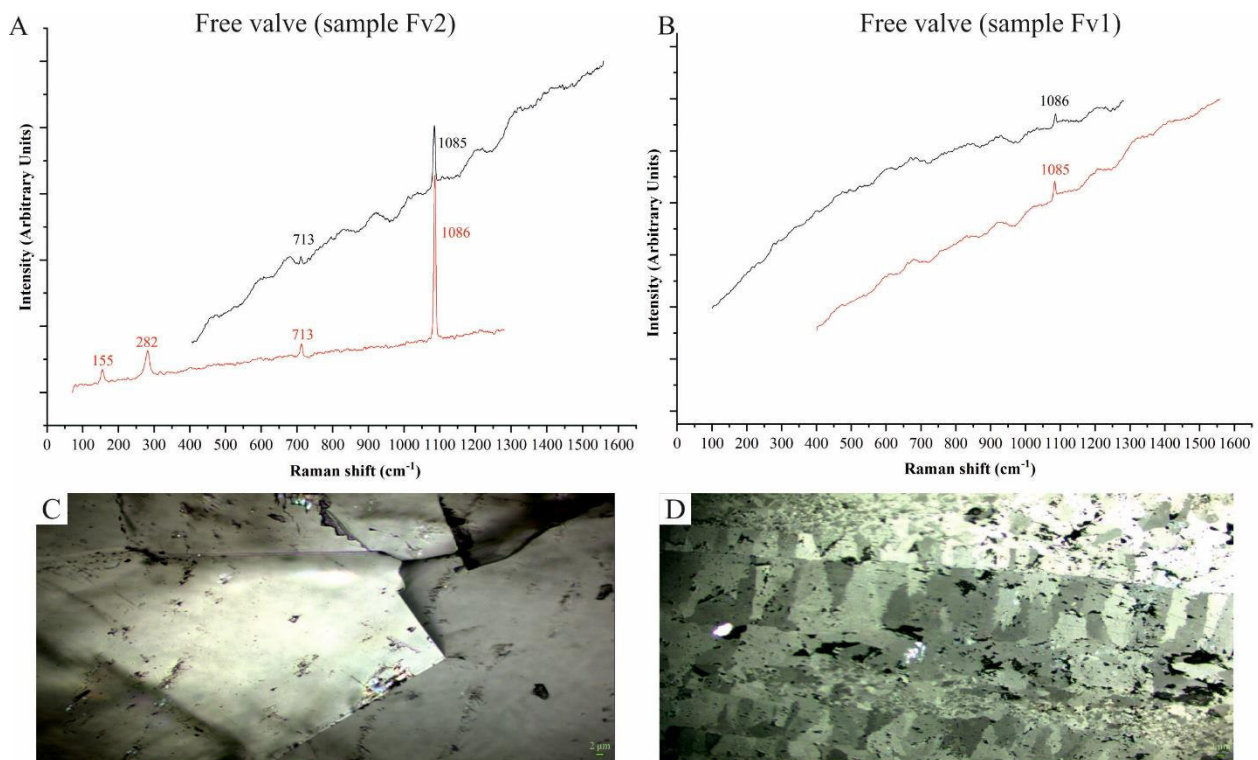
Figure 6. Raman spectra of *Lithiotis problematica* specimens. For the sample acronyms see Tab. 1. A) The red spectrum indicates the recrystallized inner area (calcite). B) The two colours indicate two different points of the same specimens. C) Microphotograph of the analysed recrystallized area (sample Fv2). Note bigger calcitic crystals. D) Microphotograph of the analysed prismatic layer (sample Fv2).

Specimen ID	Supposed pristine mineralogy	Raman Analysis							
		Lattice modes			v4	v1	v3	Raman deduced mineralogy	
Av2	Calcite		156	283	712	1086		Calcite	
	Calcite (recrystallized)		156	282	712	1086		Calcite	
Av3	Calcite		155	283		1086		Calcite	
	Calcite				707	1081	1432	?Calcite	
Fv1	Calcite					1085		?	
	Calcite					1086		?	
Fv2	Calcite				713	1085		calcite	
	Calcite (recrystallized)		155	282	713	1086		calcite	
Fv3	Calcite					1086		?	
	Calcite	142	155	281	712	1086		? calcite	
Fv5	Calcite							?	

Table 2. Raman frequencies of the studied *Lithiotis problematica* shells. In some cases, the spectra results cannot be interpreted (?). ?Calcite indicates uncertain results. Av1, Attached valve 1; Fv1, Free valve 1.

BIOGENIC CALCITE											
A.	Sample	Composition mole % MgCO₃	T	L	v4		v1		v3		
1	White coral	-	159	285	716	1011	1089	1131	1441	1522	1750
1	Pink coral	-	148	284	715	1020	1087	1134	nm	1527	nm
2	*Barnacle*	1.2	152	277	711	-	1085	-	-	-	-
2	*Diadema antillarum*	6.2	145	274	712	-	1084	-	-	-	-
2	*Lytechinus variegatus*	6.5	149	271	710	-	1084	-	-	-	-
2	*Diadema antillarum*	9.1	152	279	712	-	1086	-	-	-	-
2	*Tripneustes esculentis*	10.5	im	280	714	-	1086	-	-	-	-
2	*Lytechinus variegatus*	11.2	im	279	Nr	-	1086	-	-	-	-
2	*Lytechinus variegatus*	11.3	155	282	713	-	1085	-	-	-	-
2	*Diadema antillarum*	11.8	152	284	nr	-	1087	-	-	-	-
2	*Lytechinus variegatus*	12.0	im	277	713	-	1086	-	-	-	-

A.	Name	Value									
2	*Diadema antillarum*	12.2	153	284	715	-	1087	-	-	-	-
2	*Homotrema rubrim*	12.4	148	276	712	-	1085	-	-	-	-
2	*Echinometra lucanter*	13.3	152	282	714	-	1087	-	-	-	-
2	*Echinometra lucanter*	13.6	157	284	715	-	1087	-	-	-	-
2	*Lithothamnium corallioides*	15.5	im	270	nr	-	1086	-	-	-	-
2	*Amphiroa rigida*	19.5	im	277	714	-	1087	-	-	-	-
5	Barnacle, Italy	~ 4	155	282	713	-	1087	-	-	-	-
5	*Paracentrotus lividus* (Echinoid), Italy	~ 10	156	284	713	-	1088	-	-	-	-
5	*Cidaris* (Echinoid), Italy	~ 15	156	286	714	-	1088	-	-	-	-
CALCITE (SYNTHETIC)											
1-2	Calcite	~ 0	154	281	711	-	1085	-	1434	-	1748
3		~ 0	155	282	711	-	1085	-	-	-	-
2		1.9	155	281	711	-	1085	-	1435	-	1747
2		3.9	155	281	712	-	1086	-	1436	-	1748
2		5.7	155	282	712	-	1086	-	1436	-	1747
2		8	156	284	714	-	1087	-	1438	-	1749
2		9.9	157	284	714	-	1087	-	1438	-	1749
1		9.9	157	284	714	-	1087	-	1438	-	1750
2		12.5	156	283	714	-	1087	-	1438	-	1749
2		15	156	286	716	-	1086	-	1439	-	1750
2		25	154	278	715	-	1088	-	1439	-	1748
5	UNIMIB standard, Chihuahua, Mexico	~ 0	154	281	712	-	1086	-	-	-	-

Table 3. Main peaks for biogenic and synthetic calcite reported in literature. A., author. 1, Urmos et al., 1991; 2, Bischoff et al., 1985; 3, Behrens et al. 1995; 4, Perrin and Smith, 2007; 5, Borromeo et al., 2017; -, not reported.

		ARAGONITE																
A.	**Sample**	**Lattice modes**								**v4**				**v1**	**S-AC**	**v3**		**S-AC**
3	Aragonite (synthetic)	142	152	179	189	205	213	273	282	701	705	-	-	1082	-	-	-	-
1	Aragonite (synthetic)	143	153	180	190	206	247	261	284	701	705	-	853	1085	-	1462	1574	-
1	Porites coral	145	155	182	192	208	249	264	286	704	707		nm	1086		1463	1573	
4	*Lobophyllia corymbosa* (skeletal fibers; modern coral)	-	151	179	-	204	248	-	-	703	-	717		1085	1336	1458	1572	1603
4	*Lobophyllia corymbosa* (calcification center; modern coral)	-	152		-	202	-	-	-	704	-			1081	1344	1460	1573	1584
4	*Lobophyllia corymbosa* (calcification center; ancient coral)	148	-	179	-	201	-	-	-	703	706	717	-	1081	1343	1459	1562	1586
5	UNIMIB standard, Val Formazza, Italy	154	-		-	207	-	-	-	702	707	-	-	1087	-	-	-	-

Table 4. Main peaks for aragonite reported in literature. A., author. 1, Urmos et al., 1991; 2, Bischoff et al., 1985; 3, Behrens et al. 1995; 4, Perrin and Smith, 2007; 5, Borromeo et al., 2017; -, not reported. S-AC: semi-amorphous carbon.

B.7. Altered chalky deposit in juvenile *Lithiotis problematica* individual

The single studied specimen was deposited at the "Piero Leonardi" Museum of the University of Ferrara and was collected from Lessini Mounts (see Chapter 5 for further details).

The studied shell is likely juvenile individual (Fig. 1). In polished section, the inner part of the shell shows a completely altered brown area (calcite) and a central white region, likely preserved as aragonite (Fig. 2A). At crossed-polarized microscope this area does not show specific extinction, probably due to slight diagenetic alteration.

The inner part of the specimen has been observed in transversal section with SEM (Fig. 2A). The distinction between brownish recrystalized calcite and white area is sharp (Fig. 2B). Even though the original microstructure is not preserved, rare blades provided the spongy appearance of the "chalky" structure. During the diagenesis these thin

Figure 1. The analysed specimen of *Lithiotis problematica*. The red line points to the cutting profile. dog, direction of growth.

sub-parallel blades, which distinguished the chalky microstructure, were fused together. The altered structures observable in this sample are quite similar to those observed by Ragaini and Di Celma (2009; fig. 10) in the Pleistocene oysters from Ecuador. In the literature, the presence of chalky deposit was suggested only by Chinzei (1982, fig. 7D), who documented the "*granular texture of the inner calcitic part*", due to the alteration of original chalky microstructure. The inner calcitic part is here described as granular or prismatic grains with irregular prisms and parallel streaks (Chinzei, 1982, p. 189). As suggested by several authors (e.g., Chinzei et al., 1982; Seilacher, 1984; Vermeij, 2013), the occurrence of chalky deposits, is considered a successful feature to prevent the sinking among the "secondary soft-bottom dwellers" organisms.

The SEM-EDS analysis revealed a weakly difference in Mg content between the area with altered blades (spectrum 9; Fig. 3) and completely fused microstructure (spectrum 6; Fig. 3). The higher Mg content in the last area is likely due to more intense diagenetic alteration (see Appendix B.6 for further details).

Figure 2. *Lithiotis problematica* altered chalky deposit. A) High resolution scan of the analysed area (red arrow). B–D) Scanning electron images of studied bivalve microstructures. B) The border between completely recrystallized inner part (brown area in image A) and quite preserved chalky area (white part in image A) is sharp (red arrow). C, D) Altered chalky deposit; rare partially fused lamellae are still recognizable (black arrow).

Figure 3. SEM-EDS analysis of *Lithiotis problematica* altered chalky deposit. Mg is locally abundant (spectrum 6), corresponding to the fused (more altered) area.
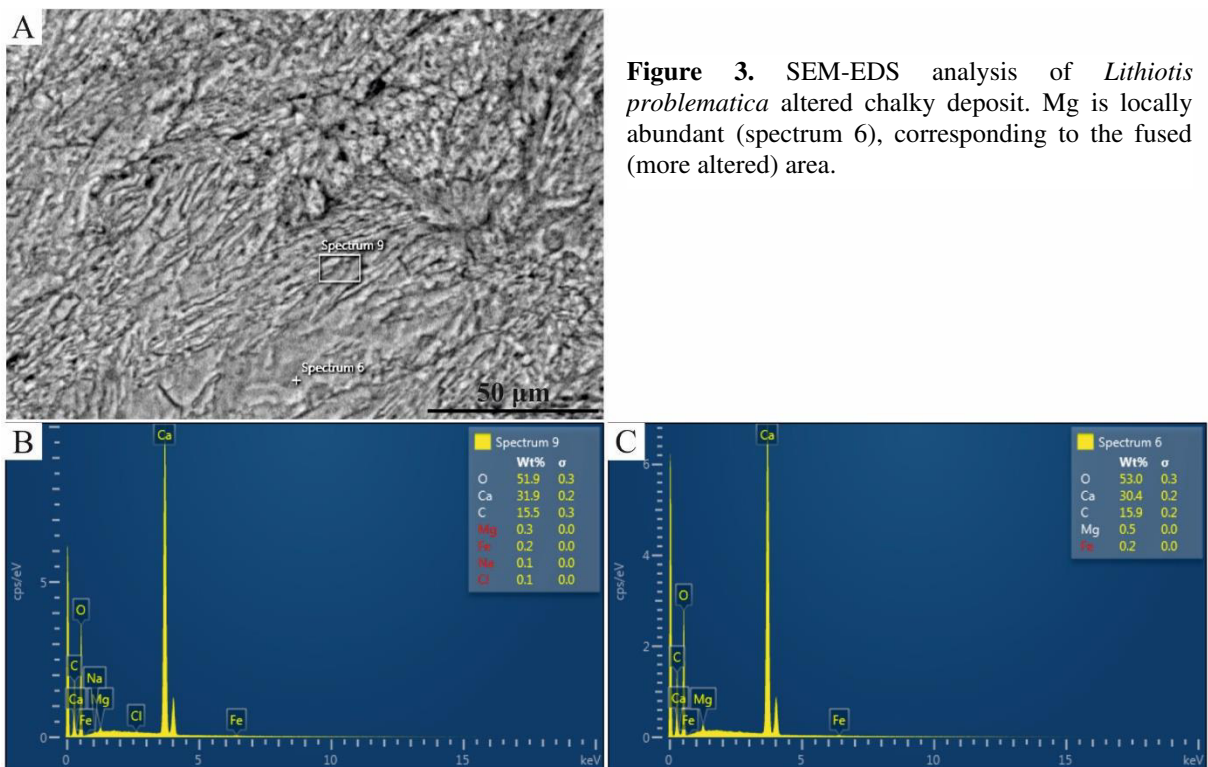
References

Aberhan, M., 1998. Paleobiogeographic patterns of pectinoid bivalves and the Early Jurassic tectonic evolution of Western Canadian Terranes. Palaios, v. 13, p. 129–148.

Aberhan, M., 2001. Bivalve palaeobiogeography and the Hispanic Corridor: time of opening and effectiveness of a proto-Atlantic seaway. Palaeogeogr. Palaeoclimatol. Palaeoecol., v. 165, p. 375–394.

Aberhan, M., and von Hillebrandt, A., 1999. The bivalve *Opisoma* in the Lower Jurassic of northern Chile. Profil., v. 16, p. 149–164.

Accorsi Benini, C., 1979. *Lithioperna*, un nuovo genere fra i grandi Lamellibranchi della facies a "*Lithiotis*". Morfologia, tassonomia ed analisi morfofunzionale. Boll. Soc. Paleontol. Ital., v. 18, p. 221–257.

Accorsi Benini, C., 1985. The large Liassic bivalves: symbiosis or longevity. Palaeogeography Palaeoclimatology Palaeoecology, v. 52, p. 21–33.

Accorsi Benini, C., Broglio Loriga, C., 1977. *Lithiotis* Gümbel, 1871 e *Cochlearites* Reis, 1903. I Revisione morfologica e tassonomica. Bollettino della Società Paleontologica Italiana, v. 16 (1), p. 15–60.

Accorsi Benini, C., Broglio Loriga, C., 1982. Microstrutture, modalità di accrescimento e periodicità nei lamellibranchi liassici (Facies a "*Lithiotis*"). Geologica Rom., v. 21, p. 795–823.

Alberti, M., Arabas, A., Fürsich, F. T., Andersen, N., and Ziółkowski, P., 2019a. The middle to upper Jurassic stable isotope record of Madagascar: Linking temperature changes with plate tectonics during the break-up of Gondwana. Gondwana Research, v. 73, p. 1–15.

Alberti, M., Fürsich, F. T., and Andersen, N., 2019b. First steps in reconstructing Early Jurassic sea water temperatures in the Andean Basin of northern Chile based on stable isotope analyses of oyster and brachiopod shells. Journal of Palaeogeography, v. 8, 33. https://doi.org/10.1186/s42501-019-0048-0.

Alberti, M., Fürsich, F. T., Abdelhady, A. A., Andersen, N., 2017. Middle to Late Jurassic equatorial seawater temperatures and latitudinal temperature gradients based on stable isotopes of brachiopods and oysters from Gebel Maghara, Egypt. Palaeogeography Palaeoclimatology Palaeoecology, v. 468, p. 301–313.

Alexandersson, E. T., 1978. Destructive diagenesis of carbonate sediments in the eastern Skagerrak, North Sea. Geology, v. 6, p. 324–327.

Alexandersson, E. T., 1979. Marine maceration of skeletal carbonates in the Skagerrak, North Sea. Sedimentology, v. 26, p. 845–852. http://doi.org/10.1111/j.1365-3091.1979.tb00977.x.

Arriaga, M. E., Caus, E., 2014. Shallow-water benthic foraminiferal turnover across the Cenomanian–Turonian boundary at Southern Apennines (Italy). In: Marchant, M., Hromic, T. (Eds.), International Symposium on Foraminifera FORAMS 2014 Chile, 19–24 January 2014, Abstract Volume, p. 45.

Aubert, A., Lazareth, C. E., Cabioch, G., Boucher, H., Yamada, T., Iryu, Y., Farman, R., 2009. The tropical giant clam *Hippopus hippopus* shell, a new archive of environmental conditions as revealed by sclerochronological and $\delta^{18}O$ profiles. Coral Reefs, v. 28, p. 989–998. https://doi.org/10.1007/s00338-009-0538-0.

Avanzini, M., Masetti, D., Romano, R., Podda, F., and Ponton, M., 2006. Calcari Grigi, Catalogo delle Formazioni - Unita Tradizionali, in: Cita, M.B., Abbate, E., Balini, M., Conti, M.A., Farloni, P., Germani, D., Groppelli, G., Manetti, P., Petti, F.M. (Eds.), Carta Geologica d'Italia 1:50000–Quaderni serie III 7(7), p. 125–135.

Baghli, H., Mattioli, E., Spangenberg, J. E., Bensalah, M., Arnaud-Godet, F., Pittet, B., Suan, G., 2019. Early Jurassic climatic trends in the south-Tethyan margin. Gondwana Research, v. 77, p. 67–81. https://doi.org/10.1016/j.gr.2019.06.016.

Barattolo, F., Romano, R., 2005. Shallow carbonate platform bioevents during the Upper Triassic–Lower Jurassic: an evolutive interpretation. Bollettino della Società Geologica Italiana, v. 124, p. 1231–142.

Barbin, V., 2013. Application of cathodoluminescence microscopy to recent and past biological materials: a decade of progress. Mineralogy and Petrology, v. 107 (3), p. 353–362.

Bassi, D., Boomer, I., Fugagnoli, A., Loriga, C., Posenato, R., Whatley, R. C., 1999. Faunal assemblages and palaeoenvironment of shallow water black shales in the Tonezza area (Calcari Grigi, Early Jurassic, Southern Alps). Annali dell'Università di Ferrara, Sezione di Scienze della Terra 8, p. 1–16.

Bassi, D., Fugagnoli, A., Posenato, R., Scott, D. B., 2008. Testate amoebae from the Early Jurassic of the western Tethys, North–East Italy. Palaeontology, v. 51, p. 1335–1339.

Bassi, D., Posenato, R., Nebelsick, J. H., 2015. Paleoecological dynamics of shallow-water bivalve carpets from a Lower Jurassic lagoonal setting, northeast Italy. Palaios, v. 30, p. 758–770. https://doi.org/10.2110/palo.2015.020.

Bassi, D., Posenato, R., Nebelsick, J. H., Owada, M., Domenicali, E., Iryu, Y., 2017. Bivalve borings in Lower Jurassic *Lithiotis* fauna from northeastern Italy and its palaeoecological interpretation. Hist. Biol., v. 29, p. 937–946.

Behrens, G., Kuhn, L. T., Ubic, R., and Heuer, A. H., 1995. Raman Spectra of Vateritic Calcium Carbonate. Spectroscopy Letters: An International Journal for Rapid Communication, v. 28 (6), p. 983–995. http://doi.org/10.1080/00387019508009934.

Berkyová, S., and Munnecke, A., 2010. "Calcispheres" as a source of lime mud and peloids - evidence from the early Middle Devonian of the Prague Basin, the Czech Republic. Bulletin of Geosciences, v. 85 (4), p. 585–602.

Berti Cavicchi, A., Bosellini, A., Broglio Loriga, C., 1971. Calcari a *Lithiotis problematica* Gümbel o calcari a "*Lithiotis*". Mem. Geopaleontol. Univ. Ferrara, v. 3, p. 41–53.

Bischoff, W. D., Sharma, S. K., MacKenzie, F. T., 1985. Carbonate ion disorder in synthetic and biogenic magnesian calcites: a Raman spectral study. American Mineralogist, v. 70 (5–6), p. 581–589.

Boehm, G., 1884. Beiträge zur Kenntniss der Grauen Kalke in Venetien. Zeitschrift der Deutschen geologischen Gesellschaft, v. 36, p. 737–782.

Böhm, G., 1891. Über *Lithiotis problematica* Gümbel. Z. Dtsch. Geol. Ges., v. 43, p. 531–532.

Boomer, I., Whatley, R., Bassi, D., Fugagnoli, A., Loriga, C., 2001. An Early Jurassic oligohaline ostracod assemblage within the marine carbonate platform sequence of the Venetian Prealps, NE Italy. Palaeogeography Palaeoclimatology Palaeoecology, v. 166, p. 331–344.

Borasio, E., 1999. Analisi di Facies del Membro di Rotzo dei Lessini (Calcari Grigi, Lias Medio). Unpubl. M.Sc. thesis, University of Ferrara (Italy), 125 pp.

Bornemann, J.G., 1886. Die Versteinerungen des cambrischen Schichtensystems der Insel Sardinien nebst vergleichenden Untersuchungen über analoge Vorkommnisse aus anderen Ländern 1. Nova Acta der Kaiserlichen Leopoldinisch-Carolinischen Deutschen Akademie der Naturforscher, v. 51 (1), p. 1–147.

Borromeo, L., Zimmermann, U., Andò, S., Coletti, G., Bersani, D., Basso, D., Gentile, P., Schulz, B., and Garzanti, E., 2017. Raman spectroscopy as a tool for magnesium estimation in Mg-calcite. J. Raman Spectrosc., v. 48, p. 983–992. http://doi.org/10.1002/jrs.5156.

Bosellini, A., 1972. Paleoecologia Dei Calcari a "*Lithiotis*" (Giurassico Inferiore, Prealpi Venete). Riv. Ital. Paleontol. Stratigr., v. 3 (78), p. 441–464.

Bosellini, A., and Broglio Loriga, C., 1971. I "Calcari Grigi" di Rotzo (Giurassico inferiore, Altopiano di Asiago) e loro inquadramento nella paleogeografia e nell'evoluzione tettonico-sedimentaria delle Prealpi Venete. Annali dell'Università di Ferrara, Nuova Serie, v. 9 (5/l), p. 1–61.

Bouchet, P., and Rocroi, J.-P., 2010. Nomenclator of Bivalve Families; with a classification of bivalve families by R. Bieler, J. G. Carter and E. V. Coan. Malacologia, v. 52 (2), p. 1–184.

Bougeault, C., Pellenard, P., Deconinck, J.-F., Hesselbo, S. P., Dommergues, J.-L., Bruneau, L., Cocquerez, T., Laffont, R., Huret, E., Thibault, N., 2017. Climatic and palaeoceanographic changes during the Pliensbachian (Early Jurassic) inferred from clay mineralogy and stable isotope (C-O) geochemistry (NW Europe). Global and Planetary Change, v. 149, p. 139–152. https://doi.org/10.1016/j.gloplacha.2017.01.005.

Brady, M., Bowie, C., 2017. Discontinuity surfaces and microfacies in a storm-dominated shallow Epeiric Sea, Devonian Cedar Valley Group, Iowa. The Depositional Record, v. 3 (2), p. 136–160. https://doi.org/10.1002/dep2.26.

Braga, J. C., Puga-Bernabéu, Á., Heindel, K., Patterson, M. A., Birgel, D., Peckmann, J., Sánchez-Almazo, I. M., Webster, J. M., Yokoyama, Y., Riding, R., 2019. Microbialites in Last Glacial Maximum and deglacial reefs of the Great Barrier Reef (IODP Expedition 325, NE Australia). Palaeogeography Palaeoclimatology Palaeoecology, v. 514, p. 1–17.

Brame, H. M. R., Martindale, R. C., Ettinger, N. P., Debeljak, I., Vasseur, R., Lathuilière, B., Kabiri, L., Bodin, S., 2019. Stratigraphic distribution and paleoecological significance of Early Jurassic (Pliensbachian–Toarcian) lithiotid-coral reefal deposits from the Central High Atlas of Morocco. Palaeogeogr. Palaeoclimatol. Palaeoecol., v. 514, p. 813–837.

Brand, U., Veizer, J., 1980. Chemical diagenesis of a multicomponent carbonate system:1, Trace elements. Journal of Sedimentary Petrology, v. 50, p. 1219–1236.

Brand, U., Logan, A., Hiller, N., Richardson, J., 2003. Geochemistry of modern brachiopods: applications and implications for oceanography and paleoceanography. Chemical Geology, v. 198, p. 305–334.

Brandolese, V., Posenato, R., Nebelsick, J. H., Bassi, D., 2019. Distinguishing core and flank facies based on shell fabrics in Lower Jurassic lithiotid shell beds. Palaeogeography Palaeoclimatology Palaeoecology, v. 526, p. 1–12. https://doi.org/10.1016/j.palaeo.2019.04.010.

Breitburg, D., Levin, L. A., Oschlies, A., Grégoire, M., Chavez, F. P., Conley, D. J., Garçon, V., Gilbert, D., Gutiérrez, D., Isensee, K., Jacinto, G. S., Limburg, K. E., Montes, I., Naqvi, S. W. A., Pitcher, G. C., Rabalais, N. N., Roman, M. R., Rose, K. A., Seibel, B. A., Telszewski, M., Yasuhara, M., and Thang, J., 2018. Declining oxygen in the global ocean and coastal waters. Science, v. 359, eaam7240. https://doi.org/10.1126/science.aam7240.

Brigaud, B., Pucéat, E., Pellenard, P., Vincent, B., Joachimski, M. M., 2008. Climatic fluctuations and seasonality during the Late Jurassic (Oxfordian–Early Kimmeridgian) inferred from δ^{18}O of Paris Basin oyster shells. Earth Planet. Sc. Lett., v. 273, p. 58–67.

Broglio Loriga, C., Neri, C., 1976. Aspetti paleobiologici e paleogeografici della facies a "*Lithiotis*" (Giurese inf.). Riv. Ital. Paleontol. Stratigr., v. 82 (4), p. 651–706.

Broglio Loriga, C., and Posenato, R., 1996. Adaptive strategies of Lower Jurassic and Eocene multivincular bivalves. Bollettino della Società Paleontologica Italiana, Special Volume 3, p. 45–61.

Brönnimann, P., 1955. Microfossils incertae sedis from the Upper Jurassic and Lower Cretaceous of Cuba. Micropaleontology, v. l, p. 28–57.

Brönnimann, P., Zaninetti, L., Bozorgnia, E., 1972. Triassic (Skythian) smaller foraminifera from the Elika Formation of the central Alborz, northern Iran and from the Siusi Formation of the Dolomites, northern Italy. Mitteilung Gesellschaft der Geologie- und Bergbaustudenten in Österreich, v. 21, p. 861–884.

Buser, S., 1965. Stratigrafski razvoj jurskih skladov na južnem Primorskem, Notranjskem in zahodni Dolenjski. Doktorska disertacija, Manuscript, 101 p., 20 PL, Naravoslovnotehni-ška fakulteta, Oddelek za geologijo, Ljubljana.

Cárdenes, V., Merinero, R., De Boever, W., Rubio-Ordóñez, A., Dewanckele, J., Cnudde, J. P., Boone, M., Van Hoorebeke, L., and Cnudde, V., 2016. Characterization of micropyrite

populations in low-grade metamorphic slate: a study using high-resolution X-ray tomography. Palaeogeography Palaeoclimatology Palaeoecology, v. 441, p. 924–935.

Carter, J. G., 1980. Environmental and biological controls of bivalve shell mineralogy and microstructure. In: Rhoads, D.C., Lutz, R.A. (Eds.), Skeletal Growth of Aquatic Organisms: Biological Records of Environmental Change (Topics in Geobiology). Plenum Publishing Corp, New York, p. 69–113.

Carter, J. G., 1990. Evolutionary significance of shell microstructure in the Palaeotaxodonta,Pteriomorphia and Isofilibranchia (Bivalvia: Mollusca). In: Carter, J.G. (Ed.), Skeletal Bio-mineralization: Patterns, Processes and Evolutionary Trends, 1. Van Nostrand Reinhold, New York, p. 135–296.

Carter et al., 2011. Paleontological contributions number 4 - a synoptical classification of bivalvia (Mollusca). Paleontological Institute, University of Kansas (USA).

Carter, J. G., Harries, P. J., Malchus, N., Sartori, A. F., Anderson, L. C., Bieler, R., Bogan, A. E., Coan, E. V., Cope, J. C. W., Cragg, S. M., García-March, J. R., Hylleberg, J., Kelley, P., Kleemann, K., Kříž, J., McRoberts, C., Mikkelsen, P. M., Pojeta J. Jr., Tëmkin, I., Yancey, T., Zieritz, A., 2012. Part N, Revised, Volume 1, Chapter 31: Illustrated Glossary of the Bivalvia, ISNN 2153-4012, The University of Kansas, Paleontological Institute, Lawrence, Kansas, USA.

Castellarin, A., Picotti, V., Cantelli, L., Claps, M., Trombetta, L., Selli, L., Carton, A., 2005. Note Illustrative della Carta Geologica D'Italia, foglio 080 Riva del Garda. APAT, Serv. Geol., Italia, Firenze, p. 1–145.

Chadwick, M., Harper E. M., Lemasson, A., Spicer J. I., Peck, L. S., 2019. Quantifying susceptibility of marine invertebrate biocomposites to dissolution in reduced pH. R. Soc. open sci., v. 6 (6), 190252. http://dx.doi.org/10.1098/rsos.190252.

Chafetz, H.S., 1986. Marine peloids: a product of bacterially induced precipitation of calcite. J Sediment Petrol., v. 56, p. 812–817.

Chagas, G. G., and Suzuki, M. S., 2005. Seasonal Hydrochemical variation in a tropical coastal lagoon (Açu lagoon, Brazil). Braz. J. Biol., v. 65 (4), p. 597–607.

Checa, A. G., Rodríguez-Navarro, A. B., Esteban-Delgado, F. J., 2005. The nature and formation of calcitic columnar prismatic shell layers in pteriomorphian bivalves. Biomaterials, v. 26 (32), p. 6404–6414. https://doi.org/10.1016/j.biomaterials.2005.04.016.

Cherchi, A., Schroeder R., 1994. Schizogony of an early Barremian cryptobiotic miliolid. Boll. Soc. Paleont. Ital., v. 2, p. 61–65.

Cherchi, A., Schroeder, R., 2005. Calcimicrobial oncoid coatings from the Pliensbachian Massone Member (Calcare Grigi Formation, Trento Platform, Italy). Preliminary communications. In: Fugagnoli, A., and Bassi, D. (eds.) Giornata di Studi Paleontologici "Prof. C. Loriga Broglio". Annali dell'Università di Ferrara, Vol. Spec., p. 45–49.

Cherns, L., Wheeley, J. R., Wright, V. P., 2011. Taphonomic bias in shelly faunas through time: early aragonitic dissolution and its implication for the fossil record. In: Allison, P.A., Bottjer, D.J. (Eds.), Taphonomy: Bias and Process through Time. Topics in Geobiology, 32. Springer Science, p. 79–105.

Chinzei, K., 1982. Morphological and structural adaptations to soft substrates in the Early Jurassic monomyarians *Lithiotis* and *Cochlearites*. Lethaia, v. 15, p. 179–197.

Chinzei, K., Savazzi, E., and Seilacher, A., 1982. Adaptational strategies of bivalves living as infaunal secondary soft bottom dwellers. Neues Jahrbuch für Geologie und Paläontologie Abhandlungen, v. 164, p. 229–244.

Cita, B. M., 1959. Osservazioni stratigrafiche sul Lias del Monte Baldo. Rivista Italiana di Paleontologia e Stratigrafia, v. 65, p. 359–365.

Clari, P., 1975. Caratteristiche sedimentologiche e paleontologiche di alcune sezioni dei Calcari Grigi del Veneto. Memorie degli Istituti di Geologia e Mineralogia dell'Università di Padova, v. 31, p. 1–63.

Clark, G. R. II, 1968. Mollusk shell: daily growth lines. Science, v. 161, p. 800–802.

Coletta, S., 2012. I bivalvi aberranti e microbiofacies della Formazione di Rotzo (Giurassico Inferiore) dell'area del Valico di Valbona (Altopiano di Tonezza, Vicenza). Unpubl. M.Sc. thesis, University of Ferrara (Italy), 87 pp.

Coniglio, M., and James, N. P., 1985. Calcified algae as sediment contributors to early Paleozoic limestones: evidence from deep-water sediments of the Cow Head Group, western Newfoundland. Journal of Sedimentary Petrology, v. 55 (5), p. 746–754.

Ćosović, V., Drobne, K., Ogorelec, B., Moro, A., Koić, M., Šoštarko, I., Tarlao, A., Tunis, G., 2008. *Decastronema barattoloi* (De Castro), characteristic fossil of the Palaeocene and the Eocene peritidal sediments from the Adriatic carbonate platform. Geologia Croatica, v. 61 (2–3), p. 321–332.

Cox, L. R., 1971. ?Family Lithiotidae Reis, 1903, p. N1199–N1200. In R. C. Moore (ed.), Treatise on Invertebrate Paleontology. Pt. N. Mollusca 6: Bivalvia 3. Geological Society of America and University of Kansas, Lawrence, Kansas.

Crippa, G., 2015. Geochemical and sclerochronological analyses of the lower Pleistocene macrofauna of western Emilia (northern Italy): palaeoenvironmental and palaeoclimatic implications. Ph.D. thesis, University of Milan (Italy), 239 pp.

Cushman, J. A., 1910. A monograph of the Foraminifera of the North Pacific Ocean. Part I. Astrorhizidae and Lituolidae. Bulletin of the United States National Museum., v. 71 (1), p. 1–134.

Danise, S., Price, G. D., Alberti, M., Holland, S. M., 2020. Isotopic evidence for partial geochemical decoupling between a Jurassic epicontinental sea and the open ocean. Gondwana Research, v. 82, p. 97–107. https://doi.org/10.1016/j.gr.2019.12.011.

Dauphin, Y., Cuif, J.P., 1999. Relation entre les teneurs en soufre des biomineraux calcaires et leurs caracteristiques mineralogiques. Annales de Sciences Naturelles, v. 2, p. 73–85.

Davenport, C. B., 1938. Growth lines in fossil pectens as indicators of past climates. J. Paleontol., v. 12, p. 514–515.

Davies, D. J., Powell, E. N., and Staff, G. M., 1989. Relative rates of shell dissolution and net sedimentary accumulation - A commentary: Can shell beds form by the gradual accumulation of biogenic debris on the sea floor? Lethaia, v. 22, p. 207–212.

De Castro, P., 1988. Observations on thaumatoporellaceans. Atti del 74° Congresso della Societá Geologica Italiana, p. A245–A249.

De Castro, P., 1990. Thaumatoporelle: Conoscenze attuali e approccio all'interpretazione. Bollettino della Società Paleontologica Italiana, v. 29 (2), p. 179–206.

De Castro, P., 2002. *Thaumatoporella parvovesiculifera* (Raineri): typification, age and historical background (Senonian, Sorrento Peninsula - southern Italy). Bollettino della Società Paleontologica Italiana, v. 41 (2–3), p. 121–129.

de Winter, N. J., 2019. Improving techniques and interpretations for reconstructing high-resolution paleoclimate in deep time from bivalve shells and tooth enamel. Ph.D. thesis, Vrije Universiteit Brussel (Belgium), 436 pp.

de Winter, N. J., Goderis, S., Van Malderen, S. J., Sinnesael, M., Vansteenberge, S., Snoeck, C., Belza, J., Vanhaecke, F., and Claeys, P., 2020. Subdaily-Scale Chemical Variability in a Torreites Sanchezi Rudist Shell: Implications for Rudist Paleobiology and the Cretaceous Day-Night Cycle. Paleoceanography and Paleoclimatology, v. 35, e2019PA003723. https://doi.org/10.1029/2019PA003723.

De Zigno, A., 1856 – 1885. Flora fossilis formationis oolithicae. Tipografia del Seminario di Padova, v. 1–2, p. 1–426.

Debeljak, I., Buser, S., 1998. Lithiotid bivalves in Slovenia and their mode of life. Geologija, v. 40, p. 11–64.

DeCarlo, T. M., 2018. Characterizing coral skeleton mineralogy with Raman spectroscopy. Nature Communications, v. 9 (1), 5325. https://doi.org/10.1038/s41467-018-07601-3.

Deconinck, J. F., and Strasser, A., 1987. Sedimentology, clay mineralogy and depositional environment of Purbeckian green marls (Swiss and French Jura). Eclogae Geol. Helv., v. 80, p. 753–772.

Dera, G., Pucéat, E., Pellenard, P., Neige, P., Delsate, D., Joachimski, M. M., Reisberg, L., Martinez, M., 2009. Water mass exchange and variations in seawater temperature in the NW Tethys during the Early Jurassic: Evidence from neodymium and oxygen isotopes of fish teeth and belemnites. Earth and Planetary Science Letters, v. 286 (1–2), p. 198–207. https://doi.org/10.1016/j.epsl.2009.06.027.

Dettman, D. L., Reische, A. K., Lohmann, K. C., 1999. Controls on the stable isotope composition of seasonal growth bands in aragonitic fresh-water bivalves (unionidae). Geochimica et Cosmochimica Acta, v. 63, p. 1049–1057.

Dettman, D. L., Flessa, K. W., Roopnarine, P. D., Schöne, B. R., Goodwin, D. H., 2004. The use of oxygen isotope variation in shells of estuarine mollusks as a quantitative record of seasonal and annual Colorado river discharge. Geochimica et Cosmochimica Acta, v. 68 (6), p. 1253–1263. https://doi.org/10.1016/j.gca.2003.09.008.

Di Domenico, G., 2014. Fast Cone-beam CT reconstruction using GPU. Proceedings of Graphic Processing Units (GPU, meeting Pisa 2014, DESY-Proc-2015-05), p. 193–198. https://doi.org/10.3204/DESY-PROC-2014-05/35.

Dillaman, R. M., and Ford, S. E., 1982. Measurement of calcium carbonate deposition in molluscs by controlled etching of radioactively labeled shells. Mar. Biol., v. 66 (2), p. 133–143.

Dubar, G., 1948. La faune domerienne du Lias marocain (domaine atlasique). Notes Memoire Service Géologique du Maroc (Rabat), v. 68, 250 pp.

Dunham, R. J., 1962. Classification of carbonate rocks according to depositional texture, in Hamm, W. E., ed., Classification of Carbonate Rocks, a Symposium: American Association of Petroleum Geologists, p. 108–121.

Elliott, G. F., 1958. Microproblematica from the Middle East. Micropaleontology, v. 4 (4), p. 419–428.

Embry, A. F., and Klovan, J. E., 1972. Absolute water depth limits of Late Devonian paleoecological zones. Geologische Rundschau, v. 61, p. 672–686.

Fairbanks, R., Evans, M., Rubenstone, J., Mortlock, R. A., Broad, K., Moore, M. D., Charles, C. D., 1997. Evaluating climate indices and their geochemical proxies measured in corals. Coral Reefs, v. 16 (Suppl. 1), p. S93–S100. https://doi.org/10.1007/s003380050245.

Feng, Q., Gong, Y., and Riding, R., 2010. Mid-Late Devonian calcified marine algae and cyanobacteria, South China. Journal of Paleontology, v. 84 (4), p. 569–587.

Flügel, E., 2010. Microfacies of Carbonate Rocks: Analysis, Interpretation and Application. Springer-Verlag, Berlin. ISBN: 354022016X.

Franceschi, M., Dal Corso, J., Posenato, R., Roghi, G., Masetti, D., Jenkyns, H. C., 2014a. Early Pliensbachian (Early Jurassic) C-isotope perturbation and the diffusion of the *Lithiotis* Fauna: Insights from the western Tethys. Palaeogeogr. Palaeoclimatol. Palaeoecol., v. 410, p. 255–263. https://doi.org/10.1016/j.palaeo.2014.05.025.

Franceschi, M., Massironi, M., Franceschi, P., Picotti, V., 2014b. Spatial analysis of thickness variability applied to an Early Jurassic Carbonate Platform in the central Southern Alps (Italy): a tool to unravel syn-sedimentary faulting. Terra Nova, v. 26, p. 239–246. http://dx.doi.org/10.1111/ter.12092.

Franceschi, M., Dal Corso, J., Cobianchi, M., Roghi, G., Penasa, L., Picotti, V., Preto, N., 2019. Tethyan carbonate platform transformations during the Early Jurassic (Sinemurian−Pliensbachian, Southern Alps): Comparison with the Late Triassic Carnian Pluvial Episode. GSA Bulletin, v. 131 (7–8), p. 1255–1275. https://doi.org/10.1130/B31765.1.

Fraser, N.M., 2002. Early Jurassic reef eclipse: paleoecology and sclerochronology of the "*Lithiotis*" facies bivalves. Ph.D. thesis, University of Southern California (USA), 258 pp.

Fraser, N.M., Bottjer, D. J., Fischer, A. F., 2004. Dissecting "*Lithiotis*" bivalves: implications for the Early Jurassic reef eclipse. Palaios, v. 19, p. 51–67.

Frollo, M. M., 1938. Sur un nouveau genre de Codiacée du Jurassique supérieur des Carpates Orientales. Bulletin de la Société Géologique de France, v. 8 (3–4), p. 269–271.

Fugagnoli, A., 2004. Trophic regimes of benthic foraminiferal assemblages in Lower Jurassic shallow water carbonates from northeastern Italy (Calcari Grigi, Trento Platform, Venetian Prealps). Palaeogeogr. Palaeoclimatol. Palaeoecol., v. 205, p. 111–130.

Fugagnoli, A., Loriga Broglio, C., 1998. Revised biostratigraphy of Lower Jurassic shallow water carbonates from the Venetian Prealps (Calcari Grigi, Trento Platform, Northern Italy). Stud. Trent. Sci. Nat. Acta Geol., v. 73, p. 35–73.

Fugagnoli, A., Giannetti, A., and Rettori, R., 2003. A new foraminiferal genus (Miliolina) from the Early Jurassic of the Southern Alps (Calcari Grigi Formation, Northeastern Italy). Revista Española de Micropaleontologia, v. 35, p. 43–50.

Fujioka, H., Takayanagi, H., Yamamoto, K., Iryu, Y., 2019. The effects of meteoric diagenesis on the geochemical composition and microstructure of Pliocene fossil *Terebratalia coreanica* and *Laqueus rubellus* brachiopod shells from northeastern Japan. Prog Earth Planet Sci, 6, 45. https://doi.org/10.1186/s40645-019-0289-7.

Fürsich, F. T., 1980. Preserved life positions of some Jurassic bivalves. Paläont. Z., v. 54, p. 289–300. https://doi.org/10.1007/BF02988131.

Fürsich, F. T., 1981. Salinity-controlled benthic associations from the Upper Jurassic of Portugal. Lethaia, v. 14 (3), p. 203–223.

Gale, L., 2015. Microfacies characteristics of the Lower Jurassic lithiotid limestone from northern Adriatic carbonate platform (central Slovenia). Geologija, letnik 58, številka 2, str., p. 121–138.

Gambarin, S., 1986. Revisione morfologico-tassonomica delle specie incluse nel gen. *Gervilleioperna* Krumbeck, 1923 (Facies a "*Lithiotis*", Formazione dei Calcari Grigi, Liassico). Unpubl. M.Sc. thesis, University of Ferrara (Italy), 101 pp.

Garbelli, C., Angiolini, L., Jadoul, F., Brand, U., 2012. Micromorphology and differential preservation of Upper Permian brachiopod low-Mg calcite. Chemical Geology, v. 298–299, p. 1–10. https://doi.org/10.1016/j.chemgeo.2011.12.019.

Geyer, O. F., 1977. Die "*Lithiotis*-Kalke" im Bereich der unterjurassischen Tethys: Neues Jahrbuch für Geologie und Paläontologie. Abhandlungen, v. 153 (3), p. 304–340.

Ghirardello, M., 2015. Sclerocronologia di bivalvi isognomonidi della Formazione di Rotzo (Giurassico Inferiore). Unpubl. B.Sc. thesis, University of Ferrara (Italy), 64 pp.

Gili, E., Skelton, P. W., Bover-Arnal, T., Salas, R., Obrador, A., Fenerci-Masse, M., 2016. Depositional biofacies model for post-OAE1a Aptian carbonate platforms of the western Maestrat Basin (Iberian Chain, Spain). Palaeogeogr. Palaeoclimatol. Palaeoecol., v. 453, p. 101–114.

Gillikin, D. P., 2005. Geochemistry of marine bivalve shells: the potential for paleoenvironmental reconstruction. Ph.D. thesis, Vrije Universiteit Brussel (Belgium), 258 pp.

Gillikin, D. P., De Ridder, F., Ulens, H., Elskens, M., Keppens, E., Baeyens, W., Dehairs, F., 2005. Assessing the reproducibility and reliability of estuarine bivalve shells (*Saxidomus giganteus*) for sea surface temperature reconstruction: implications for paleoclimate studies. Palaeogeogr Palaeoclimatol Palaeoecol, v. 228, p. 70–85.

Gillikin, D. P., Lorrain, A., Bouillon, S., Willenz, P., Dehairs, F., 2006. Stable carbon isotopic composition of *Mytilus edulis* shells: relation to metabolism, salinity, $\delta^{13}C_{DIC}$ and phytoplankton. Org. Geochem., v. 37, p. 1371–1382. https://doi.org/10.1016/j.orggeochem.2006.03.008.

Gillikin, D. P., Lorrain, A., Meng, L., and Dehairs, F., 2007. A large metabolic carbon contribution to the $\delta^{13}C$ record in marine aragonitic bivalve shells. Geochim. Cosmochim. Acta, v. 71, p. 2936–2946.

Gillikin, D. P., Hutchinson, K. A., and Kumai, Y., 2009. Ontogenic increase of metabolic carbon in freshwater mussel shells. J. Geophys. Res., v. 114, G01007. https://doi.org/10.1029/2008JG000829.

Glover, C. P., and Kidwell, S.M., 1993. Influence of Organic Matrix on the Post-Mortem Destruction of Molluscan Shells. Journal of Geology, v. 101, p. 729–747.

Göhner, D., 1980. "Covel dell'Angiolono"- ein mittelliassisches *Lithiotis*-Schlammbioherm auf der Hochebene von Lavarone (Provinz Trento, Norditalien). Neues Jahrbuch für Geologie und Paläontologie, v. 10, p. 600–619.

Golubic, S., Radoičić, R., and Seong-Joo, L., 2006. *Decastronema kotori* gen. nov., comb. nov.: a mat-forming cyanobacterium on Cretaceous carbonate platforms and its modern counterparts. Carnets de Géologie / Notebooks on Geology, Brest, Article 2006/02.

Graziano, R., 2013. Sedimentology, biostratigraphy and event stratigraphy of the Early Aptian oceanic anoxic event (OAE1A) in the Apulia Carbonate Platform margin - Ionian basin system (Gargano promontory, southern Italy). Cretaceous Research, v. 39, p. 78–111. https://doi.org/10.1016/j.cretres.2012.05.014.

Griffith, E. M., and Paytan, A., 2012. Barite in the ocean - occurrence, geochemistry and palaeoceanographic applications. Sedimentology, v. 59, p. 1817–1835.

Gröcke, D. R., and Gillikin, D. P., 2008. Advances in mollusc sclerochronology and sclerochemistry: tools for understanding climate and environment. Geo-Marine Letters, v. 28 (5–6), p. 265–268.

Grossman, E. L., and Ku, T.-L., 1986. Oxygen and carbon isotope fractionation in biogenic aragonite: temperature effects. Chemical Geology, v. 59, p. 59–74.

Grubić, A., 1961. Novo o litiotidima. - III. kongres geologa FNRJ u Budvi 1959, v. 1, p. 193–199, Titograd.

Guido, A., Papazzoni, C. A., Mastandrea, A., Morsilli, M., La Russa, M. F., Tosti, F., and Russo, F., 2011. Automicrite in a 'nummulite bank' from the Monte Saraceno (Southern Italy): evidence for synsedimentary cementation. Sedimentology, v. 58, p. 878–889.

Gümbel, C. W., 1871. Die sogennanten Nulliporen, *Lithiotis problematica*. Abhandlungen der Königlich Bayerischen Akademie der Wissenschaften Classe, v. 2 (1), p. 38–52.

Hallam, A., 1984. Continental humid and arid zones during the Jurassic and Cretaceous. Palaeogeogr. Palaeoclimatol. Palaeoecol., v. 47, p. 195–223.

Hammer, Ø., Harper, D. A. T., and Ryan, P. D., 2001. PAST: Paleontological Statistics Software Package for Education and Data Analysis. Palaeontologia Electronica 4 (1), 9 pp.

Hellings, L., Dehairs, F., Tackx, M., Keppens, E., Baeyens, W., 1999. Origin and fate of organic carbon in the freshwater part of the Scheldt Estuary as traced by stable carbon isotopic composition. Biogeochemistry, v. 47, p. 167–186.

Hellings, L., Van Den Driessche, K., Baeyens, W., Keppens, E., and Dehairs, F., 2000. Origin and fate of dissolved inorganic carbon in interstitial waters of two freshwater intertidal areas: A case study of the Scheldt Estuary, Belgium. Biogeochemistry, v. 51, p. 141–160.

Hellings, L., Dehairs, F., Van Damme, S., and Baeyens, W., 2001. Dissolved inorganic carbon in a highly polluted estuary (the Scheldt). Limnology and Oceanography, v. 46 (6), p. 1406–1414.

Henson, F. R. S., 1948. Larger imperforate Foraminifera of South-Western Asia. Families Lituolidae, Orbitolinidae and Meandropsinidae. London, British Museum (Nat. Hist.), 128 pp.

Herrera-Silveira, J. A., 1994. Spatial heterogeneity and seasonal patterns in a tropical coastal lagoon. Journal of Coastal Research, v. 10 (3), p. 738–746.

Hodgson, W. A., 1966. Carbon and oxygen isotope ratios in diagenetic carbonates from marine sediments. Geochimica et Cosmochimica Acta, v. 30, p. 1223–1233.

Hoffmann, L., Nebelsick, J., Bassi, D., Posenato, R., 2015. Microtaphofacies of Lower Jurassic limestones from the Rotzo Formation, Northern Italy. Geophysical Research Abstracts Vol. 17, EGU 2015-10561-2.

Hornung, T., Spatzenegger, A., and Joachimski, M. M., 2007. Multistratigraphy of condensed ammonoid beds of the Rappoltstein (Berchtesgaden, southern Germany): unravelling palaeoenvironmental conditions on 'Hallstatt deep swells' during the Reingraben Event (Late Lower Carnian). Facies, v. 53, p. 267–292. https://doi.org/10.1007/s10347-006-0101-1.

Hudson, J. D., 1977. Stable isotopes and limestone lithification. Journal of the Geological Society London, v. 133, p. 637–660.

Hughes, G. W., 2013. Late Permian to Late Jurassic "microproblematica" of Saudi Arabia: Possible palaeobiological assignments and roles in the palaeoenviromental reconstructions. GeoArabia, v. 18 (1), p. 57–92.

ICZN - International Commission on Zoological Nomenclature. 1999. International code of zoological nomenclature. 4th ed. International Trust of Zoological Nomenclature. London: The Natural History Museum, 306 pp.

Jones, D. S., 1983. Sclerochronology: reading the record of the molluscan shell: annual growth increments in the shells of bivalve molluscs record marine climatic changes and reveal surprising longevity. American Scientist, v. 71, p. 384–391.

Jones, D. S., Williams, D. F., Romanek, C. S., 1986. Life history of symbiont-bearing giant clams from stable isotope profiles. Science, v. 231, p. 46–48.

Jones, D. S., Arthur, M. A., Allard, D. J., 1989. Sclerochronological records of temperature and growth from shells of *Mercenaria mercenaria* from Narragansett Bay, Rhode Island. Marine Biology, v. 102, p. 225–234.

Jones, D. S., and Quitmyer, I. R., 1996. Marking time with bivalve shells: oxygen isotopes and season of annual increment formation. Palaios, v. 11, p. 340–346.

Keller, N., Del Piero, D., Longinelli A., 2002. Isotopic composition, growth rates and biological behavior of *Chamelea gallina* and *Callista chione* from the Gulf of Trieste (Italy). Mar Biol., v. 140, p. 9–15. https://doi.org/10.1007/s002270100660.

Kempe, S., and Kazmierczak, J., 1994. The role of alkalinity in the evolution of ocean chemistry, organization of living systems, and biocalcification processes. Bulletin de la Institut Océanographique (Monaco), v. 13, p. 61–117.

Kennedy, H., Richardson, C. A., Duarte, C. M., Kennedy, D. P., 2001. Oxygen and carbon stable isotopic profiles of the fan mussel, *Pinna nobilis*, and reconstruction of sea surface temperatures in the Mediterranean. Mar Biol., v. 139, p. 1115–1124. https://doi.org/10.1007/s002270100673.

Kennish, M. J., 1980. Shell microgrowth analysis: *Mercenaria mercenaria* as a type example for research in population dynamics. In: Rhoads, D. C., Lutz, R. A. (Eds.), Skeletal Growth of Aquatic Organisms: Biological Records of Environmental Change (Topics in Geobiology). Plenum Publishing Corp, New York, p. 255–294.

Kennish, M. J., and Olsson, R. K., 1975. Effects of thermal discharges on the microstructural growth of *Mercenaria mercenaria*. Geo, v. 1, p. 41–64. https://doi.org/10.1007/BF02426940.

Kershaw, S., Tang, H., Li, Y., Guo, L., 2018. Oxygenation in carbonate microbialites and associated facies after the end-Permian mass extinction: Problems and potential solutions. Journal of Palaeogeography, v. 7 (1), p. 32–47.

Kidwell, S. M., Fürsich, F. T., Aigner, T., 1986. Conceptual framework for the analysis and classification of fossil concentrations. Palaios, v. 1, p. 228–238.

Kiessling, W., Flügel, E., Golonka, J., König, D., Röper, W., Steuding, R., Haas, A., Däßler, R., 2003. The Paleoreefs Project. http://www.paleo-reefs.pal.uni-erlangen.de.

Kiessling, W., Simpson, C., 2011. On the potential for ocean acidification to be a general cause of ancient reef crises. Glob. Chang. Biol., v. 17 (1), p. 56–67. https://doi.org/10.1111/j.1365-2486.2010.02204.x.

Killam, D., 2018. The When, How and Why of Bivalve Shell Growth: Sclerochronology as a Tool to Understand Physiology in Jurassic and Future Oceans. Ph.D. thesis, UC Santa Cruz (USA), 143 pp.

King, W., 1850. A Monograph of the Permian Fossils of England. Palaeontographical Society Monograph, London, 258 pp.

Kobluk, D. R., Risk, M. J., 1977. Calcification of exposed filaments of endolithic algae, micrite envelope formation and sediment production. Journal of Sedimentary Research, v. 47 (2), p. 517–528. https://doi.org/10.1306/212F71C6-2B24-11D7-8648000102C1865D.

Kooijman, S. A. L. M., 2006. Pseudo-faeces production in bivalves. Journal of Sea Research, v. 56, p. 103–106.

Korte, C., and Hesselbo, S. P., 2011. Shallow marine carbon and oxygen isotope and elemental records indicate icehouse-greenhouse cycles during the Early Jurassic. Paleoceanography, 26, PA4219. https://doi.org/10.1029/2011PA002160.

Korte, C., Hesselbo, S., Ullmann, C., Dietl, G., Ruhl, M., Schweigert, G., Thibault, N., 2015. Jurassic climate mode governed by ocean gateway. Nat. Commun., v. 6, 10015. https://doi.org/10.1038/ncomms10015.

Kowalewski, M., Flessa, K. W., and Hallman, D. P., 1995. Ternary taphograms: Triangular diagrams applied to taphonomic analysis. Palaios, v. 10 (5), p. 478–483.

Kristan, E., 1957. Ophthalmidiidae und Tetrataxinae (Foraminifera) aus dem Rhät der Hohen Wand in Nieder-Österreich. Jahrb. Geol. Bundesandst., v. 100, p. 269–298.

Krumbeck, L., 1923. Zur Kenntnis des Jura der Insel Timor sowie des Aucellen-Horizontes von Seran und Buru. Paläontologie von Timor, v. 12 (20), p. 1–120, pl. 172–177.

Kubota, K., Shirai, K., Murakami-Sugihara, N., Seike, K., Hori, M., Tanabe, K., 2017. Annual shell growth pattern of the Stimpson's hard clam *Mercenaria stimpsoni* as revealed by sclerochronological and oxygen stable isotope measurements. Palaeogeography Palaeoclimatology Palaeoecology, v. 465, p. 307–315, https://doi.org/10.1016/j.palaeo.2016.05.016.

Lartaud, F., Emmanuel, L., de Rafelis, M., Pouvreau, S., Renard, M., 2010. Influence of food supply on the $\delta^{13}C$ signature of mollusc shells: implications for palaeoenvironmental reconstitutions. Geo-Mar Lett., v. 30, p. 23–34. https://doi.org/10.1007/s00367-009-0148-4.

Leach, W. E., 1819. Descriptions des nouvelles espèces d'animaux découvertes par le vasseau Isabelle dans un voyage au pôle boréal. Journal de Physique, de Chimie, d'Histoire Naturelle et des Arts, v. 88 (6), p. 462–467.

LeGrande, A. N., and Schmidt, G. A., 2006. Global gridded data set of the oxygen isotopic composition in seawater. Geophys. Res. Lett., v. 33, L12604. https://doi.org/10.1029/2006GL026011.

Leinfelder, R. R., Schmid, D. U., Nose, M., Werner, W., 2002. Jurassic Reef patterns - the expression of a changing globe. In: Phanerozoic Reef Patterns. 72. SEPM Special Publication, p. 465–520.

Leischner, W., 1961. Zur Kenntnis der Mikrofauna und-flora der Salzburger Kalkalpen. N. Jb. Geol. Paläont. Abh., v. 112 (1), p. 1–47.

Li, R. H., Liu, S. M., Li, Y. W., Zhang, G. L., Ren, J. L., and Zhang, J., 2014. Nutrient dynamics in tropical rivers, lagoons, and coastal ecosystems of eastern Hainan Island, South China Sea. Biogeosciences, v. 11, p. 481–506. https://doi.org/10.5194/bg-11-481-2014.

Liao, W., Bond, D. P. G., Wang, Y., He, L., Yang, H., Weng, Z., Li, G., 2017. An extensive anoxic event in the Triassic of the South China Block: A pyrite framboid study from Dajiang and its implications for the cause(s) of oxygen depletion. Palaeogeography Palaeoclimatology Palaeoecology, v. 486, p. 86–95. https://doi.org/10.1016/j.palaeo.2016.11.012.

Liu, L., Wu, Y. S., Jiang, H., Wu, N., and Jia, L., 2017. Paleoenvironmental distribution of Ordovician calcimicrobial associations in the Tarim Basin, Northwest China. Palaios, v. 32 (7), p. 462–489.

Lorrain, A., Paulet, Y. M., Chauvaud, L., Dunbar, R., Mucciarone, D., Fontugne, M., 2004. $\delta^{13}C$ variation in scallop shells: Increasing metabolic carbon contribution with body size? Geochim Cosmochim Acta., v. 68, p. 3509–3519. https://doi.org/10.1016/j.gca.2004.01.025

Lougheed, M. S., Mancuso, J. J, 1973. Hematite framboids in the Negaunee iron formation, Michigan: Evidence for their biogenic origin. Econ. Geol., v. 68, p. 202–209. https://doi.org/10.2113/gsecongeo.68.2.202

Lupher, A. W., Packard, E. L., 1929. The Jurassic and Cretaceous rudistids of Oregon. University of Oregon Publication (Geology Series), v. 1 (3), p. 203–225.

Lutz, R. A., and Rhoads, D. C., 1978. Shell structure of the Atlantic ribbed mussel, *Geukensia demissa* (Dillwyn): A reevaluation. Am. Malacol. Union Inc. Bull., p. 13–17.

Lutz, R. A., and Rhoads, D. C., 1980. Growth patterns within the Molluscan shell: an overview in Rhoads, D.C., and Lutz, R.A., eds., Skeletal Growth of Aquatic Organisms: Biological Records of Environmental Change: Plenum Press, New York, p. 203–254.

Ingram, B. L., Conrad, M. E., Ingle, J. C., 1996. Stable isotope and salinity systematics in estuarine waters and carbonates: San Francsisco Bay. Geochimica et Cosmochimica Acta, v. 60, p. 455–467.

Macintyre, I. G., 1985. Submarine cements - the peloidal question. SEPM Spec Publ, v. 36, p. 109–116.

Marchitto, T. M., Jones, G. A., Goodfriend, G. A., 2000. Precise Temporal Correlation of Holocene Mollusk Shells Using Sclerochronology. Quaternary Research, v. 246, p. 236–246. http://doi.org/10.1006/qres.1999.2107.

Martínez, R., Barragán, R., Sánchez, B., and Rojas, R., 2014. Sea level changes through the Jurassic/Cretaceous boundary in western Cuba indicated by taphonomic analysis. Boletín de la Sociedad Geológica Mexicana, v. 66 (3), p. 431–440.

Martin-Garin, B., Lathuilière, B., Geister, J., Ramseyer, K., 2010. Oxygen isotopes and climatic control of Oxfordian coral reefs. Palaios, v. 25, p. 721–729.

Masetti, D., 2002. Alcune precisazioni su facies e cicli del Membro di Rotzo dei Calcari Grigi (Piattaforma di Trento, Prealpi venete, Lias medio). Atti Ticinesi di Scienze della Terra, v. 43, p. 119–128.

Masetti, D., Claps, M., Avanzini, M., Giacometti, A., Pignatti, P., 1996. I Calcari Grigi della Piattaforma di Trento (Lias inferiore e medio, Prealpi Venete). Field guidebook, 78 riunione estiva della Società Geologica Italiana. 48 pp.

Masetti, D., Claps, M., Giacometti, A., Lodi, P., Pignatti, P., 1998. I Calcari Grigi della Piattaforma di Trento (Lias inferiore e Medio, Prealpi Venete). Atti Ticinesi di Scienze della Terra, v. 40, p. 139–183.

Masetti, D., Fantoni, R., Romano, R., Sartorio, D., Trevisani, E., 2012. Tectonostratigraphic evolution of the Jurassic extensional basins of the eastern southern Alps and Adriatic foreland based on an integrated study of surface and subsurface data. AAPG Bulletin, v. 96 (11), p. 2065–2089.

Maslov, V. P., 1956. The fossil calcareous algae of the USSR. Transactions of the USSR Academy of Sciences: Geological Science Sections, v. 160, p. 1–301.

Masuda, F., and Hirano, M., 1980. Chemical composition of some modern marine pelecypod shells. Sci. Rept. Inst. Geosc, Univ. Tsukuba, sect. B.1, p. 163–177.

Mayayo, M. J., Yuste, A., Luzón, A., Corzo, A., Muñoz, A., Pérez, A., Soriano, A., 2019. Fe-rich microspheres pseudomorphs after pyrite framboids in Holocene fluvial deposits from NE Spain: Relationship with environmental conditions and bacterial activity. Sedimentary Geology, v. 386, p. 103–117. https://doi.org/10.1016/j.sedgeo.2019.04.003.

McArthur, J. M., Janssen, N. M. M., Reboulet, S., Leng, M. J., Thirlwall, M. F., van de Schootbrugge, B., 2007. Palaeotemperatures, polar ice-volume, and isotope stratigraphy (Mg/Ca, $\delta^{18}O$, $\delta^{13}C$, $^{87}Sr/^{86}Sr$): the Early Cretaceous (Berriasian, Valanginian, Hauterivian). Palaeogeography Palaeoclimatology Palaeoecology, v. 248, p. 391–430.

McConnaughey, T. A., 1989a. ^{13}C and ^{18}O isotope disequilibria in biological carbonates. 1. Patterns. Geochimica et Cosmochimica Acta, v. 53, p. 151–162.

McConnaughey, T. A., 1989b. ^{13}C and ^{18}O isotopic disequilibrium in biological carbonates: 2. *In vitro* simulation of kinetic isotope effects. Geochimica et Cosmochimica Acta, v. 53, p. 163–171.

McConnaughey, T. A., Burdett J., Whelan, J. F., and Paull C. K., 1997. Carbon isotopes in biological carbonates: respiration and photosynthesis. Geochimica et Cosmochimica Acta, v. 61, p. 611–622.

McConnaughey, T. A., and Gillikin, D. P., 2008. Carbon isotopes in mollusk shell carbonates. Geo-Mar Lett, v. 28, p. 287–299. https://doi.org/10.1007/s00367-008-0116-4

Merinero, R., Cárdenes, V., Lunar, R., Boone, M. N., Cnudde V., 2017. Representative size distributions of framboidal, euhedral, and sunflower pyrite from high-resolution X-ray tomography and scanning electron microscopy analyses. American Mineralogist, v. 102 (3), p. 620–631. https://doi.org/10.2138/am-2017-5851.

Milano, S., Schöne, B. R., Witbaard, R., 2017. Changes of shell microstructural characteristics of *Cerastoderma edule* (Bivalvia) - A novel proxy for water temperature. Palaeogeography Palaeoclimatology Palaeoecology, v. 465 Part B, p. 395–406. https://doi.org/10.1016/j.palaeo.2015.09.051.

Monaco, P., Giannetti, A., 2001. Stratigrafia tafonomica nel Giurassico inferiore dei Calcari Grigi della Piattaforma di Trento. Atti Ticin. Sci. Terra, v. 42, p. 175–209.

Monaco, P., Giannetti, A., 2002. Three-dimensional burrow systems and taphofacies in shallowing-upward parasequences, Lower Jurassic carbonate platform (Calcari Grigi, Southern Alps, Italy). Facies, v. 47, p. 57–82.

Montaggioni, L.F., Le Cornec, F., Corrège, T., Cabioch, G., 2006. Coral barium/calcium record of mid-Holocene upwelling activity in New Caledonia, South-West Pacific. Palaeogeogr. Palaeoclimatol. Palaeoecol., v. 237, p. 436–455.

Mook, W. G., 1970. Stable carbon and oxygen isotopes of natural waters in the Netherlands. Isotope Hydrol., p. 163–190.

Mook, W. G., and Vogel, J. C., 1968. Isotopic equilibrium between shells and their environment. Science, v.159, p. 874–875.

Mook, W. G., and Tan, F. C., 1991. Stable carbon isotopes in rivers and estuaries. In: Degens E.T., Kempe S., and Richey J. E. (eds.) Biogeochemistry of Major World Rivers, John Wiley and Sons Ltd., p. 245–264.

Morse, J. W., and Cornwell, J. C., 1987. Analysis and distribution of iron sulfide minerals in recent anoxic marine sediments. Mar. Chem., v. 22, p. 55–69.

Mugridge, S.-J., Young, H. R., 1984. Rapid preparation of polished thin sections for cathodoluminescence study of carbonate rocks. The Canadian Mineralogist, v. 22 (3), p. 513–515.

Munier-Chalmas, E., 1902. Sur les Foraminifères rapportés au groupe des Orbitolites. Bulletin de la Société géologique de France (4), v. 2 (3), p. 351–353.

Murray, J.W., 2006. Ecology and Applications of Benthic Foraminifera. Cambridge University Press.

Nakayama, H., Iijima, H., Nakamura N., and Kayanne, H., 2008. Carbon and Oxygen Stable Isotope Ratios of GSJ Carbonate Reference Materials (JCp-1 and JCt-1). Bull. Geol. Surv. Japan, v. 59 (9/10), p. 461–466.

Nauss, A. L., Smith, P. L., 1988. *Lithiotis* (Bivalvia) bioherms in the Lower Jurassic of east-central Oregon, U.S.A. Palaeogeogr. Palaeoclimatol. Palaeoecol., v. 65, p. 253–268.

Neri, M., Roghi, G., Ragazzi, E., Papazzoni, C. A., 2017. First record of Pliensbachian (Lower Jurassic) amber and associated palynoflora from the Monti Lessini (northern Italy). Geobios, v. 50 (1), p. 49–63. https://doi.org/10.1016/j.geobios.2016.10.001.

Ngadiuba, K., 2015. Tafonomia di un mound a *Lithiotis problematica* (Bivalvi, Giurassico Inferiore, Altopiano di Tonezza, Vicenza). Unpubl. B.Sc. thesis, University of Ferrara (Italy), 58 pp.

Nguyen, T. M. P., Petrizzo, M. R., Speijer, R. P., 2009. Experimental dissolution of a fossil foraminiferal assemblage (Paleocene–Eocene Thermal Maximum, Dababiya, Egypt): Implications for paleoenvironmental reconstructions. Marine Micropaleontology, v. 73 (3–4), p. 241–258. https://doi.org/10.1016/j.marmicro.2009.10.005.

Nicholson, H. A., and Etheridge, R., 1878. A monograph of the Silurian fossils of the Girvan District in Ayrshire with special reference to those contained in the 'Gray Collection'. Blackwood, Edinburgh, 341 pp.

Nishida, K., Ishimura, T., Suzuki, A., Sasaki, T., 2012. Seasonal changes in the shell microstructure of the bloody clam, *Scapharca broughtonii* (Mollusca: Bivalvia: Arcidae). Palaeogeography Palaeoclimatology Palaeoecology, v. 363–364, p. 99–108. https://doi.org/10.1016/j.palaeo.2012.08.017.

Omata, T., Suzuki, A., Kawahat, H., Okamoto, M., 2005. Annual fluctuation in the stable carbon isotope ratio of coral skeletons: the relative intensities of kinetic and metabolic isotope effects. Geochim Cosmochim Acta, v. 69, p. 3007–3016.

Oschmann, W., 1993. Environmental oxygen fluctuations and the adaptive response of marine benthic organisms. Journal of the Geological Society, v. 150 (1), p. 187–191.

Ouillon, S., Douillet, P., Fichez, R., Panché, J.-Y., 2005. Enhancement of regional variations in salinity and temperature in a coral reef lagoon, New Caledonia. Comptes Rendus Geoscience, v. 337 (16), p. 1509–1517. https://doi.org/10.1016/j.crte.2005.08.005.

Owen, E. F., Wanamaker, A. D., Feindel, S. C., Schöne, B. R., and Rawson, P. D., 2008. Stable carbon and oxygen isotope fractionation in bivalve (*Placopecten magellanicus*) larval aragonite. Geochim. Cosmochim. Acta, v. 72, p. 4687–4698.

Pannella, G., 1976. Tidal growth patterns in recent and fossil mollusc bivalve shells: a tool for the reconstruction of paleotides. G. Sci Nat., v. 63, p. 539–543. https://doi.org/10.1007/BF00622786.

Parrish, J. T., Ziegler, A. M., and Scotese, C. R., 1982. Rainfall patterns and the distribution of coals and evaporites in the Mesozoic and Cenozoic. Palaeogeogr. Palaeoclimatol. Palaeoecol., v. 40, p. 67–101.

Pecorari, M., 2016. Sclerocronologia di *Lithiotis problematica*, un bivalve aberrante del Giurassico Inferiore. Unpubl. B.Sc. thesis, University of Ferrara (Italy), 85 pp.

Pentecost, A., 1981. The tufa deposits of the Malham district, North Yorkshire. Field Stud. v. 5, p. 365–387.

Perrin, C., Smith, D. C., 2007. Earliest Steps of Diagenesis in Living Scleractinian Corals: Evidence from Ultrastructural Pattern and Raman Spectroscopy. Journal of Sedimentary Research, v. 77 (6), p. 495–507. https://doi.org/10.2110/jsr.2007.051.

Pia, J., 1920. Die Siphoneae veticillatae vom Karbon bis zur Kreide. Abh. Zool. Bot. Ges. Wien, v. 11, p. 1–263.

Pia, J., 1927. Thallophyta in: HIRMER, M. Handbuch der Paläobotanik, v. 1, p. 1–136.

Plummer, H. J., 1930. Calcareous foraminifera in the Brownwood shale near Bridgeport, Texas. University of Texas bulletin, No. 3019, p. 5–21.

Posenato, R., Masetti, D., Broglio Loriga, C., 2000. I banchi a bivalvi del Giurassico Inferiore (Piattaforma di Trento): dinamica deposizionale, modalità di insediamento e sviluppo. In: Cerchi, A., Corradini, C. (Eds.), Crisi biologiche, radiazioni adattative e dinamica delle piattaforme carbonatiche. Accademia Nazionale di Scienze Lettere e Arti Modena, v. 21, p. 211–214.

Posenato, R., Masetti, D., 2005. Stop 3. The ?*Cochlearites* micromound of Monte Toraro. In: Masetti (Ed.), The Rotzo Formation (Lower Jurassic at the Val Bona Pass (Vicenza Province)). Field Excusion Book, 5th Reg. Symp. Int. Fossil Algae Ass., St. Trent. Sci. Nat. Acta Geol., v. 80 Suppl, p. 23–25.

Posenato, R., Masetti, D., 2012. Environmental control and dynamics of Lower Jurassic bivalve build-ups in the Trento Platform (Southern Alps, Italy). Palaeogeography Palaeoclimatology Palaeoecology, v. 361–362, p. 1–13. https://doi.org/10.1016/j. palaeo.2012.07.001.

Posenato, R., Bassi, D., and Nebelsick, J. H., 2013a. *Opisoma excavatum* Boehm, a Lower Jurassic photosymbiotic alatoform-chambered bivalve. Lethaia, v. 46, p. 424–437.

Posenato, R., Bassi, D., Avanzini, M., 2013b. Bivalve pavements from shallow-water black-shales in the Early Jurassic of northern Italy: a record of salinity- and oxygen-depleted environmental dynamics. Palaeogeogr. Palaeoclimatol. Palaeoecol., v. 369, p. 262–271.

Posenato, R., Bassi, D., Nebelsick, J. H., 2014. Field Trip Guide - Tonezza del Cimone (VI) 13/09/2014. 7th Int. Meeting on Taphonomy and Fossilization, Taphos 2014, 10th–13th/09/2014, Ferrara, Italy, 28 pp.

Posenato, R., Bassi, D., Trecalli, A., Parente, M., 2018. Taphonomy and evolution of Lower Jurassic lithiotid bivalve accumulations in the Apennine Carbonate Platform (southern Italy). Palaeogeogr. Palaeoclimatol. Palaeoecol., v. 489, p. 261–271. https://doi.org/10.1016/j.palaeo.2017.10.017.

Poulain, C., Lorrain, A., Mas, R., Gillikin, D. P., Dehairs, F., Robert, R., Paulet, Y.-M., 2010. Experimental shift of diet and DIC stable carbon isotopes: Influence on shell $\delta^{13}C$ values in the Manila clam *Ruditapes philippinarum*. Chemical Geology, v. 272 (1–4), p. 75–82. https://doi.org/10.1016/j.chemgeo.2010.02.006.

Pratt, B. R., 1984. *Epiphyton* and *Renalcis*; diagenetic microfossils from calcification of coccoid blue-green algae. Journal of Sedimentary Research, v. 54 (3), p. 948–971. https://doi.org/10.1306/212F853F-2B24-11D7-8648000102C1865D.

Ragaini, L., and Di Celma, C., 2009. Shell structure, taphonomy and mode of life of a Pleistocene ostreid from Ecuador. Bollettino della Società Paleontologica Italiana, v. 48 (2), p. 79–87.

Raineri, R., 1922. Alghe sifonee fossili della Libia. Atti della Società italiana di Scienze naturali e del Museo civico di Storia Naturale in Milano, v. 61 (1), p. 72–86.

Raiswell, R., Berner, R. A., 1985. Pyrite formation in euxinic and semi-euxinic sediments. Am. J. Sci., v. 285 (8), p. 710–724.

Ramanantsoa, J. D., Krug, M., Penven, P., Rouault, M., Gula, J., 2018. Coastal upwelling south of Madagascar: Temporal and spatial variability. Journal of Marine Systems, v. 178, p. 29–37. https://doi.org/10.1016/j.jmarsys.2017.10.005.

Reis, O., 1903. Über Lithiotiden. Abhandlungen der Kaiserlich-Königlichen Geologischen Reichsanstalt, v. 17 (6), p. 1–44.

Reitner, J., and Neuweiler, E., 1995. Mud mounds: a polygenetic spectrum of fine-grained carbonate buildups. Facies, v. 32, p. 1–70.

Reuter, M., Kern, A. K., Harzhauser, M., Kroh, A., Piller, W. E., 2013. Global warming and South Indian monsoon rainfall - lessons from the Mid-Miocene. Gondwana Research, v. 23 (3), p. 1172–1177. https://doi.org/10.1016/j.gr.2012.07.015.

Richardson, C. A., 1987. Tidal bands in the shell of the clam *Tapes philippinarum*. Proc. R. Soc. Lond. B, v. 230, p. 367–387.

Richardson, C. A., 2001. Molluscs as archives of environmental change. Oceanogr. Mar. Biol. Ann. Rev., v. 39, p. 103–164.

Rickard, D. T., 1970. The origin of framboids. Lithos, v. 3, p. 269–293.

Rickard, D., 2019. How long does it take a pyrite framboid to form? Earth and Planetary Science Letters, v. 513, p. 64–68.

Riding, R., 2000. Microbial carbonates: the geological record of calcified bacterial-algal mats and biofilms. Sedimentology, v. 47, p. 179–214.

Riding, R., 2002. Structure and composition of organic reefs and carbonate mud mounds: concepts and categories. Earth-Science Reviews, v. 58, p. 163–231.

Riding, R., and Toomey, D. F., 1972. The Sedimentological Role of *Epiphyton* and *Renalcis* in Lower Ordovician Mounds, Southern Oklahoma. Journal of Paleontology, v. 46 (4), p. 509–519.

Riding, R., Wray, J. L., 1972. Note on the algal genera *Epiphyton*, *Paraepiphyton*, *Tharama*, and *Chabakovia*. J. Paleontol., v. 46, p. 918–919.

Riding, R., and Liang., L., 2005. Geobiology of microbial carbonates: metazoan and seawater saturation state influences on secular trends during the Phanerozoic. Palaeogeography Palaeoclimatology Palaeoecology, v. 219, p. 1–115.

Roche, D. M., Donnadieu, Y., Pucéat, E., Paillard, D., 2006. Effect of changes in $\delta^{18}O$ content of the surface ocean on estimated sea surface temperatures in past warm climate. Paleoceanography, v. 21, PA2023.

Romano, R., Barattolo, F., Masetti, D., 2005. Biostratigraphic evidence of the middle Liassic hiatus in the Foza Section. (Eastern sector of the Trento Platform, Calcari Grigi Formation, Venetian Prealps). Boll. Soc. Geol. Ital., v. 124, p. 301–312.

Ros-Franch, S., Márquez-Aliaga, A., Damborenea, S. E., 2014. Comprehensive database on Induan (Lower Triassic) to Sinemurian (Lower Jurassic) marine bivalve genera and their paleobiogeographic record. Paleontological Contributions, v. 8, p. 1–219.

Roychoudhury, A. N., Kostka, J. E., and Cappellen, P. V., 2003. Pyritization: a palaeoenvironmental and redox proxy re-evaluated. Estuarine Coastal and Shelf Science, v. 57, p. 1–11. https://doi.org/10.1016/S0272-7714(03)00058-1.

Rzehak, A., 1895. Uber einige merkwlrdige foraminiferen aus dem Osterreichischen Tertiar. Annalen des K.K. Natllr historisches Hofmuseum, v. 10, p. 213–230.

Saint Martin, J.-P., 2010. The *Girvanella*-like remains from Messinian marine deposits (Sardinia, Italy): Lagerstätten paradigm for microbial biota? Annales de Paléontologie, v. 96 (2), p. 33–50. https://doi.org/10.1016/j.annpal.2010.10.002.

Samankassou, E., Tresch, J., Strasser, A., 2005. Origin of peloids in Early Cretaceous deposits, Dorset, South England. Facies, v. 51, p. 264–273. https://doi.org/10.1007/s10347-005-0002-8.

Sarti, C., 1981. Segnalazione di ammonite nella Formazione dei Calcari Grigi dell'Altopiano di Lavarone (Trentino). Bollettino della Società Paleontologica Italiana, v. 20, p. 49–51.

Sarti, C., Ferrari, G., 1999. The first record of an in situ ammonite from the upper part of the Calcari Grigi di Noriglio Formation of the Monte Baldo (Trentino, Northern Italy). Neues Jahrbuch für Geologie und Paläontologie. Abhandlungen, v. 213 (3), p. 313–334.

Săsăran, E., Bucur, I. I., Pleş, G., Riding, R., 2014. Late Jurassic *Epiphyton*-like cyanobacteria: Indicators of long-term episodic variation in marine bioinduced microbial calcification? Palaeogeography Palaeoclimatology Palaeoecology, v. 401, p. 122–131. https://doi.org/10.1016/j.palaeo.2014.02.026.

Savazzi, E., 1996. Preserved ligament in the Jurassic bivalve *Lithiotis*: adaptive and evolutionary significance. Palaeogeography Palaeoclimatology Palaeoecology, v. 120, p. 281–289.

Scheibner, C., and Reijmer, J. G., 1999. Facies patterns within a Lower Jurassic upper slope to inner platform transect (Jbel Bou Dahar, Morocco). Facies, v. 41 (1), p. 41–55.

Schlagintweit, F., 2013. *Thaumatoporella* ladders unravelled. Studia UBB Geologia, v. 58 (1), p. 5–9.

Schlagintweit, F., and Velić, I., 2012. Foraminiferan tests and dasycladalean thalli as cryptic microhabitats for thaumatoporellacean algae from Mesozoic (Early Jurassic–Late Cretaceous) platform carbonates. Facies, v. 58 (1), p. 79–94.

Schlagintweit, F., Hladil, J., Nose, M., Salerno, C., 2013. The Paleozoic record of *Thaumatoporella* PIA, 1927? Geologia Croatica, v. 66 (3), 155–182.

Schlagintweit, F., Kołodziej, B., Qorri, A., 2015. Foraminiferan-calcimicrobial benthic communities from Upper Cretaceous shallow-water carbonates of Albania (Kruja Zone). Cretaceous Research, v. 56, p. 432–446. https://doi.org/10.1016/j.cretres.2015.04.009.

Schmidt, D. A., 2006. Paleontology and sedimentology of calcifying microbes in the Silurian of the Ohio-Indiana region: an expanded role of carbonate-forming microbial communities. Ph.D. thesis, The Ohio State University (USA), 276 pp.

Schöne, B. R., 2013. *Arctica islandica* (Bivalvia): a unique paleoenvironmental archive of the northern North Atlantic Ocean. Glob. Planet. Chang., v. 111, p. 199–225.

Schöne, B. R., Goodwin, D. H., Flessa, K. W., Dettman, D. L., and Roopnarine, P. D., 2002. Sclerochronology and growth of the bivalve mollusks *Chione* (*Chionista*) *fluctifraga* and *C.* (*Chionista*) *cortezi* in the northern Gulf of California, Mexico. Veliger, v. 45, p. 45–54.

Schöne, B. R., Surge, D. M., 2013. Bivalve Sclerochronology. In: Rink W., Thompson J. (eds) Encyclopedia of Scientific Dating Methods. Springer, Dordrecht.

Schöne, B. R., Gillikin, D. P., 2013. Unraveling environmental histories from skeletal diaries - Advances in sclerochronology. Palaeogeography Palaeoclimatology Palaeoecology, v. 373, p. 1–5. https://doi.org/10.1016/j.palaeo.2012.11.026.

Seilacher, A., 1984. Constructional morphology of bivalves: evolutionary pathways in primary versus secondary soft-bottom dwellers. Palaeontology, v. 27, p. 207–237.

Seilacher, A., 1985. Bivalve morphology and function. In: Broadhead, T.W. (Ed.), Mollusks, Notes for a Short Course: University of Tennessee Studies in Geology, v. 13, p. 88–101.

Septfontaine, M., 1988. Vers une classification évolutive des Lituolidés (Foraminiféres) Mésozoiques en milieu de plateforme carbonatée. Rev. Paléobiol., vol. spec. 2, p. 229–256.

Sessa, J. A., Ivany, L. C., Schlossnagle, T. H., Samson, S. D., Schellenberg, S. A., 2012. The fidelity of oxygen and strontium isotope values from shallow shelf settings: Implications for temperature and age reconstructions. Palaeogeography Palaeoclimatology Palaeoecology, v. 342, p. 27–39.

Shackleton, N. J., and Kennett, J. P., 1975. Paleotemperature history of the Cenozoic and the initiation of Antarctic glaciation: Oxygen and carbon isotope analyses in DSDP sites 277, 279, and 281. Initial Reports of the Deep Sea Drilling Program, v. 29, p. 743–755.

Shiraishi, F., and Kano, A., 2004. Composition and spatial distribution of microencrusters and microbial crusts in upper Jurassic–lowermost Cretaceous reef limestone (Torinosu Limestone, southwest Japan). Facies, v. 50, p. 217–227. https://doi.org/10.1007/s10347-004-0022-9.

Skelton, P. W., Gili, E., Vicens, E., Obrador, A., 1995. The growth fabric of gregarious rudist elevators (hippuritids) in a Santonian carbonate platform in the southern Central Pyrenees. Palaeogeogr. Palaeoclimatol. Palaeoecol., v. 119, p. 107–126.

Smith, P. L., and Tipper, H. W., 1986. Plate tectonics and paleobiogeography: Early Jurassic (Pliensbachian) endemism and diversity. Palaios, v. 1, p. 399–412.

Smith, K. L., Carlucci, A. F., Jahnke, R. A., Craven, D. B., 1987. Organic carbon mineralization in the Santa Catalina Basin: benthic boundary layer metabolism. Deep Sea Res. Part A, v. 34 (2), p. 185–211.

Spalluto, L., 2011. Facies evolution and sequence chronostratigraphy of a "mid"-Cretaceous shallow-water carbonate succession of the Apulia Carbonate Platform from the northern Murge area (Apulia, southern Italy). Facies, v. 58 (1), v. 17–36. https://doi.org/10.1007/s10347- 011-0266-0.

Strub, P. T., Kosro, P. M., and Huyer, A., 1991. The nature of the cold filaments in the California Current System. J. Geophys. Res., v. 96, p. 14743–14768.

Sturani, C., 1971. Ammonites and stratigraphy of the *Posidonia alpina* beds of the Venetian Alps. (Middle Jurassic, mainly Bajocian). Mem. Ist. Geol. Min. Univ. Padova, 190 pp.

Tanaka, N., Monaghan, M. C., and Rye, D. M., 1986. Contribution of metabolic carbon to mollusk and barnacle shell carbonate. Nature, v. 320, p. 520–523.

Tasli, K., Ozer, E., Koç, H., 2006. Benthic foraminiferal assemblages of the Cretaceous platform carbonate succession in the Yavca area (Bolkar Mountains, S Turkey): biostratigraphy and paleoenvironments. Geobios, v. 39, p. 521–533.

Tasselli, A., 1982. Microstrutture, modalità di accrescimento e periodicità di alcuni lamelllibranchi liassici. Unpubl. M.Sc. thesis, University of Ferrara (Italy), 110 pp.

Tausch, L., 1890. Zur Kenntnis der Fauna der "Grauen Kalke". Abhandlungen der Kaiserlich-Königlichen Geologischen Reichsanstalt, v. 15 (2), p. 1–40.

Thurmann, J., 1832–1836. Essai sur les soulèvements jurassiques de Porrentruy. Description géognostique de la série jurassique et théorie orographique du soulèvements: Strasbourg, France. Mémoire de la Société d´Histoire Naturelle, 95 pp.

Titschack, J., Zuschin, M., Spötl, Baal, C., 2010. The giant oyster *Hyotissa hyotis* from the northern Red Sea as a decadal-scale archive for seasonal environmental fluctuations in coral reef habitats. Coral Reefs, v. 29, p. 1061–1075. https://doi.org/10.1007/s00338-010-0665-7.

Trecalli, A., Spangenberg, J., Adatte, T., Föllmi, K.B., Parente, M., 2012. Carbonate platform evidence of ocean acidification at the onset of the Early Toarcian oceanic Anoxic Event. Earth Planet. Sci. Lett., v. 357, p. 214–225. https://doi.org/10.1016/j.epsl.2012.09.043.

Urey, H. C., 1948. Oxygen isotopes in nature and in the laboratory. Science, v. 108, p. 489–496.

Urmos, J., Sharma, S. K., Mackenzie, F. T., 1991. Characterization of some biogenic carbonates with Raman spectroscopy. American Mineralogist, v. 76 (3–4), p. 641–646.

Vallentyne, J. R., 1963. Isolation of pyrite spherules from recent sediments. Limnology and Oceanography, v. 8, p. 16–30. https://doi.org/10.4319/lo.1963.8.1.0016.

Vander Putten, E., Dehairs, F., Keppens, E., Baeyens, W., 2000. High resolution distribution of trace elements in the calcite shell layer of modern *Mytilus edulis*: environmental and biological controls. Geochimica et Cosmochimica Acta, v. 64 (6), p. 997–1011. https://doi.org/10.1016/S0016-7037(99)00380-4.

Védrine, S., Strasser, A., Hug, W., 2007. Oncoid growth and distribution controlled by sea-level fluctuations and climate (Late Oxfordian, swiss Jura mountains). Facies, v. 53 (4), p. 535–552.

Veizer, J., Ala, D., Azmy, K., Bruckschen, P., Buhl, D., Bruhn, F., Carden, G.A.F., Diener, A., Ebneth, S., Godderis, Y., Jasper, T., Korte, C., Pawellek, F., Podlaha, O. G., Strauss, H., 1999. $^{87}Sr/^{86}Sr$, $\delta^{13}C$ and $\delta^{18}O$ evolution of Phanerozoic seawater. Chemical Geology, v. 161 (1–3), p. 59–88. https://doi.org/10.1016/S0009-2541(99)00081-9.

Vénec-Peyre, M.-T., 1996. Bioeroding foraminifera: a review. Mar Micropaleont., v. 28, p. 19–30.

Vermeij, G. J., 2013. The oyster enigma variations: a hypothesis of microbial calcification. Paleobiology, v. 40 (1), p. 1–13. https://doi.org/10.1666/13002.

Vilardell, O., Gili, E., 2003. Quantitative study of a hippuritid rudist lithosome in a Santonian carbonate platform in the southern Central Pyrenees. Palaeogeogr. Palaeoclimatol. Palaeoecol., v. 200, p. 31–41.

Vologdin, A. G., 1932. Archaeocyaths of Siberia, part 2. Cambrian fauna of Altai limestones. State Sci Tech Geol. Publ, Leningrad, 106 pp.

Walliser, E. O., Schöne, B. R., Tütken, T., Zirkel, J., Grimm, K. I., Pross, J., 2015. The bivalve *Glycymeris planicostalis* as a high-resolution paleoclimate archive for the Rupelian (Early Oligocene) of central Europe. Climate of the Past, v. 11 (4), p. 653–668. https://doi.org/10.5194/cp-11-653-2015.

Walliser, E. O., Mertz-Kraus, R., and Schöne, B. R., 2018. The giant inoceramid *Platyceramus platinus* as a high-resolution paleoclimate archive for the Late Cretaceous of the Western Interior Seaway. Cretaceous Research, v. 86, p. 73–90.

Walliser, E. O., Tanabe, K., Hikida, Y., Shirai, K., and Schöne, B. R., 2019. Sclerochronological study of the gigantic inoceramids *Sphenoceramus schmidti* and *S. sachalinensis* from Hokkaido, northern Japan. Lethaia, v. 52 (3), p. 410–428. https://doi.org/10.1111/let.12321.

Wanamaker, A. D., Kreutz, K. J., Borns, H. W., Introne, D. S., Feindel, S., Funder, S., Rawson, P. D., and Barber, B. J., 2007. Experimental determination of salinity, temperature, growth,

and metabolic effects on shell isotope chemistry of *Mytilus edulis* collected from Maine and Greenland. Paleoceanography, v. 22 (2), pa2217. https://doi.org/10.1029/2006PA001352.

Wang, L., Shi, X., Jiang, G., 2012. Pyrite morphology and redox fluctuations recorded in the Ediacaran Doushantuo Formation. Palaeogeography Palaeoclimatology Palaeoecology, v. 333–334, p. 218–227. https://doi.org/10.1016/j.palaeo.2012.03.033.

Wang, Q., Morse, J. W., 1995. Pyrite formation under conditions approximating those in anoxic sediments I. Pathway and morphology. Marine Chemistry, v. 52 (2), p. 99–121. https://doi.org/10.1016/0304-4203(95)00082-8.

Wefer, G., Berger, W. H., 1991. Isotope paleontology: growth and composition of extant calcareous species. Marine Geology, v. 100 (1–4), p. 207–248. https://doi.org/10.1016/0025-3227(91)90234-U.

Weidman, C., Jones, G., 1994. The long-lived mollusc *Arctica islandica*: a new paleoceanographic tool for the reconstruction of bottom temperatures for the continental shelves of the northern North. J. Geophys. Res., v. 99, p. 305–314.

Wignall, P. B., and Newton, R., 1998. Pyrite framboid diameter as a measure of oxygen deficiency in ancient mudrocks. Am J Sci, v. 298, p. 537–552.

Wignall, P. B., Hallam, A., Newton, R. J., Sha, J. G., Reeves, E., Mattioli, E., and Crowley, S., 2006. An eastern Tethyan (Tibetan) record of the Early Jurassic (Toarcian) mass extinction event. Geobiology, v. 4, p. 179–190. https://doi.org/10.1111/j.1472-4669.2006.00081.x

Wignall, P. B., Bond, D. P. G., Kuwahara, K., Kakuwa, Y., Newton, R. J., Poulton, S. W., 2010. An 80 million year oceanic redox history from Permian to Jurassic pelagic sediments of the Mino-Tamba terrane, SW Japan, and the origin of four mass extinctions. Global and Planetary Change, v. 71 (1–2), p. 109–123.

Wilkin, R. T., Barnes, H. L., Brantley, S. L., 1996. The size distribution of framboidal pyrite in modern sediments: an indicator of redox conditions. Geochim. Cosmochim. Acta, v. 60, p. 3897–3912.

Wilkin, R. T., Barnes, H. L., 1997. Formation processes of framboidal pyrite. Geochimica et Cosmochimica Acta, v. 61 (2), p. 323–339. https://doi.org/10.1016/S0016-7037(96)00320-1.

Wilkin, R. T., Arthur, M. A., Dean W. E., 1997. History of water-column anoxia in the Black Sea indicated by pyrite framboid size distributions. Earth Planet. Sci. Lett., v. 148, p. 517–525.

Wilkin, R. T., Arthur, M. A., 2001. Variations in pyrite texture, sulfur isotope composition, and iron systematics in the Black Sea: Evidence for Late Pleistocene to Holocene excursions of the O_2-H_2S redox transiton. Geochim. Cosmochim. Acta, v. 65, p. 1399–1416.

Winterer, E. L., Bosellini, A., 1981. Subsidence and sedimentation on a Jurassic passive continental margin, Southern Alps, Italy. AAPG Bull., v. 65, p. 394–421.

Woodfine, R. G., Jenkyns, H. C., Sarti, M., Baroncini, F., Violante, C., 2008. The response of two Tethyan carbonate platforms to the early Toarcian (Jurassic) oceanic anoxic event: environmental change and differential subsidence. Sedimentology, v. 55, p. 1011–1028.

Woodring, W. P., 1925. Contributions to the Geology and Palaeontology of the West Indies. Miocene Mollusks from Bowden, Jamaica. Pelecypods and Scaphopods. Carnegie Institution Publication. Carnegie Institution of Washington D.C., v. 366, p. 1–122.

Wray, J. L., 1967. Upper Devonian calcareous algae from the Canning Basin, Western Australia. Colorado School of Mines, Professional Contributions, v. 3, 76 pp.

Yamanashi, J., Takayanagi, H., Isaji, A., Asami, R., Iryu Y., 2016. Carbon and Oxygen isotope records from *Tridacna derasa* shells: toward establishing a reliable proxy for sea surface environments. PLOS ONE, v. 11 (6), e0157659. https://doi.org/10.1371/journal.pone.0157659.

Yang, R., He, S., Wang, X., Hu, Q., Hu, D., Yi, J., 2016. Paleo-ocean redox environments of the Upper Ordovician Wufeng and the first member in lower Silurian Longmaxi formations

in the Jiaoshiba area, Sichuan Basin. Canadian Journal of Earth Sciences, v. 53 (4), p. 426–440. https://doi.org/10.1139/cjes-2015-0210.

Zempolich, W. G., 1993. The drowning succession in Jurassic carbonates of the Venetian Alps, Italy, a record of supercontinent breakup, gradual eustatic rise, and eutrophication of shallow-water environments. In: Loucks, R.G., Sarg, J.F. (Eds.), Carbonate Sequence Stratigraphy: Recent Developments and Applications. Mem. Am. Assoc. Pet. Geol., v. 57, p. 63–105.

Zhang, Z., Du, Y. S., Gong, Y. M., Huang, H. W., Zeng, X. W., Li, S. S., and Ou., Y. K., 2007. Transformation from Devonian Givetian carbonate platform to Famennian bacteria-algae ecosystem in Litang isolated platform, Guangxi, and its significance. Earth Science Journal of China University of Geosciences, Wuhan, v. 32, p. 811–818.

"Questa conclusione, benché trovata da povera gente, c'è parsa così giusta,

che abbiam pensato di metterla qui, come il sugo di tutta la storia.

La quale, se non v'è dispiaciuta affatto, vogliatene bene a chi l'ha scritta […].

Ma se in vece fossimo riusciti ad annoiarvi, credete che non s'è fatto apposta."

(A. Manzoni, *I promessi sposi*)